

11-30-2009

# Linear and Nonlinear Control of Unmanned Rotorcraft

Ioannis A. Raptis  
*University of South Florida*

Follow this and additional works at: <http://scholarcommons.usf.edu/etd>

 Part of the [American Studies Commons](#), and the [Electrical and Computer Engineering Commons](#)

## Scholar Commons Citation

Raptis, Ioannis A., "Linear and Nonlinear Control of Unmanned Rotorcraft" (2009). *Graduate Theses and Dissertations*.  
<http://scholarcommons.usf.edu/etd/3482>

This Dissertation is brought to you for free and open access by the Graduate School at Scholar Commons. It has been accepted for inclusion in Graduate Theses and Dissertations by an authorized administrator of Scholar Commons. For more information, please contact [scholarcommons@usf.edu](mailto:scholarcommons@usf.edu).

Linear and Nonlinear Control of Unmanned Rotorcraft

by

Ioannis A. Raptis

A dissertation submitted in partial fulfillment  
of the requirements for the degree of  
Doctor of Philosophy  
Department of Electrical Engineering  
College of Engineering  
University of South Florida

Co-Major Professor: Kimon P. Valavanis, Ph.D.  
Co-Major Professor: Wilfrido A. Moreno, Ph.D.  
Kenneth Buckle, Ph.D.  
Elias Stefanakos, Ph.D.  
Abraham Kandel, Ph.D.  
George Vachtsevanos, Ph.D.

Date of Approval:  
November 30, 2009

Keywords: Helicopter Control, Aerial Robotics, Unmanned Aerial Vehicles, System Identification,  
Backstepping Control

© Copyright 2010, Ioannis A. Raptis

*In the loving memory of Euthimios P. Roussis, Ioannis G. Raptis and Georgios I. Raptis*

## Acknowledgements

First of all I would like to thank my advisor, Kimon Valavanis who gave me the opportunity to work in his laboratory. I am indebted for his guidance, support and friendship in all these years that we have worked together. Most importantly, I would like to thank him for giving me the help and encouragement to explore any ideas and thoughts associated with my research. I would also like to thank my co-advisor Dr. Wilfrido Moreno for helping me and guiding me with the labyrinth of the University's and the EE department's procedures.

I would also like to thank my childhood friends Nikos Kalamaras and Kostas Velivasakis for their friendship and encouragement in all the difficult times of my life. I have no words to express my gratitude to my beautiful girlfriend Diana for her love and patience all this time. Her support and encouragement helped me keep going.

I would like to thank my uncle Periklis Roussis for his love and support. I have always valued his opinion and appreciated his help by all means throughout my academic studies.

Most importantly, I would like to express my gratitude to my sister Martha and my parents Anastasios and Alexandra. Without their sacrifices I would have never been able to chase my dreams and ambitions.

This research has been partially supported by grants: ARO W911NF-06-1-0069, SPAWAR N00039-06-C-0062 and NSF IIP-0856311 (Denver University grant number 36563)

## Table of Contents

List of Tables		v
List of Figures		vi
List of Acronyms		xi
Abstract		xii
Chapter 1	Introduction	1
	1.1 Motivation	1
	1.2 Problem Statement	4
	1.3 Methods of Solution and Contributions	8
	1.3.1 Helicopter Linear Control	8
	1.3.2 Helicopter Nonlinear Control	10
	1.4 Dissertation Outline	12
Chapter 2	Literature Review	13
	2.1 Linear Control	13
	2.2 Nonlinear Control	18
Chapter 3	Helicopter Basic Equations of Motion	21
	3.1 Helicopter Equations of Motion	21
	3.2 Position and Orientation of the Helicopter	26
	3.2.1 Helicopter Position Dynamics	28
	3.2.2 Helicopter Orientation Dynamics	31
	3.3 Complete Helicopter Dynamics	33
	3.4 Remarks	34
Chapter 4	Simplified Rotor Dynamics	35
	4.1 Introduction	35
	4.2 Blade Motion	37
	4.3 Swashplate Mechanism	40
	4.4 Fundamental Rotor Aerodynamics	42
	4.5 Flapping Equations of Motion	48

4.6	Rotor Tip-Path-Plane Equation	51
4.7	First Order Tip-Path-Plane Equations	53
4.8	Main Rotor Forces and Moments	54
4.9	Remarks	56
Chapter 5	Frequency Domain System Identification	57
5.1	Mathematical Modeling	57
5.1.1	First Principles Modeling	58
5.1.2	System Identification Modeling	59
5.2	Frequency Domain System Identification	60
5.3	Advantages of the Frequency Domain Identification	62
5.4	Helicopter Identification Challenges	62
5.5	Frequency Response and Coherence Function	63
5.6	The <i>CIFER</i> <sup>®</sup> Package	66
5.7	Time History Data and Excitation Inputs	68
5.8	Linearization of the Equations of Motion	70
5.9	Stability and Control Derivatives	72
5.10	Model Identification	73
5.10.1	Experimental Platform	74
5.10.2	Parametrized State Space Model	75
5.10.3	Identification Setup	79
5.10.4	Time Domain Validation	89
5.11	Remarks	90
Chapter 6	Linear Tracking Controller Design for Small Scale Unmanned Helicopters	91
6.1	Helicopter Linear Model	91
6.2	Controller Outline	93
6.3	Decomposing the System	97
6.4	Velocity and Heading Tracking Control	101
6.4.1	Lateral-Longitudinal Dynamics	101
6.4.2	Yaw-Heave Dynamics	110
6.4.3	Stability of the Complete System Error Dynamics	114
6.5	Position and Heading Tracking	116
6.6	PID Control	121
6.7	Experimental Results	123
6.8	Remarks	124
Chapter 7	Nonlinear Tracking Controller Design for Unmanned Helicopters	129
7.1	Introduction	130
7.2	Helicopter Nonlinear Model	131
7.2.1	Rigid Body Dynamics	131
7.2.2	External Wrench Model	132
7.2.3	Complete Rigid Body Dynamics	136
7.3	Translational Error Dynamics	136
7.4	Attitude Error Dynamics	142

	7.4.1 Yaw Error Dynamics	143
	7.4.2 Orientation Error Dynamics	144
	7.4.3 Angular Velocity Error Dynamics	145
	7.5 Stability of the Attitude Error Dynamics	145
	7.6 Stability of the Translational Error Dynamics	153
	7.7 Numeric Simulation Results	162
	7.8 Remarks	167
Chapter 8	Time Domain Parameter Identification and Applied Discrete Nonlinear Control for Small Scale Unmanned Helicopters	173
	8.1 Introduction	173
	8.2 Discrete System Dynamics	174
	8.3 Discrete Backstepping Algorithm	177
	8.3.1 Angular Velocity Dynamics	177
	8.3.2 Translational Dynamics	177
	8.3.3 Yaw Dynamics	180
	8.4 Parameter Estimation Using Recursive Least Squares	183
	8.5 Parametric Model	184
	8.6 Experimental Results	185
	8.6.1 Time History Data and Excitation Inputs	185
	8.6.2 Validation	186
	8.6.3 Control Design	187
	8.7 Remarks	189
Chapter 9	Time Domain System Identification for Small Scale Unmanned Helicopters Using Fuzzy Models	193
	9.1 Introduction	193
	9.2 Takagi-Sugeno Fuzzy Models	194
	9.3 Proposed Takagi-Sugeno System for Helicopters	196
	9.4 Experimental Results	197
	9.4.1 Tuning of the Membership Functions Parameters	199
	9.4.2 Validation	199
Chapter 10	Comparison Studies	202
	10.1 Summary of the Controller Designs	202
	10.2 Experimental Results	203
	10.3 First Maneuver: Forward Flight	204
	10.4 Second Maneuver: Aggressive Forward Flight	205
	10.5 Third Maneuver: 8 Shaped	206
	10.6 Fourth Maneuver: Pirouette	207
	10.7 Remarks	209
Chapter 11	Conclusions and Future Work	223
	11.1 Summary of Contributions	225
	11.2 Results and Real-Life Implementation	227

11.3 Future Work	227
List of References	229
Appendices	239
Appendix A: Backstepping Control	240
About the Author	End Page

## List of Tables

Table 5.1	Experimental helicopter model basic specifications.	75
Table 5.2	Frequency sweeps parameters.	80
Table 5.3	Selected frequency responses and their corresponding frequency ranges (in <i>rad/sec</i> ).	81
Table 5.4	Linear state space model identified parameters.	84
Table 5.5	Transfer functions costs for each input-output pair.	85
Table 6.1	Linear tracking controller feedback gains.	125
Table 6.2	PID controller gains.	125
Table 7.1	Helicopter parameters.	164
Table 7.2	Drag and servo parameters.	164
Table 7.3	Controller gains.	164
Table 7.4	Controller outline.	166
Table 8.1	Identified system parameters.	188
Table 8.2	Values of the diagonal gain matrices.	188
Table 9.1	Gaussian membership functions.	196
Table 9.2	Gaussian centers and spreads.	198
Table 9.3	Mean error of the Takagi-Sugeno RLS in comparison with RLS identification over the verification data.	198

## List of Figures

Figure 1.1	Typical helicopter configuration.	2
Figure 1.2	This block diagram illustrates the helicopter control design problem.	7
Figure 3.1	Body-fixed coordinate system.	22
Figure 3.2	Helicopter orientation.	27
Figure 3.3	Interconnection of the helicopter dynamics in the space $SE(3)$ .	33
Figure 4.1	Representation of the rotor 3 DOF.	38
Figure 4.2	Connection of the pitch horn to the pitch link.	41
Figure 4.3	Basic configuration of the swashplate mechanism.	42
Figure 4.4	Directions of the velocity components seen by the blade element.	45
Figure 4.5	Illustration of a two dimensional blade element.	47
Figure 4.6	Aerodynamic, inertia and centrifugal forces acting on a blade element.	49
Figure 4.7	Effect of each harmonic given by (4.23) to the TPP.	52
Figure 5.1	Block diagram of the experimental platform's communication interface.	76
Figure 5.2	On-axis frequency responses of the flight data (solid line) and frequency responses predicted by the state space model (dashed line).	86
Figure 5.3	Off-axis frequency responses of the flight data (solid line) and frequency responses predicted by the state space model (dashed line).	87
Figure 5.4	Time domain validation.	88

Figure 6.1	Interconnection of the two helicopter dynamics subsystems.	99
Figure 6.2	Strict-feedback interconnection of the longitudinal-lateral helicopter dynamics subsystem.	103
Figure 6.3	Interconnection of the yaw-heave helicopter dynamics subsystem.	111
Figure 6.4	Cascade connection of the closed loop error dynamics subsystems.	115
Figure 6.5	Cascade connection of the error dynamics subsystems related with the position tracking problem.	119
Figure 6.6	Reference trajectory (solid green line), actual position trajectory of the linear (green dashed line) and PID (dashed-dotted red line) designs, expressed in inertial coordinates with respect to time.	125
Figure 6.7	Orientation angles of the linear (solid line) and PID (dashed line) designs.	126
Figure 6.8	Reference position trajectory (solid line) and the actual trajectory of the linear (dashed line) design with respect to the inertia axis.	126
Figure 6.9	Reference position trajectory (solid line) and the actual trajectory of the PID (dashed line) design, with respect to the inertia axis.	127
Figure 6.10	Control inputs of the linear design.	127
Figure 6.11	Control inputs of the PID design.	128
Figure 7.1	The helicopter's body-fixed frame, the Tip-Path-Plane angles and the thrust vectors of the main and tail rotor.	132
Figure 7.2	This block diagram illustrates the connection of the generated thrusts of the main and tail rotor with the helicopter dynamics.	133
Figure 7.3	This block diagram illustrates the interconnection of the approximated helicopter's dynamics.	136
Figure 7.4	This block diagram illustrates the translational error dynamics subsystem.	138
Figure 7.5	Resulting system dynamics after the choice of $v_d^I$ , $\rho_d$ and $T_M$ .	140
Figure 7.6	This figure illustrates the helicopter's vertical orientation vectors $\rho_3$ , $\rho_d$ with respect to inertia frame for $\rho_{3,3}, \rho_{d,3} > 0$ .	142

Figure 7.7	This figure illustrates that only the exponential convergence of $e_\rho$ can not guarantee that $\ \rho\  < 1$ for every $t \geq t_0$ .	148
Figure 7.8	This figure illustrates the existence of a value $C^*$ with $C_{max} < C^* < 1$ such that when $\ \rho\  > C^*$ then $\dot{R}(\ \rho\ ) < 0$ .	150
Figure 7.9	Block diagram of the complete helicopter dynamics after the transformation of the translational error states.	154
Figure 7.10	<i>First maneuver</i> : Reference position trajectory (dashed line) and actual helicopter trajectory (solid line) expressed in the inertial coordinates with respect to time.	167
Figure 7.11	<i>Second maneuver</i> : Reference position trajectory (dashed line) and actual helicopter trajectory (solid line) expressed in the inertial coordinates with respect to time.	168
Figure 7.12	<i>First maneuver</i> : Reference position trajectory (solid line) and actual helicopter trajectory (dashed line) with respect to the inertial axis.	170
Figure 7.13	<i>Second maneuver</i> : Reference position trajectory (solid line) and actual helicopter trajectory (dashed line) with respect to the inertial axis.	170
Figure 7.14	<i>First maneuver</i> : Euler's orientation angles.	171
Figure 7.15	<i>Second maneuver</i> : Euler's orientation angles.	171
Figure 7.16	<i>First maneuver</i> : Main and tail rotor thrust $T_M, T_T$ and the flapping angles $a, b$ .	172
Figure 7.17	<i>Second maneuver</i> : Main and tail rotor thrust $T_M, T_T$ and the flapping angles $a, b$ .	172
Figure 8.1	Interconnection of the helicopter dynamics using (8.23)-(8.27).	179
Figure 8.2	Comparison between the actual (solid line) and estimated (dashed line) linear velocities using the verification data.	190
Figure 8.3	Comparison between the actual (solid line) and estimated (dashed line) angular velocities using the verification data.	190
Figure 8.4	Reference trajectory (dashed line) and actual velocity trajectory (solid line) of the helicopter expressed in inertial coordinates with respect to time.	191
Figure 8.5	Euler's orientation angles.	191

Figure 8.6	Reference position trajectory (solid line) and the actual helicopter position (dashed line) with respect to the inertial axis.	192
Figure 8.7	Control inputs.	192
Figure 9.1	Comparison between the actual (solid line) and estimated (dotted line) linear velocities using the verification data.	200
Figure 9.2	Comparison between the actual (solid line) and estimated (dotted line) angular velocities using the verification data.	201
Figure 10.1	<i>First maneuver (Forward flight)</i> : Reference velocity trajectory (green dashed line) and actual velocity trajectory of the linear (solid blue line), PID (red dashed dotted line), nonlinear (dashed dotted black line) controller designs, expressed in inertial coordinates with respect to time.	211
Figure 10.2	<i>First maneuver (Forward flight)</i> : Orientation angles of the linear (solid blue line), PID (dashed red line) and nonlinear (dashed dotted black line) controllers designs.	211
Figure 10.3	<i>First maneuver (Forward flight)</i> : Control inputs of the linear (solid blue line), PID (dashed red line) and nonlinear (dashed dotted black line) controller designs.	212
Figure 10.4	<i>First maneuver (Forward flight)</i> : Reference position trajectory (solid line) and actual trajectory of the controller designs (dashed line) with respect to the inertial axis.	213
Figure 10.5	<i>Second maneuver (Aggressive forward flight)</i> : Reference velocity trajectory (green dashed line) and actual velocity trajectory of the linear (solid blue line), PID (red dashed dotted line), nonlinear (dashed dotted black line) controller designs, expressed in inertial coordinates with respect to time.	214
Figure 10.6	<i>Second maneuver (Aggressive forward flight)</i> : Orientation angles of the linear (solid blue line), PID (dashed red line) and nonlinear (dashed dotted black line) controllers designs.	214
Figure 10.7	<i>Second maneuver (Aggressive forward flight)</i> : Control inputs of the linear (solid blue line), PID (dashed red line) and nonlinear (dashed dotted black line) controller designs.	215
Figure 10.8	<i>Second maneuver (Aggressive forward flight)</i> : Reference position trajectory (solid line) and actual trajectory of the controller designs (dashed line) with respect to the inertial axis.	216

Figure 10.9	<i>Third maneuver (8 shaped):</i> Reference position trajectory (green dashed line) and actual position trajectory of the linear (solid blue line), PID (red dashed dotted line), nonlinear (dashed dotted black line) controller designs, expressed in inertial coordinates with respect to time.	217
Figure 10.10	<i>Third maneuver (8 shaped):</i> Orientation angles of the linear (solid blue line), PID (dashed red line) and nonlinear (dashed dotted black line) controllers designs.	217
Figure 10.11	<i>Third maneuver (8 shaped):</i> Control inputs of the linear (solid blue line), PID (dashed red line) and nonlinear (dashed dotted black line) controller designs.	218
Figure 10.12	<i>Third maneuver (8 shaped):</i> Reference position trajectory (solid line) and actual trajectory of the controller designs (dashed line) with respect to the inertial axis.	219
Figure 10.13	<i>Fourth maneuver (Pirouette):</i> Reference position trajectory (green dashed line) and actual position trajectory of the linear (solid blue line), PID (red dashed dotted line), nonlinear (dashed dotted black line) controller designs, expressed in inertial coordinates with respect to time.	220
Figure 10.14	<i>Fourth maneuver (Pirouette):</i> Orientation angles of the linear (solid blue line), PID (dashed red line) and nonlinear (dashed dotted black line) controllers designs.	220
Figure 10.15	<i>Fourth maneuver (Pirouette):</i> Control inputs of the linear (solid blue line), PID (dashed red line) and nonlinear (dashed dotted black line) controller designs.	221
Figure 10.16	<i>Fourth maneuver (Pirouette):</i> Reference position trajectory (solid line) and actual trajectory of the controller designs (dashed line) with respect to the inertial axis.	222

## List of Acronyms

SISO	Single-Input Single-Output
MIMO	Multiple-Input Multiple-Output
DOF	Degrees Of Freedom
CG	Center of Gravity
RC	Radio Controlled
FAA	Federal Aviation Administration
UDP	User Datagram Protocol
PID	Proportional Integral Derivative
PD	Proportional Derivative
TPP	Tip-Path-Plane
SMD	Spring-Mass-Damper
GAS	Globally Asymptotically Stable
UGAS	Uniformly Globally Asymptotically Stable
UGB	Uniformly Globally Bounded
LTI	Linear Time Invariant
RLS	Recursive Least Squares

## **Linear and Nonlinear Control of Unmanned Rotorcraft**

**Ioannis A. Raptis**

### **ABSTRACT**

The main characteristic attribute of the rotorcraft is the use of rotary wings to produce the thrust force necessary for motion. Therefore, rotorcraft have an advantage relative to fixed wing aircraft because they do not require any relative velocity to produce aerodynamic forces. Rotorcraft have been used in a wide range of missions of civilian and military applications. Particular interest has been concentrated in applications related to search and rescue in environments that impose restrictions to human presence and interference.

The main representative of the rotorcraft family is the helicopter. Small scale helicopters retain all the flight characteristics and physical principles of their full scale counterpart. In addition, they are naturally more agile and dexterous compared to full scale helicopters. Their flight capabilities, reduced size and cost have monopolized the attention of the Unmanned Aerial Vehicles research community for the development of low cost and efficient autonomous flight platforms.

Helicopters are highly nonlinear systems with significant dynamic coupling. In general, they are considered to be much more unstable than fixed wing aircraft and constant control must be sustained at all times. The goal of this dissertation is to investigate the challenging design problem of autonomous flight controllers for small scale helicopters. A typical flight control system is composed of a mathematical algorithm that produces the appropriate command signals required to perform autonomous flight.

Modern control techniques are model based, since the controller architecture depends on the dynamic description of the system to be controlled. This principle applies to the helicopter as well,

therefore, the flight control problem is tightly connected with the helicopter modeling. The helicopter dynamics can be represented by both linear and nonlinear models of ordinary differential equations. Theoretically, the validity of the linear models is restricted in a certain region around a specific operating point. Contrary, nonlinear models provide a global description of the helicopter dynamics.

This work proposes several detailed control designs based on both dynamic representations of small scale helicopters. The controller objective is for the helicopter to autonomously track predefined position (or velocity) and heading reference trajectories. The controllers performance is evaluated using *X-Plane*, a realistic and commercially available flight simulator.

## Chapter 1: Introduction

### 1.1 Motivation

The term Unmanned Aerial Vehicles (UAVs) is used to describe unpiloted flying vessels. This term refers to vehicles that are remotely piloted or autonomously controlled for the execution of a predefined flight task. In both cases the key attribute of these vehicles is the absence of a human pilot on board [106]. The applicability of UAVs is predominant in the execution of potentially dangerous flight missions or in cases where the small size of the vehicle restricts the presence of a pilot [70].

Potential usage of UAVs can be found in military and civilian applications, although military applications dominate the non-military ones. Civilian applications involve pipelines and power lines inspection, surveillance, rescue missions, border patrol, oil and natural gas research, fire prevention, topography, agricultural applications [106], filmmaking [70], traffic monitoring, flight in hazardous environments (i.e. in a radioactive environment) [11].

UAVs are further classified into two main categories. The first category are fixed-wing UAVs (e.g., unmanned airplanes) that require relative velocity for the production of aerodynamic forces and a runway for take-off and landing [105]. The second category are the rotorcraft UAVs. The advantages of the rotorcraft unique flight capabilities have drawn much attention through the years. The primary characteristic attribute of the rotorcraft is the use of rotary wings to produce the thrust force necessary for motion. The main benefit of using a rotorcraft is its ability to move in all directions of the Cartesian space while preserving an independent heading. Therefore, rotorcraft have an advantage relative to fixed wing aircraft because they do not require any relative velocity to produce aerodynamic forces [40] and also due to their vertical flight capability.

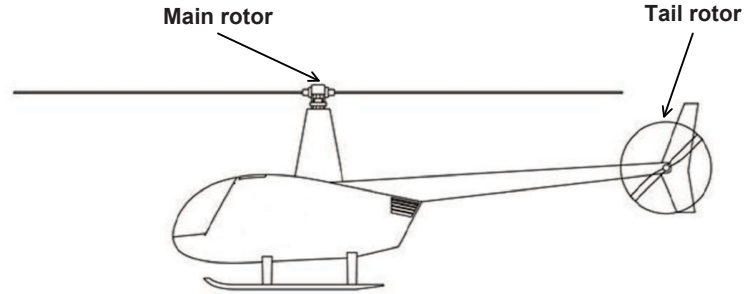


Figure 1.1: Typical helicopter configuration. The helicopter motion is produced by two engine driven rotors: The main and tail rotor.

The main representative of the rotorcraft family is the helicopter. The typical configuration of a helicopter involves two engine driven rotors: The main and the tail rotor. The main rotor produces the thrust force for the vertical lift of the helicopter. The tail rotor compensates the torque produced by the main rotor and controls the heading of the helicopter. The change of the helicopter's fuselage attitude angles results in the tilt of the main rotor and, therefore, the production of the propulsive forces for the longitudinal/lateral motion of the helicopter.

Small scale helicopters retain all the flight characteristics and physical principles of their full scale counterpart. In addition, they are naturally more agile and dexterous compared to full scale helicopters. Their flight capabilities, reduced size and cost have monopolized the attention of the UAV research community for the development of low cost and efficient autonomous flight platforms.

The design of an autonomous small scale helicopter flight platform requires several expertise in diverse fields of engineering. Some of the challenges towards the development of an autonomously flying helicopter involve sensor integration and sensor fusion to obtain accurate measurements, flight controller design, path planning and communications. Advances in sensor technology, computational efficiency and the constantly reduced size of processors provide a significant boost in the development of on-board hardware for the UAVs.

The goal of this dissertation is to examine the challenging design problem of autonomous flight controllers for small scale unmanned helicopters. A typical flight controller system is composed of a mathematical algorithm that produces the appropriate command signals required to

perform any autonomous flight. The control algorithm receives the measurement signals from several sensors and triggers a suitable output for operating the helicopter. The controller's output is also referred to as the controller's feedback signal. An important requirement of the controller design is to guarantee the stability of the helicopter during the autonomous flight operation.

The most reliable approach for designing the control algorithm and also examining the stability properties of the autonomous flight system, is via modern control theory. According to this theoretical framework, the flight controller design is based on the helicopter dynamic model. This model is a mathematical system of ordinary differential equations. The dynamic model describes the helicopter response to any given input.

Helicopters are highly nonlinear systems with significant dynamic coupling. The dynamic coupling is attributed to two main sources. The first one is the helicopter nonlinear equations of motion. The second one is the dynamic coupling between the generated aerodynamic forces and moments. In addition, there is also significant parameter and model uncertainty due to complicated aerodynamic nature of the thrust generation. Furthermore, helicopters are considered to be much more unstable than fixed wing aircraft and constant control action must be sustained at all times. The above helicopter characteristics constitute very challenging obstacles to the controller design problem.

As in most control applications, the helicopter model that is used for control design purposes is just an approximation of the actual nonlinear helicopter dynamics. To this extent, in order to develop a generic flight control system which applies to most standard small scale helicopter platforms, the designer must successfully solve the following intermediate tasks:

- Derive the structure and the order of a parametric dynamic model that best describes the helicopter motion. The order of the model should be kept to minimum such that the parametric model includes only the absolutely necessary variables that are required for the representation of the helicopter dynamics. Dynamic systems of high order are very impractical since they significantly increase the complexity of the control design. The parametric model should provide a physically meaningful dynamic description for a large family of small scale helicopters.

- Based on the parametric helicopter model, determine a nominal feedback control law such that the helicopter tracks a predefined reference trajectory. The design should guarantee that the control inputs remain bounded while the helicopter tracks the reference trajectory.
- Finally, for a particular helicopter, determine which is the best methodology for accurately extracting the values of the parametric model.

Most of the current work published in the field of helicopter control restrict its analysis only in a subset of the above design challenges. This dissertation is one of the few research efforts that encompass a thorough examination of all of the above design issues. The characteristics of the helicopter dynamics (high uncertainty, nonlinear coupled dynamics) constitute the helicopter control problem stimulating for both its theoretical and real-life implementation viewpoint. The objective of this work is to provide mathematically consistent methodologies that can be applied into actual small scale helicopter platforms.

## 1.2 Problem Statement

The helicopter dynamics are inherently nonlinear with significant dynamic coupling among the state variables and control inputs. The dynamic coupling expresses the fact that any change in a control input affects multiple state variables of the helicopter. Therefore, each input effects not only the state variables of interest, but also produces unintended secondary responses. To suppress the unwanted excitation of secondary state variables a simultaneous coordination of all the control inputs is required at all time instances. The nonlinear nature and the cross coupling effect of the helicopter dynamics places them among the most complex aerial vehicles.

The helicopter has four control inputs. Two cyclic commands that manipulate the longitudinal/lateral motion, one collective command that controls the vertical motion and finally the pedal command that controls the heading motion of the helicopter. Since the control inputs are significantly less than the motion variables, the helicopter is further classified as an underactuated system.

The actual helicopter dynamics are represented in mathematical terms by the differential equations of the following nonlinear system:

$$\dot{x} = f(x, u_c) \quad (1.1)$$

where  $x \in \mathbb{R}^n$  is the helicopter's state and  $u_c \in \mathbb{R}^4$  is the control input vector. Control techniques based on modern control theory are model based, in the sense that the controller architecture depends on the dynamic description of the system. Therefore, knowledge of the helicopter's dynamic model is required for the design of autonomous flight controllers.

However, the actual helicopter dynamics are unknown and as in most engineering applications, they are approximated by physically meaningful mathematical models of lower order. To this point, it must be stated that the approximated model is just an "abstraction" since it is practically impossible to provide a complete representation of the actual helicopter dynamics [81]. However, this does not mean that it is impossible to develop a model, that sufficiently represents the dynamics of the helicopter under certain operating flight conditions.

Generally, there are two ways to approximate the actual helicopter dynamics. The first is by a Linear Time Invariant (LTI) model. The second representation is via a model of nonlinear differential equations. Typically, the validity of the LTI model is restricted in the vicinity of a particular operating condition of the helicopter. For the description of a wide portion of the flight envelope, multiple linear models are required for different operating conditions. The LTI model is represented by a set of first-order linear differential equations, written in the form:

$$\begin{aligned} \dot{x}_l &= Ax_l + Bu_c \\ y &= C_l x_l \\ y_m &= C_l^m x_l \end{aligned} \quad (1.2)$$

where  $x_l$  is the vector of the helicopter's linear model state variables,  $y_m$  is the vector of the helicopters available measurements and  $y$  is the vector of the helicopter outputs that need to be con-

trolled. The dimension of the output vector can not exceed the number of the control inputs. The design problem is to find a feedback law of the measurement vector, i.e.,  $u_l = \Phi_l(y_m)$ , such that when  $u_c = u_l$ , then the helicopter output asymptotically tracks a reference trajectory denoted by  $y_r$ . Hence, the objective is:

$$\lim_{t \rightarrow \infty} \|y(t) - y_r(t)\| = 0 \quad (1.3)$$

By applying modern control design techniques, the architecture of the feedback law  $u_l$  will be (in general) depended on the structure of the linear system given by (1.2).

Nonlinear models are used to provide a global description of the helicopter dynamics for the complete flight envelope. They are more elaborate and complex compared to linear models, however, only a single model is required for the description of the helicopter dynamics. When a nonlinear dynamic representation is chosen, the helicopter dynamics can be written as:

$$\begin{aligned} \dot{x}_n &= \phi(x_n, u_c, \mu) \\ y &= C_n x_n \\ y_m &= C_n^m x_n \end{aligned} \quad (1.4)$$

where  $\mu$  denotes the parameter vector of the nonlinear model. Of course, even in the case of the nonlinear representation, the output and the measurement vector of the helicopter are identical with the linear model case. However, the dimensions of the state vectors  $x_n$  and  $x_l$  are (in general) different since the two models might have different orders. Similarly to the linear case, the control objective is the design of a feedback law  $u_n = \Phi_n(y_m)$  such that when  $u_c = u_n$ , then the asymptotic tracking of (1.3) is achieved. Since  $u_n$  depends on the state space equations of (1.4) then, in principal,  $u_l$  and  $u_n$  will be different. The block diagram of the helicopter tracking control problem is illustrated in Figure 1.2. In either case the design challenges are:

- The determination of the order and structure of the parametric model (1.2) or (1.4). These parametric models should encapsulate the dynamic behavior of a large family of small scale helicopters.

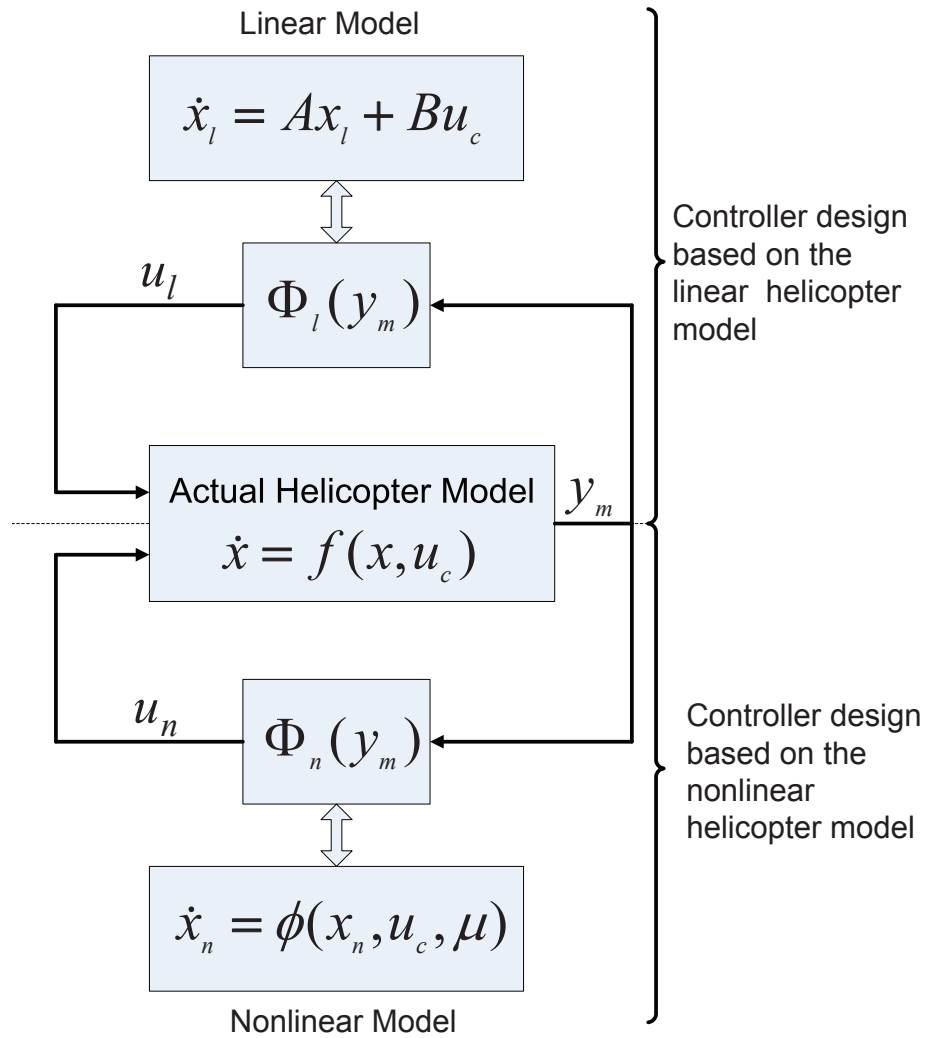


Figure 1.2: This block diagram illustrates the helicopter control design problem. The helicopter dynamics can be represented by a linear or nonlinear system of differential equations. In either case the feedback control law depends on the model choice.

- The derivation of a consistent methodology for designing the feedback laws  $u_l = \Phi_l(y_m)$  or  $u_n = \Phi_n(y_m)$  which guarantee that the tracking objective given in (1.3) is achieved.
- The calculation of the matrices  $A$ ,  $B$  or the parameter vector  $\mu$  such that the predicted response from (1.2) and (1.4) is the same with the actual helicopter response obtained by flight data. The identified parameters are required for the implementation of the control laws  $u_l$  and  $u_n$ , respectively.

### 1.3 Methods of Solution and Contributions

This research provides a complete and consistent solution to the helicopter controller design problem. All intermediate challenges associated with the helicopter controller design are addressed for both the linear and the nonlinear representations of the helicopter dynamics. The proposed solutions incorporate a fine balance between theoretical control challenges and real-life application issues. The proposed controllers performance and applicability are evaluated using the commercially available flight simulator *X-Plane*. The experimental part of this research was conducted in the *X-Plane* environment for a small scale *Raptor 90 SE* Radio Controlled (RC) helicopter. Depending on the helicopter model representation, the controller designs proposed in this work are classified as linear and nonlinear.

#### 1.3.1 Helicopter Linear Control

The proposed control design is based on a linear Multiple-Input Multiple-Output (MIMO) coupled helicopter model. Typical design techniques that deal with the tracking problem of linear systems are the internal model approach and the integral control design. The disadvantage of the internal model approach is its complex design while the integral control is restricted only in cases where the reference output is a constant signal. The proposed design guarantees the asymptotic tracking of arbitrary continuous reference trajectories with the only requirement that the reference signal and its higher derivatives are bounded.

The main novelty of the proposed controller is its ability to “pass” the intuitive notion of helicopter piloting to the mathematical controller design. This is achieved by decoupling the rotor dynamics into two separate subsystems. The first subsystem involves the coupled dynamics of the longitudinal/lateral motion while the second subsystem is composed by the yaw/heave dynamics of the helicopter. This separation provides a more distinct effect of the helicopter inputs to the state variables of the two subsystems. The intuitive operation of the vehicle dictates that the two cyclic commands are used for the generation of longitudinal and lateral motion. The two collective commands of the main and tail rotor are mainly used for the production of the vertical lift and regulating the helicopter’s heading.

The basic idea of the controller design is to determine a desired state vector for each subsystem such that when the helicopter state variables converge to their desired state values then the tracking error tends asymptotically to zero. The desired state vectors for each subsystem, are composed by the components of the reference outputs vectors and their higher derivatives.

The second contribution of the proposed design is the development of a recursive procedure for the derivation of the aforementioned desired state vectors for each subsystem. The recursive procedure is based on the backstepping design of systems in pure feedback form. However, the linear helicopter dynamics are not in feedback form. This fact is attributed to the coupling between the helicopter’s external forces and moments. Similarly to [47], a simplified helicopter model that neglects the coupling between the helicopter forces and moments is in pure feedback form. This approximation is based on the rational assumption that the forces produced by the flapping motion of the main rotor blades are negligible compared to the forces produced by the tilt of the fuselage. Since the approximate system is in pure feedback form, it is also feedback linearizable and differentially flat. The derivation of the desired state vectors is based on the differential flatness property of the two subsystems.

For the linear model representation of the helicopter dynamics the model structure proposed in [70] is adopted. This linear model has been successfully used for the parametric identification of several small scale helicopters of different specifications [8, 10, 27, 28, 89, 90]. The proposed model is a linear coupled system of the helicopter motion variables and the main rotor flapping

dynamics. The model validity is evaluated by performing frequency domain system identification using flight test data obtained for the *Raptor 90 SE*. The frequency domain identification procedure of the *Raptor 90 SE* takes place by using the *CIFER*<sup>©</sup> package developed by the NASA Rotorcraft Division (Ames Research Center) [105]. The identified model is later used to evaluate the controller's performance.

Finally, a second controller is introduced which does not require the knowledge of the helicopter model. In many practical control applications the MIMO dynamic model of the helicopter is not available. A fundamental controller composed by four SISO Proportional Integral Derivative (PID) feedback loops is presented. This control scheme is very common start up design point in real-life applications, since it does not require knowledge of the helicopter model and the controller gains can be empirically tuned.

### 1.3.2 Helicopter Nonlinear Control

The adopted nonlinear model of the helicopter dynamics is based on [47]. The helicopter model is represented by the rigid body nonlinear equations of motion enhanced by a simplified model of force and torque generation. The first controller design is based on the backstepping design principle for systems in feedback form. The intermediate backstepping control signals (a.k.a. pseudo controls) for each level of the feedback system are appropriately chosen to stabilize the overall helicopter dynamics. The resulting system error dynamics can be separated in two interconnected subsystems representing the error in translational and attitude dynamics, respectively. This separation reflects the inherited time scaling that exists in the helicopter dynamics. The attitude dynamics are significantly faster compared to the dynamics of the translational motion.

One of the novelties of the proposed controller is that the thrust magnitude is used to compensate the translational error dynamics in all Cartesian directions and not only for the heave dynamics. Furthermore, apart from stabilizing the attitude dynamics, the control design can guarantee that the helicopter will not overturn for every allowed reference trajectory. In addition, the use of

nested saturations in the intermediate pseudo controls of the translational dynamics can guarantee that the physical constraints of the helicopter motion and power will be preserved.

Theoretically, the proposed controller is applicable for both full scale and small scale helicopters. However, the adopted nonlinear model is significantly simplified and does not include higher order dynamics such as engine, inflow velocity and main rotor lead-lag dynamics that are required for the modeling of full scale helicopters.

Although this controller has significant theoretical potential, the extraction of the model parameters from the continuous time nonlinear model using time domain identification is computationally inefficient. The identification procedure is significantly simplified when the nonlinear dynamic model is discretized. A second controller is introduced that applies the backstepping methodology for the discrete time system. Similarly to the continuous time case, the discretized model has a cascade structure. The main contribution of the developed controller is the design freedom in the convergence rate for each state variable of the cascade structure. This is of particular interest since control of the convergence rate in each level of the cascade structure provides better flight results. Furthermore, the stability of the resulting dynamics can be simply inspected by the eigenvalues of a linear system without the necessity of Lyapunov's functions. Those eigenvalues are determined by the designer.

For the identification of the parameters of the nonlinear discrete time system, a simple recursive least squares algorithm is performed. The identified model and the controller performance were evaluated for the *Raptor 90 SE*. Finally, the identification results of the previous methodology can be significantly improved if the discrete nonlinear helicopter dynamics are represented by a Takagi-Sugeno fuzzy system. After the development of the Takagi-Sugeno system, a standard RLS algorithm is used to estimate its parameters. The resulting fuzzy system is an interpolator of nonlinear discrete systems, which depends on the helicopter's flight condition.

## 1.4 Dissertation Outline

This dissertation is organized as follows. Chapter 2 presents the literature review related to the helicopter control problem. The review includes a description of several flight control systems that have been implemented to a variety of helicopter types.

The next two Chapters provide the necessary information for the understanding of both linear and nonlinear helicopter models. In particular, Chapter 3 presents an analytical derivation of the helicopter's kinematic equation of motion, when the helicopter is treated as a rigid body.

The goal of Chapter 4 is to present a simplified model of the main rotor dynamics that encapsulates the coupling effects between the fuselage motion and the main rotor. Chapter 4 presents the sequence of all the intermediate events that take place from the implementation of the cyclic commands to the generation of the blades flapping motion. The concepts described in this Chapter are important for the understanding of the external aerodynamic forces and moments models, used by both the linear and nonlinear representations of the helicopter dynamics.

The Chapters 5 and 6 are related to the linear controller design for helicopters. Chapter 5 gives a description of the frequency domain identification method which is used for the extraction of low order linear helicopter models.

Chapter 6 introduces a tracking controller design based on the linear helicopter dynamics.

Chapter 7 provides a backstepping tracking controller based on the nonlinear helicopter dynamics.

Chapter 8 introduces a discrete time applied backstepping controller and a simple time domain identification method for the determination of helicopter's model unknown parameters.

Chapter 9 shows how a Takagi-Sugeno fuzzy system can improve the time domain identification results.

Chapter 10 provides an extensive comparison and evaluation of the controller designs that have been presented in the previous Chapters.

Concluding remarks and future work follow in Chapter 11. Finally, Appendix A provides background information about the backstepping control method.

## Chapter 2: Literature Review

This Chapter presents the literature review of several flight controller designs for rotorcraft. Flight control systems have been tested in a wide range of rotorcraft types and configurations. The review includes applications for several rotorcraft types such as full-scale, small-scale and experimental platforms, which are gimbaled on a vertical stand. The flight control systems that exist in the literature use tools from all the fields of control theory by incorporating into the design classical, modern and intelligent control techniques.

Flight control systems are mainly classified as linear and nonlinear. Typically, this classification is based on the rotorcraft model representation that is used by the controller. Linear control designs are more application-oriented and have been implemented on the majority of rotorcraft autonomous platforms. Their popularity stems from the simplicity of the control design, which minimizes both the computational effort and the design time. On the contrary, nonlinear controllers are mostly valued for their theoretical contribution to the rotorcraft control problem and their implementation to actual platforms is limited. In what follows both linear and nonlinear control designs are covered and compared.

### 2.1 Linear Control

Classical control techniques disregard the multivariable nature of the rotorcraft dynamics and the strong coupling that exists between the rotorcraft states and the control inputs. In the controller designs of this type, each control input is responsible for the regulation of a particular rotorcraft output. The interaxis couplings that exist between the rotorcraft outputs are disregarded, and each control input is associated with a Single-Input Single-Output (SISO) feedback loop. The SISO

feedback loops that correspond to the control inputs are completely independent with each other. The SISO feedback loops are designed based on typical loop shaping techniques. The stability of the feedback loop is determined by the phase and gain margins of the latter. These margins dictate the admissible amount of gain and phase that can be injected by the controller such that the feedback loop dynamics are stable. These margins, however, can easily lead to erroneous conclusions in the case of multivariable systems [108].

In [89] a PID controller composed by four independent SISO loops is applied to the *Kyosho Concept 60 Graphite* small scale radio controlled helicopter as part of the *Berkeley AeRobot (BEAR)* project. In order to evaluate the closed loop characteristics of the PID scheme an eleven state linear model was identified based on the model structure proposed by [72]. The model parameters were identified by using the prediction error method that is a time domain identification approach. The PID design did not manage to suppress the coupling effect between the lateral and longitudinal motion of the helicopter and the flight controller was limited only to hover flight. The results indicate that SISO techniques have moderate performance and multivariable approaches are required to eliminate the inherent cross coupling effect of the helicopter dynamics. A similar multi-loop PID design has been implemented in [44] for a *Yamaha R-50* small scale helicopter. Similar shortcomings of this classical control approach restricted the autonomous flight of the helicopter only to hover mode.

A simple classical control design composed of Proportional Derivative (PD) SISO feedback loops is also investigated in [70] for the *Yamaha R-50* helicopter. The helicopter model is derived by performing a frequency domain identification method. The identified helicopter dynamics are represented by a thirteen state linear model of the motion variables, the rotor and stabilizer bar characteristics. The identified linear model is used for the optimization of the flight control system. In this particular case, the use of a notch filter is suggested for compensating the effect of the stabilizer bar on the helicopter's attitude dynamics. The particular case study indicates that although the performance of flight control systems based on classical control techniques is limited, accurate knowledge of the helicopter's model can significantly improve the design of the feedback loops.

The majority of linear flight controllers that have been applied to autonomous helicopter platforms, are based on the  $\mathcal{H}_\infty$  feedback control approach. The  $\mathcal{H}_\infty$  control scheme was initially introduced in [68]. The main advantage of the  $\mathcal{H}_\infty$  approach, is its ability to cope with both model uncertainty and disturbance rejection. The  $\mathcal{H}_\infty$  based controller design can be easily adjusted to classical control techniques and at the same time compensate for the multivariable effects of the helicopter. The work reported in [80] provides very strong arguments of why the  $\mathcal{H}_\infty$  approach is a reasonable and suitable control solution for flight vehicles.

The typical structure of an  $\mathcal{H}_\infty$  controller is composed of two parts. The first part is the loop shaping portion of the problem where the input channel is pre-compensated and post-compensated in a similar way that takes place in the classical control techniques of SISO systems. The pre-compensator includes Proportional Integral (PI) compensators for increasing the low-frequency gain of the system, disturbance rejection and attenuate the steady state error. The post compensator is typically used for noise elimination, therefore, it is typically composed by low pass filters. The second portion of the controller, is the  $\mathcal{H}_\infty$  synthesis part, where a static feedback gain is calculated in order to stabilize the multivariable system dynamics and at the same time being optimal with respect to a performance index. More about  $\mathcal{H}_\infty$  control can be found in [12, 17, 78, 92, 113].

In [108] an observer based multivariable controller was designed, using a singular value loop shaping method based on a two degree of freedom  $\mathcal{H}_\infty$  optimization. The controller objective was the development of an Attitude-Command Attitude-Hold (ACAH) flight system for the full scale Westland Lynx helicopter. Contrary to autonomous flight applications, the ACAH flight system is integrated to manned flight operations. The goal of the ACAH flight controller is for the helicopter to track an attitude and heave velocity command that is generated by the pilot's stick input. The principle of the controller design is to suppress the interaxis coupling of the helicopter dynamics, thus decreasing the pilot's workload. The pilot is only charged with the generation of the reference attitude and heave velocity commands that are necessary for the helicopter's motion. The  $\mathcal{H}_\infty$  controller design was based on an eight rigid-body states and four actuator states linear model. The model was obtained by linearizing a more elaborate nonlinear model in hover mode.

The controller performance was evaluated through flight simulations. Although the controller was designed for hover and low speed operations, the simulation results indicated satisfactory performance for speeds up to 90 *knots*.

The design of an ACAH flight system based on a static  $\mathcal{H}_\infty$  loop shaping approach, is also reported in [83] for the Bell 205 full scale helicopter. This work addresses the common problem that exists in multivariable modern control theory, according to which the controller order is equal to the order of the plant to be controlled. This fact is of particular importance for the design of helicopter flight control systems, since the order of a full scale helicopter model may reach up to thirty states! The order of the controller can be reduced by model reduction techniques, however, it is preferable to design from the beginning a flight controller of minimum order via the use of output feedback. When the complete state vector of a system is not available for feedback purposes, instead, only a subset of the state variables can be used by the controller; then the control law is classified as an output feedback controller. This research demonstrated the design of high performance and low order  $\mathcal{H}_\infty$  controllers by applying linear matrix inequality optimization techniques. The helicopter model was derived by linearizing a thirty two states nonlinear model at hover. The linearized model was further truncated to twelve states by removing the dynamics associated with the main rotor. The performance of the developed ACAH system was tested in a series of helicopter maneuvers with satisfactory results.

An alternate  $\mathcal{H}_\infty$  static output feedback controller design is proposed in [26–28] for the stabilization of an autonomous small scale helicopter at hover. The output feedback approach allows the design of multivariable feedback loops using a reduced set of states which results in minimization of the flight controller's order. The structure of the proposed feedback loops reflect the physical flight intuition for helicopters such that the controller design is well suited for the particular application. The loop shaping part of the  $\mathcal{H}_\infty$  controller attenuates the effects of helicopter high frequency unmodeled dynamics. In most cases, the output feedback controller design problem requires the solution of three nonlinear coupled matrix equations. In the reported work, a novel iterative algorithm is introduced that solves the  $\mathcal{H}_\infty$  synthesis part of the controller by solving only two-coupled matrix equations and does not require the knowledge of an initial stabilizing

gain. The controller structure is composed of two main loops. The first loop is responsible for the stabilization of the attitude dynamics while the second loop is used for position tracking. The controller design is based on a thirteen state linear model of the coupled fuselage and rotor dynamics. The model order and structure are obtained by [70]. The identified parameter values have been obtained for the small scale *Raptor 90* radio controlled helicopter. The controller performance is evaluated by numeric simulations and it is restricted to hover flights.

Promising flight results for an autonomous small scale helicopter have been obtained in the work reported in [51, 53–55]. In this research, an  $\mathcal{H}_\infty$  loop shaping controller was implemented on the Carnegie Mellon University's *Yamaha R-50*. This approach applies a blending of multi-variable control techniques and system identification for the development of the flight control system. The helicopter nonlinear model is derived by using the MOdeling for Flight Simulation and Control Analysis (MOSCA) modeling technique [52]. MOSCA combines first principles and system identification techniques for the derivation of both linear and nonlinear helicopter models. A thirty state nonlinear model is derived that includes the fuselage, main rotor, stabilizer bar and inflow dynamics. The helicopter nonlinear dynamics are further linearized in several linear models which correspond to certain operating conditions of the helicopter. Based on the multiple linear models a gain scheduled  $\mathcal{H}_\infty$  loop-shaping controller is applied.

*Gain scheduling* is a control technique according to which the gains of the controller are varying depending on certain variables, which are called *scheduling variables*. The scheduling variables could be functions of the system's state variables or exogenous variables that describe the operating conditions of the system. The main design idea is to control a nonlinear system using a family of linear controllers. The nonlinear system dynamics are linearized over a finite number of operating points. The operating points are parametrized by the scheduling variables. For each linearized model that corresponds to a particular operating point, a linear controller is designed. The overall control law operates as an interpolator of the multiple linear controllers whose gain parameters depend on the scheduling variables. More details about gain scheduling can be found in [43, 87]. The gain scheduling approach has emerged from avionics control applications, where

the linearization of the vehicle's nonlinear dynamics around several operating points is a common procedure.

An interesting comparative study between several controller designs is given in [109, 110]. Both classical and multivariable linear controllers are included in the study. An eighteen state linear model, which represents the helicopter dynamics at hover, was used for the flight controllers design. The flight controllers were tested in a radio controlled helicopter mounted on a mechanical structure that allows the motion of the helicopter in all directions of the Cartesian space. For hovering the multivariable techniques had superior performance in comparison with the classical control designs. From the multivariable designs LQR,  $\mathcal{H}_2$  and  $\mathcal{H}_\infty$  designs were evaluated. The flight validation indicates that in the multivariable design case it is preferable to design multiple feedback loops which correspond to independent subsystems of the helicopter dynamics, thus, decomposing the problem. This approach is preferable from establishing the controller design directly to the complete helicopter dynamics. The low order subsystems should appeal to the physical flight intuition and should be as decoupled as possible. In the particular case the initial linear model was decomposed to a subsystem representing the longitudinal/lateral motion and a second subsystem of the heave and yaw dynamics.

An example of a linear controller design for a helicopter in a vertical stand is also given in [56]. The gimbaled like device on which the helicopter was connected to, allows only a three degrees of freedom motion of the latter. A discrete Linear Quadratic Regulator is used with an augmented Kalman filter for state estimation. The work in [2] compares a simple eigenstructure assignment with full state feedback controller versus a typical LQR design. The helicopter model under consideration does not include the flapping dynamics and the verification takes place by numerical simulations. Other robust designs of helicopter control are reported in [6, 50, 82, 97]

## 2.2 Nonlinear Control

In general, most control designs are based on linearized helicopter dynamics using the widely adopted concept of stability derivatives. However, in recent years there is considerable research

related to helicopter flight control based on nonlinear dynamic representations. The nonlinear controller designs are mostly valued for their theoretical contribution to the helicopter flight control problem. Their applicability is still an open challenge mainly due to the increased order and nonlinear structure of the controller. However, their contribution to the understanding of the limitations and capabilities of the helicopter control problem is significant.

Detailed models of helicopter nonlinear dynamics can be found in [40, 79, 84]. However, such models are of high order and impractical for controller design purposes. In [47, 48] a simplified nonlinear model of the helicopter dynamics is introduced. The helicopter model is represented by the nonlinear dynamic equations of motion of the helicopter enhanced by a simplified model of the aerodynamic force and torque generation. The particular model has been adopted in most work related to the helicopter nonlinear controller design. The reported work indicates that exact input-output linearization fails to linearize the helicopter model resulting in unstable zero dynamics. This work has shown that the use of an approximate model that disregards the thrust forces produced by the main rotor flapping motion, is full state linearizable. This derivation is very important since if the system dynamics are not input-output linearizable most nonlinear control techniques would be inapplicable. A feedback linearization controller is proposed based on the approximated model dynamics. It is proven that the proposed controller, based on the approximated model, achieves bounded tracking of the position and yaw reference trajectories.

However, helicopters are characterized by significant parametric and model uncertainty due to the complicated aerodynamic nature of the thrust generation. Therefore, linearization and nonlinear terms cancellation techniques are poorly suited. It is important that the controller design exhibits sufficient robustness towards potentially significant uncertainty. A design that guarantees bounded tracking in the presence of parametric and model uncertainty is reported in cite [37]. The proposed control law incorporates stabilization techniques for feedforward systems with input saturation and adaptive nonlinear output regulation techniques.

The work reported in [66, 67] addresses the design of an autopilot for the helicopter capable of letting its vertical/lateral and longitudinal dynamics and yaw attitude dynamics tracking arbitrary references with only some bound requirements on the higher order time derivatives imposed by

functional controllability. This work is an extension of [37] by including the main rotor dynamics and allowing the tracking of arbitrary trajectories. In addition, in the reported work the controller design is based on the pitch-roll-yaw attitude convention instead of quaternions which are used in [37]. Similarly to [37], the final control structure is a mix of feedforward actions and nested saturation control laws. The proposed controller is able to enforce very aggressive maneuvers characterized by large attitude angles and to cope with possible large uncertainties affecting the physical parameters.

As previously mentioned, most nonlinear designs neglect the effect of thrust force components associated with the tilt of the main rotor disk. This is common practice since those parasitic forces have a minimal effect on translational dynamics. This simplification results in a set of system equations having a feedback form, which is ideal for backstepping control design established in [49]. Backstepping control implementation for helicopters is presented in [11, 21, 64, 65] and similar designs for a quadrotor in [32, 33, 42].

Approaches of nonlinear control that use Neural Networks (NN) and nonlinear inversion are reported in [14, 15, 34, 38, 39, 45]. In all the aforementioned cases, the nonlinear inversion requirement and the augmentation of a NN increases significantly the order of the controller. To this extent the derivation of the controller using the nonlinear equation of motion of the helicopter becomes impractical. Therefore these cases have applied the controllers based on the linearized dynamics of the helicopter around hover. In [34, 45] the analysis is even more restricted by using a simplified model of only the longitudinal and heave motion of the helicopter. In [38, 39] the controller was experimentally implemented to a *Yamaha R-50* helicopter for a simple step command response.

## Chapter 3: Helicopter Basic Equations of Motion

The objective of this Chapter is to provide the basic equations of motion of the helicopter, when the helicopter is treated as a rigid body. The equations of motion are derived by implementing Newton's second law that deals with vector summations of all forces and moments as applied to the helicopter, relative to an inertial reference frame. However, for practical reasons, analysis may be significantly simplified if motion is described relative to a reference frame rigidly attached to the helicopter. When this is the case, the equations of motion are derived relative to this non-inertial body-fixed frame. The end result of this Chapter is the complete state space representation of the helicopter equations of motions in the configuration space.

### 3.1 Helicopter Equations of Motion

The first assumption toward dynamic modeling of a helicopter is to consider it as a rigid body with six Degrees Of Freedom (DOF). The DOF dictate the minimal number of parameters that are required to specify an object's configuration [95]. The motion of a rigid body is defined relative to a Cartesian inertial frame. A frame is composed of a point in space and three orthonormal vectors that form a basis. Therefore, in order to derive the equations of motion, two frames are required. The first one is the inertial frame (Earth-fixed frame) defined as  $\mathcal{F}_I = \{O_I, \vec{i}_I, \vec{j}_I, \vec{k}_I\}$ . A typical convention of the Earth-fixed frame, is the North-East-Down system where  $\vec{i}_I$  points North,  $\vec{j}_I$  points East and  $\vec{k}_I$  points at the center of the Earth. The second frame is the body-fixed reference frame defined as  $\mathcal{F}_B = \{O_B, \vec{i}_B, \vec{j}_B, \vec{k}_B\}$  where the center  $O_B$  is located at the Center of Gravity (CG) of the helicopter. The vector  $\vec{i}_B$  is pointing forward through the helicopter nose,  $\vec{j}_B$  is pointing at the right side of the fuselage and  $\vec{k}_B$  points downwards, such that  $\{\vec{i}_B, \vec{j}_B, \vec{k}_B\}$  constitutes a

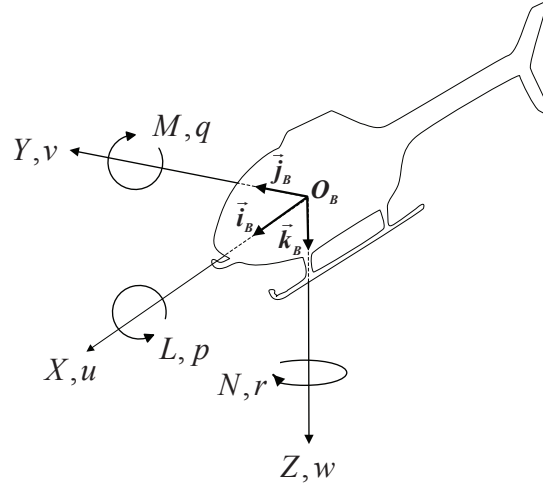


Figure 3.1: Body-fixed coordinate system. The components of the external forces and moments acting on the fuselage are denoted by  $f^B = [X \ Y \ Z]^T$  and  $\tau^B = [L \ M \ N]^T$ , respectively. The linear and angular velocity components are denoted by  $v^B = [u \ v \ w]^T$  and  $\omega^B = [p \ q \ r]^T$ , respectively.

right-handed Cartesian coordinate frame ( $\vec{k}_B = \vec{i}_B \times \vec{j}_B$ ). The directions of the body-fixed frame orthonormal vectors  $\{\vec{i}_B, \vec{j}_B, \vec{k}_B\}$  are shown in Figure 3.1.

There are two ways to represent free vectors in space. The first is through the synthetic approach, where the free vectors are considered as geometric entities. In the second approach, the geometric entities are represented by coordinates. This is called analytic approach [95]. In the analytic approach, the vector representation depends on the coordinate frame of reference. The advantage of the analytic approach is that the operations between vectors may be tackled by algebraic methods (equations). For example, a vector  $\vec{w}$  can be represented analytically by the coordinate triple  $w^B = [w_1^B \ w_2^B \ w_3^B]^T \in \mathbb{R}^3$ , with respect to the body-fixed frame, or by the triple  $w^I = [w_1^I \ w_2^I \ w_3^I]^T \in \mathbb{R}^3$ , with respect to the inertial frame. In general, the triples  $w^B$  and  $w^I$  will be different, however, they both represent the same geometric entity  $\vec{w}$ . In order to provide a clear understanding of the derivation of the helicopter's equations of motion, in this Chapter both approaches will be adopted.

An inertial frame makes the analysis impractical since moments and products of inertia vary with time. This is not the case when a body-fixed frame is considered, where moments and prod-

ucts of inertia are constant. Therefore, the equations of motion will be derived with respect to the body-fixed frame.

The linear velocity vector of the fuselage CG is denoted by  $\vec{v}$ . The coordinate vector of the linear velocity is  $v^B = [u \ v \ w]^T$ , with respect to the body-fixed frame. Similarly, the angular velocity  $\vec{\omega}$  of the fuselage, is represented in the body-fixed frame by  $\omega^B = [p \ q \ r]^T$ .

The sum of all external forces acting on the fuselage are denoted by  $f^B = [X \ Y \ Z]^T$ , with respect to the body-fixed frame. Similarly, the sum of all external moments (torques) are denoted by  $\tau^B = [L \ M \ N]^T$ , as shown in Figure 3.1. Positive direction of the angular velocity and moment components refers to the right-hand rule about the respective axis.

The equations of Newton's second law are valid only in an inertial reference frame. Therefore, Newton's second law for the translational motion of the helicopter is given by:

$$\vec{f} = m \left. \frac{d\vec{v}}{dt} \right|_I \quad (3.1)$$

where  $m$  denotes the total mass of the helicopter. The operand  $\left. \frac{d(\circ)}{dt} \right|_I$  denotes the time derivative of a vector in space as viewed by an observer in the inertial reference frame. From basic kinematic principles, which can be found in [31, 111], the time derivative of  $\vec{v}$  with respect to the inertial reference frame, is equal to:

$$\left. \frac{d\vec{v}}{dt} \right|_I = \left. \frac{d\vec{v}}{dt} \right|_B + \vec{\omega} \times \vec{v} \quad (3.2)$$

The operator  $(\times)$  is the vector cross product. The term  $\left. \frac{d\vec{v}}{dt} \right|_B$  denotes the time derivative of the velocity vector  $\vec{v}$  with respect to the body-fixed reference frame. In general,  $\left. \frac{d(\circ)}{dt} \right|_B$  denotes the derivative of a vector from the viewpoint of an observer in the body-fixed frame. At this point a comment should be made about vector differentiation: As indicated in [31], the operands  $\left. \frac{d(\circ)}{dt} \right|_I$  and  $\left. \frac{d(\circ)}{dt} \right|_B$  when performed on a free vector in space will provide in general a different result. The first one is the time rate of change of a vector as viewed by an observer from the inertial frame, while the second one is the time rate of change viewed by an observer of a rotating frame. The change of the vector's direction due to the angular velocity of the body-fixed frame, is not con-

ceivable by the observer on the body-fixed frame. On the contrary, this change is detected by the observer of the inertial frame. A simple coordinate conversion will not provide accurate results since both of them are viewing a different change.

Since  $\vec{v} = u\vec{i}_B + v\vec{j}_B + w\vec{k}_B$ , then  $\left. \frac{d\vec{v}}{dt} \right|_B = \dot{u}\vec{i}_B + \dot{v}\vec{j}_B + \dot{w}\vec{k}_B$ . Therefore, substituting (3.2) to (3.1), the analytic expression of Newton's second law for the translational motion is:

$$\begin{aligned} X/m &= \dot{u} + qw - rv \\ Y/m &= \dot{v} + ru - pw \\ Z/m &= \dot{w} + pv - qu \end{aligned} \quad (3.3)$$

To conclude the derivation of the equations of motion, Newton's second law is applied to all moments that act on the CG. The reference point for calculating the angular momentum and the external moments is rigidly attached to the *CG* of the helicopter. Furthermore, using the body-fixed reference frame for the analysis is advantageous since the moments and the products of inertia do not vary with time given that the mass distribution of the helicopter does not change.

Let  $\vec{H}$  denote the vector of the helicopter angular momentum and  $H^B = [h_x \ h_y \ h_z]^T$  its coordinates with respect to the body-fixed frame. From [31], the angular momentum components of the body-fixed reference frame are given by  $H^B = \mathcal{I}\omega^B$ , where  $\mathcal{I}$  denotes the inertia matrix:

$$\mathcal{I} = \begin{bmatrix} \mathcal{I}_{xx} & -\mathcal{I}_{xy} & -\mathcal{I}_{xz} \\ -\mathcal{I}_{yx} & +\mathcal{I}_{yy} & -\mathcal{I}_{yz} \\ -\mathcal{I}_{zx} & -\mathcal{I}_{zy} & +\mathcal{I}_{zz} \end{bmatrix} \quad (3.4)$$

The respective moments of inertia are:

$$\mathcal{I}_{xx} = \sum (y_m^2 + z_m^2)dm \quad \mathcal{I}_{yy} = \sum (x_m^2 + z_m^2)dm \quad \mathcal{I}_{zz} = \sum (x_m^2 + y_m^2)dm$$

The products of inertia are:

$$\mathcal{I}_{xy} = \mathcal{I}_{yx} = \sum x_m y_m dm \quad \mathcal{I}_{xz} = \mathcal{I}_{zx} = \sum x_m z_m dm \quad \mathcal{I}_{yz} = \mathcal{I}_{zy} = \sum y_m z_m dm$$

The above sums apply to all elementary masses  $dm$  of the helicopter, and  $x_m$ ,  $y_m$  and  $z_m$  are the distances of each elementary mass from the CG. It is assumed that the principal axes coincide with the axes of the body-fixed frame, therefore, it follows that  $\mathcal{I}_{xy} = \mathcal{I}_{yx} = 0$ ,  $\mathcal{I}_{yz} = \mathcal{I}_{zy} = 0$  and  $\mathcal{I}_{zz} = \mathcal{I}_{zx} = 0$ .

Newton's second law for the rotational motion dictates that the external moments acting on the helicopter are equal to the time rate of change of the angular momentum with respect to the inertial reference frame. Therefore:

$$\vec{\tau} = \left. \frac{d\vec{H}}{dt} \right|_I \quad (3.5)$$

From differentiation of free vectors, one has:

$$\left. \frac{d\vec{H}}{dt} \right|_I = \left. \frac{d\vec{H}}{dt} \right|_B + \vec{\omega} \times \vec{H} \quad (3.6)$$

The term  $\left. \frac{d\vec{H}}{dt} \right|_I$  is the time rate of change of the angular momentum with respect to the inertial frame. The time derivative components of the angular momentum  $\left. \frac{d\vec{H}}{dt} \right|_B$ , are given by:

$$\begin{aligned} \dot{h}_x &= \mathcal{I}_{xx}\dot{p} \\ \dot{h}_y &= \mathcal{I}_{yy}\dot{q} \\ \dot{h}_z &= \mathcal{I}_{zz}\dot{r} \end{aligned} \quad (3.7)$$

Substituting (3.6) and (3.7) to (3.5), the analytic expression of Newton's second law for the rotational motion of the helicopter is:

$$L = \mathcal{I}_{xx}\dot{p} + qr(\mathcal{I}_{zz} - \mathcal{I}_{yy})$$

$$M = \mathcal{I}_{yy}\dot{q} + pr(\mathcal{I}_{xx} - \mathcal{I}_{zz}) \quad (3.8)$$

$$N = \mathcal{I}_{zz}\dot{r} + pq(\mathcal{I}_{yy} - \mathcal{I}_{xx})$$

Therefore, the final form of the equations of motion with respect to the inertia frame, but expressed in the body-fixed frame coordinate components, are given by (3.3) for the translational and by (3.8) for the rotational motion of the helicopter. A compact form of the helicopter equations of motion expressed in the body-fixed frame, is the following:

$$\begin{bmatrix} mI_3 & 0 \\ 0 & \mathcal{I} \end{bmatrix} \begin{bmatrix} \dot{v}^B \\ \dot{\omega}^B \end{bmatrix} + \begin{bmatrix} \omega^B \times mv^B \\ \omega^B \times \mathcal{I}\omega^B \end{bmatrix} = \begin{bmatrix} f^B \\ \tau^B \end{bmatrix} \quad (3.9)$$

From [75], the above equations are called *Newton-Euler equations* in the body-fixed frame's coordinates.

### 3.2 Position and Orientation of the Helicopter

The motion of the helicopter is defined by the position and orientation of the body-fixed frame relative to the inertial frame. The Newton-Euler equations provide information about the translational and angular velocity of the helicopter. However, neither of them give information about the helicopter's current position and orientation. The helicopter equations of motion are completed by determining the position and orientation dynamics of the latter. Derivation follows [20] but with additional details for clarification purposes.

Let  $\mathcal{F}_1 = \{O_B, \vec{i}_1, \vec{j}_1, \vec{k}_1\}$  define an intermediate frame that is aligned with  $\mathcal{F}_I$  and centered on the CG of the helicopter. The helicopter orientation at any time instant may be obtained by performing three consecutive rotations of  $\mathcal{F}_1$  until it is aligned with  $\mathcal{F}_B$ . The rotations are performed at a specific order, they cannot be considered as vectors and they are not commutative [111]. Therefore, the rotation order is important for consistency, as follows (see Figure 3.2):

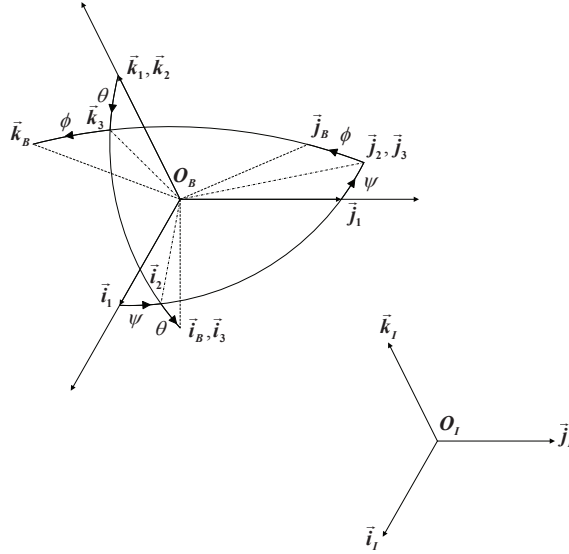


Figure 3.2: Helicopter orientation.

- A rotation of an angle  $\psi$  about  $\vec{k}_1$ . This rotation moves the helicopter to the direction defined by  $\mathcal{F}_2 = \{O_B, \vec{i}_2, \vec{j}_2, \vec{k}_2\}$ , bringing  $\vec{i}_2$  parallel to the plane defined by  $\vec{i}_B$  and  $\vec{k}_1$ .
- A rotation of an angle  $\theta$  about  $\vec{j}_2$ . This rotation moves the helicopter to the direction described by  $\mathcal{F}_3 = \{O_B, \vec{i}_3, \vec{j}_3, \vec{k}_3\}$ , aligning  $\vec{i}_3$  with  $\vec{i}_B$ .
- A rotation of an angle  $\phi$  about axis  $\vec{i}_3$  bringing  $\mathcal{F}_3$  to its final orientation  $\mathcal{F}_B$ .

In the above convention, each rotation is performed about an axis whose location depends on the preceding rotations [16]. The intermediate frames and each rotation is shown in detail in Figure 3.2. These angles with the particular sequence of rotations are also known as *Z-Y-X Euler angles*. The Euler angles orientation vector is denoted by  $\Theta = [\phi \ \theta \ \psi]^T$ . Positive direction of each angle refers to the right-hand rule about the respective axis. Any arbitrary rotation of the body-fixed frame relative to the inertia frame can be parametrized by the three Euler angles.

### 3.2.1 Helicopter Position Dynamics

Expressing the helicopter position relative to the body-fixed frame is meaningless and such an action cannot take place. Therefore, the position dynamics are derived with respect to the inertial frame. Before we present the position dynamics, we introduce the description that relates the coordinate vectors of the body-fixed and inertial frames. This description is called the *rotation matrix* and it provides a systematic way to express the relative orientation of the two frames.

Denote by  $v^I = [v_x^I \ v_y^I \ v_z^I]^T$  the linear velocity's coordinate vector with respect to the inertial frame. The linear velocity vector of the helicopter, relative to  $\mathcal{F}_B$  and  $\mathcal{F}_I$ , respectively, is:

$$\vec{v} = u\vec{i}_B + v\vec{j}_B + w\vec{k}_B \quad (3.10a)$$

$$\vec{v} = v_x^I\vec{i}_1 + v_y^I\vec{j}_1 + v_z^I\vec{k}_1 \quad (3.10b)$$

Using the definition of the Euler angles, the unit vectors of the body-fixed frame  $\mathcal{F}_B$  are written relative to the frame  $\mathcal{F}_3$  as:

$$\begin{aligned} \begin{bmatrix} \vec{i}_B \\ \vec{j}_B \\ \vec{k}_B \end{bmatrix} &= \begin{bmatrix} 1 & 0 & 0 \\ 0 & \cos \phi & \sin \phi \\ 0 & -\sin \phi & \cos \phi \end{bmatrix} \begin{bmatrix} \vec{i}_3 \\ \vec{j}_3 \\ \vec{k}_3 \end{bmatrix} \\ &= R_\phi^T(\phi)[\vec{i}_3 \ \vec{j}_3 \ \vec{k}_3]^T \end{aligned} \quad (3.11)$$

Similarly, the unit vectors of the frame  $\mathcal{F}_3$  are expressed relative to the frame  $\mathcal{F}_2$  as:

$$\begin{aligned} \begin{bmatrix} \vec{i}_3 \\ \vec{j}_3 \\ \vec{k}_3 \end{bmatrix} &= \begin{bmatrix} \cos \theta & 0 & -\sin \theta \\ 0 & 1 & 0 \\ \sin \theta & 0 & \cos \theta \end{bmatrix} \begin{bmatrix} \vec{i}_2 \\ \vec{j}_2 \\ \vec{k}_2 \end{bmatrix} \\ &= R_\theta^T(\theta)[\vec{i}_2 \ \vec{j}_2 \ \vec{k}_2]^T \end{aligned} \quad (3.12)$$

Finally, the unit vectors of the frame  $\mathcal{F}_2$  relative to  $\mathcal{F}_1$  are expressed as:

$$\begin{bmatrix} \vec{i}_2 \\ \vec{j}_2 \\ \vec{k}_2 \end{bmatrix} = \begin{bmatrix} \cos \psi & \sin \psi & 0 \\ -\sin \psi & \cos \psi & 0 \\ 0 & 0 & 1 \end{bmatrix} \begin{bmatrix} \vec{i}_1 \\ \vec{j}_1 \\ \vec{k}_1 \end{bmatrix} \quad (3.13)$$

$$= R_{\psi}^T(\psi) [\vec{i}_1 \quad \vec{j}_1 \quad \vec{k}_1]^T \quad (3.14)$$

By consecutive substitutions of (3.11), (3.12) and (3.13) to (3.10a), one obtains:

$$\begin{aligned} \vec{v} &= [u \ v \ w] [\vec{i}_B \quad \vec{j}_B \quad \vec{k}_B]^T \\ &= [u \ v \ w] R_{\phi}^T(\phi) [\vec{i}_3 \quad \vec{j}_3 \quad \vec{k}_3]^T \\ &= [u \ v \ w] R_{\phi}^T(\phi) R_{\theta}^T(\theta) [\vec{i}_2 \quad \vec{j}_2 \quad \vec{k}_2]^T \\ &= [u \ v \ w] R_{\phi}^T(\phi) R_{\theta}^T(\theta) R_{\psi}^T(\psi) [\vec{i}_1 \quad \vec{j}_1 \quad \vec{k}_1]^T \end{aligned} \quad (3.15)$$

Denote by  $R(\Theta)$  the product:

$$R(\Theta) = R_{\psi}(\psi) R_{\theta}(\theta) R_{\phi}(\phi) \quad (3.16)$$

Equating the right hand sides of (3.10b) and (3.15), one gets:

$$\begin{bmatrix} v_x^I \\ v_y^I \\ v_z^I \end{bmatrix} = R(\Theta) \begin{bmatrix} u \\ v \\ w \end{bmatrix} \quad (3.17)$$

where:

$$R(\Theta) = \begin{bmatrix} \cos \theta \cos \psi & \sin \phi \sin \theta \cos \psi - \cos \phi \sin \psi & \cos \phi \sin \theta \cos \psi + \sin \phi \sin \psi \\ \cos \theta \sin \psi & \sin \phi \sin \theta \sin \psi + \cos \phi \cos \psi & \cos \phi \sin \theta \sin \psi - \sin \phi \cos \psi \\ -\sin \theta & \sin \phi \cos \theta & \cos \phi \cos \theta \end{bmatrix} \quad (3.18)$$

The matrix  $R(\Theta)$  is called the rotation matrix and it is parametrized with respect to the three Euler angles. The rotation matrix  $R$  is used to map vectors from the body-fixed frame  $\mathcal{F}_B$  to the inertial frame  $\mathcal{F}_I$ . The rotation matrix belongs to the Special Orthogonal group of order 3 denoted by  $SO(3)$ .

**Property 3.1.** *The rotation matrix has the following properties [95]:*

1.  $RR^T = R^T R = I$
2.  $\det(R) = 1$
3. *Each column (and each row) of  $R$  is a unit vector*
4. *Each column (and each row) of  $R$  are mutually orthogonal*

When the rotation matrix is parametrized by the Z-Y-X Euler angles, singularities occur at  $\theta = \pm\pi/2$ . More specifically, when  $\theta = \pm\pi/2$ , then, the inverse problem of retrieving the Euler angles from the rotation matrix, does not have a solution [75]. Such singularities occur in any 3-D representation of  $SO(3)$ .

The rotation matrix facilitates the derivation of the position and translational velocity dynamics with respect to the inertial frame. Denote by  $p^I = [p_x^I \ p_y^I \ p_z^I]^T$  the position of the helicopter CG. Then, the position and velocity dynamics with respect to the inertial frame are:

$$\dot{p}^I = v^I \tag{3.19}$$

$$\dot{v}^I = \frac{1}{m} R f^B \tag{3.20}$$

Any rigid motion is defined by the ordered pair  $(p^I, R)$  where  $p^I \in \mathbb{R}^3$  and  $R \in SO(3)$ . The group  $SE(3) = \mathbb{R}^3 \times SO(3)$  is the configuration space of the helicopter and it is known as the *Special Euclidean group*.

### 3.2.2 Helicopter Orientation Dynamics

Consider that during an infinitesimal time interval  $dt$  the helicopter is subjected to three infinitesimal rotations  $d\psi$ ,  $d\theta$  and  $d\phi$  resulting in a position defined by angles  $\psi + d\psi$ ,  $\theta + d\theta$  and  $\phi + d\phi$ . Although finite rotations cannot be treated as vectors, infinitesimal rotations may be treated as such, thus, according to [20], the vector that represents the above rotation is:

$$\hat{n} = d\phi \vec{i}_B + d\theta \vec{j}_3 + d\psi \vec{k}_2 \quad (3.21)$$

Then, the angular velocity can be expressed as:

$$\vec{\omega} = \frac{d\hat{n}}{dt} = \dot{\phi} \vec{i}_B + \dot{\theta} \vec{j}_2 + \dot{\psi} \vec{k}_1 \quad (3.22a)$$

and:

$$\vec{\omega} = p \vec{i}_B + q \vec{j}_B + r \vec{k}_B \quad (3.22b)$$

By using the expressions (3.11)-(3.13) and equating the right hand sides of (3.22a) and (3.22b), one has:

$$\begin{bmatrix} p \\ q \\ r \end{bmatrix} = \begin{bmatrix} \dot{\phi} \\ 0 \\ 0 \end{bmatrix} + R_\phi^T(\phi) \begin{bmatrix} 0 \\ \dot{\theta} \\ 0 \end{bmatrix} + R_\phi^T(\phi) R_\theta^T(\theta) \begin{bmatrix} 0 \\ 0 \\ \dot{\psi} \end{bmatrix} \Rightarrow$$

$$\begin{bmatrix} p \\ q \\ r \end{bmatrix} = \begin{bmatrix} 1 & 0 & -\sin \theta \\ 0 & \cos \phi & \sin \phi \cos \theta \\ 0 & -\sin \phi & \cos \phi \cos \theta \end{bmatrix} \begin{bmatrix} \dot{\phi} \\ \dot{\theta} \\ \dot{\psi} \end{bmatrix} \quad (3.23)$$

Based on the above equation, the orientation dynamics of the helicopter are given by:

$$\dot{\Theta} = \Psi(\Theta)\omega^B \quad (3.24)$$

where:

$$\Psi(\Theta) = \begin{bmatrix} 1 & \sin \phi \tan \theta & \cos \phi \tan \theta \\ 0 & \cos \phi & -\sin \phi \\ 0 & \sin \phi / \cos \theta & \cos \phi / \cos \theta \end{bmatrix} \quad (3.25)$$

For an arbitrary motion, the components of the rotation matrix are time varying. The derivative of the rotation matrix is given by:

$$\dot{R} = R\hat{\omega}^B \quad (3.26)$$

where  $\hat{\omega}^B$  denotes the skew symmetric matrix of the vector  $\omega^B$ . For a vector  $w = [w_1 \ w_2 \ w_3]^T$  the skew symmetric matrix is defined as:

$$\hat{w} = \begin{bmatrix} 0 & -w_3 & w_2 \\ w_3 & 0 & -w_1 \\ -w_2 & w_1 & 0 \end{bmatrix}$$

The multiplication of the matrix  $\hat{w}$  with a vector  $h$ , produces the coordinates of the cross product  $w \times h$ .

**Proposition 3.1.** For two vectors  $g_1$  and  $g_2$  of  $\mathbb{R}^3$ , the skew symmetric matrix has the following properties:

1.  $\hat{g}_1 g_1 = 0$
2.  $R(\hat{g}_1 g_2) = \widehat{(Rg_1)}(Rg_2)$
3.  $\hat{g}_1 + \hat{g}_1^T = 0$
4.  $R\hat{g}_1 R^T = \widehat{Rg_1}$

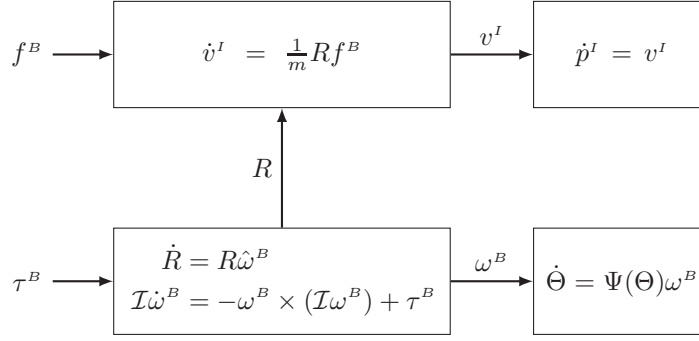


Figure 3.3: Interconnection of the helicopter dynamics in the space  $SE(3)$ .

The derivation of (3.26) is not presented here because it is out of the scope of this Chapter. However, more details may be found in [75, 95]. The rotation matrix dynamics are very important, since they appear in the linear velocity dynamics given in (3.20). Although the orientation dynamics are also given in (3.25), working with the rotation matrix in control applications is more preferable due to the special properties of the rotation matrix.

### 3.3 Complete Helicopter Dynamics

Having defined the position and orientation dynamics, the complete state space representation of the helicopter equations of motion in the configurations space  $SE(3)$  is:

$$\dot{p}^I = v^I \quad (3.27)$$

$$\dot{v}^I = \frac{1}{m} R f^B \quad (3.28)$$

$$\dot{R} = R \hat{\omega}^B \quad (3.29)$$

$$\mathcal{I} \dot{\omega}^B = -\omega^B \times (\mathcal{I} \omega^B) + \tau^B \quad (3.30)$$

where  $[p^I \ v^I \ R \ \omega^B] \in \mathbb{R}^3 \times \mathbb{R}^3 \times SO(3) \times R^3$ . Integration of the above equations provides all the required information for determining the helicopter motion in the configuration space. The interconnection of the helicopter dynamics in  $SE(3)$  is illustrated in Figure 3.3.

As mentioned earlier, the orientation of the helicopter is parametrized by the Z-Y-X Euler angles. In this case each intermediate rotation takes place about an axis of a frame that is produced by a preceding rotation. In aviation applications it is preferable that each rotation takes place about the axis of a fixed frame. Exactly the same equations are derived if the final orientation is produced by a  $\phi$  angle about the axis  $\vec{i}_I$ , then an angle  $\theta$  about  $\vec{j}_I$  and finally an angle  $\psi$  about the axis  $\vec{k}_I$ . In this convention the angles  $\phi$ ,  $\theta$  and  $\psi$  are called pitch, roll and yaw angles, respectively.

The helicopter rigid body dynamics given in (3.27)-(3.30) are completed by defining the external body frame force  $f^B$  and torque  $\tau^B$ .

### 3.4 Remarks

This Chapter has presented an analytical derivation of the helicopter's basic equations of motion. The linear and angular velocity dynamics are obtained from Newton's second law for translational and rotational motion. The orientation of the helicopter with respect to a stationary inertial frame is determined by three orientation angles. The rotation matrix is parametrized by the orientation angles and constitutes a systematic tool for mapping vectors from the inertial frame to the body fixed frame and vice versa. The position and orientation dynamics complete the description of the helicopter's motion in the configurations space. The final requirement towards the derivation of the helicopter's mathematical model is the determination of the external forces and moments applied to the helicopter. The main source of force and torque generation of the helicopter is produced by the main and tail rotor. The main rotor itself is a dynamical system. A detailed model of the aerodynamic forces and moments of the main rotor would be of high order and significant complexity. The next Chapter presents a simplified model of the main rotor dynamics which is suitable for control design purposes.

## Chapter 4: Simplified Rotor Dynamics

The helicopter's main source of propulsion is provided by the main and tail rotor. The aerodynamic forces and moments are nonlinear functions of motion characteristics and controls. Due to the complexity and the uncertainty associated with the aerodynamic phenomena, a detailed model of the forces and moments produced by the main rotor would be of high order and completely impractical for any controller design. In this Chapter, the modeling approach presented in [47, 56, 70, 72] is followed, which provides a simplified derivation of the main rotor dynamics and the produced thrust force vector, adequate for controller design purposes.

### 4.1 Introduction

There are four control commands associated with helicopter piloting. The control input vector is defined as  $u_c = [u_{lon} \ u_{lat} \ u_{ped} \ u_{col}]^T$ , where  $u_{col}$  and  $u_{ped}$  are the collective controls of the main and tail rotor, correspondingly. The collective commands control the magnitude of the main and tail rotor thrust by a uniform change in the pitch angles of all the rotor's blades. The other two control commands,  $u_{lon}$  and  $u_{lat}$ , are the cyclic controls of the helicopter, which control the inclination of the Tip-Path-Plane (TPP) on the longitudinal and lateral direction. The TPP is the plane on which the tips of the blades lie and it is used to provide a simplified representation of all the rotor blades [70].

For the main rotor thrust generation, a simplified approach is followed based on [47, 70, 72]. According to that, the thrust vector produced by the rotor disk is perpendicular to the TPP. The main rotor blades apart from rotating about the shaft axis, they also exhibit a flapping motion

normal to the plane of rotation. Since the thrust vector is normal to the TPP, by controlling the TPP inclination, the pilot indirectly controls the direction of the propulsion forces.

The TPP is itself a dynamic system. The dynamics of the TPP represent the rotor dynamics. The rotor is affected by both the pilot's control commands and the helicopter's motion. On the other hand, the helicopter's motion itself is controlled by the applied rotor forces and moments. Therefore, there is an obvious coupling between the rotor and fuselage dynamics. The work presented in [70] and [104] provides a simplified model of the rotor dynamics that is integrated with the rigid body model, in order to arrive at a "hybrid model" of the helicopter dynamics.

The goal of this Chapter is to present a simplified model of the rotor dynamics, which encapsulates the cross coupling effect between the rotor and the fuselage. The second task is to derive a practical description of the thrust force and moment components, produced by the main rotor. In general, the rotor mathematical modeling is a very complex procedure. The complexity of the model, without considering any simplification assumptions, will significantly increase. As pointed in [18], the model complexity depends on the application the model is designed for. For control applications, the proposed model provides a practical and physically meaningful description of the rotor dynamics. The main results of this Chapter associated with the rotor dynamics are based on [70].

In order for the reader to understand the final derivation of the simplified rotor dynamics and to obtain a fair insight of the physical concepts that effect the rotor behavior, a series of intermediate steps are presented. The first step is to introduce the additional DOF of the blades. The control of the rotor is mainly produced by the variation of the blades pitch angle. By changing the pitch angle, the aerodynamic loads of the blades are also altered. This is a way of controlling the lift forces applied to each blade. To this extent, a generic description of the basic mechanical design that produces the variation of the pitch angle is given.

Simplified aerodynamics concepts are presented next, which result in the derivation of the aerodynamic forces applied to each blade. By giving a description of the aerodynamic forces and by considering the additional inertia forces acting on the blade, the blade's equations of motion are derived. The adoption of some physically meaningful simplification assumptions leads to

the derivation of the so called Tip-Path-Plane dynamic equations, which essentially are the main rotor dynamics. Finally, using the Tip-Path-Plane equations, the force and moment components produced by the main rotor are derived.

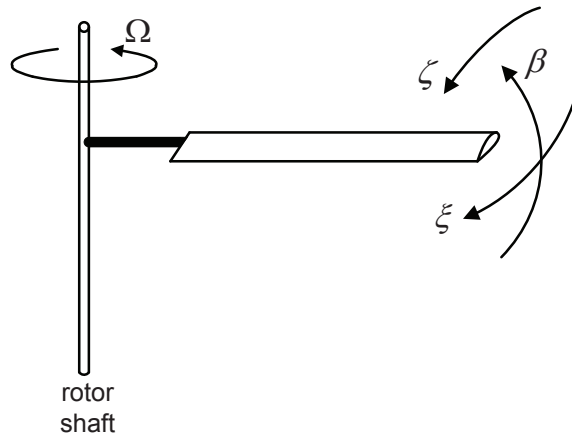
## 4.2 Blade Motion

The most common rotor configuration consists of two (or more) identical blades attached to the rotor hub [40]. The rotor hub is connected to the rotor shaft. The blades perform rotational motion around the rotor shaft with a constant angular velocity  $\Omega$ .

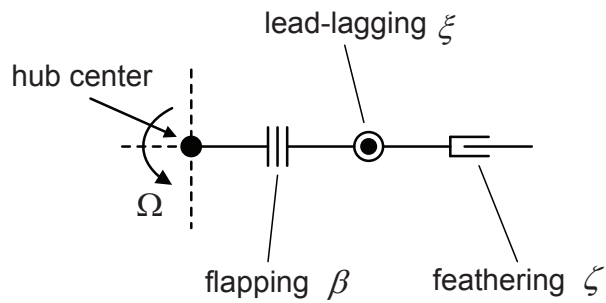
Apart from the rotational motion around the shaft, the blades also have three additional DOF. These DOF are illustrated in Figure 4.1. More specifically:

- *Flapping*: This DOF produces a motion of the blade that is parallel to the plane that includes the blade and the shaft, and it is denoted by the flapping angle  $\beta$ . The flapping angle is defined to be positive when the blade moves upwards.
- *Lead-Lagging*: This DOF produces a motion of the blade that is parallel to the hub plane. The lagging angle is denoted by  $\xi$ . Lagging is positive when the blade opposes the direction of rotation produced by the rotor.
- *Feathering*: This DOF produces a pitching motion of the blade about the blade span. The feathering angle is denoted by  $\zeta$ . Feathering angle is considered positive for nose up motion of the blade.

The necessity for free motion of the blade with respect to these additional DOF was apparent from early helicopter designs. The feathering angle controls the aerodynamic forces that are generated on the blades. Those aerodynamic forces control the thrust force that is necessary for the motion of the helicopter. However, the generation of aerodynamic forces has as a result the appearance of large moments on the root of the blade. Those moments are transmitted to the hub and then to the rest of the helicopter's body. A rotor configuration that allows the flapping motion



(a) The 3 DOF of the rotor blade in space. The Figure is based on [40].



(b) Top view of the rotor hub where each DOF of the rotor blade is represented by a blade hinge. The Figure is based on [40].

Figure 4.1: Representation of the rotor 3 DOF.

of the blade is needed in order to relief the blade root from those arising moments. The immediate result of the flapping motion is the generation of Coriolis moments on the blade in the plane of rotation [7]. A second configuration is needed to allow the lagging motion of the blade so those moments are relieved.

There are several hub designs that allow the motion of the blades. The traditional approach is the use of mechanical hinges at the blade root for the flapping and lagging motion. Modern designs have substituted the use of hinges by flexible elements in the root of the hub that allow the flapping and lagging motion. In addition, there are configurations that use both approaches. A general classification of the rotor hub depending on the mechanical configuration that is used to facilitate the flapping and lagging motion according to [40, 58] is the following :

- *Articulated rotor*: This type of rotor hub provides a flap and a lag hinge for every individual blade. There is also a feathering bearing for the control of the blade pitch. This is the most classical means to provide blade motion. This configuration allows the blade to move independently from the others.
- *Teetering rotor*: This type of rotor is composed of two blades that are connected together, forming a continuous structure with a single flap hinge. The two blades are connected to the flap hinge in such a way that when the one blade flaps upwards the other blade flaps downwards. This type of rotor does not include lag hinges.
- *Hingeless rotor*: The hingeless rotor allows the flap and lag motion by structural bending in the root of the blade. This configuration does not require hinges. The structural bending at the root of the blade is made by an attachment to the hub of a cantilever root restraint. A feathering bearing or hinge is used for changes in the pitch angle of each blade. This design provides a relative stiff rotor hub and as a result the hub and blade loads are higher than those of hinged configurations.

### 4.3 Swashplate Mechanism

Helicopter flight control is achieved by varying the pitch angle of the blades. Feathering is the pitching motion of the blade about the span of the blades. The feathering motion changes the blade's angle of attack, providing a way to control the thrust and the rotor moments that are applied to the rotor. The feathering angle (as well as the flapping angle) are measured relatively to a reference plane. This reference plane is perpendicular to the rotor shaft and it is denoted as the *hub plane*. The total pitch angle of each blade is given by the equation:

$$\zeta = \zeta_0 - \zeta_{1c} \cos \psi_b - \zeta_{1s} \sin \psi_b \quad (4.1)$$

The angle  $\zeta_0$  is called collective pitch and it controls the magnitude of the thrust vector. The two angles  $\zeta_{1c}$  and  $\zeta_{1s}$  are called cyclic pitch angles. The two cyclic pitch angles control the orientation of the thrust vector. More specifically,  $\zeta_{1c}$  controls the lateral orientation of the thrust vector while  $\zeta_{1s}$  controls the longitudinal orientation. The blade's position is described by the azimuth angle  $\psi_b = \Omega t$ . The azimuth angle is considered zero when the blade is aligned with the tail facing backwards.

There are several types of mechanical designs that produce the collective and cyclic angles of the blades. A generic description of the most standard configuration is given in [40] and it is described here. This configuration is composed of two main mechanical parts. The first part is associated with the creation of the blade's feathering angle and it is illustrated in Figure 4.2. The pitch motion of the blades takes place about a pitch bearing or a hinge. This bearing is rigidly attached to one of the tips of the pitch horn. The other tip of the pitch horn is connected to the pitch link. The pitch horn and the pitch link are connected in such a way that the vertical motion of the pitch link produces the blade's pitch motion. What is needed is a mechanical arrangement that provides the periodic pitch angle described by (4.1). The most standard mechanical configuration for this task is the use of the swashplate mechanism.

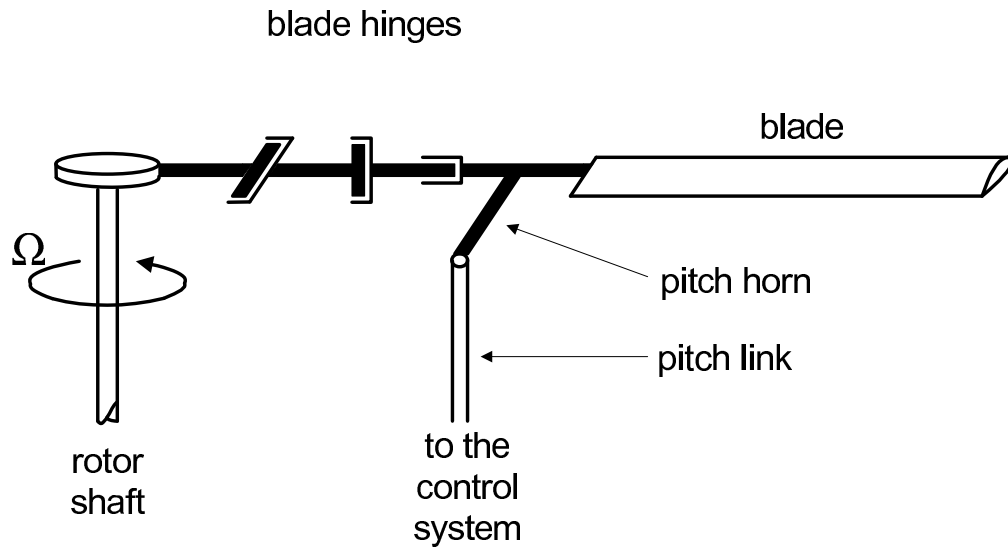


Figure 4.2: Connection of the pitch horn to the pitch link. The pitch link is also attached to the swashplate. The blade's 3 DOF are represented by three blade hinges. This Figure is based on [40].

There is a wide variety of designs for the swashplate. Here, we present the fundamental principle of the swashplate's function. This description is based on [40]. A schematic of the basic swashplate's components is illustrated in Figure 4.3.

The swashplate is composed of two rings that are concentric with the shaft. One of the rings has the ability to rotate about the shaft while the other one is constantly nonrotating. Bearings lie between the two rings. The blade pitch links are attached to the rotating ring while the pilot's controls are attached to the nonrotating ring. The two rings are attached to the shaft in such a way that the swashplate surface can take an arbitrary orientation relative to the shaft.

Moving the swashplate vertically to the shaft results in a uniform change of the blade's pitch independently of the position of the blade. Therefore, the vertical motion of the swashplate produces the collective pitch angle  $\zeta_0$ . On the other hand, a longitudinal or lateral tilt of the swashplate creates a sinusoidal variation of the pitch angle depending on the azimuthal position of the

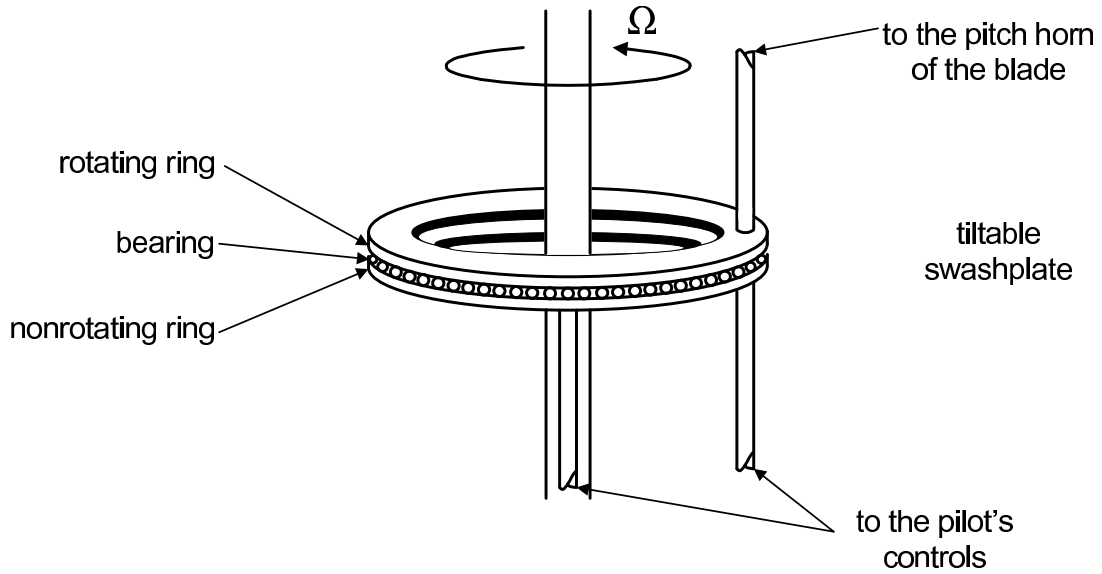


Figure 4.3: Basic configuration of the swashplate mechanism. This Figure is based on [40].

blade. It is obvious that the control of the swashplate tilt produces the cyclic control angles  $\zeta_{1s}$  and  $\zeta_{1c}$  of the rotor blades.

Therefore, the cyclic control angles can be written as linear functions of the controls inputs of the pilot's stick. Hence:

$$\zeta_{1c} = B_{lat}\delta_{lat} \quad \zeta_{1s} = A_{lon}\delta_{lon} \quad (4.2)$$

#### 4.4 Fundamental Rotor Aerodynamics

The objective of this Section is to provide a relatively simplified analysis of the rotor aerodynamics. The mathematical analysis will be kept to the minimum required in order to reduce complexity, however it will provide insight to the dominating behavior of the rotor. In order to determine the aerodynamic forces that are applied to the blade the first step is to analyze the velocity components of the blade relative to the air, over the complete blade span. This analysis, in general, is a very difficult task. This is due to the complexity associated with the modeling of the inflow velocity throughout the rotor disk.

As indicated in [40] and [58] the blade element analysis considers each blade element as a two dimensional airfoil. The aerodynamic behavior of neighboring blade elements is independent of each other. An induced inflow velocity on each blade element should be accounted, which is a product of the rotor wake. Analytical ways of calculating the induced velocity may be found using momentum theory, vortex theory or nonuniform inflow calculations [40]. In general the calculation of the inflow velocity is a very challenging task, due to its non uniformity across the blade span, so mathematical simplifications should be applied in order to minimize the complexity of the analysis. Finally, after determining the velocity components of the blade element, we calculate the aerodynamic forces acting on this element. The complete dynamic behavior of the blade is obtained by integrating the applied forces of the individual elements throughout the blade span.

In what follows, the hub plane is considered as the reference plane. To facilitate the analysis denote by  $\mathcal{F}_h = \{O_h, \vec{i}_h, \vec{j}_h, \vec{k}_h\}$  a reference frame attached to the main rotor where  $\vec{i}_h = -\vec{i}_B$ ,  $\vec{j}_h = \vec{j}_B$  and  $\vec{k}_h = -\vec{k}_B$ . The center  $O_h$  is located at the center of the rotor hub such that  $\vec{i}_h$  is aligned with the blade when  $\psi_b = 0$ .

Let  $V_\infty$  denote the free stream velocity which is the helicopter's forward velocity with respect to the air. The free stream velocity, illustrated in Figures 4.4(a) and 4.4(c), is directed straight to the front part of the helicopter with an angle  $\alpha_{hb}$  with respect to the hub plane (positive when the free stream velocity is facing downwards to the hub). Therefore, the free stream velocity has a component  $V_\infty \cos \alpha_{hb}$ , which lies in the plane of the hub, and a component  $V_\infty \sin \alpha_{hb}$ , which is normal to the hub plane. Usually in the literature, the in plane component is defined as the non dimensional quantity called rotor advance ratio denoted by  $\mu$  that is the in plane free stream component normalized by the blade's tip speed. Therefore:

$$\mu = \frac{V_\infty \cos \alpha_{hb}}{\Omega R_b} \quad (4.3)$$

where  $R_b$  denotes the blade's radius. The rotor blades perform three types of motion. The first one is out of plane flapping motion described by the flapping angle  $\beta$ . There is also feathering motion

about the blade axis with a feathering angle  $\zeta$  measured relative to the hub plane. Last, the blade performs a rotational motion about the rotor's shaft with angular velocity  $\Omega$ .

The velocity accounted by each blade element is due to the helicopter forward motion, the blade's flapping motion, the rotor's inflow velocity and the rotor's rotation about the shaft.

Three velocity vectors are required for the description of the total air velocity  $U$  as seen by the blade element. Those vectors are two in plane components and one out of plane component normal to the hub plane. The first in plane component is denoted by  $U_T$ . It is tangential to the blade and parallel to the disk plane. We consider that the positive direction of  $U_T$  is opposing the rotational blade motion.

The second in plane component is the radial component of the blade, denoted by  $U_R$  that lies on the hub plane, it is parallel to the blade axis and positive direction is considered outwards. Both of them can be seen in Figure 4.4(a). Finally the out of plane component is denoted by  $U_P$  and it is perpendicular to the hub plane with positive direction facing downwards as illustrated in Figures 4.4(a) and 4.4(b).

The tangential velocity  $U_T$  is affected by the rotor rotation and the forward velocity. The component due to rotor rotation is  $\Omega r$  (where  $r$  is the radial distance of the blade element), while the tangential to the blade forward velocity component is  $(V_\infty \cos \alpha_{hb}) \sin \psi_b$ . Therefore, the complete form of  $U_T$  with respect to the azimuthal angle  $\psi_b$  and the radial distance  $r$  of the blade element is given by:

$$U_T(r, \psi_b) = (V_\infty \cos \alpha_{hb}) \sin \psi_b + \Omega r \quad (4.4)$$

The radial component of the blade element is solely produced by the freestream velocity, therefore:

$$U_R(\psi_b) = (V_\infty \cos \alpha_{hb}) \cos \psi_b \quad (4.5)$$

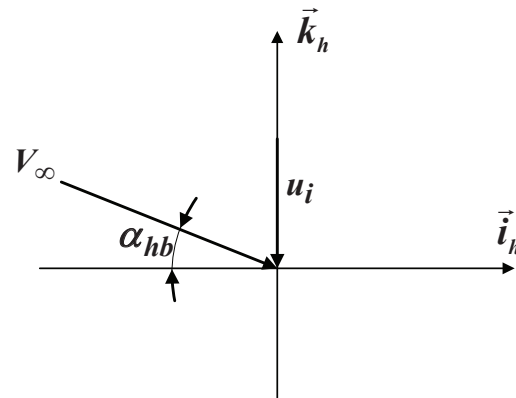
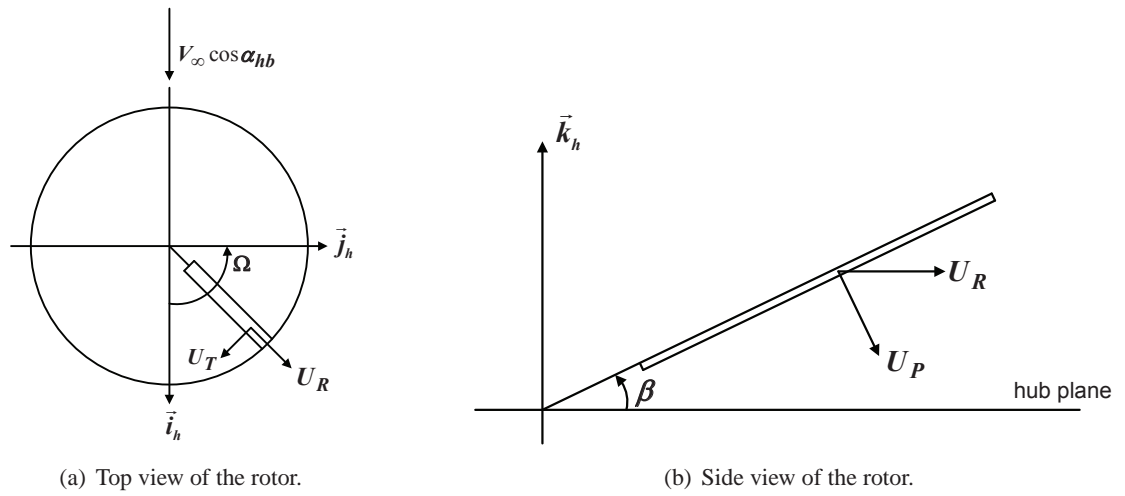


Figure 4.4: Directions of the velocity components seen by the blade element. This Figure also illustrates the direction of the free stream and inflow velocity.

In general the effect of the radial component towards the calculation of the air velocity of the blade element is neglected. However, this component should be considered when calculating explicitly the effect of the rotor drag [58].

The out of plane velocity vector consists of four velocity components. The first one is the velocity due to blade flapping given by  $r\dot{\beta}$ . The second one is the perpendicular to the blade element component due to the radial velocity  $U_R$  given by  $U_R \sin \beta$ . The third is the effect of the forward velocity described by  $(V_\infty \sin \alpha_{hb}) \cos \beta$ . Lastly, there is the influence of the inflow velocity  $u_i$ , which is perpendicular to the rotor hub with component  $u_i \cos \beta$ . The complete out of plane velocity is given by:

$$U_P(r, \psi_b) = r\dot{\beta} + U_R \sin \beta + (V_\infty \sin \alpha_{hb}) \cos \beta + (u_i) \cos \beta \quad (4.6)$$

By considering a small flapping angle  $\beta$ , the following simplified equation is obtained:

$$U_P(r, \psi_b) = r\dot{\beta} + U_R \beta + (V_\infty \sin \alpha_{hb}) + u_i \quad (4.7)$$

A schematic description of the velocities, aerodynamic angles and elemental forces acting on a blade element is given in Figure 4.5. The magnitude of the velocity seen by the blade element is given by:

$$U = \sqrt{U_T^2 + U_P^2} \quad (4.8)$$

The relative inflow angle (or induced angle of attack) is given by:

$$\phi_b = \tan^{-1} \left( \frac{U_P}{U_T} \right) \quad (4.9)$$

The blade's angle of attack is a function of the blade pitch angle  $\zeta$  and the produced inflow angle  $\phi_b$ . The complete expression of the angle of attack is given by:

$$\alpha_b = \zeta - \phi_b \quad (4.10)$$

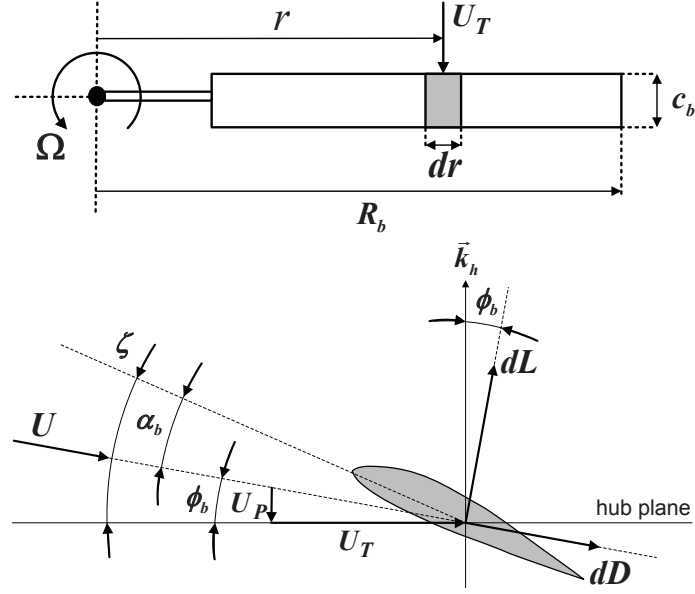


Figure 4.5: Illustration of a two dimensional blade element. The figure illustrates the velocity components of the blade element, the aerodynamic angles and the elemental aerodynamic forces. This figure is based on [70].

The aerodynamic lift and drag vectors of the blade element are normal and parallel, respectively, to the resultant velocity  $U$  seen by the blade element.

From [58] the incremental lift  $dL$  produced at the blade element is:

$$dL = \frac{1}{2} \rho_a U^2 c_b C_{l\alpha} \alpha_b dr \quad (4.11)$$

In the above equation  $\rho_a$  is the air density,  $c_b$  is the blade chord and  $C_{l\alpha}$  is the airfoil's lift curve slope. The drag component, denoted  $dD$ , of the element blade is given by:

$$dD = \frac{1}{2} \rho_a U^2 c_b C_d dr \quad (4.12)$$

where  $C_d$  is a drag constant which depends on the blade's geometry. The components of the forces acting parallel and perpendicular to the hub plane are given by:

$$dF_x = dL \sin \phi_b + dD \cos \phi_b \quad (4.13)$$

$$dF_z = dL \cos \phi_b - dD \sin \phi_b \quad (4.14)$$

The complete forces are obtained by integrating the above equations for all the blade elements along the blade's length. The above equations indicate that the cyclic inputs and the helicopter forward motion through the air, produce periodic aerodynamic forces with a frequency related to  $\Omega$ . Actually, as indicated in [7, 40, 58, 70], the periodic aerodynamic loads produced by feathering have a frequency equal or closed to  $\Omega$ . An analytical description of the aerodynamic forces is too complex and it is out of the scope of this work. These periodic forces result to the periodic flapping motion of the blade. The blade's flapping motion is described in the next Section.

#### 4.5 Flapping Equations of Motion

This Section presents the rotor equations of motion associated with the flapping of the blades. Flapping is assumed to take place about a hinge located at the intersection of the shaft with the hub plane (no hinge offset). To complete the model of the flapping hinge, a linear torsional spring is added at the hinge with stiffness  $K_\beta$ . This model approach is based on [7, 79] and it is a successful way to represent uniformly a variety of hinged and hingeless rotors. This modeling approach is also able to capture the effect of the hinge offset. Apart from the flapping motion, the blade is rotating with angular velocity  $\Omega$  about the shaft. The effect of the rotational and translational accelerations of the fuselage on the blade motion is disregarded. This is a typical simplification assumption, however, details about this effect can be found in [79]. Furthermore, mass uniformity of the blade is assumed. The mass per unit length of the blade is denoted by  $m_b$ . The mass of a blade element with radial distance  $r$  from the blade root is  $m_b dr$ .

The first thing towards this analysis is the determination of the forces acting on the blade element. The first force component is the periodic aerodynamic lift force  $dF_a$ , acting on the blade element. This force component is perpendicular to the blade element facing upwards. In addition, there are two inertia forces acting on the blade. The first one is the inertia force component opposing the flapping motion. The acceleration of the blade element due to flapping is  $\ddot{\beta}r$ , there-

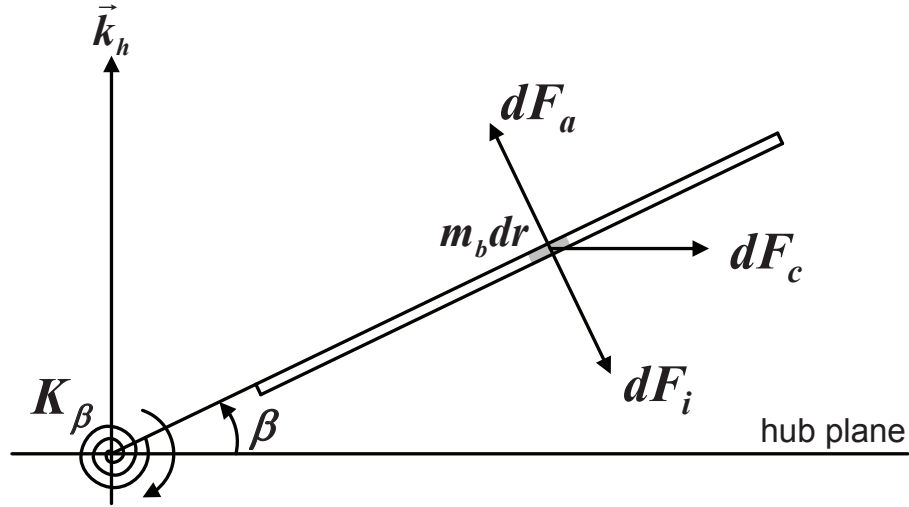


Figure 4.6: Aerodynamic, inertia and centrifugal forces acting on a blade element. The flapping angle of the blade is denoted by  $\beta$ . A centered torsional spring of stiffness  $K_\beta$  is placed at the root of the blade. This figure is based on [70].

fore, the inertia force due to flapping  $dF_i$  is  $m_b dr \ddot{\beta} r$ , which is perpendicular to the blade facing downwards. The second inertia force is the centrifugal force  $dF_c = m_b dr \Omega^2 r \cos \beta$ , which is parallel to the hub plane directed radially outwards, due to the centripetal acceleration  $\Omega^2 r \cos \beta$ . The inertia force due to Coriolis acceleration (this force is in the in-plane direction) and the weight force acting on the blade are disregarded since they produce significant smaller forces than the forces produced by flapping.

The flapping equation of motion is derived by equating all moments that act on the blade. The total moment is derived by calculating the elementary moments acting on a blade element and then by integrating along the complete blade length. Since the force components that are collinear with the the blade axis do not produce any moments, the moment equation takes the form:

$$\int_0^{R_b} m_b \Omega r^2 \cos \beta \sin \beta dr + \int_0^{R_b} m_b \ddot{\beta} r^2 dr + K_\beta \beta = \int_0^{R_b} r dF_a dr \quad (4.15)$$

By assuming small angle approximation for  $\beta$ , the above equations takes the form:

$$(\ddot{\beta} + \Omega^2 \beta) \int_0^{R_b} m_b r^2 dr + K_\beta \beta = \int_0^{R_b} r dF_a dr \quad (4.16)$$

The integral of the first term is the inertia of the blade given by:

$$\mathcal{I}_b = \int_0^{R_b} m_b r^2 dr \quad (4.17)$$

Equation (4.16) takes a more intuitive form if the flapping angle  $\beta$  is expressed as a function of the azimuthal angle  $\psi_b$  of the blade, instead of time. The operand ( $'$ ) denotes the derivative of  $\beta$  with respect to  $\psi_b$ . The relation between the azimuthal angle and time is given by  $\psi_b = \Omega t$  so regarding the derivatives of  $\beta$  with respect to  $\psi_b$  the following equalities hold:

$$\dot{\beta} = \frac{\partial \beta}{\partial \psi_b} \frac{\partial \psi_b}{\partial t} = \Omega \beta' \quad (4.18)$$

$$\ddot{\beta} = \frac{\partial \dot{\beta}}{\partial \psi_b} \frac{\partial \psi_b}{\partial t} = \Omega^2 \beta'' \quad (4.19)$$

Considering (4.18) and (4.19), then (4.16) results in:

$$\beta'' + \lambda_\beta^2 \beta = \frac{1}{\Omega^2 \mathcal{I}_b} \int_0^{R_b} r dF_a dr \quad (4.20)$$

where the flapping frequency ratio  $\lambda_\beta$  [70, 79] is given by the expression:

$$\lambda_\beta^2 = \frac{K_\beta}{\Omega^2 \mathcal{I}_b} + 1 \quad (4.21)$$

The dynamics of (4.20) resemble the equation of motion of a single DOF Spring-Mass-Damper (SMD) system. The description of the latter is given by the equation  $m\ddot{x} + c\dot{x} + kx = F$  where  $m$  denotes the mass of the object,  $c$  is the damping coefficient,  $k$  is the spring stiffness and  $F$  is the external applied force. For this system, the natural frequency is given by  $\omega_n = \sqrt{k/m}$  and it is independent of the damping coefficient. For (4.20) it is obvious that the natural frequency of blade flapping is equal to the flapping frequency ratio  $\lambda_\beta$ . The aerodynamic term in the right hand side of (4.20) includes the damping term.

## 4.6 Rotor Tip-Path-Plane Equation

From the analysis of the previous Section, it is apparent that the flapping motion depends on the azimuthal angle of the blade. Therefore, the flapping motion is a periodic function with fundamental frequency  $\Omega$  and period  $T_b = 2\pi/\Omega$ . Every periodic function can be expressed as a Fourier series, so the flapping motion can be expanded to the following infinite sum:

$$\begin{aligned}\beta(\psi_b) &= \beta_0 - \sum_{n=1}^{\infty} (b_{nc} \cos n\psi_b + b_{ns} \sin n\psi_b) \\ &= \beta_0 - b_{1c} \cos \psi_b - b_{1s} \sin \psi_b - b_{2c} \cos 2\psi_b - b_{2s} \sin 2\psi_b - \dots\end{aligned}\quad (4.22)$$

where  $\beta_0$ ,  $\beta_{nc}$ , and  $\beta_{ns}$  denote the Fourier series coefficients. Practical observations have shown that only the first harmonics of the infinite series are sufficient to approximate the flapping behavior of the blade since the contribution of higher harmonics can be considered negligible. In this case, following the classical approach of [13], the form of the flapping angle  $\beta$  is represented by the first harmonic terms of (4.22) with time varying coefficients, therefore:

$$\beta(\psi_b) = \beta_0(t) - \beta_{1c}(t) \cos \psi_b - \beta_{1s}(t) \sin \psi_b \quad (4.23)$$

The above equation indicates that the tips of the blade curve a circularly path. The plane that this circular path lies on, is referred to as *Tip-Path-Plane (TPP)* or *rotor disk*. In order for the reader to understand the blade motion described by (4.23) the following analysis examines individually the effect of the first-harmonic coefficients to the TPP. For simplicity, the coefficients  $\beta_0$ ,  $\beta_{1c}$ , and  $\beta_{1s}$  are considered constant with time. Denote by  $[x_h \ y_h \ z_h]^T$  the coordinates of the tip of the blade with respect to the hub frame  $\mathcal{F}_h$ .

If the flapping angle is composed only by the  $\beta_0$  coefficient, then the blades form a cone as they rotate and the TPP is a circle parallel to the hub plane as illustrated in Figure 4.7(a).

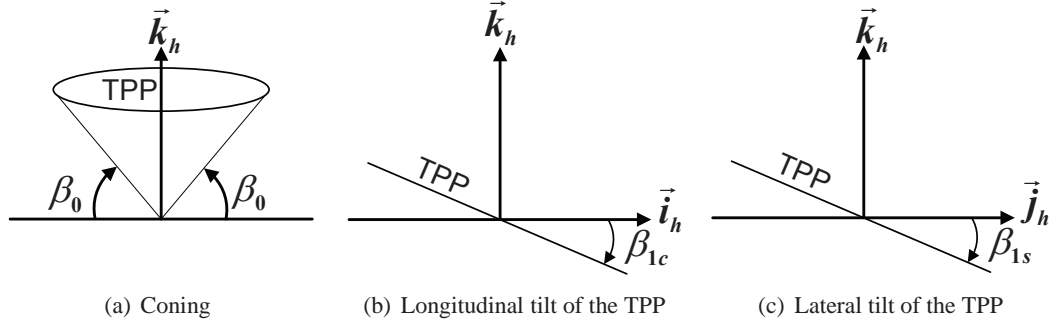


Figure 4.7: Effect of each harmonic given by (4.23) to the TPP.

Regarding the  $\beta_{1c}$  term, if small angle approximation is used and the flapping angle is given by  $\beta(\psi_b) = -\beta_{1c} \cos \psi_b$ , then the coordinate of the tip of the blade on the  $\vec{k}_h$  axis is:

$$z_h = R_b \sin \beta \approx R_b \beta = -R_b \beta_{1c} \cos \psi_b \approx -\beta_{1c} x_h \quad (4.24)$$

In this case the TPP lies on a plane that is tilted about the  $\vec{j}_h$  axis with an angle  $\beta_{1c}$  downwards as illustrated in Figure 4.7(b). Following the same analysis for the motion of  $\beta(\psi_b) = -\beta_{1s} \sin \psi_b$ , one obtains:

$$z_h = R_b \sin \beta \approx R_b \beta = -R_b \beta_{1s} \sin \psi_b \approx -\beta_{1s} y_h \quad (4.25)$$

and the TPP will be a plane tilted about the  $\vec{i}_h$  axis downwards having an angle  $\beta_{1s}$  with the reference plane. The lateral tilt of the TPP is illustrated in Figure 4.7(c). The TPP equation described by (4.23) results in a longitudinal and lateral tilt of the cone produced by  $\beta_0$ . The tilt angles of the cone are  $\beta_{1c}$  and  $\beta_{1s}$ , respectively.

The dynamics of the first harmonic terms of (4.23) provide the dynamic equations of the TPP. Those equations are derived by substituting (4.23) to (4.20), and equating, respectively, the non-periodic term, the terms including  $\cos \psi_b$  and the terms with  $\sin \psi_b$ . A detailed analysis of this approach, providing a thorough mathematical representation is given in [13]. Let  $\mathbf{a} = [\beta_0 \ a \ b]^T$  denote the state vector of the TPP (following the notation given in [70]) where  $a$  stands for  $\beta_{1c}$  and  $b$  for  $\beta_{1s}$ . The TPP dynamic equations are given by the following differential equation of the state

vector  $\mathbf{a}$ :

$$\ddot{\mathbf{a}} + D\dot{\mathbf{a}} + K\mathbf{a} = F \quad (4.26)$$

where  $D$  is the damping matrix,  $K$  is the stiffness matrix and  $F$  is the matrix of the forcing function. As mentioned earlier, the complete formulation on the above equation can be found in [13]. Those equations are further simplified in order to provide a practical model of the TPP dynamics. Those simplifications are introduced in [70] and they are presented in the next Section.

#### 4.7 First Order Tip-Path-Plane Equations

For the derivation of a simplified model of the rotor dynamics the work in [70] has adopted the detailed dynamic equations of the TPP presented in [13] also considering some additional simplification assumptions. The model proposed in [70] is suitable for system identification since it includes the necessary components that capture the dynamic behavior that affect the helicopter without burdening the model with unnecessary complexity. The simplification assumptions are the following:

- The effect of the inflow ratio is disregarded.
- The coning angle is considered constant, therefore its associated dynamics are omitted.
- The effect of the hinge offset is disregarded.
- The pitch-flap coupling ratio is zero.
- The effect of the forward velocity is disregarded ( $\mu = 0$ ).

The TPP model presented in [13] provides a very extensive description of the TPP dynamics. If we do not consider the above simplification assumptions the resulting TPP model is going to be very complex and completely impractical for control design purposes. Then based on [70], the

simplified flapping dynamics are given by:

$$\tau_f \dot{a} = -a - \tau_f q + A_b b + A_{lon} u_{lon} \quad (4.27a)$$

$$\tau_f \dot{b} = -b - \tau_f p + B_a a + B_{lat} u_{lat} \quad (4.27b)$$

The above equations are an approximation of the TPP dynamics produced by the helicopter motion and control inputs. The term  $\tau_f$  denotes the main rotor time constant and it is given by:

$$\tau_f = \frac{16}{\gamma \Omega} \quad (4.28)$$

The rotor's time constant depends on the angular velocity  $\Omega$  and the Lock number  $\gamma$ . The Lock number is given by:

$$\gamma = \frac{\rho_a a c_b R_b^4}{\mathcal{I}_b} \quad (4.29)$$

Finally, the main rotor cross coupling terms  $A_b$  and  $B_a$  are:

$$A_b = -B_a = \frac{8}{\gamma} (\lambda_\beta^2 - 1) \quad (4.30)$$

#### 4.8 Main Rotor Forces and Moments

The final part of the rotor description deals with the derivation of a simplified model of the forces and moments produced by the main rotor. The thrust vector produced by the main rotor is considered perpendicular to the Tip-Path-Plane (TPP). Since the thrust vector is normal to the TPP, by controlling the TPP inclination, the pilot indirectly controls the direction of the propulsion forces.

Let  $\vec{T}_M$  denote the thrust vector of the main rotor and  $T_M$  its magnitude. The body-fixed frame coordinate vector of the thrust is denoted by  $T_M^B$ . By simple geometry the following equations are

derived:

$$T_M^B = \begin{bmatrix} X_M \\ Y_M \\ Z_M \end{bmatrix} = \begin{bmatrix} -\sin a \cos b \\ \cos a \sin b \\ -\cos a \cos b \end{bmatrix} T_M \approx \begin{bmatrix} -a \\ b \\ -1 \end{bmatrix} T_M \quad (4.31)$$

The above equations are simplified by assuming small angle approximation ( $\cos(\cdot) \approx 1$  and  $\sin(\cdot) \approx (\cdot)$ ) for the flapping angles. The small angle assumption is adopted by [40, 47, 70].

The generated thrust torque is the result of the above force and the rotor's stiffness moments. Denote by  $h_M^B = [x_m \ y_m \ z_m]^T$  the position of the main rotor shaft. Let  $\vec{\tau}_\beta$  denote the vector of the main rotor moments due to the hub stiffness  $K_\beta$ . Then, the main rotor moment vector is given by  $\vec{\tau}_M = \vec{h}_M \times \vec{T}_M + \vec{\tau}_\beta$ . The components of the hub stiffness moments vector in the body-fixed frame are given by:

$$\tau_\beta^B = \begin{bmatrix} L_\beta \\ M_\beta \\ N_\beta \end{bmatrix} = \begin{bmatrix} b \\ a \\ 0 \end{bmatrix} K_\beta \quad (4.32)$$

In the ideal case that the CG is aligned with the shaft, i.e.  $h_M^B = [0 \ 0 \ -l_h]$  then the pitch and roll moments of the main rotor are given by:

$$L_M = -(-l_h)Y_M + L_\beta$$

$$M_M = -l_h X_M + M_\beta$$

Hence:

$$L_M = (l_h T_M + K_\beta)b \quad (4.33a)$$

$$M_M = (l_h T_M + K_\beta)a \quad (4.33b)$$

Therefore, the pitch and roll moments about the CG depend on the main rotor thrust magnitude and the stiffness of the hub. The above simplified case is presented because it provides insight to the development of the linear helicopter model. In the case that the nonlinear helicopter dynamics

are considered the more elaborate description  $\vec{\tau}_M = \vec{h}_M \times \vec{T}_M + \vec{\tau}_\beta$ , is used for the representation of the moment produced by the main rotor.

#### 4.9 Remarks

This Chapter has presented a description of the intermediate concepts that are related with the flapping dynamics of the blades. The flapping motion is initially triggered by a change in the cyclic pitch of the blades. The pitch variation alters the blade's angle of attack resulting to the generation of periodic aerodynamic forces that act upon the blade. The flapping motion is produced by the aerodynamic, centrifugal, inertial and hub stiffness moments that act on the blade. The flapping dynamics equations are based on the work presented in [70]. In the reported work the simplified rotor dynamics (flapping dynamics) are derived by significantly simplifying the more elaborate model presented in [13]. The particular rotor model is physically meaningful and has been successfully applied to system identification modeling of several helicopters. The flapping dynamics given in (4.27) are suitable for small scale helicopters since for full scale helicopters an accurate model would also require the addition of the coning dynamics effect. The rotor model is augmented to the rigid body dynamics to produce the complete helicopter model. The main rotor thrust vector is considered perpendicular to the TPP. This modeling assumption is adopted by both linear and nonlinear helicopter models. The task of the next section is to present a reliable system identification methodology for the extraction of linear helicopter models. The presented methodology is based in the work reported in [70, 105] and it a successful approach for the system identification modeling of small scale helicopters.

## Chapter 5: Frequency Domain System Identification

Helicopter flight controller design requires knowledge of a mathematical model that accurately describes the dynamic behavior of the helicopter. This mathematical model is represented by a set of ordinary differential equations. Establishing such a model in the case of helicopters is a challenging task. This Chapter provides a thorough description of a frequency domain identification procedure for the extraction of linear models that correspond to certain operating conditions of the helicopter. This methodology has been established in [105] and has been successfully applied for a small scale helicopter in the work reported in [70]. The frequency domain identification procedure is evaluated for an experimental small scale Radio Controlled (RC) *Raptor 90 SE* helicopter through the *X-Plane* flight simulator. The *Raptor 90 SE* helicopter is used for the evaluation and comparison of the several controller designs and identification methods that are presented in this research.

### 5.1 Mathematical Modeling

Helicopter dynamics are nonlinear and of high order. For typical aircraft models there is a distinct separation between the dynamics associated with the lateral and longitudinal motion. This separation can not take place in the case of a helicopter, where there exists a strong coupling among the system dynamics.

The prime coupling effect is encountered by the interaction of the fuselage and main rotor dynamics. As indicated from the previous Chapter, the rotor is a dynamical system itself, affected by both the environment, through the air flow (inflow) passing through the rotor blades, and the fuselage motion. In many cases, the fuselage rigid body dynamics representation is not adequate

and the additional effect of the rotor should be encountered [70]. An additional source of complexity is the description of the aerodynamic forces and moments acting on the helicopter. Those forces and moments are complicated, with significant changes in their behavior, depending on the operating condition of the helicopter.

Two approaches may be followed for the derivation of a mathematical model representing the helicopter dynamics. The first modeling approach is the derivation of a mathematical model from *first principles* modeling, while the second is through *system identification*. In some parts those two methods are complementary to each other and in many cases the use of both of them is mandatory for increasing the accuracy of the derived model.

### 5.1.1 First Principles Modeling

When the first principles modeling method is used, the system equations are derived by the implementation of physics laws. Obviously, this approach, requires an a priori knowledge of all the parameters that affect the helicopter motion and aerodynamics. The typical end result of first principles modeling is a set of nonlinear differential equations of high order that cover a wide portion of the flight envelope. A common use of the first principles modeling method is for the development of simulation models. The main disadvantage of this approach is the large number of parameters to be determined. Those parameters involve geometrical characteristics, mass and inertias, drag coefficients and aerodynamic parameters. Many of the latter parameters can be easily obtained by simple experimental tests (such as masses and inertias), however their majority requires more sophisticated experiment methods such as wind tunnel tests [105]. The difficulty of obtaining an accurate estimate of many of the helicopter parameters render the first principles modeling method impractical for many applications.

### 5.1.2 System Identification Modeling

System identification is the procedure of deriving a mathematical model of the system based on experimental data of the system's control inputs and measured outputs. Two types of models can be derived by this method. The first type is the *nonparametric models* and examples of such models are the impulse response and frequency responses. The nonparametric models are directly produced by experimental data and provide an input-output description of the system. These model types are just collections of data and do not require any knowledge of the system structure.

The challenge of the system identification procedure, is to derive a *parametric model* of the system. Examples of parametric models are the transfer functions and the state space models. The first step towards the extraction of a parametric model, is the derivation of a parametrized model, which will serve as a logical guess of the actual system model. The use of an optimization algorithm determines the parameters of the model that minimize (in a least-square sense) the error between the actual system responses and the model responses. The first question that arises is what is a suitable guess of the initial parametrized model in terms of model order, structure and the initial values of the parameters. Estimates of those characteristics can be obtained by analysis of the nonparametric model combined with information obtained by the first principles approach.

The system identification procedure is an iterative process. Depending on the identification results, the parametrized model can be refined in terms of order and structure until a satisfactory identification error is achieved. When the parametrized model is known, the system identification method reduces to the parameter estimation problem. There exist many system identification methods, which are well described in [61, 62, 93]. A major classification amongst the system identification methodologies depends on whether the compared responses are considered in the time domain or the frequency domain. Frequency domain system identification has been proven a successful approach for extracting accurate linear models of aircraft and helicopters.

## 5.2 Frequency Domain System Identification

The inability of the first principles modeling approach to provide accurate and practical models for control design, lead to the development of more suitable system identification approaches. In particular, frequency domain identification has been regarded as an ideal solution for extracting linear helicopter models of high accuracy. One of the main advantages of this approach is the use of actual flight data for the derivation and validation of the model. Additionally, this has a coherent flow of the design steps starting from the input-output characterization of the helicopter (nonparametric modeling), continuing with the extraction of the state space model (parametric modeling) and finally validating the predicted model in the time domain. This method is classified as an output-error method where the fitting error is defined between the actual flight data frequency responses and the frequency responses predicted by the model.

The initial step of the identification procedure is the excitation of the helicopter by specially designed input signals such as frequency sweeps. The intention of the test data inputs is to excite the helicopter dynamics over a desired frequency range. The choice of the desired frequency range (model bandwidth) has an important role in the identification process. The model bandwidth has to be wide enough in order to encapsulate all the dynamic effects of interest (i.e., fuselage dynamics and rotor dynamics).

After some preprocessing to eliminate the noise effects and other types of inconsistencies in the time domain output data, the second phase is the computation of the input-output frequency responses using a Fast Fourier Transform. This phase of the process constitutes the nonparametric model of the helicopter.

The next step is the design of the parametrized linear state space model, using information from the first principles physical laws and the nonparametric modeling phase. The linear model has the form:

$$\dot{x}(t) = A(\Pi)x(t) + B(\Pi)u_c(t - \tau) \quad (5.1)$$

$$y(t) = Cx(t) + u_c(t - \tau) \quad (5.2)$$

where  $x$  is the state space vector,  $y$  is the measurement vector,  $\Pi$  denotes the unknown model parameter vector and  $\tau$  is the system's delay. The matrices  $C$ ,  $D$  are usually known, based on standard kinematic equations. The objective of parametric modeling is the extraction of the model matrices  $A$ ,  $B$  (depended on  $\Pi$ ) and the time delay  $\tau$ .

The frequency domain identification method is only suitable for the derivation of linear state space models. Although the helicopter dynamics are nonlinear, around certain trimmed flight conditions, the nonlinearities from the equations of motion and aerodynamics are relatively mild. When this is the case, a linearized model is adequate to accurately predict the helicopter's response. Usually, the validity of the linearized model is satisfactory in a relatively wide area of the flight envelope around the trim point. However, a single linear model in most cases is not enough for a global representation of the flight envelope. Different models are required for each operating condition.

After the determination of the linearized model, an optimization algorithm is used to tune the identification parameters, such that a good fit is achieved between the parametrized system's responses and the flight data responses. The frequency response magnitude and phase errors are denoted by the vector  $\epsilon(\omega, \Pi)$  for a frequency  $\omega$ . The objective is the minimization of a cost function  $J(\Pi)$ , which is the sum of the weighted squared errors  $\epsilon(\omega, \Pi)$  over a finite number of frequencies. More specifically:

$$J(\Pi) = \sum_{j=1}^n \epsilon(\omega_j, \Pi)^T W \epsilon(\omega_j, \Pi) \quad (5.3)$$

where  $W$  is a weight matrix. The above procedures constitute the parametric modeling part of the problem. If the parameter identification does not provide a satisfactory result, the parametrized model is revisited in terms of order and structure until a satisfactory minimization of the cost function is achieved.

The final step of the identification procedure is the validation of the model. This step takes place in the time domain, with different flight data from the identification procedure. For the same input sequence, the helicopter responses from the flight data are compared with the predicted

values of the model, obtained by integration of the state space model. Again, if the validation portion of the problem is not satisfactory the designer should modify the parametric modeling setup and repeat the procedure.

### 5.3 Advantages of the Frequency Domain Identification

Based on [70, 105], some of the advantages for using frequency domain identification for helicopter modeling are the following:

- Biases and reference shifts from the trim condition are removed by the identification process.
- The frequency response estimates are unbiased from measurement noise, given that the latter is uncorrelated with the excitation signals.
- Accurate identification of time delays.
- The frequency range of each frequency response is selected individually. Therefore, only the most accurate data are involved in the calculations.
- The model structure and order selection are facilitated by the nonparametric model.
- The frequency domain identification is computationally more efficient from its time domain counterpart. The time domain identification requires the integration of the system state space equations for each iterative step. Integration of the system equation does not take place in the frequency domain scheme. In addition, frequency domain identification requires less data points than the time domain identification.

### 5.4 Helicopter Identification Challenges

The identification process encounters some particular difficulties in the case of helicopters. Based on [70, 105] those difficulties are listed below:

- In many cases where the helicopter is operating at low velocities (hover, low speed cruising) the control input has similar magnitude with the measurement noise. Common noise source could be produced by structural vibrations caused from gear boxes, the engine as well as the rotor.
- The helicopter is a MIMO system with significant dynamic coupling (or *interaxis coupling*). For any primary axis response (*on-axis* response) caused by one of the inputs, unintended secondary axis responses (*off-axis* responses) result.
- A linear model based solely on the rigid body dynamics will not be sufficient to accurately describe the helicopter responses. A model of higher order is needed including additional subsystems such as the rotor dynamics. Furthermore, the rotor dynamics are not independent from the rest of the model so a coupled fuselage-rotor model is required.
- The helicopter dynamics are in general unstable or critically stable. During the execution of the excitation control signals, required for the experimental data collection, additional feedback is required to sustain the vehicle in a range of a certain operating condition. The presence of feedback deteriorates the identification results.

## 5.5 Frequency Response and Coherence Function

Consider a Linear Time Invariant (LTI) system with input and output signals  $x(t)$  and  $y(t)$ , respectively. Denote by  $h(t)$ , the impulse response that characterizes the previous LTI system. The time domain relation of the output  $y(t)$  with respect to the input  $x(t)$  of the system, is given by the convolution integral [23, 77], namely:

$$y(t) = \int_{-\infty}^{\infty} h(t - \tau)x(\tau)d\tau \quad (5.4)$$

The frequency domain representation of the signals  $x(t)$ ,  $y(t)$  and  $h(t)$  is given by the *Fourier transform*. More specifically:

$$\begin{aligned} X(j\omega) &= \int_{-\infty}^{\infty} x(t)e^{-j\omega t} dt \\ Y(j\omega) &= \int_{-\infty}^{\infty} y(t)e^{-j\omega t} dt \\ H(j\omega) &= \int_{-\infty}^{\infty} h(t)e^{-j\omega t} dt \end{aligned} \quad (5.5)$$

where  $\omega$  is the real continuous time angular frequency variable in radians. The system input-output mapping is easier represented in the frequency domain by:

$$Y(j\omega) = H(j\omega)X(j\omega) \quad (5.6)$$

The Fourier transform  $H(j\omega)$  of the impulse response is called frequency response of the system.

It is a complex valued function with real and imaginary parts,  $H_R(j\omega)$  and  $H_I(j\omega)$ , respectively.

The frequency response can be expressed in polar form as:

$$H(j\omega) = |H(j\omega)| e^{j\angle H(j\omega)} \quad (5.7)$$

where:

$$|H(j\omega)| = \sqrt{H_R^2(j\omega) + H_I^2(j\omega)} \quad \text{and} \quad \angle H(j\omega) = \tan^{-1} \left( \frac{H_I(j\omega)}{H_R(j\omega)} \right) \quad (5.8)$$

The frequency domain can be also derived by the input and output spectral densities. The quantities  $S_{xx}$  and  $S_{xy}$  are the auto spectral density and cross spectral density, respectively. The auto spectral density and cross spectral density are functions commonly used in stochastic processes [5, 46]. The two-sided auto spectral density  $S_{xx}(j\omega)$  and cross spectral density  $S_{xy}(j\omega)$  are given

by:

$$S_{xx}(j\omega) = 2 \int_{-\infty}^{\infty} \mathcal{R}_{xx}(\tau) e^{-j\omega\tau} d\tau \quad S_{xy}(j\omega) = 2 \int_{-\infty}^{\infty} \mathcal{R}_{xy}(\tau) e^{-j\omega\tau} d\tau \quad (5.9)$$

where  $\mathcal{R}_{xx}(\tau)$  and  $\mathcal{R}_{xy}(\tau)$  denotes the auto correlation and cross correlation, respectively, given

by:

$$\mathcal{R}_{xx}(\tau) = \lim_{T \rightarrow \infty} \frac{1}{T} \int_{-\infty}^{\infty} x(t)x(t+\tau)dt \quad \mathcal{R}_{xy}(\tau) = \lim_{T \rightarrow \infty} \frac{1}{T} \int_{-\infty}^{\infty} x(t)y(t+\tau)dt \quad (5.10)$$

The equality that relates the spectral densities with the frequency response is:

$$S_{xy}(j\omega) = H(j\omega)S_{xx}(j\omega) \quad \implies \quad H(j\omega) = \frac{S_{xy}(j\omega)}{S_{xx}(j\omega)} \quad (5.11)$$

An important quantity, particularly useful in the frequency domain identification of MIMO systems is the coherence function. The latter is defined for the SISO case as:

$$\gamma_{xy}^2(j\omega) = \frac{|S_{xy}(j\omega)|^2}{|S_{xx}(j\omega)||S_{yy}(j\omega)|} \quad (5.12)$$

The coherence function is a normalized metric with its values ranging for zero to unity. It is an indicator of the linearity between the input and the output [46]. A value of the coherence function close to unity, indicates that the output is significantly linearly correlated with the input of the system. Possible causes for a low value of the coherence function are [46]:

- Presence of noise
- The input-output mapping is nonlinear
- The input does not effect the output

In the case of MIMO systems the equivalent metric is denoted as partial coherence. A low partial coherence in a MIMO system, is usually an indicator of that the specific input-output pair

is uncorrelated, therefore, the corresponding frequency response should not be included in the identification process. More about partial coherence can be found in [105].

All of the above functions will be calculated in a digital computer. The discretization of the continuous signals  $x(t)$  and  $y(t)$  by a sampling period  $T_s$  will lead to the concept of the *Discrete Fourier Transform* (DFT). Denote  $N$  the total number of sampled data. The DFTs for the  $N$  samples of  $x(t)$  and  $y(t)$  are given by [73, 76]:

$$X(k\Omega_s) = \sum_{n=0}^{N-1} x(t_0 + nT_s) e^{-j2\pi kn/N} \quad (5.13)$$

$$Y(k\Omega_s) = \sum_{n=0}^{N-1} y(t_0 + nT_s) e^{-j2\pi kn/N} \quad (5.14)$$

where  $\Omega_s$  is the frequency resolution and  $t_0$  is the first sampling time instant. Finally the discrete estimates of the auto spectral and cross spectral density,  $\hat{S}_{xx}$  and  $\hat{S}_{xy}$ , respectively, are given by [46, 70]:

$$\hat{S}_{xx}(k\Omega_s) = \frac{2}{NT_s} |X(k\Omega_s)|^2 \quad (5.15)$$

$$\hat{S}_{xy}(k\Omega_s) = \frac{2}{NT_s} X^\dagger(k\Omega_s) Y(k\Omega_s) \quad (5.16)$$

$$(5.17)$$

where the upper script  $\dagger$  denotes the complex conjugate value of the variable.

## 5.6 The *CIFER*<sup>©</sup> Package

The *CIFER*<sup>©</sup> package is an effective tool to tackle the aircraft and rotorcraft complete identification problem. *CIFER*<sup>©</sup> (Comprehensive Identification from FrEQUENCY Responses) [105] has been developed as a joint venture of the Army/NASA Rotorcraft Division (Ames Research Center). The program is composed of six utility packages that interact with a sophisticated database of frequency responses. The importance of a well organized and flexible database system is very

crucial in a large scale MIMO identification procedure of an air vehicle. The *CIFER*<sup>©</sup> package is designed to cover all the intermediate steps necessary for the development of an air vehicle parametric model. The key characteristic of *CIFER*<sup>©</sup> is its ability to generate and analyze high quality frequency responses for MIMO systems, by using sophisticated DFT and windowing algorithms. The six utility packages of *CIFER*<sup>©</sup> are [70, 105]:

- *FRESPID*: This utility package calculates the SISO frequency responses for each input-output pair. For the calculation of the FFTs a chirp-z algorithm is used. The user provides to the utility the time domain flight records of the input and output measurements. Biases and shifts are removed by the time domain data, and the flight records are concatenated into a single record. The time domain data are additionally filtered (to eliminate high frequency noise) and additionally processed by overlapping windowing. The later actions are necessary to improve the fidelity and the speed of the chirp-z transform. Finally the databased is updated with the estimated frequency responses and coherence functions
- *MISOSA*: This utility package receives the frequency responses previously calculated from *FRESPID* and removes the effect of secondary inputs which are possibly correlated with the primary input (conditioning). *MISOSA* outputs the conditioned frequency responses and partial coherence.
- *COMPOSITE*: This module optimizes the frequency responses for each spectral window applied by *FRESPID* and *MISOSA*, to provide the best possible estimated frequency response and highest coherence function, over the desired bandwidth.
- *NAVFIT*: This module belongs to the parametric portion of the identification procedure. *NAVFIT* calculates the transfer function model that best fits the estimated SISO frequency response.
- *DERIVID*: This program estimates the MIMO state space representation whose frequency response is the best fit for the estimated frequency responses obtained by the flight data. The parameters of the model can be considered free or constrained by a different parameter,

during the identification process. The unknown parameters are extracted by the application of a nonlinear iterative secant algorithm.

- *VERIFY*: This module is the final step of the identification procedures. *VERIFY* compares the time domain response of the identified model versus the experimental data. The data used by *VERIFY* should be dissimilar with the flight records obtained by the identification procedure.

## 5.7 Time History Data and Excitation Inputs

An issue of primary concern is the design of the excitation inputs used to collect data for the identification part. It is important to note that the behavior of the actual model that is required to be encapsulated by the identifier should be included in the data used for the identification [105]. In general regarding system identification, the design of the excitation signal is an open subject which depends on the model to be identified. The excitation signal must be capable of exciting the actual system modes that are needed to appear in the identified model.

A description of excitation signals specially designed for aircraft identification may be found in [46]. Some of those signals are frequency sweeps, impulse multisines and doublets. In this work frequency sweeps are used. Frequency sweeps are sinusoidal signals with variable frequency. The frequency of the signal increases logarithmically over time. Following this approach the excitation signal is capable of covering the desired frequency band. Frequency sweeps are commonly used in frequency identification techniques where the model is identified over a predefined frequency range.

Observations regarding the frequency sweeps are presented in [46, 105]. The most important feature is that they are not required to have constant amplitude. Variations in the frequency sweeps instead of being avoided are welcome since they enrich the frequency content of the signal. The symmetry of those signals allows the helicopter to sustain its position around a certain operating condition.

When the frequency sweep is applied to one of the helicopter's control inputs the rest should be implemented in such a way to adjust the helicopter in the neighborhood of the operating point. As indicated in [105] the rest of the control inputs should be uncorrelated with the main excitation signal and at the same time suppress any unwanted flight behavior. During the system identification procedure, frequency sweep data collected by several maneuvers can be concatenated, so it is very important that the data start and end at the trim condition. A 3 sec period in trim at the beginning and at the end is suggested.

The design of the frequency sweeps requires that the frequency bandwidth is determined a-priori. In general a good bandwidth for helicopter identification lies between 0.3-12 rad/sec [105]. The recorded length of the data for each sweep following a rule of thumb should be four to five times the period that corresponds to the minimum frequency. Let  $[\omega_{min} \ \omega_{max}]$  be the desired frequency interval that the excitation signal should contain. Then, the period that corresponds to the smallest frequency will be  $T_{max} = 2\pi/\omega_{min}$ . The suggested recorded length should be  $T_{rec} \geq 4T_{max}$ . The proposed excitation signal is given by  $u = A \sin [f(t)]$  where  $A$  is the amplitude of the signal and:

$$f(t) = \int_0^{T_{rec}} v(t) dt \quad (5.18)$$

$$K(t) = C_2[\exp(C_1 t/T_{rec}) - 1] \quad (5.19)$$

$$v(t) = \omega_{min} + K(t)(\omega_{max} - \omega_{min}) \quad (5.20)$$

From [105], the proposed parameters of (5.19) are  $C_1 = 4.0$  and  $C_2 = 0.0187$ . Further, based on [105] a brief summary of the most important guidelines that should be accounted in the frequency sweep signals, are the following:

- The sinusoidal should be as symmetric as possible to maintain the helicopter at trim. The symmetric input will also assist the FFT to identify and remove the trim values.
- The sweep signal should provide satisfactory excitation over the frequency range of interest. Special attention should be given to the low frequency excitation (0.3-1 rad/sec). At

least two periods of the minimum frequency of interest should be included in the excitation signal.

- The amplitude does not have to be constant.
- The increase in frequencies is not important. Furthermore, the maneuver should start and end with a 3 *sec* operation at trim.
- Most importantly, the secondary control commands should be as uncorrelated as possible with the primary excitation. The use of low frequency pulses is recommended to keep the *off-axis* responses bounded. However, although the *off-axis* responses should not diverge from the trim condition, they should not be suppressed either. Those effects are produced by the cross-coupled nature of the helicopter dynamics and this information should be included in the identification process.

## 5.8 Linearization of the Equations of Motion

Equations describing the helicopter motion are nonlinear differential equations. Linearizing these equations, under specific assumptions, is a common practice that simplifies greatly calculations and at the same time provides an adequate description of the actual behavior of the helicopter. Derivations follow the work described in [20].

Model linearization is based on small disturbance theory. According to that theory, analysis is done under small perturbations of motion characteristics (related to forces, momentums, velocities, angular velocities, etc.) from a steady non-accelerating reference flight. The rationale behind this approach is the fact that external aerodynamic forces and moments acting on the CG depend mainly on helicopter's control inputs and motion variables such as linear and angular velocities. When this is the case, the perturbed aerodynamic forces and moments may be considered as linear functions of the disturbances [20].

The helicopter is assumed to perform a reference trimmed flight when the disturbances occur. In this equilibrium operation, the state variable  $x$  of the helicopter can be approximated by  $x =$

$x_0 + \delta x$ , where  $x_0$  is the trimmed value of the state and  $\delta x$  the perturbation from the reference flight condition. The small perturbations logic applies for the control inputs as well. Since in the identification procedure we are going to consider only the hover representation of the helicopter, the equilibrium state values will be:

$$u_0 = v_0 = w_0 = p_0 = q_0 = r_0 = \theta_0 = \phi_0 = 0$$

The perturbation quantities and their derivatives will have very small values; therefore, their products are negligible. Without loss of generality, it is assumed that the trigonometric quantities of the perturbed variables, for example  $\delta\theta$ , will be  $\cos \delta\theta = 1$  and  $\sin \delta\theta = \delta\theta$ . Therefore:

$$\sin(\theta_0 + \delta\theta) = \sin \theta_0 \cos \delta\theta + \cos \theta_0 \sin \delta\theta = \delta\theta \quad (5.21)$$

$$\cos(\theta_0 + \delta\theta) = \cos \theta_0 \cos \delta\theta - \sin \theta_0 \sin \delta\theta = 1 \quad (5.22)$$

Based on the above assumptions, substitutions into (3.3) and (3.8) result in the following perturbed equations:

$$\begin{aligned} m\delta\dot{u} &= -mg\delta\theta + X_0 + \Delta X \\ m\delta\dot{v} &= mg\delta\phi + Y_0 + \Delta Y \\ m\delta\dot{w} &= mg + Z_0 + \Delta Z \end{aligned} \quad (5.23)$$

$$\begin{aligned} \mathcal{I}_{xx}\delta\dot{p} &= L_0 + \Delta L \\ \mathcal{I}_{yy}\delta\dot{q} &= M_0 + \Delta M \\ \mathcal{I}_{zz}\delta\dot{r} &= N_0 + \Delta N \end{aligned} \quad (5.24)$$

$$\begin{aligned} \delta\dot{\theta} &= \delta q \\ \delta\dot{\phi} &= \delta p \\ \delta\dot{\psi} &= \delta r \end{aligned} \quad (5.25)$$

In the above equations  $\Delta X, \Delta Y, \Delta Z$  denote the perturbed values of the external aerodynamic forces and  $\Delta L, \Delta M, \Delta N$  denote the perturbed values of the moments about the CG. When the helicopter is at trim, the trimmed values of the moments about the CG will be zero. In addition, only the trimmed force component  $Z_0$  is compensating for the gravitational force. Hence, at trim:

$$\begin{aligned}\delta \dot{u} &= -g\delta\theta + \Delta X/m \\ \delta \dot{v} &= g\delta\phi + \Delta Y/m \\ \delta \dot{w} &= \Delta Z/m\end{aligned}\tag{5.26}$$

$$\begin{aligned}\delta \dot{p} &= \Delta L/\mathcal{I}_{xx} \\ \delta \dot{q} &= \Delta M/\mathcal{I}_{yy} \\ \delta \dot{r} &= \Delta N/\mathcal{I}_{zz}\end{aligned}\tag{5.27}$$

## 5.9 Stability and Control Derivatives

The last step towards the linearization of the initial rigid body equation relates to expressing the perturbed values of the external aerodynamic forces and moments in a linear way. The analysis of the perturbed external aerodynamic forces and moments follows the assumption that the latter are continuous functions of the helicopter disturbed motion variables and the helicopter controls [20, 70, 79]. The linearization of those perturbed values is a very common method with very practical results although it is not based on a consistent mathematical background, and to this extent there might be cases that this modeling method will not provide adequate results [20, 79].

Due to the assumption that the perturbed forces and moments are functions of the disturbed values of the helicopter's motion and controls, it follows that the former can be expressed as a Taylor series. The linear form of those quantities follows by neglecting high order terms. Notation wise, the expansion of the aerodynamic force (or moment) is normalized by the mass (or corresponding inertia). An example is the expansion of the aerodynamic moment  $\Delta L$ , as:

$$\frac{1}{\mathcal{I}_{xx}}\Delta L = \frac{1}{\mathcal{I}_{xx}}\frac{\partial L}{\partial u}\delta u + \dots + \frac{1}{\mathcal{I}_{xx}}\frac{\partial L}{\partial p}\delta p + \dots + \frac{1}{\mathcal{I}_{xx}}\frac{\partial L}{\partial a}\delta a \dots + \frac{1}{\mathcal{I}_{xx}}\frac{\partial L}{\partial u_i}\delta u_i \quad (5.28)$$

where  $u_i$  denotes a helicopter's control variable. Typically, the products of the partial derivatives are notated i.e as:

$$L_u = \frac{1}{\mathcal{I}_{xx}}\frac{\partial L}{\partial u} \quad (5.29)$$

The above partial derivatives, with respect to the helicopter's perturbed motion variables and control inputs, are called stability and control derivatives, respectively. Those derivatives are calculated under the trim flight condition. The calculation of the stability derivatives is beyond the scope of this work; however, details may be found in [7, 79, 84, 86]. In general not all stability derivatives are necessary for linearization of the forces or moments. As mentioned in [70] an important part of system identification is to decide which derivatives are important in the calculations of the perturbed forces and moments. Everything will take place at hover.

## 5.10 Model Identification

The previous Sections of this Chapter provided an outline of the frequency domain identification method for helicopter modeling. This Section presents the identification results obtained by *CIFER*<sup>©</sup> for a small scale helicopter, operating in a flight simulator environment. The flight tests throughout this work are conducted using the *X-Plane* flight simulator for a *RC Raptor 90 SE* helicopter. At first, the description of the experimental platform is given. The parametrized model with the associated stability derivatives is also provided. After the presentation of the parametrized model, the set-up and final results of the identification procedure obtained by *CIFER*<sup>©</sup> follow. Finally the accuracy of the extracted model is validated in the time domain. The end result of this Section will be a linear dynamic system representing the helicopter response at hover.

### 5.10.1 Experimental Platform

The system identification accuracy and the performance of the controller designs are evaluated by using the commercial flight simulator *X-Plane*. The helicopter model in *X-Plane* is treated as the “black box” portion of the problem, since no a-priori knowledge of the model parameters is used in the identification process or the control design. *X-Plane* is an awarded flight simulator certified by the Federal Aviation Administration (FAA).

Apart from the realistic flight simulation capabilities, *X-Plane* incorporates a series of additional useful features, making it an ideal solution for experimentation and validation of unmanned flight. The user has the ability to modify and customize those models in order to achieve the desired flight characteristics. In addition, *X-Plane* supplies a plethora of flight data, which are required for the model identification process and the control feedback. The main advantage of *X-Plane*, in comparison with other simulators such as *Microsoft's Flight Simulator* and *FlightGear*, is the ability to import and export real-time data. This is of particular importance, since the control inputs can be obtained by an external autopilot. In addition, the autopilot requires the helicopter's state at every sampling instant, which is available by the exported data of *X-Plane*.

The helicopter used for experimentation in *X-Plane*, is a customized *Raptor 90 SE* RC helicopter, based on the *Raptor 70* flight model [19]. The basic specifications of this model can be found in Table 5.1. The *X-Plane* helicopter model, has been additionally calibrated by an experienced pilot, in such a way that the flight behavior of the latter will accurately resemble the behavior of the actual helicopter. However, in the software model, the yaw rate exhibits significant sensitivity to the pedal input. This sensitivity in the yaw rate results from the absence of a gyro feedback mechanism in the simulator model. The gyro is a typical feature of actual small scale helicopters and inserts additional feedback for controlling the heading.

The experimental platform, in which the flight testing took place, is based on a communication interface between *MATLAB/SIMULINK* and *X-Plane*. The code of the control algorithm is developed and stored in *SIMULINK*. At every sampling instant, the control algorithm receives the state measurement from *X-Plane* and outputs the control commands. The flight simulator

Table 5.1: Experimental helicopter model basic specifications.

Full length of fuselage	6.6 (ft)
Full width of fuselage	1 (ft)
Total height	2.12 (ft)
Main rotor radius	3 (ft)
Tail rotor radius	0.7 (ft)
Main rotor designed angular speed	1250 (RPM)
Tail rotor designed angular speed	5000 (RPM)
Full equipped weight	16 (lb)

receives the control commands and visualizes the flight response. The communication between *SIMULINK* and *X-Plane* takes place through a User Datagram Protocol (UDP) connection. The block diagram of the communication interconnections is depicted in Figure 5.1. The communication of the software packages is based on the work presented in [19]. The sampling rate is slightly variable around an average value. This average value can be chosen by the user and it has a maximum value of  $100Hz$ . Most of the experiments were conducted at  $60Hz$ .

### 5.10.2 Parametrized State Space Model

One of the most critical parts in the frequency domain identification method is the determination of the parametrized model. As indicated in Section 5.9, the key challenge is to decide about which stability derivatives should be included in the development of the parametrized model. The linear parametrized model used for parameter identification of the *Raptor 90 SE* is based on Mettler's model that is described in [70–72] for the Carnegie Mellon's *Yamaha R-50* and MIT's *X-Cell .60*.

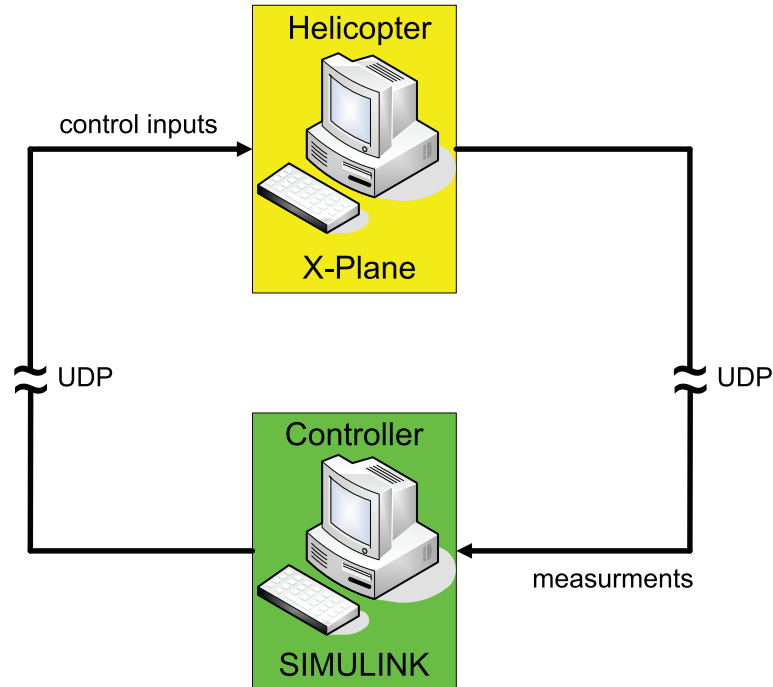


Figure 5.1: Block diagram of the experimental platform's communication interface.

The structure of the parametrized model proposed by Mettler has been already successfully used for the parametric identification of several helicopters, of different sizes and specifications [8, 10, 27, 28, 89, 90]. The ability of this model structure to establish a generic solution to the small scale helicopter identification problem is based on two important factors: The first factor is that Mettler's parametrized model provides a physically meaningful representation of the system dynamics. All stability derivatives included in this model are related to kinematic and aerodynamic effects of the fuselage and the main rotor. The second component is the ability to represent the several cross coupling effects that dominate the helicopter motion. This ability stems from the integration of the rotor model with the linearized equations of motion.

The adopted parametrized model in this work has two main differences with respect to Mettler's model. The first difference is the absence of the stabilizer bar dynamics. The stabilizer bar provides additional damping to the pitch and roll rates. This mechanism is not included in the *X-Plane Raptor 90 SE* helicopter model. In addition, as mentioned in Section 5.10.1, the Raptor does not include a gyro feedback. The absence of the gyro results in very high yaw rate response to

the pedal input. This fact was an obstacle in the application of the frequency sweeps of the pedal command. Small sinusoidal oscillation of the pedal resulted in very high deviations of the yaw rates. To tackle this problem, the pedal input used was:

$$u_{ped} = -\lambda_r r + \bar{u}_{ped} \quad (5.30)$$

where  $\lambda_r$  is a positive gain. This was a practical way to provide some additional feedback to the yaw response, in order to conduct the experiments. The frequency sweep excitation is applied through the input  $\bar{u}_{ped}$  instead of a direct transmission through  $u_{ped}$ . Although the experiments associated with the pedal command were conducted in closed loop, this did not create a problem in the identification procedure. The additional yaw damping from the feedback term in (5.30) is absorbed by the stability derivative  $N_r$ . In this case, it is important to clarify, that the parametrized model considers  $\bar{u}_{ped}$  as the pedal input command.

The parametrized model represents the linearized dynamics of the perturbed states and control inputs of the helicopter from a trimmed reference flight condition. The trim operating condition considered is the hover mode. Although the parametrized model is associated with the perturbed values of the states and inputs, for notation simplicity, the  $\delta$ 's defined in Section 5.8 will be dropped. The linear state-space parametrized model is given by:

$$\dot{x} = Ax + Bu$$

where the state and control vectors are, respectively:

$$x = [u \ v \ \theta \ \phi \ q \ p \ a \ b \ w \ r]^T \quad \text{and} \quad u_c = [u_{lon} \ u_{lat} \ u_{col} \ \bar{u}_{lat}]^T$$

The matrices  $A$  and  $B$  of the parametrized model are composed by the stability and control derivatives of the helicopter. The state space matrices of the parametrized linear model, for the *Raptor*

90 SE, are:

$$A = \begin{bmatrix} X_u & 0 & -g & 0 & 0 & 0 & X_a & 0 & 0 & 0 \\ 0 & Y_v & 0 & g & 0 & 0 & 0 & Y_b & 0 & 0 \\ 0 & 0 & 0 & 0 & 1 & 0 & 0 & 0 & 0 & 0 \\ 0 & 0 & 0 & 0 & 0 & 1 & 0 & 0 & 0 & 0 \\ M_u & M_v & 0 & 0 & 0 & 0 & M_a & 0 & 0 & 0 \\ L_u & L_v & 0 & 0 & 0 & 0 & 0 & L_b & 0 & 0 \\ 0 & 0 & 0 & 0 & -1 & 0 & -1/\tau_f & A_b & 0 & 0 \\ 0 & 0 & 0 & 0 & 0 & -1 & B_a & -1/\tau_f & 0 & 0 \\ 0 & 0 & 0 & 0 & 0 & 0 & Z_a & Z_b & Z_w & Z_r \\ 0 & N & 0 & 0 & 0 & N_p & 0 & 0 & N_w & N_r \end{bmatrix} \quad B = \begin{bmatrix} 0 & 0 & 0 & 0 \\ 0 & 0 & 0 & 0 \\ 0 & 0 & 0 & 0 \\ 0 & 0 & 0 & 0 \\ 0 & 0 & 0 & 0 \\ 0 & 0 & 0 & 0 \\ A_{lon} & A_{lat} & 0 & 0 \\ B_{lon} & B_{lat} & 0 & 0 \\ 0 & 0 & Z_{col} & 0 \\ 0 & 0 & N_{col} & N_{ped} \end{bmatrix}$$

To finalize the description of the parametrized model, we are going to provide some additional details for some of the key stability and control derivatives of the above matrices. Since the trim operating condition is the hover mode, it is assumed that the magnitude of the main rotor thrust will be equal to the weight of the helicopter. Therefore  $T_M = mg$ . Based on (4.31) the linear velocity stability derivatives can be approximated by:

$$X_a = \frac{1}{m} \frac{\partial X}{\partial a} = \frac{1}{m} \frac{\partial(-T_M a)}{\partial a} = -g$$

$$Y_b = \frac{1}{m} \frac{\partial Y}{\partial b} = \frac{1}{m} \frac{\partial(T_M b)}{\partial b} = g$$

The above equations impose a constraint to the values of  $X_a$  and  $Y_b$ , reducing the number of the unknown parameters in the parameter estimation phase. Based on (4.33), the stability derivatives for the pitch and roll moments, can be calculated by:

$$M_a = \frac{1}{\mathcal{I}_{xx}} \frac{\partial M}{\partial a} = \frac{1}{\mathcal{I}_{xx}} \frac{\partial[(l_h T_M + K_\beta)] a}{\partial a} = \frac{l_h mg + K_\beta}{\mathcal{I}_{xx}}$$

$$L_b = \frac{1}{\mathcal{I}_{yy}} \frac{\partial L}{\partial b} = \frac{1}{\mathcal{I}_{yy}} \frac{\partial[(l_h T_M + K_\beta)] b}{\partial b} = \frac{l_h mg + K_\beta}{\mathcal{I}_{yy}}$$

Some additional stability derivatives that require further clarification are the following:

- $A_{lat}$ ,  $B_{lon}$ : These stability derivatives are added to the flapping dynamics to capture potential unmodeled off-axis effects.
- $M_u$ ,  $M_v$  and  $L_u$ ,  $L_v$ : According to [70], these speed derivatives are included to capture the effect of airspeed to the angular dynamics. In theory, the angular dynamics are not affected by the airspeed. It would make more sense to include them in the rotor dynamics. However, as indicated in [70], the identification results are significantly better when those moments are included in the pitch and roll equations.

As mentioned earlier, the above parametrized model provides an excellent generic description of the small scale helicopter dynamics. The dimensions of the parametrized model can be increased by the inclusion of the stabilizer bar and gyro feedback dynamics. The challenge is determine which of those parameters should be included in the model and the determination of their arithmetic values.

### 5.10.3 Identification Setup

The identification procedure for the *Raptor 90 SE* starts with the collection of the experimental time domain flight data. For the collection of each flight data record, the helicopter is set to hover and a computerized frequency sweep excitation signal is applied to one of the four control inputs. While the frequency sweep is executed by the primary input of interest, the rest of the control commands should maintain the helicopter in the vicinity of the reference operating point. In addition, as indicated in Section 5.7, the secondary inputs should be as uncorrelated as possible from the main input. For each control input, five to six flight records are collected. The bandwidth of the excitation signal is ranging between  $0.3 \text{ rad/sec}$ - $28 \text{ rad/sec}$ . The computerized sweeps applied are based on (5.18)-(5.20). The minimum and maximum frequency of the excitation sweeps as well as the duration of the flight records, for each control input are given in Table 5.2.

Table 5.2: Frequency sweeps parameters. Those parameters correspond to (5.18)-(5.20).

	$\omega_{min}$	$\omega_{max}$	$T_{rec}$
	(rad/sec)	(rad/sec)	(sec)
$u_{lon}$	1	28	$7T_{max}$
$u_{lat}$	0.8	28	$7T_{max}$
$u_{col}$	0.3	27	$4T_{max}$
$\bar{u}_{ped}$	0.8	25	$7T_{max}$

For each flight record, the maximum frequency  $\omega_{max}$ , of the corresponding excitation signal is slightly varied from the value given in Table 5.2. This variation will produce a different excitation signal for each flight record. Identical excitations do not provide additional spectral information. The sampling rate of the experiments was set at  $60Hz$ . *X-Plane* provides availability to all the helicopter states and control inputs. The collected measurements for the identification process, are the following:

- Euler angles  $\phi, \theta, \psi$
- Angular velocities  $p, q, r$
- Body frame accelerations  $\dot{u}, \dot{v}$  and linear velocity  $w$ .

For translational motion, the body frame accelerations  $\dot{u}, \dot{v}$  were chosen instead of the velocity measurements  $u$  and  $v$ , respectively. The body frame acceleration measurements for these directions provide a more symmetrical response around the trim value, facilitating the calculations of the respective FFTs.

After the collection of the time domain experimental data, flight records excited by the same primary control input, are concatenated into a single record. The concatenated flight records are additionally filtered by a low pass filter with a cutoff frequency of  $13 Hz$ . The time domain experimental data are inserted to the *CIFER*<sup>©</sup> software. The three modules *FRESPID*, *MISOSA* and *COMPOSITE*, process the time domain experimental data to produce a high quality MIMO

Table 5.3: Selected frequency responses and their corresponding frequency ranges (in  $rad/sec$ ). The dashed entries indicate that the specific input-output pair was not included in the identification process. The bold entries highlight the *on-axis* responses.

	$u_{lon}$	$u_{lat}$	$u_{col}$	$\bar{u}_{ped}$
$\dot{i}$	<b>0.5-12.5</b>	–	–	–
$\dot{v}$	–	<b>0.51-22</b>	–	–
$w$	–	–	<b>0.20942-27</b>	–
$\phi$	–	<b>0.51-27</b>	–	–
$\theta$	<b>0.5-18</b>	–	–	–
$p$	0.5 – 18	<b>0.51-27</b>	–	–
$q$	<b>0.5-18</b>	0.51 – 27	–	–
$r$	–	0.51 – 27	1 – 10	<b>1-10</b>

frequency response database. This database is composed by the *conditioned frequency responses* and *partial coherences* for each input-output pair.

After the calculation of the flight data frequency responses, the next task is the extraction of the parametric model. *CIFER*<sup>©</sup> uses the *DERIVID* module to determine the parameters of the state space model, such that the estimated frequency responses from the latter, are the best fits to the flight data frequency responses.

The first action required by the parametric modeling process is the determination of the flight data frequency response input-output pairs, which will be included in the identification process. From these frequency responses, the frequency range of interest should also be determined. For the *Raptor 90 SE*, the selected frequency responses and their corresponding ranges are depicted in Table 5.3. The criterion for the frequency response selection is the coherence function  $\gamma^2$ . Frequency responses for which the coherence function has values greater than 0.7 over the desired frequency range of the model will be included. Frequency responses with  $\gamma \leq 0.7$  over their entire range are dropped.

After determining the frequency response pairs that will be included in the identification process, we are ready to proceed with the extraction of the state space model. This part initially requires the determination of the structure and order of the parametrized state space model. The selected parametrized model is described in Section 5.10.2. The next step is to decide about logical initial guesses for the values of the model parameters. *DERIVID* uses an optimization algorithm which calculates the parameter vector  $\Pi$ , such that the cost function defined in (5.3) for each input-output pair, is minimized. The optimization algorithm is based on an iterative robust secant algorithm that reduces the phase and magnitude error between the state space model and the flight data frequency responses. The execution of the optimization algorithm continues, until the average of the selected frequency responses cost functions  $J_a$ , is minimized.

The extraction of the parametric model is an iterative procedure, which continues until the most suitable stability and control derivatives of the state space model are selected. In order to determine which stability or control derivatives are going to participate in the state space model, apart from the frequency responses cost functions, *DERIVID* provides two additional statistical metrics. The first one is the percentage of the Cramér-Rao (CR) bound for each parameter. The CR bound gives a lower bound of the standard deviation of the parameter. A high CR bound indicates that the parameter is unreliable and should be disqualified from the model, or fixed to a certain value. The second statistical metric is the percentage of the insensitivity of each parameter with respect to the cost function. A high insensitive parameter will have a minimal or any effect to the calculation of the cost function. Therefore, this parameter should be dropped from the model. A summary of the guidelines for the selection of the state space model's derivatives based on [105] is:

- $J_a \leq 100$
- $CR\% \leq 20\%$
- $Insensitivity\% \leq 10\%$

The identified stability and control derivatives for the *Raptor 90 SE*, with their respective CR bound and insensitivity percentage, can be seen in Table 5.4. The on-axis frequency responses,

obtained by the flight data and those predicted by the state space model are given in Figure 5.2. The same comparison for the off-axis responses is given in Figure 5.3. The identification results illustrate a very good fit between the frequency responses obtained by the flight data and those predicted by the state space model. The cost value for each frequency response of the input-output pairs that participated in the identification process, is depicted in Table 5.5. The average cost  $J_a$ , is well below the suggested guideline value. Those results indicate that the identification procedure has accurately extracted a linear state space model of the *Raptor 90 SE* dynamics.

Table 5.4 indicates that some of the identified parameters exhibit high CR bounds and insensitivities. The larger values are encountered in the translational velocity damping derivatives  $X_u$  and  $Y_v$ . The same issue with the specific parameters was also encountered for the *Yamaha R50* model described in [70]. Although the sign and the value of this parameters makes sense, the statistical metrics indicate that they are completely unreliable. According to [70], the large uncertainty of the specific stability derivatives resulted from the lack of low frequency excitation. High statistical metrics are also associated with the speed derivatives of the roll and pitch rates. In particular,  $M_v$  and  $L_u, L_v$  exhibit very high CR bounds and insensitivities. Those parameters could be dropped from the model without sacrificing the accuracy of the identification results. However, they were intentionally preserved to keep the final state space dynamics as close as possible to the parametrized model.

Finally, the mismatch in the heave responses depicted in Figure 5.2, indicate that *X-Plane* accounts for the main rotor inflow dynamics. The most important parameters of the state space model are the main rotor flapping spring derivatives  $M_a$  and  $L_b$ . The high value of those two variables indicate the the *Raptor 90 SE* is a super maneuverable and highly agile helicopter. This was an anticipated result since small scale helicopters of this type have very rigid blades. Apart from the excellent fit of the actual and predicted frequency responses, the identification result indicate that the flight simulator may duplicate real flight applications.

Table 5.4: Linear state space model identified parameters. The dashed entries indicate that the specific derivatives were not included in the state space model.

	Value	CR %	Insensitivity %		Value	CR %	Insensitivity %
<b>A matrix</b>							
$X_u$	-0.03996	118.7	58.24	$B_a$	0.6168	9.090	1.923
$Y_v$	-0.05989	127.4	62.24	$Z_a$	—	—	—
$M_u$	0.2542	12.25	4.195	$Z_b$	—	—	—
$M_v$	-0.06013	28.95	7.091	$Z_w$	-2.055	7.351	2.546
$M_a$	307.571	6.815	1.097	$Z_r$	—	—	—
$L_u$	-0.02440	36.81	10.63	$N$	2.982	6.991	1.908
$L_v$	-0.1173	246.6	94.13	$N_p$	—	—	—
$L_b$	1172.4817	5.751	1.462	$N_w$	-0.7076	15.95	4.400
$A_b$	0.7713	8.896	1.860	$N_r$	-10.71	6.729	1.233
$g$	-9.389	3.331	0.9953	$1/\tau_f$	30.71	7.474	0.9838
<b>B matrix</b>							
$A_{lon}$	4.059	3.005	0.9285	$Z_{col}$	-13.11	5.026	1.688
$A_{lat}$	-0.01610	14.66	3.356	$N_{col}$	3.749	7.161	2.602
$B_{lon}$	-0.01017	23.79	7.206	$N_{ped}$	26.90	6.189	1.825
$B_{lat}$	4.085	2.900	0.8280				

Table 5.5: Transfer functions costs for each input-output pair.

$\dot{u}/u_{lon}$	54.087
$\theta/u_{lon}$	56.108
$p/u_{lon}$	48.502
$q/u_{lon}$	60.196
$\dot{v}/u_{lat}$	29.704
$\phi/u_{lat}$	36.271
$p/u_{lat}$	38.068
$q/u_{lat}$	55.421
$r/u_{lat}$	42.551
$w/u_{col}$	89.496
$r/u_{col}$	20.147
$r/\bar{u}_{ped}$	20.178
<b>Average</b>	<b>45.894</b>

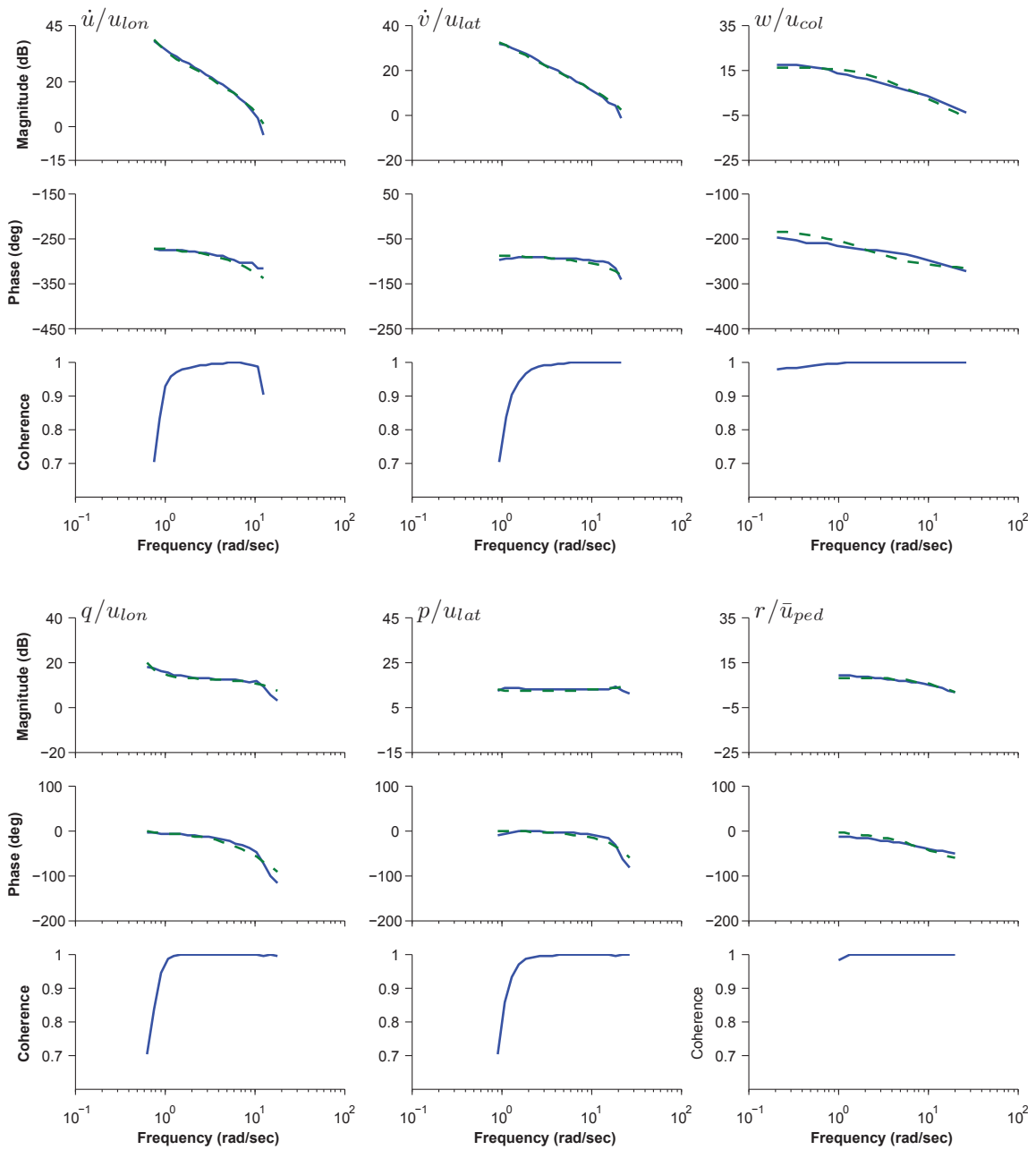


Figure 5.2: On-axis frequency responses of the flight data (solid line) and frequency responses predicted by the state space model (dashed line).

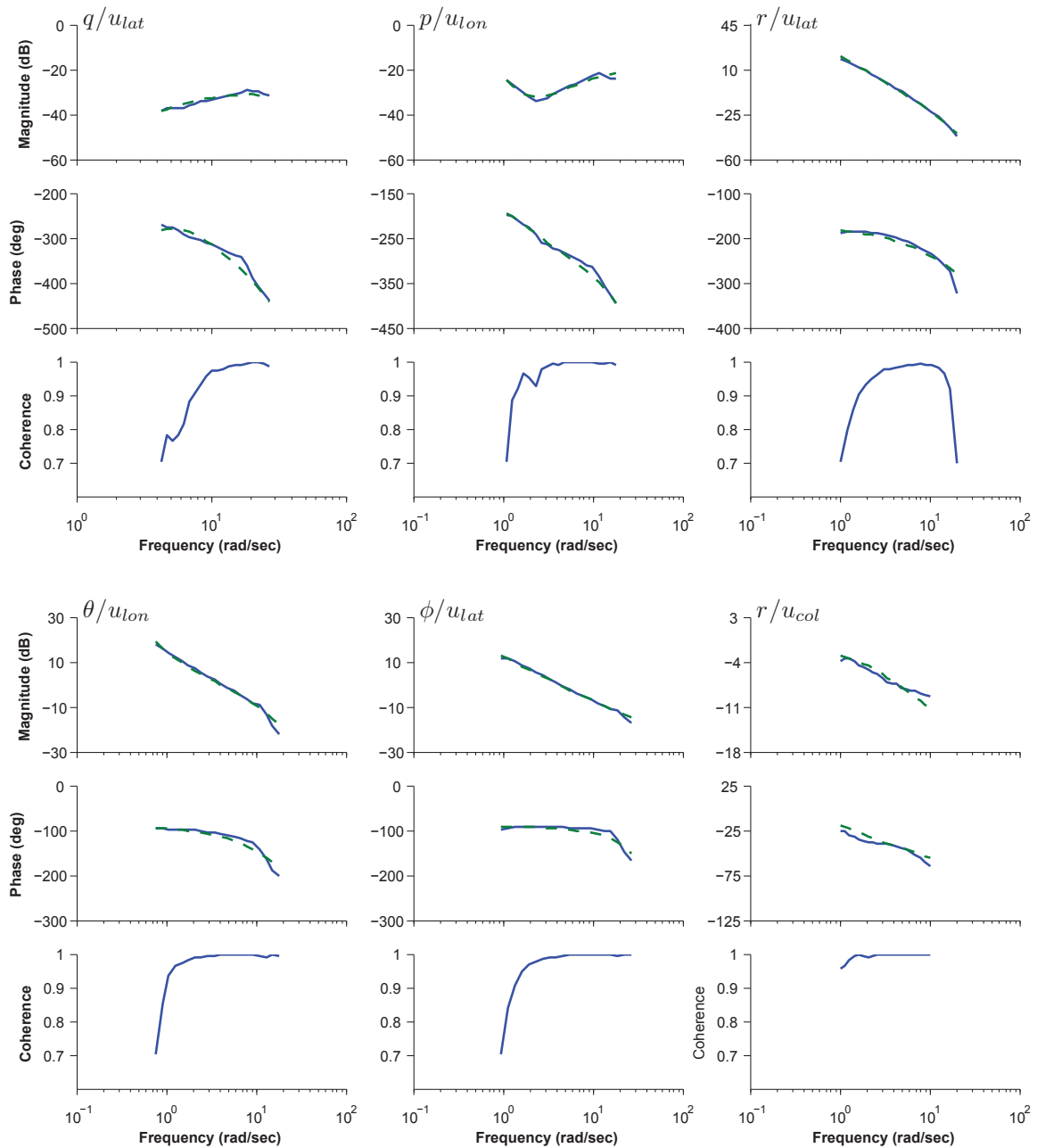


Figure 5.3: Off-axis frequency responses of the flight data (solid line) and frequency responses predicted by the state space model (dashed line).

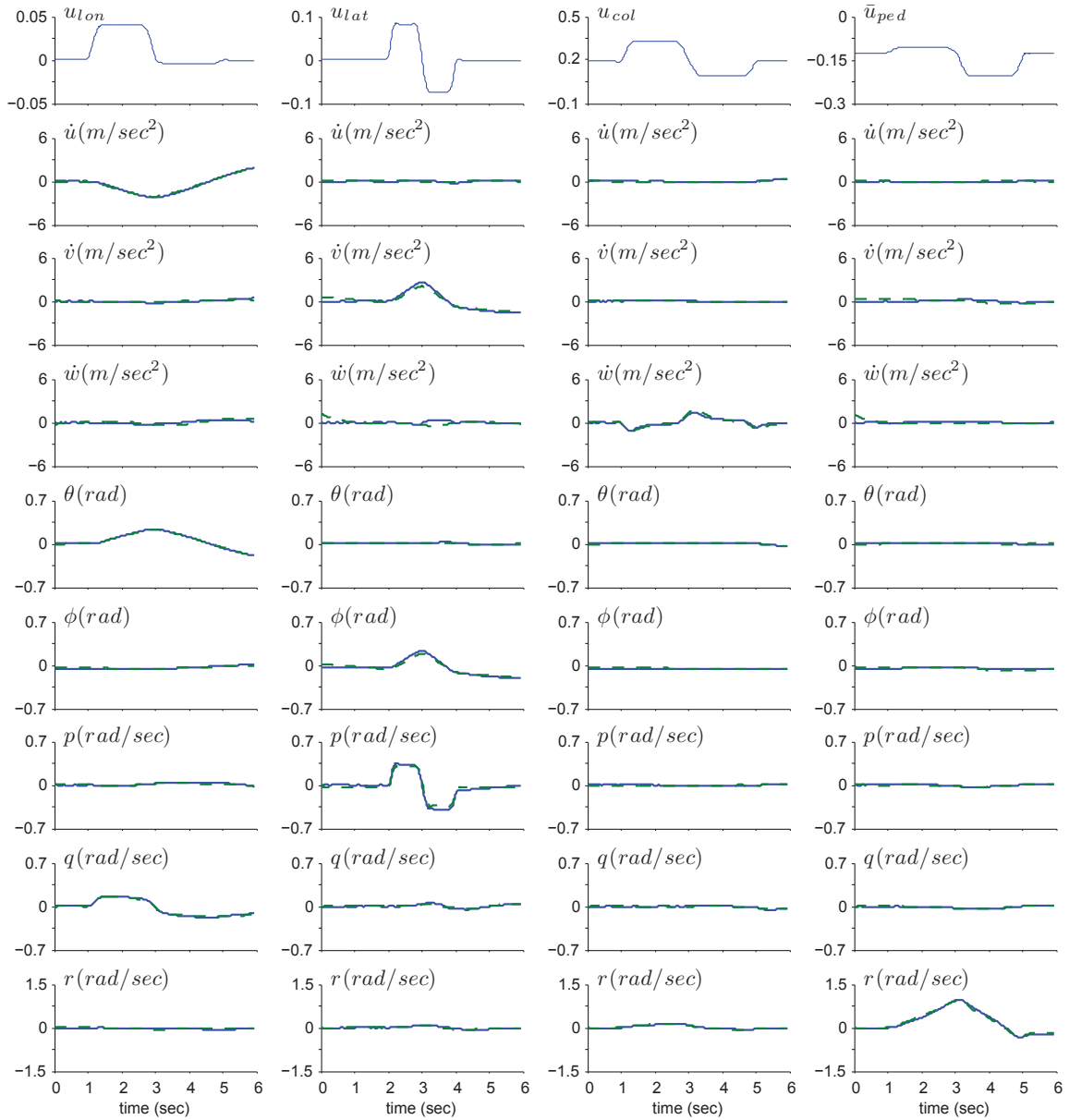


Figure 5.4: Time domain validation.

#### 5.10.4 Time Domain Validation

The final step of the identification procedure is the validation of the extracted state space model in the time domain. The time domain validation is important for evaluating the predictive accuracy and limitations of the identified model. The time domain flight data used for the validation part are obtained by applying special control inputs which are dissimilar with the ones used in the identification process. These inputs are steps or roughly symmetric doublets. These types of inputs are used due to their relative large frequency content [70]. The time domain responses of the identified model obtained by the integration of the state space equations, are compared with the corresponding responses of the flight data. The inputs to the state space model used for the integration process are identical with the ones obtained by the flight data.

To obtain the validation flight data, four individual flight records are collected, each corresponding to one of the control inputs. In every individual flight record, a roughly symmetric doublet is applied by the corresponding primary input, while the rest of the control commands retain their trimmed value. The doublet should be applied in such a way that the on-axis responses of the corresponding input are sufficiently diverged from the trimmed condition. A large deviation from the operating point will reveal the identified model predictive limitations. Before each doublet is applied, the helicopter is set to hover mode. The time domain validation comparison results are depicted in Figure 5.4, in a similar way with [70]. The time domain responses for each record are illustrated in columns. The first row shows the executed doublet of each primary control input. The validation comparison indicates an excellent fit between the predicted values from the linear state space model and the flight data. Therefore, the identified model provides a reliable dynamic representation of the helicopter around the hovering operating condition and it is appropriate for control design.

## 5.11 Remarks

The identification process described in this Chapter considers hovering as the reference flight operating point. Therefore, the model is limited to an area of the flight envelope around the specific operating condition. To derive a linear model for a different flight mode, the same procedures should be repeated. However, the execution of the frequency sweeps for a different reference flight condition from hover is a very tedious process. For example, in the case of forward flight, the helicopter should cruise in a constant translational velocity when the sweeps are applied. This experimental procedure introduces practical limitations. Firstly, it is very difficult to sustain a constant translational velocity in all the flight records. In addition, the retainment of the helicopter around the desired operating point when the sweeps are applied is an additional limiting factor. This limitation is more apparent when the low frequency portion of the sweep is executed. To this extent, the experimental data acquired from the cruise mode have inferior quality compared with the data collected when the helicopter is in hover. Therefore, the system identification modeling method has potential shortcomings in the development of linear models which correspond to flight modes different from hover. Having decided the order and the structure of a generic parametric linear helicopter model at hover, the next step is the development of a systematic procedure for the design of linear helicopter flight controllers. The next Chapter provides a position and heading tracking controller based on the linear helicopter model.

The individual experiments are arranged in columns for the doubled -input experiments. The first row shows the piloted doublet applied to the respective control input and the remaining rows show the responses to the vehicles states.

## Chapter 6: Linear Tracking Controller Design for Small Scale Unmanned Helicopters

In the previous Chapter we provided an analytical methodology for the extraction of a linear dynamic model for a small scale helicopter based on [70, 105]. Modern control techniques are model based, in the sense that the controller architecture depends on the dynamic description of the system. Therefore, the knowledge of the helicopter linear dynamic model is very valuable for the design of autonomous flight controllers. This Chapter presents a systematic procedure for the design of a flight controller based on the linear dynamic representation of the helicopter. The controller objective is for the helicopter to track predefined reference trajectories of the inertial position and the yaw angle.

### 6.1 Helicopter Linear Model

The goal of this Section is to derive a flight controller based on the helicopter's linear dynamic model. The proposed controller should also be applicable to any small scale helicopter. This claim requires the adoption of a nominal linear dynamic model structure, which is capable of capturing the dynamic behavior of a wide family of small scale helicopters. An ideal solution to this requirement is the use of the parametrized model described in Section 5.10.2 as a basis for the controller design.

The specific model represents the dynamic response of the helicopter perturbed state vector from the reference flight condition. In this case, the reference operating condition is hover. At hover, the trim values of the linear and angular velocity are:

$$v_o^B = \omega_o^B = [0 \ 0 \ 0]^T \quad (6.1)$$

From the above equations it is apparent that when the helicopter operates around hover, the helicopter's state is equal to the perturbed state vector about the reference operating point. The helicopter linear model is based on Section 5.10.2 and it is repeated here for clarification purposes.

The adopted state space model is:

$$\dot{x} = Ax + Bu_c \quad (6.2)$$

where the state and control vectors are:

$$x = [u \ v \ \theta \ \phi \ q \ p \ a \ b \ w \ r \ \psi]^T \quad \text{and} \quad u_c = [u_{lon} \ u_{lat} \ u_{col} \ u_{lat}]^T \quad (6.3)$$

The matrices  $A$  and  $B$  of the state space model are given by:

$$A = \begin{bmatrix} X_u & 0 & -g & 0 & 0 & 0 & X_a & 0 & 0 & 0 & 0 \\ 0 & Y_v & 0 & g & 0 & 0 & 0 & Y_b & 0 & 0 & 0 \\ 0 & 0 & 0 & 0 & 1 & 0 & 0 & 0 & 0 & 0 & 0 \\ 0 & 0 & 0 & 0 & 0 & 1 & 0 & 0 & 0 & 0 & 0 \\ M_u & M & 0 & 0 & 0 & 0 & M_a & 0 & 0 & 0 & 0 \\ L_u & L_v & 0 & 0 & 0 & 0 & 0 & L_b & 0 & 0 & 0 \\ 0 & 0 & 0 & 0 & -1 & 0 & -1/\tau_f & A_b & 0 & 0 & 0 \\ 0 & 0 & 0 & 0 & 0 & -1 & B_a & -1/\tau_f & 0 & 0 & 0 \\ 0 & 0 & 0 & 0 & 0 & 0 & Z_a & Z_b & Z_w & Z_r & 0 \\ 0 & N & 0 & 0 & 0 & N_p & 0 & 0 & N_w & N_r & 0 \\ 0 & 0 & 0 & 0 & 0 & 0 & 0 & 0 & 0 & 1 & 0 \end{bmatrix}$$

$$B^T = \begin{bmatrix} 0 & 0 & 0 & 0 & 0 & 0 & A_{lon} & B_{lon} & 0 & 0 & 0 \\ 0 & 0 & 0 & 0 & 0 & 0 & A_{lat} & B_{lat} & 0 & 0 & 0 \\ 0 & 0 & 0 & 0 & 0 & 0 & 0 & 0 & Z_{col} & N_{col} & 0 \\ 0 & 0 & 0 & 0 & 0 & 0 & 0 & 0 & 0 & N_{ped} & 0 \end{bmatrix}$$

The above state space representation is slightly different from the parametrized model of Section 5.10.2, since it includes the yaw dynamics given by  $\dot{\psi} = r$ . The yaw dynamics are excluded from the identification process since they do not include any unknown stability derivatives and also the yaw is decoupled from the rest of the state variables. However, the controller design requires the inclusion of the yaw to the state space model. The overall dynamics constitute a coupled linear system of the helicopter motion variables and the main rotor flapping dynamics.

The order of the above model can be increased by including the dynamics of the stabilizer bar and the yaw damping system. These two subsystems provide additional damping to the angular velocity dynamics. Since they constitute additional feedback sources of the angular dynamics, their presence in the state space system does not influence the controller design. Therefore, their effect has been omitted from the helicopter model.

The proposed linear model (usually with the inclusion of the yaw gyro dynamics) has been successfully adopted for control applications in a large number of small scale unmanned helicopters [8, 10, 27, 28, 89, 90]. To this extent, the linear model proposed by [70] provides a generalized and physically meaningful solution to the development of practical linear models for small scale helicopters. For any particular small scale helicopter, the numeric values of the matrices  $A$  and  $B$  entries can be estimated by following the identification procedure described in the previous Chapter.

## 6.2 Controller Outline

Having established the helicopter linear dynamic model, the next step is the design of the autonomous flight controller. The controller's ultimate objective is for the helicopter to autonomously track predefined bounded position and heading reference trajectories. The linear model given in (6.2) does not include the helicopter position dynamics. Therefore, the controller design starts with the tracking problem of a reference translational velocity and heading profile. The integration of the position tracking to the control problem follows. The initial output of interest of the

helicopter is:

$$y = [u \ v \ w \ \psi]^T = Cx \quad (6.4)$$

The first design task is for the helicopter to track the reference output  $y_r = [u_r \ v_r \ w_r \ \psi_r]^T$ . The tracking problem requires the determination of the control signal  $u_c(t)$  as a function of the state variables of the vector  $x(t)$  and the reference output  $y_r(t)$  (with its higher derivatives) such that:

$$\lim_{t \rightarrow \infty} \|y(t) - y_r(t)\| = 0 \quad (6.5)$$

while the state of the system  $x(t)$  and, thus, the control input  $u_c(t)$  remain bounded for any bounded reference output  $y_r(t)$ . An additional difficulty of the tracking control problem is the availability of the state variables from measurements. Not all of the helicopter states can be measured, hence only a subset of the state variables can be used by the controller for feedback purposes. In real life applications, only the helicopter motion state variables can be directly measured. On the other hand, the flapping angles are typically absent from the available measurements. It is assumed that there is availability of the following measurement vector:

$$y_m = [u \ v \ w \ p \ q \ r \ \theta \ \phi \ \psi]^T = C_m x \quad (6.6)$$

The complete state can be reconstructed for control purposes by a Kalman filter or a state estimator [3, 23, 41]. Both of these choices increase the system dynamics order. However, in manned flight applications, the pilot is able to operate the helicopter without accounting for the flapping angles. Therefore, we set the same requirement for the unmanned case restricting the controller's feedback information only to the measured vector  $y_m$ . This problem is classified as output feedback. When  $y_m = x$ , then we have full state state feedback.

In the case of linear systems, the tracking problem with output feedback can be tackled with two different approaches. Tracking with integral control and tracking via the use of an internal model. In the internal model approach, the reference output signal is generated by a fixed reference dynamic system driven by a bounded input. This reference system is called *internal model*.

The structure of the internal model is used by the controller yielding a dynamic feedback scheme. Typical application of such control design is met when the reference output is a constant signal or sinusoidal with constant frequency [43]. The internal model approach has very important robust and adaptive properties, however the design is relatively complex. In the case of MIMO systems the generated internal model should consider the relative degree vector that corresponds to the output (the relative degree vector components indicates how many time each output should be differentiated until the input appears). Likewise with the integral control, the use of the internal model becomes relatively complicated when the desired output is an arbitrary continuous signal of time. More details about the internal model approach can be found in [9, 36].

The use of integral control for the tracking problem results in the design of a dynamic feedback controller. Integral control provides a reliable and consistent solution when the desired output has constant values over time. However, in the case of a time varying output profile, the integral control design requires the determination of a steady state response  $x_{ss}(t)$  and a steady state control input  $u_c^{ss}(t)$ , such that when  $y(t)$  tends to  $y_r(t)$ , the following equality holds:

$$\dot{x}_{ss} = Ax_{ss} + Bu_c^{ss} \quad (6.7)$$

The determination of the pair  $(x_{ss}, u_c^{ss})$  is a difficult task, rendering the integral control design impractical for the tracking problem of a time varying output. More details about the integral control of linear systems can be found in [23, 43].

Instead of following the above standard methodologies, we adopt a tracking design which is simple, mathematically consistent and well suited to the specific problem. The first part of the design involves the determination of a desired state vector  $x_d$  which is composed only by the components of the reference output vector  $y_r$  and their higher derivatives. Denote  $e = x - x_d$  the error between the actual helicopter state and its desired value. The desired vector  $x_d$  should be chosen in such a way that, given:

$$\lim_{t \rightarrow \infty} \|e(t)\| = 0 \quad \text{then} \quad \lim_{t \rightarrow \infty} \|y(t) - y_r(t)\| = 0 \quad (6.8)$$

The proposed controller design provides a recursive methodology for the derivation of a desired state vector  $x_d$  and a desired control input  $u_c^d$  that satisfies (6.8) and also:

$$\dot{x}_d = Ax_d + Bu_c^d \quad (6.9)$$

The role of the desired state vector  $x_d$  and the control input  $u_c^d$  is identical with the steady state vector  $x_{ss}$  and the input vector  $u_c^{ss}$  which is required by the integral control methodology. The contribution of the proposed design is the development of a simple recursive procedure for the derivation of the pair  $(x_d, u_c^d)$  that satisfies (6.8)-(6.9).

The choice of the pair  $(x_d, u_c^d)$  is based on the backstepping design approach. Details about the backstepping design methodology can be found in the Appendix A. In the particular case the backstepping design is not used for the stabilization of the tracking error but it is restricted to the determination of the desired state and control input vectors. Backstepping provides a systematic methodology for the output tracking problem of systems in feedback form.

Due to the presence of the stability derivatives  $X_a$  and  $Y_b$  in (6.2), the helicopter model can not be categorized in this class of systems. A common simplification practice, followed in [37, 47, 66], is to neglect the effect of the lateral and longitudinal forces produced by the TPP tilt. Those parasitic forces have a minimal effect on the translational dynamics compared to the propulsion forces produced by the stability derivatives  $X_\theta$  and  $Y_\phi$  (in (6.2) are denoted by  $-g$  and  $g$ , respectively). This assumption is physically meaningful and results into a linear system of feedback form.

Systems of strict-feedback form are feedback linearizable and therefore differentially flat. The differentially flatness property is the key attribute of the approximated system to which the controller design is based on. A system is called differentially flat when there exists output functions (called flat outputs) such that all the state and input vectors can be expressed in terms of the flat outputs and their higher derivatives [48]. Details about the differential flatness property of nonlinear systems may be found in [22, 107]. The concept of differential flatness has been also

used in [47, 48] for the development of a nonlinear controller based on nonlinear inversion for the helicopter tracking problem.

Having defined the desired state  $x_d$  and control vector  $u_c^d$ , we introduce the stabilizing controller of the system. The controller signal is constructed by the following superposition:

$$u_c = u_c^d + u_c^{fb} \quad (6.10)$$

Then the error dynamics take the form:

$$\dot{e} = Ae + Bu_c^{fb} \quad (6.11)$$

The above system is identical with the system given in (6.2). The difference is that the state space vector is substituted by the error vector. The second control component can be chosen from a variety of output feedback techniques, such that the error  $e$  is rendered globally asymptotically stable (GAS).

### 6.3 Decomposing the System

It is emphasized that the controller design must incorporate the physical limitations of helicopter flight. A common mistake in the development of flight controllers is the blind adoption of a mathematical control scheme without considering the physical structure of the helicopter model. It is typical that the flight control problem is forced to suit a specific controller design rather than the controller design being tailored based on the problem. A challenging and rigorous mathematical control scheme will perform significantly poor in a real life application if the fundamental notion of helicopter flight is disregarded by the designer.

The helicopter piloting fundamental intuition dictates that the cyclic commands  $u_{lon}$  and  $u_{lat}$ , are used to manipulate the pitch and roll moments with ultimate objective the production of translational motion. The collective command  $u_{col}$  controls the magnitude of the thrust of the main rotor producing the necessary lifting force, while the pedal command controls the heading of the

helicopter. To this extent the ideal solution is for each control command to be as much independent as possible from the others. The ideal solution to the problem is to construct 4 independent SISO feedback loops for each control input. However, since the system is a highly coupled linear system this approach can not guarantee a rigorous and mathematically consistent stability analysis.

Having said that, a close inspection of the model structure given in (6.2), indicates that the helicopter dynamics can be separated in to two interconnected subsystems. The first subsystem represents the helicopter longitudinal and lateral motion. The second subsystem represents the coupled yaw and heave dynamics. In particular, the lateral-longitudinal subsystem is given by:

$$\dot{x}_{ll} = A_{ll}x_{ll} + B_{ll}u_{ll} \quad (6.12)$$

where:

$$x_{ll} = [u \ v \ \theta \ \phi \ q \ p \ a \ b]^T \quad \text{and} \quad u_{ll} = [u_{lon} \ u_{lat}]^T \quad (6.13)$$

and:

$$A_{ll} = \begin{bmatrix} X_u & 0 & -g & 0 & 0 & 0 & X_a & 0 \\ 0 & Y_v & 0 & g & 0 & 0 & 0 & Y_b \\ 0 & 0 & 0 & 0 & 1 & 0 & 0 & 0 \\ 0 & 0 & 0 & 0 & 0 & 1 & 0 & 0 \\ M_u & M_v & 0 & 0 & 0 & 0 & M_a & 0 \\ L_u & L_v & 0 & 0 & 0 & 0 & 0 & L_b \\ 0 & 0 & 0 & 0 & -1 & 0 & -1/\tau_f & A_b \\ 0 & 0 & 0 & 0 & 0 & -1 & B_a & -1/\tau_f \end{bmatrix} \quad B_{ll} = \begin{bmatrix} 0 & 0 \\ 0 & 0 \\ 0 & 0 \\ 0 & 0 \\ 0 & 0 \\ 0 & 0 \\ A_{lon} & A_{lat} \\ B_{lon} & B_{lat} \end{bmatrix} \quad (6.14)$$

The yaw-heave dynamics subsystem is given by:

$$\dot{x}_{yh} = A_{yh}x_{yh} + B_{yh}u_{yh} + D_{yh}x_{ll} \quad (6.15)$$

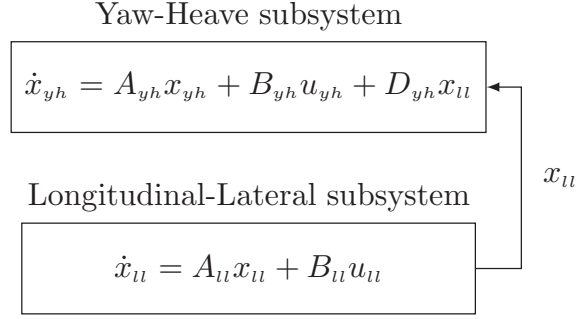


Figure 6.1: Interconnection of the two helicopter dynamics subsystems.

where:

$$x_{yh} = [\psi \ w \ r]^T \quad \text{and} \quad u_{yh} = [u_{col} \ u_{ped}]^T \quad (6.16)$$

and:

$$A_{yh} = \begin{bmatrix} 0 & 0 & 1 \\ 0 & Z_w & Z_r \\ 0 & N_w & N_r \end{bmatrix} \quad B_{yh} = \begin{bmatrix} 0 & 0 \\ 0 & Z_{col} \\ N_{ped} & N_{col} \end{bmatrix}$$

$$D_{yh} = \begin{bmatrix} 0 & 0 & 0 & 0 & 0 & 0 & 0 & 0 \\ 0 & 0 & 0 & 0 & 0 & 0 & Z_a & Z_b \\ 0 & 0 & 0 & 0 & 0 & 1 & 0 & 0 \end{bmatrix} \quad (6.17)$$

The interconnection of the two subsystems is shown in Figure 6.1. The controller design requires that the following assumptions associated with the helicopter linear model given in (6.2), should hold:

**Assumption 6.1.** The matrix pairs  $(A_{ll}, B_{ll})$  and  $(A_{yh}, B_{yh})$  are controllable.

**Assumption 6.2.** The matrix  $B \in \mathbb{R}^{8 \times 4}$  has four linearly independent rows.

**Assumption 6.3.** The stability derivatives  $g$ ,  $M_a$  and  $L_b$  are nonzero.

The above assumptions are substantially necessary conditions required by the controller design. If the linear model does not satisfy all of the above conditions then most likely the modeling

identification process has lead to erroneous results. They reflect the fact that the linear model has to be physically meaningful. Intuitively, from manned flight applications, the pilot commands can regulate the position and heading of the helicopter in all of the configuration space. Regarding Assumption 6.1, lack of controllability indicates poor identification results, wrong model structure or a helicopter that can not fly properly! In addition, each input must have a direct effect to the helicopter's motion, therefore, Assumption 6.3 should hold as well. Finally, if  $M_a = 0$  or  $L_b = 0$  it implies that no moments are transmitted to the helicopter. Therefore, the above assumptions provide a validity check of the helicopter linear model.

Before we proceed, we introduce a preliminary control action for the input vectors  $u_{ll}$ ,  $u_{yh}$  that cancels out the coupling effect of the control derivatives and normalizes the  $B_{ll}$  and  $B_{yh}$  matrices, respectively. Hence:

$$u_{ll} = (B_{ll}^n)^{-1}v_{ll} \quad u_{yh} = (B_{yh}^n)^{-1}v_{yh} \quad (6.18)$$

where:

$$B_{ll}^n = \begin{bmatrix} A_{lon} & A_{lat} \\ B_{lon} & B_{lat} \end{bmatrix} \quad B_{yh}^n = \begin{bmatrix} 0 & Z_{col} \\ N_{ped} & N_{col} \end{bmatrix} \quad (6.19)$$

Based on Assumption 6.3 the above inverse matrices are nonsingular. Singularity in any of them indicates erroneous parameter values. Substituting the above preliminary control actions the two subsystems become:

$$\dot{x}_{ll} = A_{ll}x_{ll} + \bar{B}_{ll}v_{ll} \quad (6.20)$$

$$\dot{x}_{yh} = A_{yh}x_{yh} + \bar{B}_{yh}v_{yh} + D_{yh}x_{ll} \quad (6.21)$$

where:

$$\bar{B}_{ll} = \begin{bmatrix} 0_{6 \times 2} \\ I_2 \end{bmatrix} \quad \bar{B}_{yh} = \begin{bmatrix} 0_{2 \times 1} \\ I_2 \end{bmatrix} \quad (6.22)$$

From the above analysis, the initial system is now viewed as two interconnected subsystems in cascade form. The backstepping design is performed independently for each subsystem resulting in the cascaded error dynamics of the helicopter. Stabilization of nonlinear systems in cascade has been extensively studied in [63, 94, 98]. Contrary to the nonlinear systems, the case for the LTI systems is much more easier in terms of analysis. If the controller is designed such that the two error dynamics subsystems are rendered GAS (by ignoring the interconnection effect), then the complete error dynamics system is rendered GAS, as well. This approach is based on the *separation principle*, which emerges from the *superposition property* of LTI systems. The stability analysis of the controller design is given in detail in the following Sections.

At this point, the controller structure requires the design of two independent feedback loops for each subsystem. This approach results in a mathematically consistent and systematic methodology, which reflects the intuitive flight notion. The lateral/longitudinal motion is regulated independently from the heading and vertical motion of the helicopter. The same decomposition of the helicopter dynamics is also reported in [109].

## **6.4 Velocity and Heading Tracking Control**

This Section provides a detailed presentation of the controller design for the velocity and heading tracking of the helicopter. The control problem is focused on the design of two feedback loops for each subsystem. After the introduction of the two feedback loops the stability analysis of the overall system dynamics is given.

### **6.4.1 Lateral-Longitudinal Dynamics**

The longitudinal and lateral motion of the helicopter are not directly controlled through the cyclic inputs but rather via a sequence of intermediate events. The cyclic inputs produce pitch and roll moments to the helicopter fuselage. Those moments result in a change of the pitch and roll attitude angles. The attitude change results in the tilt of the helicopter main rotor disc. By tilting

the rotor disc the main rotor thrust is also tilted to produce the necessary propulsion forces for lateral and longitudinal motion. The effect of the translational forces produced by the flapping motion of the the main rotor is parasitic and negligible compared to the main source of propulsion, which is the roll and pitch tilt of the main rotor.

As indicated in Section 6.2, neglecting the effect of the stability derivatives  $X_a$  and  $Y_b$  is a common practice that results in a more physically meaningful design. When the latter stability derivatives are omitted from the helicopter model, the lateral-longitudinal dynamics have a strict-feedback form.

The complete description of the longitudinal-lateral subsystem is given by:

$$\begin{aligned}\dot{x}_u &= A_u^{fb} x_u + \bar{B}_u v_u \\ y_u &= C_u x_u \\ y_u^m &= C_u^m x_u\end{aligned}\tag{6.23}$$

where:

$$\begin{aligned}x_u &= [u \ v \ \theta \ \phi \ q \ p \ a \ b]^T \\ v_u &= [v_{lon} \ v_{lat}]^T \\ y_u &= [u \ v]^T \\ y_u^m &= [u \ v \ \theta \ \phi \ q \ p]^T\end{aligned}$$

In the above equations  $y_u^m$  is the measurement vector available for feedback and  $y_u$  is the output of the subsystem. The reference output vector is  $y_u^r = [u_r \ v_r]^T$ . The matrix  $A_u^{fb}$ , is identical to  $A_u$  with the only difference that the stability derivatives  $X_a$  and  $Y_b$  are omitted. The interconnection of the approximated longitudinal-lateral subsystem is shown in Figure 6.2.

From Section 6.2, the first goal of the controller design for this subsystem is to determine a desired state vector  $x_u^d$  and a desired control input  $v_u^d$ , with both of them being functions of the  $y_u^r$

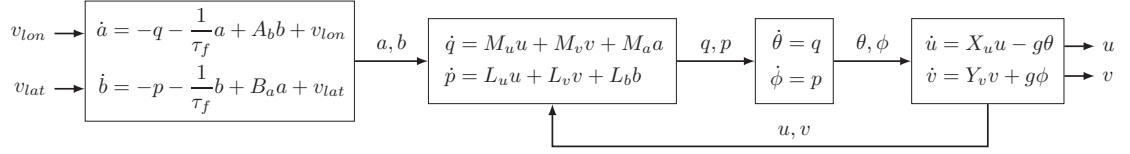


Figure 6.2: Strict-feedback interconnection of the longitudinal-lateral helicopter dynamics subsystem. The terms associated with the  $X_a$  and  $Y_b$  stability derivatives are disregarded.

components and their higher derivatives, such for the error  $e_u = x_u - x_u^d$  given that:

$$\lim_{t \rightarrow \infty} \|e_u\| = 0 \quad \text{then} \quad \lim_{t \rightarrow \infty} \|y_u(t) - y_u^r(t)\| = 0 \quad (6.24)$$

To do so the control law of this subsystem is obtained by the following superposition:

$$v_u = v_u^d + v_u^{fb} = \begin{bmatrix} v_{lon}^d \\ v_{lat}^d \end{bmatrix} + \begin{bmatrix} v_{lon}^{fb} \\ v_{lat}^{fb} \end{bmatrix} \quad (6.25)$$

The initial task is to select the pair  $(x_u^d, v_u^d)$  such that they satisfy the requirement of (6.24) and also:

$$\dot{x}_u^d = A_u^{fb} x_u^d + \bar{B}_u v_u^d \quad (6.26)$$

If the pair  $(x_u^d, v_u^d)$  satisfies the above equation then the error dynamics become:

$$\dot{e}_u = A_u^{fb} e_u + \bar{B}_u v_u^{fb} \quad (6.27)$$

The final step is the selection of an output feedback control law  $v_u^{fb}$  which stabilizes  $e_u$  such that the tracking objective of (6.24) is achieved.

For the derivation of the desired state vector  $x_u^d$  and control input  $v_u^d$  we are going to apply a recursive procedure based on the backstepping methodology. The backstepping approach is ideal for the control design of systems in feedback form. In this case, however, the backstepping procedure is not used for the stabilization of the system but it is only restricted to the derivation of the pair  $(x_u^d, v_u^d)$  such that (6.24) and (6.26) are satisfied. The applicability of this approach

is based on the fact that the longitudinal-lateral subsystem is in strict-feedback form therefore it is differentially flat. Therefore, the derivation of the desired state and the nominal desired input based on the reference output is feasible.

The derivation of the error dynamics and the selection of the desired states and inputs is going to take place simultaneously. The basic idea of the recursive procedure is to start from the top state equations of the subsystem and gradually derive the desired state variables and the error dynamics of each level by moving downwards in each step, until the bottom set of state equations is reached. In each step the desired values of the state variables of lower levels is chosen in such a way that they cancel out the desired values of state variables of higher levels.

The procedure begins by deriving the error dynamics of the translational velocity variables. Therefore, one has:

$$\begin{aligned}\dot{e}_u &= \dot{u} - \dot{u}_d = -\dot{u}_d + X_u \underbrace{(e_u + u_d)}_u - g \underbrace{(e_\theta + \theta_d)}_\theta \\ &= -\dot{u}_d + X_u u_d - g\theta_d + X_u e_u - g e_\theta\end{aligned}\quad (6.28)$$

$$\begin{aligned}\dot{e}_v &= \dot{v} - \dot{v}_d = -\dot{v}_d + Y_v \underbrace{(e_v + v_d)}_v + g \underbrace{(e_\phi + \phi_d)}_\phi \\ &= -\dot{v}_d + Y_v v_d + g\phi_d + X_u e_v + g e_\phi\end{aligned}\quad (6.29)$$

The desired pitch and and roll angles are chosen such that they cancel out the values  $\dot{u}_d$ ,  $u_d$  and  $\dot{v}_d$ ,  $v_d$ , respectively. More precisely:

$$\theta_d = \frac{1}{-g} [\dot{u}_d - X_u u_d] \quad \phi_d = \frac{1}{g} [\dot{v}_d - Y_v v_d] \quad (6.30)$$

The choice of the desired translational velocity components is  $u_d = u_r$  and  $v_d = v_r$  such that when:

$$\lim_{t \rightarrow \infty} \|[e_u \ e_v]^T\| = 0 \quad \text{then} \quad \lim_{t \rightarrow \infty} \|y_u(t) - y_u^r(t)\| = 0 \quad (6.31)$$

It is apparent that the desired angles of (6.30) are functions of only the  $y_{li}^T$  vector components and their first derivatives (i.e.  $\theta_d := w_\theta(\dot{u}_r, u_r)$  and  $\phi_d := w_\phi(\dot{v}_r, v_r)$ ). The particular choice of (6.30) is also physically meaningful since it indicates that the desired attitude is proportional to the reference acceleration and velocity. With the above choice of the desired roll and pitch angles, the translational velocity error dynamics become:

$$\dot{e}_u = X_u e_u - g e_\theta \quad (6.32)$$

$$\dot{e}_v = Y_v e_v + g e_\phi \quad (6.33)$$

The attitude angles error dynamics are:

$$\begin{aligned} \dot{e}_\theta &= \dot{\theta} - \dot{\theta}_d = -\dot{\theta}_d + \underbrace{(e_q + q_d)}_q \\ &= -\dot{\theta}_d + q_d + e_q \end{aligned} \quad (6.34)$$

$$\begin{aligned} \dot{e}_\phi &= \dot{\phi} - \dot{\phi}_d = -\dot{\phi}_d + \underbrace{(e_p + p_d)}_p \\ &= -\dot{\phi}_d + p_d + e_p \end{aligned} \quad (6.35)$$

The desired values of the pitch and roll angular velocities are chosen such that they cancel out the effect of  $\dot{\theta}_d$  and  $\dot{\phi}_d$ . Therefore:

$$q_d = \dot{\theta}_d \quad p_d = \dot{\phi}_d \quad (6.36)$$

The roll and pitch attitude error dynamics become:

$$\dot{e}_\theta = e_q \quad (6.37)$$

$$\dot{e}_\phi = e_p \quad (6.38)$$

Similarly, the angular velocity error dynamics are:

$$\begin{aligned}\dot{e}_q &= \dot{q} - \dot{q}_d = -\dot{q}_d + M_u \underbrace{(e_u + u_d)}_u + M_v \underbrace{(e_v + v_d)}_v + M_a \underbrace{(e_a + a_d)}_a \\ &= -\dot{q}_d + M_u u_d + M_v v_d + M_a a_d + M_u e_u + M_v e_v + M_a e_a\end{aligned}\quad (6.39)$$

$$\begin{aligned}\dot{e}_p &= \dot{p} - \dot{p}_d = -\dot{p}_d + L_u \underbrace{(e_u + u_d)}_u + L_v \underbrace{(e_v + v_d)}_v + L_b \underbrace{(e_b + b_d)}_b \\ &= -\dot{p}_d + L_u u_d + L_v v_d + L_b b_d + L_u e_u + L_v e_v + L_b e_b\end{aligned}\quad (6.40)$$

The values of the desired flapping angles  $a_d$  and  $b_d$  are chosen as:

$$a_d = \frac{1}{M_a} [\dot{q}_d - M_u u_d - M_v v_d] \quad b_d = \frac{1}{L_b} [\dot{p}_d - L_u u_d - L_v v_d] \quad (6.41)$$

Hence, the angular error velocity dynamics, become:

$$\dot{e}_q = M_u e_u + M_v e_v + M_a e_a \quad (6.42)$$

$$\dot{e}_p = L_u e_u + L_v e_v + L_b e_b \quad (6.43)$$

Finally, the flapping angles error dynamics, are:

$$\begin{aligned}\dot{e}_a &= \dot{a} - \dot{a}_d = -\dot{a}_d - \underbrace{(e_q + q_d)}_q - \frac{1}{\tau_f} \underbrace{(e_a + a_d)}_a + A_b \underbrace{(e_b + b_d)}_b + v_{lon} \\ &= -\dot{a}_d - q_d - \frac{1}{\tau_f} a_d + A_b b_d - e_q - \frac{1}{\tau_f} e_a + A_b e_b + v_{lon}^d + v_{lon}^{fb}\end{aligned}\quad (6.44)$$

$$\begin{aligned}\dot{e}_b &= \dot{b} - \dot{b}_d = -\dot{b}_d - \underbrace{(e_p + p_d)}_p - \frac{1}{\tau_f} \underbrace{(e_b + b_d)}_b + B_a \underbrace{(e_a + a_d)}_a + v_{lat} \\ &= -\dot{b}_d - p_d - \frac{1}{\tau_f} b_d + B_a a_d - e_p - \frac{1}{\tau_f} e_b + B_a e_a + v_{lat}^d + v_{lat}^{fb}\end{aligned}\quad (6.45)$$

The components of the control vector  $v_{li}^d$  are chosen such that they cancel out the terms of all the desired state values and only the error state variables remain to the flapping error dynamic

equations. Thus:

$$v_{lon}^{ds} = \dot{a}_d + q_d + \frac{1}{\tau_f} a_d - A_b b_d \quad v_{lat}^{ds} = \dot{b}_d + p_d + \frac{1}{\tau_f} b_d - B_a a_d \quad (6.46)$$

It is easy to verify that the derived pair  $(x_u^d, v_u^d)$  satisfies the differential equation of (6.26). The components of  $x_u^d$  and  $v_u^d$  are composed by the reference values  $u_r$  and  $v_r$  and their higher derivatives up to the fourth order. Therefore the components of  $y_u^r$  should belong to  $C^4$ . The final form of the longitudinal-lateral subsystem error dynamics is:

$$\begin{aligned} \dot{e}_u &= A_u^{fb} e_u + \bar{B}_u v_u^{fb} \\ Y_u &= e_u \\ Y_u^m &= C_u^m e_u \end{aligned} \quad (6.47)$$

where:

$$\begin{aligned} e_u &= [e_u \ e_v \ e_\theta \ e_\phi \ e_q \ e_p \ e_a \ e_b]^T \\ Y_u^m &= [e_u \ e_v \ e_\theta \ e_\phi \ e_q \ e_p]^T \end{aligned}$$

The initial tracking problem of the longitudinal and lateral dynamics has been converted to the stabilization problem of the error vector  $e_u$ . The measurement vector  $Y_u^m$  does not have available all the state variables of the system (6.47) since the flapping angles  $a$  and  $b$  can not be measured. When the complete state vector of a system is not available for feedback purposes and only a subset of the state variables can be used by the controller, then the control law is classified as an output feedback controller. In particular, instead of integrating in the initial system the dynamics of a state estimator, we require a static feedback control law of the form:

$$v_u = -K_u Y_u^m \quad (6.48)$$

such that for the closed loop system:

$$\dot{e}_u = (A_u^{fb} - \bar{B}_u K_u C_u^m) e_u \quad (6.49)$$

the closed loop matrix  $A_u^{cl} = A_u^{fb} - \bar{B}_u K_u C_u^m$  is Hurwitz. A square matrix is called Hurwitz if all of its eigenvalues have strictly negative real parts.

A very good study of the output feedback problem is given in [99] and [100]. Stabilization via output feedback can be achieved by two ways: Eigenvalue placement and in the context of the Linear Quadratic Regulator (LQR). The eigenvalue placement approach, typically requires the solution of very complicated heuristic algorithms for the calculation of the output feedback gain. For this reason we adopt the LQR approach. In this case, the objective is to chose  $K_u$  of (6.48) such that  $A_u^{cl}$  is Hurwitz and, in addition, the gain selection minimizes the following quadratic performance index:

$$J_u = \int_{t_0}^{\infty} \left( e_u^T Q_u e_u + (v_u^{fb})^T R_u v_u^{fb} \right) dt \quad (6.50)$$

where  $Q_u \leq 0$  (positive semi-definite) and  $R_u > 0$  (positive definite) are diagonal matrices. The  $Q_u$  and  $R_u$  matrices are the design parameters of the LQR controller. The principle of the optimality problem is to regulate the state error vector to zero, with the least possible state deviation and control energy. The trade off between control energy and state deviation is specified by the relative values of  $Q_u$  and  $R_u$ . For a larger weighting matrix  $R_u$ , the control input is forced to be smaller in magnitude relative to the state norm. Contrary, a larger  $Q_u$  matrix, requires that the error state vector deviates less from zero by injecting more control energy to the system.

The LQR controller design for LTI systems with output feedback was initially introduced in [59]. The necessary condition for the solution of the above optimality problem is the existence of three matrices namely,  $K_u$ ,  $S_u$  and  $P_u$ , which are solutions to the following coupled equations [59, 74]:

$$0 = \left( A_u^{cl} \right)^T S_u + S_u A_u^{cl} + Q_u + (C_u^m)^T K_u^T R_u K_u C_u^m \quad (6.51)$$

$$0 = P_u \left( A_u^{cl} \right)^T + A_u^{cl} P_u + I_8 \quad (6.52)$$

$$0 = R_u K_u C_u^m P_u (C_u^m)^T - \bar{B}_u^T S_u P_u (C_u^m)^T \quad (6.53)$$

Generally, optimal control with output feedback, results in such coupled nonlinear matrix equations [60]. There are several iterative algorithms for the solution of the above problem. However, the most practical convergent algorithm that results in a local minimum solution is given in [60] based on [74]. The iterative algorithm is the following:

- Step 1: Initialize the iteration procedure by setting  $n = 0$ . Determine an initial gain  $K_{u,0}$  such that the  $A_{u,0}^{cl} = A_u^{fb} - \bar{B}_u K_{u,0} C_u^m$  is Hurwitz.
- Step 2 ( $n$ -th iteration): Set  $A_{u,n}^{cl} = A_u^{fb} - \bar{B}_u K_{u,n} C_u^m$ . Solve for  $S_n$  and  $P_n$  the following Lyapunov equations:

$$\begin{aligned} 0 &= \left( A_{u,n}^{cl} \right)^T S_n + S_n A_{u,n}^{cl} + Q + (C_u^m)^T K_{u,n}^T R_u K_{u,n} C_u^m \\ 0 &= P_n \left( A_{u,n}^{cl} \right)^T + A_{u,n}^{cl} P_n^T + I \end{aligned}$$

Set  $J_{u,n} = tr(S_n)$  and evaluate the gain update direction:

$$\Delta K = R_u^{-1} \bar{B}_u^T S_n P_n (C_u^m)^T \left( C_u^m P_n (C_u^m)^T \right)^{-1} - K_n$$

Update the feedback gain by:

$$K_{u,n+1} = K_{u,n} + \alpha \Delta K$$

In the above equation chose  $\alpha \in (0 \ 1]$  such that the closed loop matrix  $A_{u,n}^{cl}$  is Hurwitz and:

$$\Delta J_u = \|J_{u,n+1} - J_{u,n}\| = \|tr(S_{n+1}) - tr(S_n)\| \leq \epsilon$$

where  $\epsilon$  is a very small number. If  $\Delta J_u \leq \epsilon$  proceed to Step 3, else set  $n = n + 1$  and repeat Step 2.

- Step 3: Terminate the algorithm by setting  $K_{ll} = K_{ll,n+1}$  and  $J_{ll} = J_{ll,n+1}$ .

The disadvantage of the specific numerical algorithm, is the requirement to guess an initial stabilizing gain  $K_{ll,0}$ , at the first step of the algorithm. A practical solution to this problem is to initially calculate the state feedback gain by a regular eigenvalue placement algorithm. Then, omit the entries that correspond to the unmeasured states, and use the rest of the gain components that correspond to the measure states as the initial output feedback gain  $K_{ll,0}$ . The above algorithm was presented because standard software packages such as *MATLAB* do not include built-in routines for the calculation of the output feedback gain. Contrary, *MATLAB* provides a complete set of algorithms for the solution of generalized Lyapunov equations and the extraction of full state feedback gains via eigenvalue placement or performance index optimization.

#### 6.4.2 Yaw-Heave Dynamics

The goal of this Section is the design of the second control law, responsible for the heading and vertical velocity tracking. The yaw-heave dynamics subsystem, is summarized by the following equations:

$$\begin{aligned}\dot{x}_{yh} &= A_{yh}x_{yh} + \bar{B}_{yh}v_{yh} + D_{yh}x_{ll} \\ y_{yh} &= C_{yh}x_{yh} \\ y_{yh}^m &= x_{yh}\end{aligned}\tag{6.54}$$

where:

$$\begin{aligned}x_{yh} &= [\psi \ r \ w]^T \\ v_{yh} &= [v_{ped} \ v_{col}]^T \\ y_{yh} &= [\psi \ w]^T\end{aligned}$$

In the above equations,  $y_{yh}$  is the output vector and  $y_{yh}^m$  is the measurement vector. The reference

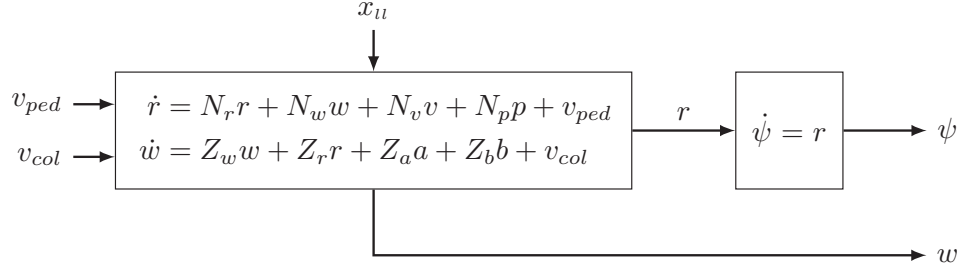


Figure 6.3: Interconnection of the yaw-heave helicopter dynamics subsystem. The yaw-heave dynamics are additionally perturbed by the longitudinal-lateral dynamics state vector  $x_{ll}$ .

output is denoted by  $y_{yh}^r = [\psi_r \ w_r]^T$ . The yaw-heave subsystem is in cascade connection with the longitudinal-lateral subsystem via the matrix  $D_{yh}$ . The interconnection of the yaw-heave subsystem dynamics is shown in Figure 6.3. The design procedure is similar with the one presented in Section 6.4.1. The controller design requires the determination of a desired state vector  $x_{yh}^d$  and a desired nominal control input  $v_{yh}^d$ , such that when the error  $e_{yh} = x_{yh} - x_{yh}^d$  is regulated to zero, then the output  $y_{yh}$  of the yaw heave subsystem asymptotically tracks the reference output vector  $y_{yh}^r$ . The obvious choice of the desired yaw and heave velocity is  $\psi_d = \psi_r$  and  $w_d = w_r$ . Thus, when:

$$\lim_{t \rightarrow \infty} \|[e_\psi \ e_w]^T\| = 0 \quad \text{then} \quad \lim_{t \rightarrow \infty} \|y_{yh}(t) - y_{yh}^r(t)\| = 0 \quad (6.55)$$

The control law for the yaw-heave subsystem, is obtained as the following superposition:

$$v_{yh} = v_{yh}^d + v_{yh}^{fb} = \begin{bmatrix} v_{ped}^d \\ v_{col}^d \end{bmatrix} + \begin{bmatrix} v_{ped}^{fb} \\ v_{col}^{fb} \end{bmatrix} \quad (6.56)$$

The choice of the controller component  $v_{yh}^d$  and the desired state vector  $x_{yh}^d$  should satisfy:

$$\dot{x}_{yh}^d = A_{yh} x_{yh}^d + \bar{B}_{yh} v_{yh}^d + D_{yh} x_{ll}^d \quad (6.57)$$

where the state vector  $x_{ll}^d$  is defined in Section 6.4.1. The input  $v_{yh}^d$  and the desired state  $x_{yh}^d$ , are derived by using a similar recursive backstepping procedure with the one described in Section 6.4.1.

The choice of  $v_{yh}^d$  and  $x_{yh}^d$  components emerge from the inspection of the error vector  $e_{yh} = x_{yh} - x_{yh}^d$  dynamics. The error dynamics of the yaw-heave subsystem are given by:

$$\begin{aligned}\dot{e}_\psi &= \dot{\psi} - \dot{\psi}_d = -\dot{\psi}_d + \underbrace{(e_r + r_d)}_r \\ &= -\dot{\psi}_d + r_d + e_r\end{aligned}\quad (6.58)$$

$$\begin{aligned}\dot{e}_r &= \dot{r} - \dot{r}_d = -\dot{r}_d + N \underbrace{(e_v + v_d)}_v + N_p \underbrace{(e_p + p_d)}_p + N_w \underbrace{(e_w + w_d)}_w + N_r \underbrace{(e_r + r_d)}_r + v_{ped} \\ &= -\dot{r}_d + Nv_d + N_pp_d + N_w w_d + N_r r_d + Ne_v + N_p e_p + N_w e_w + N_r e_r + v_{ped}^d + v_{ped}^{fb}\end{aligned}\quad (6.59)$$

$$\begin{aligned}\dot{e}_w &= \dot{w} - \dot{w}_d = -\dot{w}_d + Z_a \underbrace{(e_a + a_d)}_a + Z_b \underbrace{(e_b + b_d)}_b + Z_r \underbrace{(e_r + r_d)}_r + Z_w \underbrace{(e_w + w_d)}_w + v_{col} \\ &= -\dot{w}_d + Z_a a_d + Z_b b_d + Z_r r_d + Z_w w_d + Z_a e_a + Z_b e_b + Z_r e_r + Z_w e_w + v_{col}^{ds} + v_{col}^{fb}\end{aligned}\quad (6.60)$$

The desired angular velocity  $r_d$ , and the components of  $v_{yh}^d$ , are chosen such that they cancel out all the terms associated with the rest desired state variables and only the error terms remain to the yaw-heave subsystem error dynamics. Thus:

$$r_d = \dot{\psi}_d \quad (6.61)$$

$$v_{ped}^{ds} = \dot{r}_d - Nv_d - N_pp_d - N_w w_d - N_p p_d \quad (6.62)$$

$$v_{col}^{ds} = \dot{w}_d - Z_a a_d - Z_b b_d - Z_r r_d - Z_w w_d \quad (6.63)$$

Based on the above choice, it is easy to verify that (6.57) is satisfied. The desired state vector  $x_{yh}^d$  and the control input  $v_{yh}^d$  are functions of the components of the  $y_{yh}^r, y_{ll}^r$  vectors and their higher derivatives. Moreover,  $\psi_r$  and  $w_r$  should belong to  $C^2$  and  $C^1$ , respectively. The dependence of  $v_{yh}^d$  to the components of  $y_{ll}^r$  stems from the interconnection of the two subsystems through the matrix  $D_{yh}$ . Using the equations given in (6.61)-(6.63), the error dynamics of the yaw-heave

subsystem become:

$$\begin{aligned}\dot{e}_{yh} &= A_{yh}e_{yh} + \bar{B}_{yh}v_{yh}^{fb} + D_{yh}e_{ll} \\ Y_{yh} &= e_{yh} \\ Y_{yh}^m &= e_{yh}\end{aligned}\quad (6.64)$$

where:

$$e_{yh} = [e_\psi \ e_r \ e_v]^T$$

In the above equations  $Y_{yh}^m$  denotes the vector of available measurements. Similarly with the longitudinal-lateral subsystem, the tracking problem of  $y_{yh}^r$  is converted to the regulation of  $e_{yh}$  to zero. However, in the particular case, the full state vector of the system in (6.64) is available for feedback. The design objective is to determine a static feedback law  $v_{yh}^{fb}$  of the form:

$$v_{yh}^{fb} = -K_{yh}e_{yh}\quad (6.65)$$

such that the closed loop stability matrix  $A_{yh}^{cl} = A_{yh} - \bar{B}_{yh}K_{yh}$  of the yaw-heave error subsystem is Hurwitz. As it will be illustrated later if this condition is satisfied, the solution of the complete error dynamics is GAS given that  $A_{ll}^{cl}$  is Hurwitz as well.

Since full state feedback is available, there is a variety of options for determining the feedback gain  $K_{yh}$ . The first choice for calculating  $K_{yh}$  is via the LQR method. Similarly with the output feedback case,  $K_{yh}$  is calculated such that  $A_{yh}^{cl}$  is Hurwitz, and the gain selection minimizes the following performance index:

$$J_{yh} = \int_{t_0}^{\infty} \left( e_{yh}^T Q_{yh} e_{yh} + \left( v_{yh}^{fb} \right)^T R_{yh} v_{yh}^{fb} \right) dt\quad (6.66)$$

In the above equality,  $Q_{yh} \geq 0$  and  $R_{yh} > 0$  are diagonal matrices of appropriate dimensions. Likewise to  $Q_{ll}$  and  $R_{ll}$ , the matrices  $Q_{yh}$  and  $R_{yh}$  are chosen by the designer such that a fine

balance between the system response and the control effort is achieved. In the case of full state feedback, the particular optimization problem is much easier than its output feedback counterpart. The controller state feedback gain is given by:

$$K_{yh} = R_{yh}^{-1} \bar{B}_{yh}^T P_{yh} \quad (6.67)$$

where the matrix  $P_{yh}$  is the solution of the *algebraic Riccati equation*:

$$0 = P_{yh} \bar{B}_{yh} R_{yh}^{-1} \bar{B}_{yh}^T P_{yh} - Q_{yh} - P_{yh} A_{yh} - A_{yh}^T P_{yh} \quad (6.68)$$

The solution of the algebraic Riccati equation, is provided by *MATLAB* by using the `care.m` built-in routine. A different approach is to determine the feedback gain  $K_{yh}$  by direct eigenvalue placement. The advantage of this method is that the eigenvalue position provides a quantitative perception of the system's response. *MATLAB* provides the `place.m` built-in routine, for accurate eigenvalue placement with full state feedback for MIMO systems.

### 6.4.3 Stability of the Complete System Error Dynamics

In Sections 6.4.1 and 6.4.2, we have given a detailed presentation of how to define the feedback gain matrices  $K_{ul}$  and  $K_{yh}$ , such that the the close loop matrices  $A_{ul}^{cl} = A_{ul}^{fb} - \bar{B}_{ul} K_{ul} C_{ul}^m$  and  $A_{yh}^{cl} = A_{yh} - \bar{B}_{yh} K_{yh}$  are Hurwitz. By applying the control laws  $v_{ul}^{fb}$  and  $v_{yh}^{fb}$ , the complete error system dynamics take the form:

$$\begin{bmatrix} \dot{e}_{yh} \\ \dot{e}_{ul} \end{bmatrix} = \begin{bmatrix} (A_{yh} - \bar{B}_{yh} K_{yh}) & D_{yh} \\ 0_{8 \times 3} & (A_{ul}^{fb} - \bar{B}_{ul} K_{ul} C_{ul}^m) \end{bmatrix} \begin{bmatrix} e_{yh} \\ e_{ul} \end{bmatrix} \quad (6.69)$$

The cascade connection of the closed loop error dynamics is shown in Figure 6.4. The stability of the complete error dynamics system given in (6.69), is specified by the following Theorem:

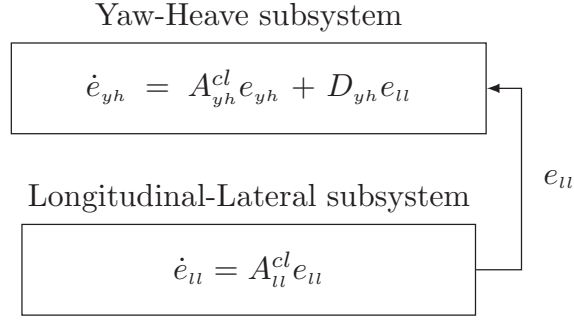


Figure 6.4: Cascade connection of the closed loop error dynamics subsystems.

**Theorem 6.1.** *Given that the feedback gains  $K_{ul}$  and  $K_{yh}$  are selected such that the matrices  $A_{ul}^{cl} = A_{ul}^{fb} - \bar{B}_{ul}K_{ul}C_{ul}^m$  and  $A_{yh}^{cl} = A_{yh} - \bar{B}_{yh}K_{yh}$  are Hurwitz, then the solution  $e(t) = [e_{yh}(t) \ e_{ul}(t)]$  of the complete error dynamics system of (6.69) is GAS.*

*Proof.* The proof of the Theorem begins with a standard result from linear algebra. If  $\mathcal{A} \in \mathbb{R}^{n \times n}$ ,  $\mathcal{B} \in \mathbb{R}^{m \times m}$  are square matrices, and  $\mathcal{C} \in \mathbb{R}^{n \times m}$ , then the following property holds:

$$\det \left( \begin{bmatrix} \mathcal{A} & \mathcal{C} \\ 0_{m \times n} & \mathcal{B} \end{bmatrix} \right) = \det(\mathcal{A}) \cdot \det(\mathcal{B})$$

where  $\det(\cdot)$  denotes the determinant of a matrix. Denote by  $\lambda$  the eigenvalues of the composite error dynamics system of (6.69). By definition, the eigenvalues of (6.69) satisfy the following equalities:

$$\det \left( \begin{bmatrix} A_{yh}^{cl} - \lambda I_{3 \times 3} & D_{yh} \\ 0 & A_{ul}^{cl} - \lambda I_{8 \times 8} \end{bmatrix} \right) = \det(A_{yh}^{cl} - \lambda I_{3 \times 3}) \cdot \det(A_{ul}^{cl} - \lambda I_{8 \times 8}) = 0$$

Therefore the eigenvalues of the composite error system, are the union of the eigenvalues of  $A_{yh}^{cl}$  and  $A_{ul}^{cl}$ . Since both of those matrices are Hurwitz, then all the eigenvalues of (6.69) have strictly negative real parts. Therefore the complete error dynamics system of (6.69) is GAS.  $\square$

## 6.5 Position and Heading Tracking

The ultimate goal of the controller design is for the helicopter to track a predefined position trajectory of the inertial frame expressed by the reference vector  $p_r^I = [p_{r,x}^I \ p_{r,y}^I \ p_{r,z}^I]^T$ . The helicopter position expressed in the body-fixed frame, is denoted by the coordinate vector  $p^B = [p_x^B \ p_y^B \ p_z^B]^T$ . The position error expressed in the body-fixed frame is given by  $e_p^B = p^B - p_r^B$ . The position error dynamics are derived by using the properties of the rotation matrix  $R$ , described in Chapter 3. The rotation matrix is used for mapping coordinate vectors from the body-fixed frame to the inertial frame. For the position error expressed in the body-fixed frame the following equalities hold:

$$e_p^B = p^B - p_r^B = R^T p^I - R^T p_r^I \quad (6.70)$$

Using the analysis of Chapter 3, the position error dynamics are given by:

$$\begin{aligned} \dot{e}_p^B &= R^T (\dot{p}^I - \dot{p}_r^I) + \dot{R}^T (p^I - p_r^I) \\ &= R^T (v^I - v_d^I) + (R\hat{\omega}^B)^T (p^I - p_r^I) \\ &= v^B - v_d^B + (\hat{\omega}^B)^T (p^B - p_r^I) \\ &= e_v^B - \hat{\omega}^B e_p^B \\ &= e_v^B + \hat{e}_p^B \omega^B \end{aligned} \quad (6.71)$$

For deriving the position error dynamics we have used the following:

$$v_d^I = \dot{p}_r^I \quad v^I = \dot{p}^I \quad \dot{R} = R\hat{\omega}^B \quad \hat{\omega}^B e_p^B = -\hat{e}_p^B \omega^B \quad (6.72)$$

The position error dynamics are not linear since they include the nonlinear term  $\hat{e}_p^B \omega^B$ . The latter term expresses the contribution of the angular velocity to the position error dynamics.

The choice of a linear model for the representation of the helicopter dynamics is limited to a certain range of a particular operating condition. In this case, the operating condition of inter-

est is the hover flight mode. Since the linear model of (6.2) is restricted to a certain range of the hover mode, the tracking problem of arbitrary position and velocity trajectories becomes dubious. However, experimental results of real life applications indicate that the accuracy of linear dynamic models is satisfactory enough for a relative wide range of the flight envelope around the reference operating condition. Therefore, it is assumed that the adopted linear model of (6.2) provides a quasi-global description of the helicopter dynamics. Linearization is also applied to the nonlinear position error dynamics, assuming that  $e_p^B$  is the perturbed value of the position error from the reference steady state vector  $e_{p,o}^B = [0 \ 0 \ 0]^T$ . Similarly,  $\omega^B$  is considered as the angular velocity's perturbed value from the trim vector  $\omega_o^B = [0 \ 0 \ 0]^T$ . In this case, the term  $\hat{e}_p^B \omega^B$  can be disregarded since it is considered as a product of two perturbed values<sup>1</sup>. This approximation adds up to all simplification assumptions that take place in order to obtain the linear dynamic model of the helicopter given in (6.2). Therefore, the approximated position error dynamics are given by:

$$\dot{e}_p^B = e_v^B \quad (6.73)$$

The composite error system is additionally enhanced by the integral of the position and yaw error dynamics. The presence of integral terms in the control law is very beneficial in terms of robustness performance. The feedback integral components attenuate the steady state tracking error caused by potential parametric and model uncertainty. Denote by  $\eta_p^B = [\eta_x^B \ \eta_y^B \ \eta_z^B]^T$  and  $\eta_\psi$  the integral of the position and yaw error. Thus:

$$\dot{\eta}_p^B = e_p^B \quad \text{and} \quad \dot{\eta}_\psi = e_\psi \quad (6.74)$$

The structure of the control laws for the position tracking problem will be identical to the velocity tracking case. The composite error dynamics are still separated into two subsystems corresponding to the lateral-longitudinal and yaw-heave motion. Having said that, the longitudinal-

---

<sup>1</sup>More details about linearization may be found in Section 5.8.

lateral dynamics are given by:

$$\begin{aligned}\dot{\varepsilon}_{ll} &= \mathcal{A}_{ll}\varepsilon_{ll} + \mathcal{B}_{ll}v_{ll}^{fb} \\ \mathcal{Y}_{ll}^m &= \mathcal{C}_{ll}^m\varepsilon_{ll}\end{aligned}\quad (6.75)$$

where:

$$\begin{aligned}\varepsilon_{ll} &= [\eta_x^B \ \eta_y^B \ e_x^B \ e_y^B \ e_u \ e_v \ e_\theta \ e_\phi \ e_q \ e_p \ e_a \ e_b]^T \\ \mathcal{Y}_{ll}^m &= [\eta_x^B \ \eta_y^B \ e_x^B \ e_y^B \ e_u \ e_v \ e_\theta \ e_\phi \ e_q \ e_p]^T\end{aligned}$$

and:

$$\mathcal{A}_{ll} = \left[ \begin{array}{c|cc} 0_{4 \times 2} & I_{4 \times 4} & 0_{4 \times 6} \\ \hline 0_{8 \times 2} & 0_{8 \times 2} & A_{ll}^{fb} \end{array} \right] \quad \mathcal{B}_{ll} = \left[ \begin{array}{c} 0_{4 \times 2} \\ \hline \bar{B}_{ll} \end{array} \right] \quad (6.76)$$

The yaw-heave error dynamics are given by:

$$\begin{aligned}\dot{\varepsilon}_{yh} &= \mathcal{A}_{yh}\varepsilon_{yh} + \mathcal{B}_{yh}v_{yh}^{fb} + \mathcal{D}_{yh}\varepsilon_{ll} \\ \mathcal{Y}_{yh}^m &= \varepsilon_{yh}\end{aligned}\quad (6.77)$$

where:

$$\varepsilon_{yh} = [\eta_z^B \ \eta_\psi \ e_z^B \ e_\psi \ e_w \ e_r]^T$$

and:

$$\mathcal{A}_{yh} = \left[ \begin{array}{c|cc} 0_{3 \times 2} & I_{3 \times 3} & 0_{3 \times 1} \\ \hline 0_{3 \times 2} & 0_{3 \times 1} & A_{yh} \end{array} \right] \quad \mathcal{B}_{yh} = \left[ \begin{array}{c} 0_{3 \times 2} \\ \hline \bar{B}_{yh} \end{array} \right] \quad \mathcal{D}_{yh} = \left[ \begin{array}{c|c} 0_{3 \times 3} & O_{3 \times 8} \\ \hline 0_{3 \times 4} & D_{yh} \end{array} \right] \quad (6.78)$$

The interconnection of the new complete error dynamics subsystems is illustrated in Figure 6.5.

Similarly to the velocity tracking case, the control design is reduced to the calculation of two

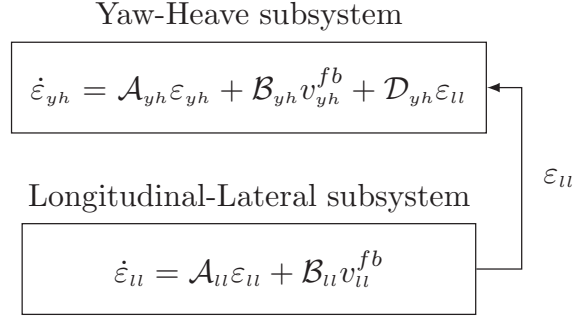


Figure 6.5: Cascade connection of the error dynamics subsystems related with the position tracking problem.

feedback gain matrices  $\mathcal{K}_{ll}$  and  $\mathcal{K}_{yh}$ , such that by applying the following feedback control laws:

$$v_{ll}^{fb} = -\mathcal{K}_{ll}\mathcal{Y}_{ll}^m \quad (6.79)$$

$$v_{yh}^{fb} = -\mathcal{K}_{yh}\mathcal{Y}_{yh}^m \quad (6.80)$$

the closed loop matrices  $\mathcal{A}_{ll}^{cl} = \mathcal{A}_{ll} - \mathcal{B}_{ll}\mathcal{K}_{ll}\mathcal{C}_{ll}^m$  and  $\mathcal{A}_{yh}^{cl} = \mathcal{A}_{yh} - \mathcal{B}_{yh}\mathcal{K}_{yh}$  are Hurwitz. The feedback gains can be calculated by performing the methodologies described in Sections 6.4.1 and 6.4.2. For example, following the LQR method the gains are selected such that they minimize the following quadratic performance indexes:

$$\mathcal{J}_{ll} = \int_{t_0}^{\infty} \left( \varepsilon_{ll}^T \mathcal{Q}_{ll} \varepsilon_{ll} + \left( v_{ll}^{fb} \right)^T \mathcal{R}_{ll} v_{ll}^{fb} \right) dt \quad (6.81)$$

$$\mathcal{J}_{yh} = \int_{t_0}^{\infty} \left( \varepsilon_{yh}^T \mathcal{Q}_{yh} \varepsilon_{yh} + \left( v_{yh}^{fb} \right)^T \mathcal{R}_{yh} v_{yh}^{fb} \right) dt \quad (6.82)$$

However, in order to follow the LQR or eigenvalue placement methodologies, the pairs  $(\mathcal{A}_{ll}, \mathcal{B}_{ll})$  and  $(\mathcal{A}_{yh}, \mathcal{B}_{yh})$  must be controllable. The necessary condition for controllability of the pairs  $(\mathcal{A}_{ll}, \mathcal{B}_{ll})$  and  $(\mathcal{A}_{yh}, \mathcal{B}_{yh})$  is established by the following Theorem:

**Theorem 6.2.** *Given that Assumptions 6.1, 6.2 and 6.3 hold, then the pairs  $(\mathcal{A}_{ll}, \mathcal{B}_{ll})$  and  $(\mathcal{A}_{yh}, \mathcal{B}_{yh})$  are controllable.*

*Proof.* Based on Assumptions 6.1 and 6.2, the pair  $(A_u^{fb}, \bar{B}_{y_h})$  is controllable. Let  $T(s) = [sI_8 - A_u^{fb} | \bar{B}_u]$  where  $s \in \mathbb{R}$ . From the Popov-Belevitch-Hautus (PBH) test, for every  $s \in \mathbb{R}$  we have  $\text{rank}(T(s)) = 8$ . We need to show that  $\text{rank}(T(s)) = 12$  for every  $s \in \mathbb{R}$ , where  $T(s) = [sI_{12} - \mathcal{A}_u | \mathcal{B}_u]$ .

- For  $s \neq 0$  one has:

$$\text{rank}(T(s)) = \text{rank} \left( \left[ \begin{array}{cc|cc|c} sI_2 & -I_2 & 0_{2 \times 2} & 0_{2 \times 6} & 0_{4 \times 2} \\ 0_{2 \times 2} & sI_2 & -I_2 & 0_{2 \times 6} & \\ \hline 0_{2 \times 2} & 0_{2 \times 2} & -A_u^{fb} & -B_u & \end{array} \right] \right)$$

Since  $s \neq 0$ , the first four rows are linearly independent. Therefore:

$$\text{rank}(T(s)) = 4 + \text{rank} \left( [A_u^{fb} | B_u] \right) = 4 + 8 = 12$$

- For  $s = 0$  one has:

$$\text{rank}(T(0)) = \left( \left[ \begin{array}{cc|cc|c} 0_{2 \times 2} & -I_2 & 0_{2 \times 2} & 0_{2 \times 6} & 0_{4 \times 2} \\ 0_{2 \times 2} & 0_{2 \times 2} & -I_2 & 0_{2 \times 6} & \\ \hline 0_{2 \times 2} & 0_{2 \times 2} & -A_u^{fb} & -B_u & \end{array} \right] \right)$$

The first two rows are linearly independent. Therefore:

$$\text{rank}(T(0)) = 2 + \left( \left[ \begin{array}{cc|c} -I_2 & 0_{2 \times 6} & 0_{2 \times 2} \\ \hline -A_u^{fb} & -B_u & \end{array} \right] \right)$$

The matrix of the right hand side of the above equation, is square and lower triangular with nonzero elements in its main diagonal (this fact is guaranteed by Assumption 6.3). Hence, the rank of this matrix is 10 and  $\text{rank}(T(0)) = 12$ .

We have proved that for every  $s \in \mathbb{R}$ , we have  $\text{rank}(T(s)) = 12$ . Therefore given that the pair  $(A_u^{fb}, \bar{B}_u)$  is controllable, then the pair  $(\mathcal{A}_u, \mathcal{B}_u)$  is controllable as well. The proof for the

controllability of  $(\mathcal{A}_{yh}, \mathcal{B}_{yh})$  based on the controllability of the pair  $(\mathcal{A}_{yh}, \mathcal{B}_{yh})$  is derived similarly to the above analysis.  $\square$

By applying the control laws  $v_{il}^{fb} = -\mathcal{K}_{il}\mathcal{Y}_{il}^m$  and  $v_{yh}^{fb} = -\mathcal{K}_{yh}\mathcal{Y}_{yh}^m$ , the complete error system dynamics take the form:

$$\dot{\varepsilon} = \mathcal{A}_{\varepsilon}^{cl} \varepsilon \quad (6.83)$$

where:

$$\varepsilon = \begin{bmatrix} \varepsilon_{yh} \\ \varepsilon_{il} \end{bmatrix} \quad \mathcal{A}_{\varepsilon} = \left[ \begin{array}{c|c} (\mathcal{A}_{yh} - \mathcal{B}_{yh}\mathcal{K}_{yh}) & \mathcal{D}_{yh} \\ \hline 0_{8 \times 3} & (\mathcal{A}_{il} - \mathcal{B}_{il}\mathcal{K}_{il}\mathcal{C}_{il}^m) \end{array} \right] \quad (6.84)$$

The stability of the complete error dynamics system of (6.83) is established by the following Theorem:

**Theorem 6.3.** *Given that the feedback gains  $\mathcal{K}_{il}$  and  $\mathcal{K}_{yh}$  are selected such that the matrices  $\mathcal{A}_{il}^{cl} = \mathcal{A}_{il} - \mathcal{B}\mathcal{K}_{il}\mathcal{C}_{il}^m$  and  $\mathcal{A}_{yh}^{cl} = \mathcal{A}_{yh} - \mathcal{B}_{yh}\mathcal{K}_{yh}$  are Hurwitz, then the solution  $\varepsilon(t) = [\varepsilon_{yh}(t) \ \varepsilon_{il}(t)]$  of the complete error dynamics system in (6.83), is GAS.*

*Proof.* The proof is derived similarly to Theorem 6.1. The eigenvalues of (6.83) have strictly negative real parts based on the determinant property of square matrices in block triangular form.  $\square$

## 6.6 PID Control

In many practical control applications the MIMO dynamic model of the helicopter is not available. In this Section we present a fundamental controller composed by four SISO Proportional Integral Derivative (PID) feedback loops. This control scheme is a very common start up design point in real life applications, since it does not require the knowledge of the helicopter model and the controller gains can be empirically tuned.

The design of the cyclic feedback loops is based on the simple fact that the longitudinal and lateral velocity of the helicopter is produced from the pitch and roll tilt of the fuselage. Therefore, the helicopter velocity is considered proportional to the helicopter attitude [70]. The structure of the feedback law is composed by two main loops: The *inner loop* and the *outer loop*. The inner

loop regulates the helicopter attitude to the desired angles  $\theta_{des}$  and  $\phi_{des}$ . The feedback signal of the inner loop is proportional to the attitude error. The outer loop generates the desired attitude angles. The desired pitch and roll angles are proportional to the position and velocity error in the longitudinal and lateral directions, respectively. The cyclic commands are given by:

$$u_{lon} = -K_{\theta}(\theta - \theta_{des}) = -K_{\theta}(\theta - K_{\eta,x}\eta_x^B - K_x e_x^B - K_u e_u) \quad (6.85)$$

and:

$$u_{lat} = -K_{\phi}(\phi + \phi_{des}) = -K_{\phi}(\phi + K_{\eta,y}\eta_y^B + K_y e_y^B + K_v e_v) \quad (6.86)$$

In order for the above feedback law to perform well, the attitude error should be regulated to zero faster than the translational error. To do so, the control law gains should be chosen appropriately such that a distinct time scaling is achieved between the attitude dynamics and the translational dynamics. The pedal and collective feedback loops are more direct than the cyclic loops. Each of them is composed solely from the yaw and heave error and their corresponding velocity error. Therefore the pedal and the collective input are given by:

$$u_{ped} = -K_{\eta,\psi}\eta_{\psi} - K_{\psi}e_{\psi} - K_r e_r \quad (6.87)$$

and:

$$u_{col} = -K_{\eta,z}\eta_z^B - K_y e_x^B - K_v e_v \quad (6.88)$$

The PID control design does not take into consideration the cross coupling effect that usually exists in the helicopter dynamics. Therefore, the four closed loops are completely independent with each other. The gains of the control feedback loop are tuned by simple trial and error. The gain tuning procedure can be significantly improved by the knowledge of a simple non-parametric

model of the helicopter. The non-parametric model can be extracted with the methodologies described in Chapter 5.

## 6.7 Experimental Results

The performance of the proposed linear tracking controller and the PID design is evaluated using the *Raptor 90 SE RC* helicopter in the *X-Plane* simulator. Details about the Raptor model and *X-Plane* can be found in Section 5.10.1. The stability and control derivatives of the Raptor's linear model are given in Table 5.4. Both controller performance was tested by the execution of a velocity tracking maneuver. The desired maneuver is a trapezoidal velocity profile in the lateral and longitudinal directions of the inertial space. Throughout the maneuver the desired heading remains constant with the value  $\psi_d = 0$ . The linear tracking controller's gains of (6.79)-(6.80) are shown in Table 6.1. The PID gains are given in Table 6.2. The controller responses versus the desired trajectory are illustrated in Figure 6.6. The pitch, roll and yaw orientation angles for the two controllers are depicted in Figure 6.7. The position of the helicopter in the inertial coordinates is given in Figures 6.8 and 6.9. Finally the control inputs for the two designs are given in Figures 6.10 and 6.11.

Based on the results, the performance of both controller designs was satisfactory. Although the reference trajectory requires that the helicopter executes a cruising maneuver (longitudinal velocity up to  $17 \text{ m/sec}$  and lateral velocity up to  $3 \text{ m/sec}$ ) a single linear controller based only on the hover linear model, was adequate. To this extent, the identification of multiple models for different operating conditions was redundant. It was expected that the PID performance would be inferior to the linear design, however the flight results indicate that both the designs provided equally successful results. The success of the PID controller is attributed to the attenuated cross coupling effect amongst the Raptor dynamics. This fact is supported by the off-axis responses of the helicopter illustrated in Figure 5.3. The magnitude of the  $q/u_{lat}$  and  $p/u_{lon}$  responses lie in the zone of  $-20$  to  $-40 \text{ dB}$ . This is an indicator of negligible cross coupling between the helicopter dynamics.

## 6.8 Remarks

This Chapter has presented a position (or velocity) and heading tracking controller for small scale helicopters. The analysis is restricted to this class of rotorcraft because the adopted generic linear model, to which the controller is based on, may be inadequate for full scale helicopters. Models for full scale helicopters are in principle of higher order by including additional dynamics such as coning, engine dynamics and other aerodynamic effects like the inflow velocity's dynamics. The linear design is based on the linearized helicopter dynamics around hover. The design can be expanded such that the overall control law can be an interpolator of multiple controllers where each of them corresponds to a linear model of a different operating condition of the helicopter. It is important however that all of the linearized models have the same structure and order with the base hover model and only their parameters may vary. In addition, it is important that for all the linear models, it is physically meaningful to be approximated by a system of strict-feedback form such that the principle of differential flatness holds. The output feedback controllers  $v_{it}^{fb}$  and  $v_{yh}^{fb}$  are not restricted only to the proposed designs of this Chapter but they could be chosen from a wide variety of linear controller designs that exist in the literature. To this extent, the popular method of  $\mathcal{H}_\infty$  may be also applied. The suggested output feedback control laws of this Chapter are only indicators for a straightforward design.

To eliminate the necessity of multiple linear models a single nonlinear model should be used leading to a nonlinear controller design. This is the goal of the next Chapter where a nonlinear backstepping controller is proposed based on the nonlinear helicopter dynamics. The helicopter dynamics are based on the complete nonlinear equations of motions enhanced by a simplified model of the main and tail rotor forces and moments generation.

Table 6.1: Linear tracking controller feedback gains.

$\mathcal{K}_{ll} =$	$\begin{bmatrix} -1.9187 & 0.4710 & -4.3711 & 1.0374 & -3.1353 & 0.6882 & 9.8054 & 1.9041 & 0.5662 & 0.2395 \\ -0.1242 & 0.6031 & -0.2734 & 1.3663 & -0.1847 & 0.9682 & 0.5038 & 2.9687 & 0.0632 & -0.5391 \end{bmatrix}$
	$\mathcal{K}_{yh} = \begin{bmatrix} 0 & 0 & 42 & 0 & 10.9451 & 0 \\ 0 & 0 & 0 & 60 & 0 & 1 \end{bmatrix}$

Table 6.2: PID controller gains.

$K_\theta$	0.7566	$K_y$	0.3252
$K_{\eta,x}$	0	$K_v$	0.2493
$K_x$	0.3256	$K_{\eta,\psi}$	0
$K_u$	0.1628	$K_\psi$	3
$K_\phi$	0.4569	$K_r$	0.35
$K_{\eta,y}$	0	$K_{\eta,z}$	0
$K_w$	0.6060	$K_z$	1.6018

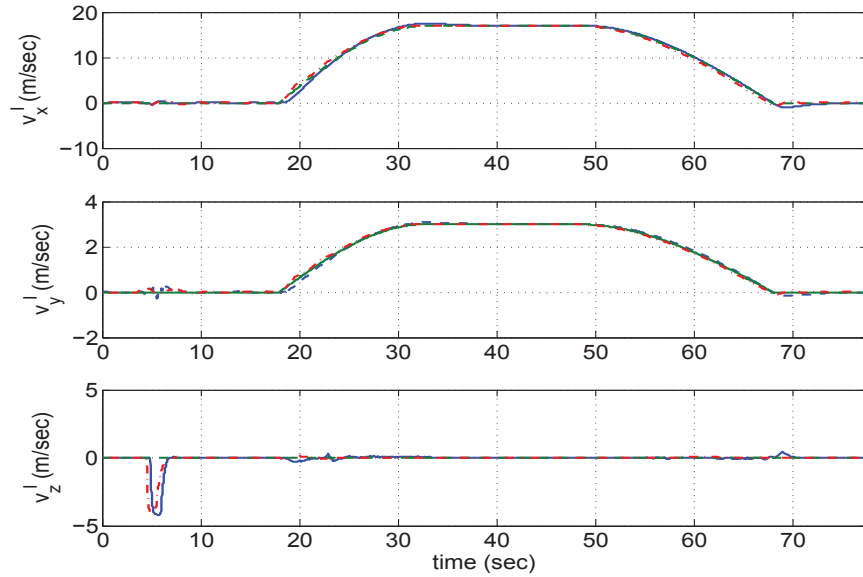


Figure 6.6: Reference trajectory (solid green line), actual position trajectory of the linear (green dashed line) and PID (dashed-dotted red line) designs, expressed in inertial coordinates with respect to time.

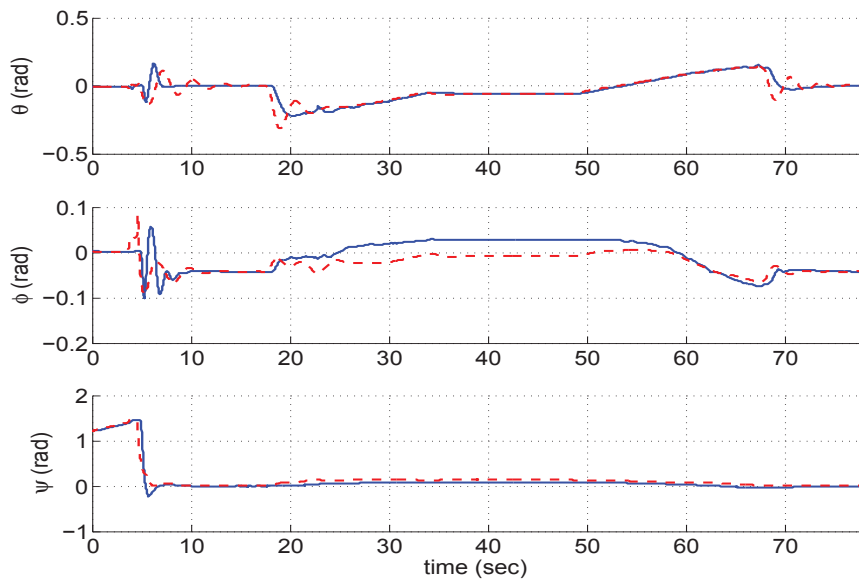


Figure 6.7: Orientation angles of the linear (solid line) and PID (dashed line) designs.

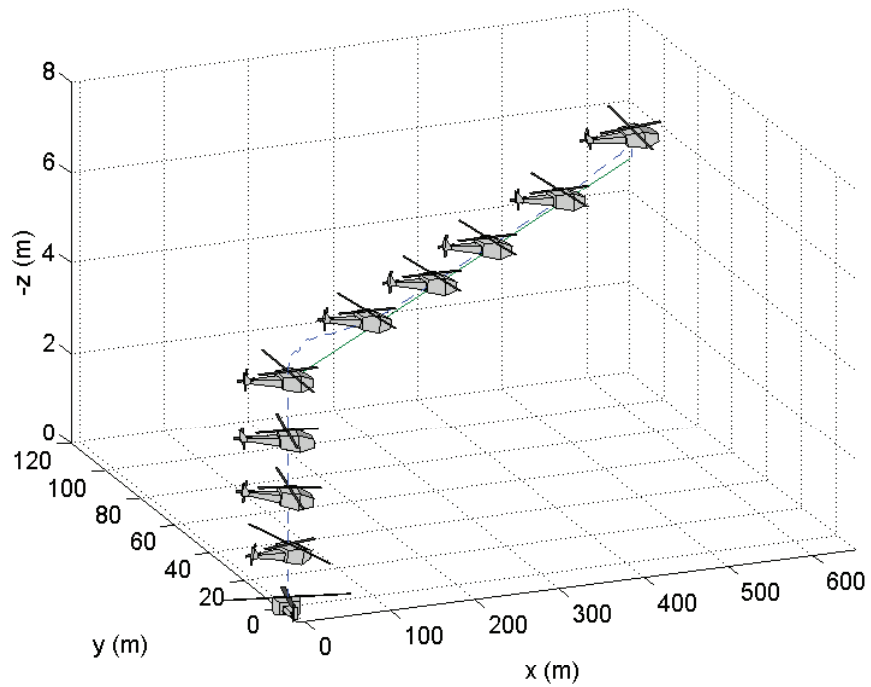


Figure 6.8: Reference position trajectory (solid line) and the actual trajectory of the linear (dashed line) design with respect to the inertia axis.

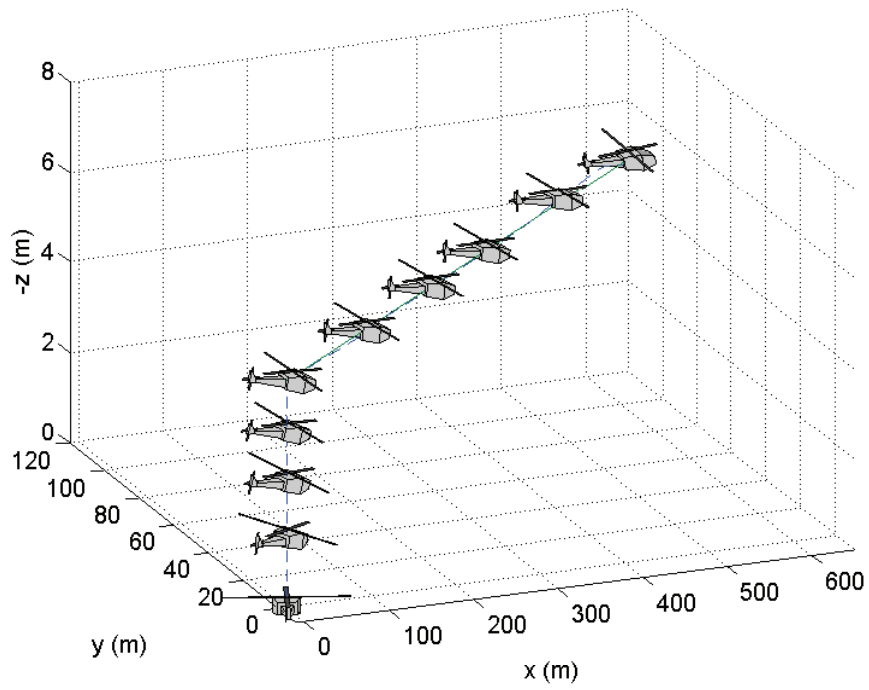


Figure 6.9: Reference position trajectory (solid line) and the actual trajectory of the PID (dashed line) design, with respect to the inertia axis.

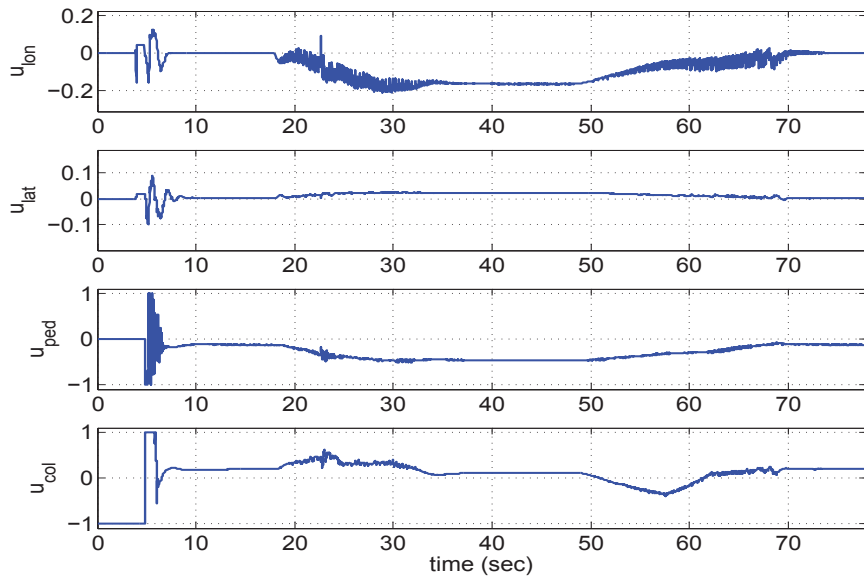


Figure 6.10: Control inputs of the linear design.

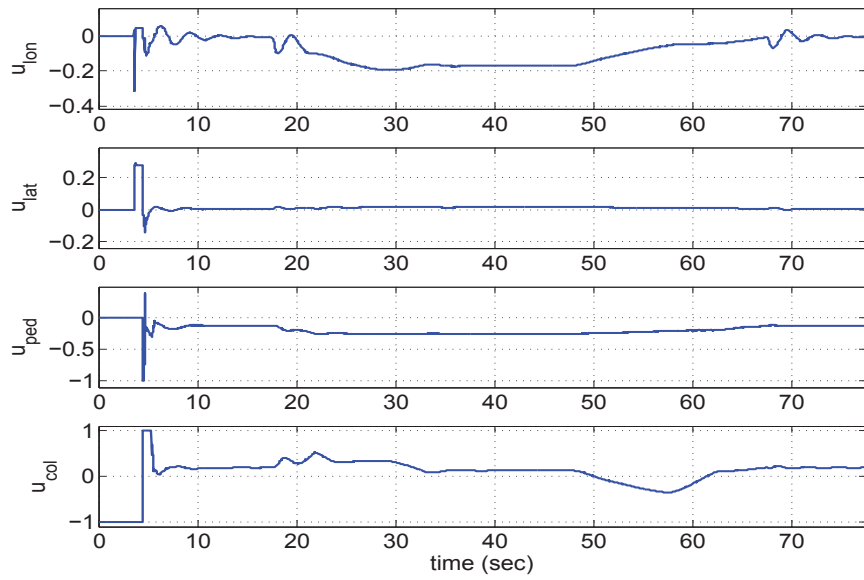


Figure 6.11: Control inputs of the PID design.

## Chapter 7: Nonlinear Tracking Controller Design for Unmanned Helicopters

The previous Chapter presented a tracking controller of the position and heading of a helicopter based on the linearized helicopter dynamics. The adopted parametric linear model, to which the flight controller is based on, represented the quasi steady state behavior of the helicopter dynamics at hover.

Real life case studies indicate that the validity of linear models is restricted only to flight operation around the trim point of reference. A wider description of the flight envelope requires the identification of multiple linear models where each of them corresponds to a different operating condition of the helicopter. Therefore, multiple controllers should be designed where each of them is based on the linear model of a particular operating condition. The output of overall control law is produced by a scheduling process of these multiple controllers depending on the helicopter's operating condition.

However, as indicated in Chapter 5 the experimental procedure for the extraction of linear models parameters, for operating conditions other than hover, is a tedious and in many cases unreliable process. The ideal solution to this problem would be the design of a single controller based on a model that provides a global description of the helicopter dynamics. The goal of this Chapter is the design of a position and heading control law based on the nonlinear helicopter dynamics. The resulting control law, from a theoretical view point, is valid for the complete flight envelope and is applicable to both full scale and small scale helicopters.

## 7.1 Introduction

In general, most controller designs are based on the linearized helicopter dynamics using the widely adopted concept of stability derivatives [25, 28, 54–56, 89]. However, in recent years there is considerable research related to helicopter flight control based on nonlinear dynamic representations [24, 30, 47, 88, 91].

This Chapter presents a nonlinear tracking controller design for helicopters. The main objective is for the helicopter to track a predefined, possibly aggressive, position and yaw reference trajectories with certain bounds that reflect the helicopter's physical limitations. The helicopter model is represented by the rigid body equations of motion enhanced by a simplified model of force and torque generation. The helicopter nonlinear model is based on the work reported in [47].

The controller is based on the backstepping design principle for systems in feedback form. The intermediate backstepping control signals (a.k.a. pseudo controls) for each level of the feedback system are appropriately chosen to stabilize the overall helicopter dynamics. The resulting system error dynamics can be separated in two interconnected subsystems representing the error in translational and attitude dynamics, respectively. The distinction of the two subsystems indicate the time scaling separation that exists in actual helicopters where the position dynamics are significantly slower than the attitude dynamics.

The incorporation of nested saturation feedback functions in the backstepping design preserves the helicopter's motion and power physical constraints. The intermediate control signals related to the attitude dynamics exploit the structural properties of the rotation matrix and are enhanced with terms that guarantee that the helicopter will not overturn while tracking the desired position trajectory. The attitude dynamics are rendered exponentially stable while the translational dynamics are globally asymptotically stable. Numerical simulations illustrate the applicability of the proposed design.

## 7.2 Helicopter Nonlinear Model

Before we proceed with the helicopter nonlinear model we introduce some mathematical notation that is required for the following analysis. The abbreviations  $C_t$  and  $S_t$  with  $t \in \mathbb{R}$  represent the trigonometric functions  $\cos(t)$  and  $\sin(t)$ , respectively. The operands  $\|(\cdot)\|$ ,  $|(\cdot)|$  denote the Euclidean norm and the  $\|(\cdot)\|_1$  norm of a vector, respectively.

The helicopter model considered in this Section is composed by the nonlinear equations of motion accompanied by a simplified model of the forces and moments that are produced by the main and tail rotor. These aerodynamic forces and moments are complex nonlinear functions of the motion characteristics and controls which are dominated by high uncertainty. Detailed models of the helicopter nonlinear dynamics can be found in [7, 40, 84]. However, such models are of high order and impractical for the development of flight controllers. In this Section, the derivation of the external forces and moments that act on the helicopter are based on the simplified model of the generated main rotor thrust that is covered Chapter 4.

### 7.2.1 Rigid Body Dynamics

The helicopter rigid body nonlinear equations of motion have been already derived in Chapter 3 and are briefly repeated here for clarification purposes. Let  $p^I = [p_x^I \ p_y^I \ p_z^I]^T$  denote the position vector of the CG of the helicopter with respect to the inertial coordinates, and  $v^I = [v_x^I \ v_y^I \ v_z^I]^T$  denote the linear velocity vector in inertial coordinates. The angular velocity with respect to the body frame is  $\omega^B = [p \ q \ r]^T$ . Based on Chapter 3, the complete rigid body dynamic equations of the helicopter in the configuration space  $SE(3) = \mathbb{R}^3 \times SO(3)$  are:

$$\dot{p}^I = v^I \quad (7.1)$$

$$\dot{v}^I = \frac{1}{m} R f^B \quad (7.2)$$

$$\dot{R} = R \hat{\omega}^B \quad (7.3)$$

$$\mathcal{I} \dot{\omega}^B = -\omega^B \times (\mathcal{I} \omega^B) + \tau^B \quad (7.4)$$

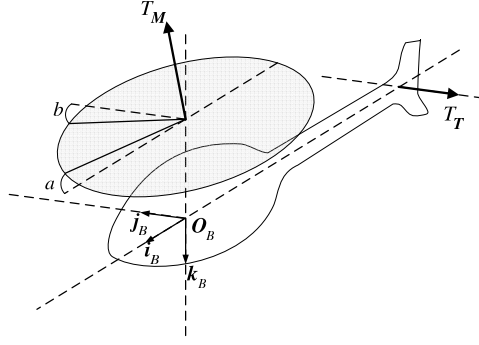


Figure 7.1: The helicopter's body-fixed frame, the Tip-Path-Plane angles and the thrust vectors of the main and tail rotor.

The rotation matrix  $R$  is parametrized with respect to the three Euler angles roll ( $\phi$ ), pitch ( $\theta$ ) and yaw ( $\psi$ ) and maps vectors from the body fixed frame  $\mathcal{F}_B$  to the inertia frame  $\mathcal{F}_I$ . The controller design of this Chapter makes extensive use of the rotation matrix so its components are repeated here:

$$R = \begin{bmatrix} C_\psi C_\theta & -S_\psi C_\phi + C_\psi S_\theta S_\phi & S_\phi S_\psi + C_\phi S_\theta C_\psi \\ S_\psi C_\theta & C_\phi C_\psi + S_\phi S_\theta S_\psi & -C_\psi S_\phi + S_\psi S_\theta C_\phi \\ -S_\theta & C_\theta S_\phi & C_\theta C_\phi \end{bmatrix}$$

The orientation vector is given by  $\Theta = [\phi \ \theta \ \psi]^T$  and the associated orientation dynamics are governed by:

$$\dot{\Theta} = \Psi(\Theta)\omega^B \quad (7.5)$$

The components of  $\Psi(\Theta)$  matrix are given in (3.25). The helicopter's rigid body dynamics given in (7.1)-(7.4) are completed by defining the external body-fixed frame force  $f^B$  and torque  $\tau^B$ .

The vector  $F^B = [f^B \ \tau^B]^T$  is called the external wrench that acts on the helicopter [75].

## 7.2.2 External Wrench Model

This Chapter follows the modeling approach of [47, 56, 70, 72], which provides a simplified external wrench model adequate for controller design purposes. Most of the concepts associated

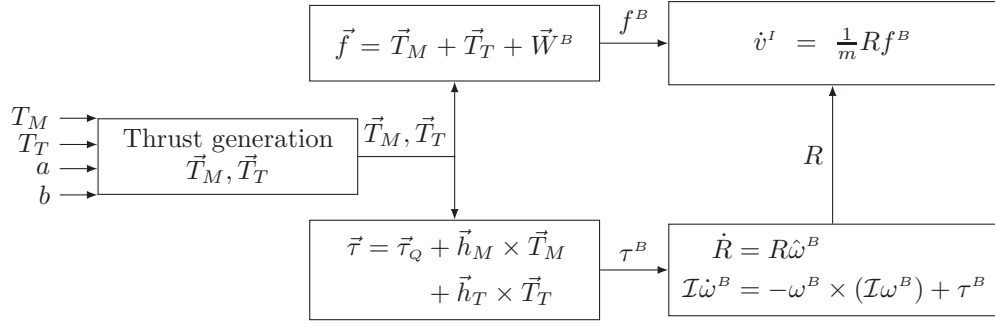


Figure 7.2: This block diagram illustrates the connection of the generated thrusts of the main and tail rotor with the helicopter dynamics. The vector  $\vec{W}^B$  represents the weight force expressed in the body fixed frame.

with the derivation of the simplified external wrench model have been already covered in Chapter 4. The main assumption is that the thrust vector produced by the main rotor is considered perpendicular to the TPP.

There are four control inputs associated with helicopter piloting. The control input vector in this Chapter is defined as  $u_c = [a \ b \ T_M \ T_T]^T$ . The components  $T_M$  and  $T_T$  are the magnitudes of the generated thrusts by the main and tail rotor, respectively. The magnitude of the main and tail rotor thrust is produced by a uniform change in the pitch angles of the main and tail rotor blades. The flapping angles  $a$ ,  $b$  represent the tilt of the TPP at the longitudinal and lateral axis, respectively. The vectors of the body-fixed frame, the flapping angles and the thrust vectors are depicted in Figure 7.1.

From Section 4.8 the components of the main rotor thrust vector  $\vec{T}_M$ , expressed in the body-fixed frame, are given by:

$$T_M^B = \begin{bmatrix} X_M \\ Y_M \\ Z_M \end{bmatrix} = \begin{bmatrix} -S_a C_b \\ C_a S_b \\ -C_a C_b \end{bmatrix} T_M \approx \begin{bmatrix} -a \\ b \\ -1 \end{bmatrix} T_M \quad (7.6)$$

As indicated from Section 4.8, the above equation is simplified by assuming small angle approximation ( $\cos(\cdot) \approx 1$  and  $\sin(\cdot) \approx (\cdot)$ ) for the flapping angles. The small angle assumption is

adopted by [40, 47, 70]. For the body-fixed components of the tail rotor thrust vector, one has:

$$T_T^B = \begin{bmatrix} 0 \\ Y_T \\ 0 \end{bmatrix} = \begin{bmatrix} 0 \\ -1 \\ 0 \end{bmatrix} T_T \quad (7.7)$$

Therefore, by including the helicopter's weight the complete force vector is:

$$f^B = \begin{bmatrix} X_M \\ Y_M + Y_T \\ Z_M \end{bmatrix} + R^T \begin{bmatrix} 0 \\ 0 \\ mg \end{bmatrix} \quad (7.8)$$

A common simplification practice followed in [37, 47, 66] is to neglect the effect of the lateral and longitudinal forces produced by the TPP tilt and the effect of the tail rotor thrust. Those parasitic forces have a minimal effect on the translational dynamics compared to the  $Z_M$  component<sup>1</sup>. In this case, the only two forces applied to the helicopter are the main rotor's thrust vector at the direction of  $\vec{k}_B$  of the body frame and the weight force. Therefore, (7.8) becomes:

$$f^B = \begin{bmatrix} 0 \\ 0 \\ -T_M \end{bmatrix} + R^T \begin{bmatrix} 0 \\ 0 \\ mg \end{bmatrix} \quad (7.9)$$

The generated torques are the result of the above forces and the rotors moments. Denote  $h_M^B = [x_m \ y_m \ z_m]^T$  and  $h_T^B = [x_t \ y_t \ z_t]^T$  as the position vectors of the main and tail rotor shafts, respectively (expressed in the body-fixed coordinate frame). Let  $\vec{\tau}_M = \vec{h}_M \times \vec{T}_M$  and  $\vec{\tau}_T = \vec{h}_T \times \vec{T}_T$  be

<sup>1</sup>The override of the  $f^B$  components in the  $\vec{i}_B$  and  $\vec{j}_B$  directions of the body-fixed frame achieves the decoupling of the helicopter external force and moment model. The work reported in [47] indicates that if the complete description of the force vector given in (7.8) is used, then the state space dynamics of the nonlinear helicopter model can not be input-output linearizable and the zero-dynamics of the system will be unstable. If the system dynamics are not input-output linearizable most of the standard control methodologies will be inapplicable. If the proposed approximation takes place, the helicopter nonlinear model becomes full state linearizable by considering the position and the yaw as outputs. To the authors knowledge there is not any controller design in the literature that is based on the exact model and in all case studies this approximation is performed. The use of the approximated model also took place in Chapter 6 indicating that for the helicopter control problem only practical stability can be achieved based on the approximated model.

the torques generated by  $\vec{T}_M$  and  $\vec{T}_T$ , respectively. The complete torque vector will be:

$$\tau^B = \tau_Q^B + \begin{bmatrix} y_m Z_M - z_m Y_M - z_t Y_T \\ z_m X_M - x_m Z_M \\ x_m Y_M - y_m X_M + x_t Y_T \end{bmatrix} \quad (7.10)$$

with  $\tau_Q^B = [R_M \ M_M \ N_M]^T$ . The  $\vec{\tau}_Q$  is produced by the main rotor moment vector  $\vec{\tau}_\beta$  due to the hub stiffness and the main rotor anti-torque denoted by  $Q_M$ . The components of  $\tau_M^B = [R_M \ M_M \ N_M]^T$  are:

$$\begin{aligned} R_M &= K_\beta b - Q_M S_a C_b & M_M &= K_\beta a + Q_M S_b C_a \\ N_M &= -Q_M C_a C_b & Q_M &= C^M |T_M|^{1.5} + D^M \end{aligned}$$

The positive constants  $C^M$  and  $D^M$  are associated with the generation of the reaction torque  $Q_M$ . A detailed description of  $\vec{\tau}_Q$  can be found in [30, 47]. Figure 7.2 depicts the association of the generated thrusts with the helicopter's rigid body dynamics. Substituting (7.6), (7.7) to (7.10) a more compact form of the torque can be given as:

$$\tau^B = A(T_M)v_c + B(T_M) \quad (7.11)$$

where:

$$v_c = (a \ b \ T_T)^T \quad (7.12)$$

with  $A(T_M) \in \mathbb{R}^{3 \times 3}$  being an invertible matrix for bounded  $T_M$  and  $B(T_M) \in \mathbb{R}^{3 \times 1}$ .

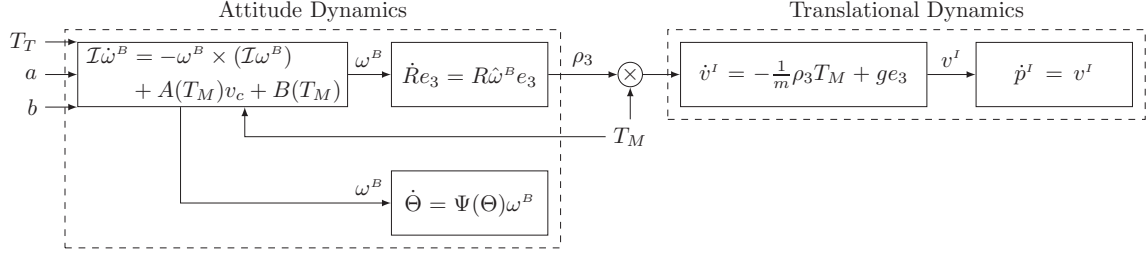


Figure 7.3: This block diagram illustrates the interconnection of the approximated helicopter's dynamics.

### 7.2.3 Complete Rigid Body Dynamics

Using the force simplification assumption given in (7.9) and the applied torque given by (7.11), the translational and angular velocity helicopter dynamics are expressed as:

$$\dot{v}^I = -\frac{1}{m} R e_3 T_M + g e_3 \quad (7.13)$$

$$\mathcal{I}\dot{\omega}^B = -\omega^B \times (\mathcal{I}\omega^B) + A(T_M)v_c + B(T_M) \quad (7.14)$$

where  $e_3 = [0 \ 0 \ 1]^T$ . The interconnection of the helicopter dynamics is shown in Figure 7.3. The helicopter dynamics can be further separated in two interconnected subsystems representing the attitude and the translational dynamics, respectively.

### 7.3 Translational Error Dynamics

Consider a helicopter described by the dynamic equations (7.1), (7.3) and (7.13), (7.14). The objective is to design a controller regulating position  $p^I$  and the yaw angle  $\psi$  to the reference values  $p_r^I = [p_{r,x}^I \ p_{r,y}^I \ p_{r,z}^I]^T$  and  $\psi_r$ , respectively. The proposed controller design requires that the components of  $p_r^I$  and their higher time derivatives are bounded. This is an expected restriction, which reflects the helicopter's physical constraints. Furthermore, the controller design assumes availability of all helicopter's state variables of the translational and attitude dynamics. The con-

troller design is based on the backstepping procedure for systems in feedback form. A description of the backstepping methodology can be found in Appendix A.

Let  $R = [\rho_1 \ \rho_2 \ \rho_3]$  where  $\rho_i$  with  $i = 1, 2, 3$  are the column vectors of the rotation matrix. Denote  $\rho_{i,j}$  the element of the  $j$ th row and  $i$ th column of the rotation matrix. Let  $e_\rho$  denote the orientation error between the actual direction of the thrust vector  $\rho_3$ , minus a desired direction denoted by  $\rho_d = [\rho_{d,1} \ \rho_{d,2} \ \rho_{d,3}]^T$ . Following standard procedure of the backstepping design, the translational error dynamics of the helicopter can be written as:

$$\dot{e}_p = \dot{p}^I - \dot{p}_r^I = -\dot{p}_r^I + v_d^I + e_v \quad (7.15)$$

$$\dot{e}_v = \dot{v}^I - \dot{v}_d^I = ge_3 - \dot{v}_d^I - \frac{1}{m}\rho_d T_M - \frac{1}{m}e_\rho T_M \quad (7.16)$$

The elements of the unitary vector  $\rho_3$  express the inertia coordinates of the body's frame vector  $\vec{k}_B$ . The term  $-\rho_3 T_M$  represents the helicopter's thrust force. Obviously,  $\rho_3$  dictates the direction of the thrust vector while  $T_M$  its magnitude. As illustrated in Figure 7.3, the thrust magnitude  $T_M$  is a direct control command while the direction vector  $\rho_3$  is indirectly manipulated by the attitude dynamics. The translational error dynamics subsystem is shown in Figure 7.4.

The main design idea of this step is to choose the desired velocity dynamics  $v_d^I$ , the desired direction and magnitude of the thrust vector ( $\rho_d$  and  $T_M$ , respectively) in such a way so that the translational error dynamics will be globally asymptotically stable (GAS) by disregarding initially the effect of  $e_\rho$ . The resulting translational error dynamics subsystem can be viewed as GAS nominal system perturbed by the orientation error  $e_\rho$ . As it will be illustrated, the proposed choice of  $v_d^I, \rho_d, T_M$  followed by the exponential stability of the orientation error  $e_\rho$ , will guarantee that the complete translational error dynamics will be uniformly globally asymptotically stable (UGAS) for any initial condition of the position and translational velocity.

The following desired values will be chosen:

$$v_d^I = \dot{p}_r^I \quad (7.17)$$

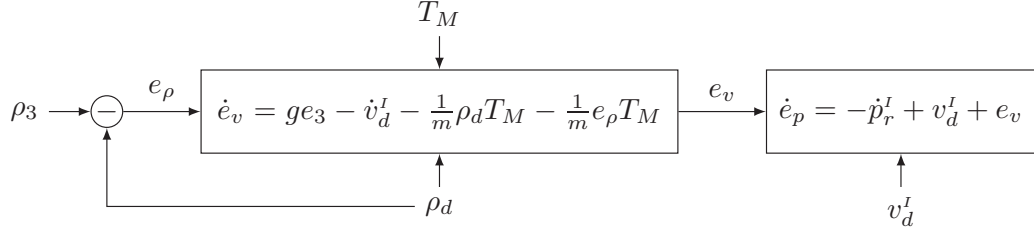


Figure 7.4: This block diagram illustrates the translational error dynamics subsystem.

$$\rho_d = \frac{-\ddot{p}_r^I + ge_3 + \Sigma_2(e_v + \Sigma_1(W(e_v + e_p)))}{\left\| -\ddot{p}_r^I + ge_3 + \Sigma_2(e_v + \Sigma_1(W(e_v + e_p))) \right\|} \quad (7.18)$$

$$T_M = m \left\| -\ddot{p}_r^I + ge_3 + \Sigma_2(e_v + \Sigma_1(W(e_v + e_p))) \right\| \quad (7.19)$$

where  $W = \text{diag}(w_1, w_2, w_3)$  with  $w_i > 0$  for  $i = 1, 2, 3$  and:

$$\begin{aligned} S(e_p, e_v) &= \Sigma_2(e_v + \Sigma_1(W(e_v + e_p))) \\ &= \begin{bmatrix} \sigma_{2,1}(e_{v,x} + \sigma_{1,1}(w_1(e_{v,x} + e_{p,x}))) \\ \sigma_{2,2}(e_{v,y} + \sigma_{1,2}(w_2(e_{v,y} + e_{p,y}))) \\ \sigma_{2,3}(e_{v,z} + \sigma_{1,3}(w_3(e_{v,z} + e_{p,z}))) \end{bmatrix} \end{aligned} \quad (7.20)$$

The function  $\sigma$  denotes a saturation function, which is defined as follows:

**Definition 7.1.** The function  $\sigma : \mathbb{R} \rightarrow \mathbb{R}$  is a continuous, twice differentiable, nondecreasing function for which given two positive numbers  $L, M$  with  $L \leq M$  the following properties hold:

- P.1.  $\sigma(s) = s$  when  $|s| \leq L$ ;
- P.2.  $|\sigma(s)| \leq M$  for every  $s \in \mathbb{R}$ ;
- P.3.  $s\sigma(s) > 0$  for every  $s \neq 0$ ;
- P.4.  $|\sigma(s)| \leq |s|$  for every  $s \in \mathbb{R}$ ;

P.5.  $\sigma(s)$  is globally Lipschitz in  $s$ , with Lipschitz constant  ${}^\sigma L$ . Hence:

$$\forall s_1, s_2 \in \mathbb{R} \quad |\sigma(s_1) - \sigma(s_2)| \leq {}^\sigma L |s_1 - s_2|$$

The above definition of the linear saturation function is similar to the definition given in [102]. Two additional properties are added. The twice differentiability and the globally Lipschitz property (P.5) that are necessary for the backstepping design.

The choice of the desired thrust vector  $-\rho_d T_M$  given in (7.18), (7.19) is twofold. Firstly, by (7.18) it is obvious that  $\rho_d$  is chosen to be a unitary vector. Secondly, due to the use of the nested saturation feedback, given that the desired acceleration  $\ddot{p}_r^I$  is bounded by (7.19) the thrust magnitude  $T_M$  will be bounded as well. This fact is of particular importance since due to the physical constraints of the helicopter actuation, stability should be achieved with limited control resources.

The helicopter during the flight operation is required not to overturn while tracking the reference maneuver. More specifically it is required that  $|\phi(t)| < \pi/2$  and  $|\theta(t)| < \pi/2$  for every  $t \geq t_0$ . Apart from the physical helicopter flight limitations, this condition is necessary to avoid singularities in the rotation matrix representation by the Euler angles. Similar constraints apply by the use of quaternions for the attitude representation [4, 37]. Since  $\rho_{3,3} = C_\theta C_\phi$  the helicopter will not overturn if the inequality  $\rho_{3,3}(t) > 0$  is preserved for every  $t \geq t_0$ . When the helicopter is tracking its desired orientation, dictated by the directional vector  $\rho_d$ , the same limitation should apply. In other words,  $|\phi_d(t)| < \pi/2$  and  $|\theta_d(t)| < \pi/2$  for every  $t \geq t_0$ . From (7.18) an additional constraint is imposed on the choice of the saturation vector  $S(e_p, e_v)$  and the desired position trajectory. This constraint is sufficient to guarantee that  $\rho_{d,3} = C_{\theta_d} C_{\phi_d} > 0$  for every  $t \geq t_0$ .

**Property 7.1.** *If for every  $t \geq t_0$  the saturation level  $M_{2,3}$  of the function  $\sigma_{2,3}$  and the predefined value of  $\ddot{p}_{r,z}^I$  satisfy the inequality:*

$$g - M_{2,3} > \max_{t \geq t_0} \ddot{p}_{r,z}^I(t)$$

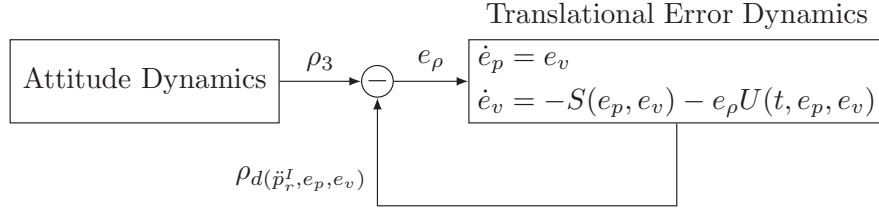


Figure 7.5: Resulting system dynamics after the choice of  $v_d^I$ ,  $\rho_d$  and  $T_M$ .

then  $\rho_{d,3}(t) > 0$  and consequently  $|\phi_d(t)|, |\theta_d(t)| < \pi/2$  for every  $t \geq t_0$ .

The above property can be easily verified by the following series of inequalities:

$$\begin{aligned} & \rho_{d,3}(t) > 0 \\ \Rightarrow & -\ddot{p}_{r,z}^I(t) + g + \sigma_{2,3} \left( e_{v,z} + \sigma_{1,3} (w_3(e_{v,z} + e_{p,z})) \right) > 0 \\ \Rightarrow & g - M_{2,3} > \max_{t \geq t_0} \ddot{p}_{r,z}^I(t) \end{aligned}$$

Substitution of the desired values given in (7.17)-(7.19) will result in the following representation of the translational error dynamics:

$$\dot{e}_p = e_v \quad (7.21)$$

$$\dot{e}_v = -S(e_p, e_v) - \underbrace{(\rho_3(\Theta) - \rho_d(t))}_{e_\rho} U(t, e_p, e_v) \quad (7.22)$$

where:

$$U(t, e_p, e_v) = \left\| -\ddot{p}_r^I + g e_3 + \Sigma_2 \left( e_v + \Sigma_1 (W(e_v + e_p)) \right) \right\| \quad (7.23)$$

Regarding  $U(\cdot)$  the following property will hold:

**Property 7.2.** Given that  $\rho_{d,3}(t) > 0$  for every  $t \geq t_0$ , then the following inequalities will hold:

$$U_{min} \leq U(t, e_p, e_v) \leq U_{max}$$

with:

$$U_{min} = g - M_{2,3} - \max_{t \geq t_0} \ddot{p}_{r,z}^I(t) > 0$$

$$U_{max} = \max_{t \geq t_0} \|\ddot{p}_r^I(t)\| + g + \sqrt{3}(M_{2,1} + M_{2,2} + M_{2,3})$$

The resulting system dynamics, up to this point, can be seen in Figure 7.5. The translational error dynamics subsystem can be considered as a GAS nominal system of a single integrator controlled by a nested saturation feedback law. Chains of integrators controlled by linear saturation functions have been extensively investigated in [102]. The nominal system is perturbed by a bounded term of the orientation error  $e_\rho$ . The stability analysis of the resulting translational error dynamics will be investigated in detail in Section 7.6, after we establish some useful stability results associated with the attitude error dynamics subsystem.

Before we proceed with the analysis of the attitude dynamics subsystem, the following observation is mentioned. Since  $\rho_3$  and  $\rho_d$  are unitary vectors there is an additional constraint expressed by the equality  $\rho_{3,3} = \sqrt{1 - \rho_{3,1}^2 - \rho_{3,2}^2}$  given that  $\rho_{3,3} \geq 0$ . Due to this constraint it is shown that only exponential decay of the vector  $e_\rho = \rho - \rho_d$  with  $\rho = [\rho_{3,1} \ \rho_{3,2}]^T$  and  $\rho_d = [\rho_{d,1} \ \rho_{d,2}]^T$  is required. The vectors  $\rho$  and  $\rho_d$  lie in the  $x - y$  plane of the inertia frame. Given that the controller design guarantees that the helicopter will not overturn ( $\rho_{3,3}(t) > 0$  for every  $t > t_0$ ) the exponential convergence of  $\rho_{3,3}$  to  $\rho_{d,3}$  follows. A representation of the orthonormal vectors  $\rho_3, \rho_d$  can be seen in Figure 7.6.

**Definition 7.2.** Denote the open and connected sets:

1.  $\mathcal{P} = (0 \ 1]$
2. The two dimensional set  $\mathcal{Q} = \{v \in \mathbb{R}^2 : \|v\| < 1\}$
3. The two dimensional set  $\mathcal{E} = (-2 \ 2) \times (-2 \ 2)$

A consequence of the angle bounds  $|\theta|, |\phi| < \pi/2$  and  $|\theta_d|, |\phi_d| < \pi/2$  are the statements of the following Proposition:

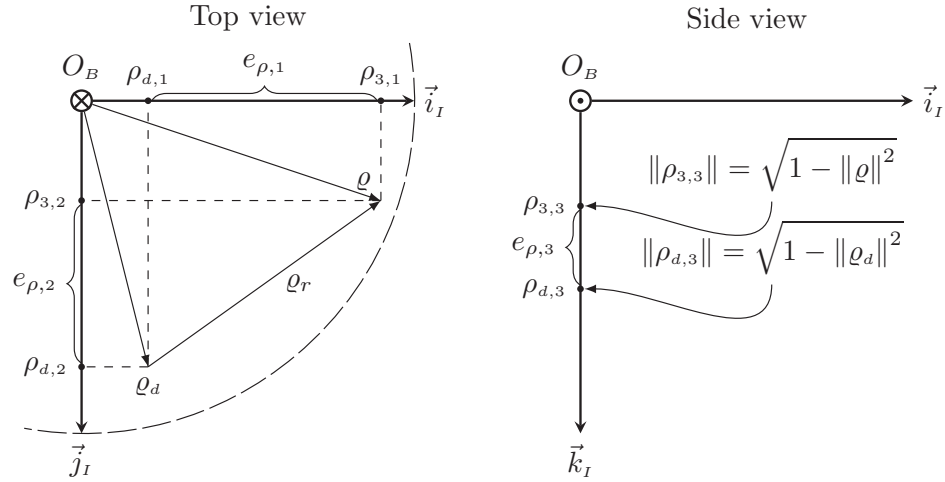


Figure 7.6: This figure illustrates the helicopter's vertical orientation vectors  $\rho_3, \rho_d$  with respect to inertia frame for  $\rho_{3,3}, \rho_{d,3} > 0$ .

**Proposition 7.1.** When  $\rho_{3,3}, \rho_{d,3} \in \mathcal{P}$  then:

1.  $|\phi|, |\phi_d|, |\theta|, |\theta_d| < \pi/2$
2.  $\varrho, \varrho_d \in \mathcal{Q}$
3.  $e_\varrho \in \mathcal{E}$

This Section has introduced the applied pseudo controls associated with the translational error dynamics. Additional comments and conditions were presented related to the orientation restrictions of the helicopter during the flight maneuver, that are necessary for the analysis of the attitude dynamics. The detailed stability analysis of the translational error dynamics subsystem is given in Section 7.6, after some useful results associated with the stability of the attitude dynamics are established in Sections 7.4 and 7.5.

#### 7.4 Attitude Error Dynamics

This Section presents the attitude error dynamics subsystem. Furthermore, the proposed pseudo controls and the input vector  $v_c$  for the stabilization of the attitude error are provided. Apart from

the stabilization part, additional goal for the control law is to keep  $|\theta(t)|, |\phi(t)| < \pi/2$  for every  $t \geq t_0$  for any initial condition of the attitude dynamics for which the helicopter is not overturned.

#### 7.4.1 Yaw Error Dynamics

The yaw dynamics are obtained by the equation:

$$\dot{\psi} = \Psi_3(\Theta) \omega^B \quad (7.24)$$

where  $\Psi_3(\Theta)$  is the third row of the matrix  $\Psi(\Theta)$  defined in (3.25). Let  $e_\psi = \psi - \psi_r$  be the error of the yaw angle, then the error dynamics will be:

$$\begin{aligned} \dot{e}_\psi &= -\dot{\psi}_r + \Psi_3(\Theta) \omega^B \\ &= -\dot{\psi}_r + \frac{S_\phi}{C_\theta} q + \frac{C_\phi}{C_\theta} r \end{aligned} \quad (7.25)$$

Using the yaw angular velocity  $r$  as pseudo control, the error dynamics for the yaw angle can be written as:

$$\dot{e}_\psi = -\dot{\psi}_r + \frac{S_\phi}{C_\theta} q + \frac{C_\phi}{C_\theta} r_d + \alpha(\phi, \theta) e_\omega \quad (7.26)$$

where  $e_\omega = \omega^B - \omega_d^B$ , with  $e_\omega = [e_{\omega,x} \ e_{\omega,y} \ e_{\omega,z}]$ ,  $\omega_d^B = [p_d \ q_d \ r_d]^T$  and  $\alpha(\phi, \theta) = \left[0 \ 0 \ \frac{C_\phi}{C_\theta}\right]$ . The value of  $r_d$  will be chosen in such a way to cancel out the nonlinear terms and stabilize the yaw error dynamics. The choice is:

$$r_d = \frac{C_\theta}{C_\phi} \left[ \dot{\psi}_r - \frac{S_\phi}{C_\theta} q - \lambda_\psi e_\psi \right] \quad (7.27)$$

where  $\lambda_\psi$  is a positive gain. The yaw dynamics become:

$$\dot{e}_\psi = -\lambda_\psi e_\psi + \alpha(\phi, \theta) e_\omega \quad (7.28)$$

## 7.4.2 Orientation Error Dynamics

As mentioned earlier due to the constraint of orthonormality of the vector  $\rho_3$  the orientation analysis can be restricted to the vector  $\varrho \in \mathcal{E}$ . As it will be shown, exponential stabilization of the error dynamics  $e_\varrho = \varrho - \varrho_d$  will guarantee the exponential stabilization of  $e_\rho$ . The reduced orientation error dynamics are:

$$\dot{e}_\varrho = -\dot{\varrho}_d + Z(\Theta) \begin{bmatrix} p_d \\ q_d \end{bmatrix} + Z(\Theta) \begin{bmatrix} e_{\omega,x} \\ e_{\omega,y} \end{bmatrix} \quad (7.29)$$

where:

$$Z(\Theta) = \begin{bmatrix} -\rho_{2,1} & \rho_{1,1} \\ -\rho_{2,2} & \rho_{1,2} \end{bmatrix} \text{ with }^2 Z^{-1}(\Theta) = \frac{1}{\rho_{3,3}} \begin{bmatrix} \rho_{1,2} & -\rho_{1,1} \\ \rho_{2,2} & -\rho_{2,1} \end{bmatrix} \quad (7.30)$$

The choice of the angular velocity pseudo controls is:

$$\begin{bmatrix} p_d \\ q_d \end{bmatrix} = Z^{-1}(\Theta) \left( \dot{\varrho}_d - \Lambda_1 e_\varrho - \frac{k}{\rho_{3,3}} e_\varrho \right) \quad (7.31)$$

where  $\Lambda_1 = \text{diag}(\lambda_{1,1}, \lambda_{1,2})$  with  $\lambda_{1,i}, k > 0$  for  $i = 1, 2$ . The reduced orientation error dynamics take the form:

$$\begin{aligned} \dot{e}_\varrho &= -\Lambda_1 e_\varrho - \frac{k}{\rho_{3,3}} e_\varrho + Z(\Theta) \begin{bmatrix} e_{\omega,x} \\ e_{\omega,y} \end{bmatrix} \\ &= -\Lambda_1 e_\varrho - \frac{k}{\rho_{3,3}} e_\varrho + Z_0(\Theta) e_\omega \end{aligned} \quad (7.32)$$

with  $Z_0(\Theta) = [Z(\Theta) \ 0_{2 \times 1}]$ . It can be easily verified that  $\|Z(\Theta)\| = \|Z_0(\Theta)\| = 1$ .

<sup>2</sup>Note that  $\rho_{3,3} = \rho_{1,1}\rho_{2,2} - \rho_{1,2}\rho_{2,1}$ .

### 7.4.3 Angular Velocity Error Dynamics

The angular velocity error dynamics  $e_\omega$  based on (7.14) have the following form:

$$\begin{aligned}
 \mathcal{I}\dot{e}_\omega &= \mathcal{I}(\dot{\omega}^B - \dot{\omega}_d^B) \\
 &= -\mathcal{I}\dot{\omega}_d^B - \hat{\omega}^B \mathcal{I}\omega^B + A(T_M)v_c + B(T_M) \\
 &= -\mathcal{I}\dot{\omega}_d^B - \hat{e}_\omega \mathcal{I}\omega^B - \hat{\omega}_d^B \mathcal{I}\omega^B + A(T_M)v_c + B(T_M)
 \end{aligned} \tag{7.33}$$

The initial objective of  $v_c$  is to remove the effect of  $A(T_M)$  and  $B(T_M)$ . Therefore the initial choice of  $v_c$  is:

$$v_c = A^{-1}(T_M) [-B(T_M) + \tilde{v}] \tag{7.34}$$

The vector  $\tilde{v}$  is an additional stabilizing term of the following form:

$$\tilde{v} = \mathcal{I}\dot{\omega}_d^B + \hat{\omega}_d^B \mathcal{I}\omega^B - e_\psi \alpha(\phi, \theta)^T - \Lambda_2 e_\omega \tag{7.35}$$

where  $\Lambda_2 \in \mathbb{R}^{3 \times 3}$  is a diagonal matrix of positive gains.

### 7.5 Stability of the Attitude Error Dynamics

Applying the control  $v_c$  of (7.34), (7.35) and the pseudo controls given in (7.27), (7.31), the error attitude dynamics become:

$$\begin{aligned}
 \dot{e}_\rho &= -\Lambda_1 e_\rho - \frac{k}{\rho_{3,3}} e_\rho + Z_0(\Theta) e_\omega \\
 \dot{e}_\psi &= -\lambda_\psi e_\psi + \alpha(\phi, \theta) e_\omega \\
 \mathcal{I}\dot{e}_\omega &= -\hat{e}_\omega \mathcal{I}\omega^B - e_\psi \alpha(\phi, \theta)^T - \Lambda_2 e_\omega
 \end{aligned} \tag{7.36}$$

The complete error vector of the attitude dynamics is given by the state vector  $[e_\psi \ e_\rho \ e_\omega]^T \in \mathcal{Z}$  where  $\mathcal{Z} = \mathbb{R} \times \mathcal{E} \times \mathbb{R}^3$ . Precondition for the continuity of the right hand side of (7.36) is for  $\rho_{3,3}$  to belong to the set  $\mathcal{P}$ .

**Theorem 7.1.** *Given that  $\rho_{3,3}(t)$  and the desired value of  $\rho_{d,3}(t)$  belong to  $\mathcal{P}$  for every  $t \geq t_0$ , and the choice of gains:*

$$\begin{aligned}\lambda_{1,1} &= \kappa_1 + \theta_1^2 & \lambda_{1,2} &= \kappa_2 + \eta_1^2 \\ \lambda_{2,min} &= \zeta + \theta_2^2 + \eta_2^2\end{aligned}$$

where  $\lambda_{2,min}$  is the minimum entry of the gain matrix  $\Lambda_2$  and  $\theta_1, \theta_2, \eta_1, \eta_2, \zeta > 0$  with  $\theta_1\theta_2 \geq 1/2$ ,  $\eta_1\eta_2 \geq 1/2$ , then the error dynamics of the system described by equations (7.36) are exponentially stable for any initial condition  $[e_\psi(t_0) \ e_\rho(t_0) \ e_\omega(t_0)] \in \mathcal{Z}$ .

*Proof.* The stability analysis of the attitude dynamics begins by considering the below Lyapunov quadratic function of the associated attitude variables:

$$V(e_\psi, e_\rho, e_\omega) = \frac{1}{2}e_\psi^2 + \frac{1}{2}e_\rho^T e_\rho + \frac{1}{2}e_\omega^T \mathcal{I} e_\omega$$

The derivative of  $V(e_\psi, e_\rho, e_\omega)$  along the trajectories of the attitude dynamics, for every  $[e_\psi \ e_\rho \ e_\omega] \in \mathcal{Q}$  and  $\rho_{3,3} \in \mathcal{P}$  will be:

$$\begin{aligned}\dot{V}(e_\psi, e_\rho, e_\omega) &= e_\psi \dot{e}_\psi + e_\rho^T \dot{e}_\rho + e_\omega^T \mathcal{I} \dot{e}_\omega \\ &= -\lambda_\psi e_\psi^2 - e_\rho^T \Lambda_1 e_\rho - \frac{k}{\rho_{3,3}} e_\rho^T e_\rho - e_\omega^T \Lambda_2 e_\omega + e_\rho^T Z_0(\Theta) e_\omega \\ &\leq -\lambda_\psi \|e_\psi\|^2 - \frac{k}{\rho_{3,3}} e_\rho^T e_\rho - \lambda_{1,1} \|e_{\rho,1}\|^2 - \lambda_{1,2} \|e_{\rho,2}\|^2 \\ &\quad - \lambda_{2,min} \|e_\omega\|^2 + e_{\rho,1} [1 \ 0] Z_0(\Theta) e_\omega + e_{\rho,2} [0 \ 1] Z_0(\Theta) e_\omega \\ &\leq -\lambda_\psi \|e_\psi\|^2 - \lambda_{1,1} \|e_{\rho,1}\|^2 - \lambda_{1,2} \|e_{\rho,2}\|^2 - \lambda_{2,min} \|e_\omega\|^2 \\ &\quad + (\theta_1 \|e_{\rho,1}\| - \theta_2 \|e_\omega\|)^2 + (\eta_1 \|e_{\rho,1}\| - \eta_2 \|e_\omega\|)^2 \\ &\quad + \|e_{\rho,1}\| \|e_\omega\| + \|e_{\rho,2}\| \|e_\omega\|\end{aligned}$$

$$\begin{aligned}
&\leq -\lambda_\psi \|e_\psi\|^2 - (\lambda_{1,1} - \theta_1^2) \|e_{\rho,1}\|^2 - (\lambda_{1,2} - \eta_1^2) \|e_{\rho,2}\|^2 \\
&\quad - (2\theta_1\theta_2 - 1) \|e_{\rho,1}\| \|e_\omega\| - (2\eta_1\eta_2 - 1) \|e_{\rho,2}\| \|e_\omega\| \\
&\quad - (\lambda_{2,\min} - \theta_2^2 - \eta_2^2) \|e_\omega\|^2 \\
&\leq -\lambda_\psi \|e_\psi\|^2 - \kappa_1 \|e_{\rho,1}\|^2 - \kappa_2 \|e_{\rho,2}\|^2 - \zeta \|e_\omega\|^2
\end{aligned}$$

This proves the theorem. □

The exponential decay of the vector  $e_\rho$  from Theorem 7.1 results in the following inequalities:

$$\|e_{\rho,1}\| \leq \|e_{\rho,1}(t_0)\| e^{-\kappa_1(t-t_0)} \quad \text{and} \quad \|e_{\rho,2}\| \leq \|e_{\rho,2}(t_0)\| e^{-\kappa_2(t-t_0)}, \quad \forall t \geq t_0 \quad (7.37)$$

**Theorem 7.2.** *For the system in (7.36), given a desired orientation vector  $\rho_d(t)$  with the vector component  $\rho_{d,3}(t) > 0$  for every  $t \geq t_0$ , the helicopter will not overturn, satisfying  $\rho_{3,3}(t) > 0$  for every  $t \geq t_0$ . The latter inequality of the vector component  $\rho_{3,3}$  holds for every initial state of the angular velocity and the orientation of the thrust vector, given that  $\rho_{3,3}(t_0) > 0$ .*

*Proof.* The necessary condition for the helicopter not to overturn is  $\rho_{3,3}(t) > 0$  for every  $t \geq t_0$ .

This condition requires that  $\|\varrho\| < 1$  for every  $t \geq t_0$ .

If Property 7.1 holds, then  $\rho_{d,3}(t) > 0$  for every  $t \geq t_0$ . Let  $\min_{t \geq t_0} \rho_{d,3}(t) = c_{\min} > 0$ . Define the positive constant  $C_{\max}$  given by  $\max_{t \geq t_0} (\rho_{d,1}^2(t) + \rho_{d,2}^2(t)) = C_{\max}^2$ . Since:

$$\min_{t \geq t_0} \rho_{d,3}^2(t) = 1 - \max_{t \geq t_0} (\rho_{d,1}^2(t) + \rho_{d,2}^2(t)) \Rightarrow c_{\min}^2 = 1 - C_{\max}^2$$

it follows that  $0 \leq C_{\max} < 1$ . From Theorem 7.1, the error variables  $e_{\rho,1}$  and  $e_{\rho,2}$  are exponentially stable in  $\mathcal{E}$ . The exponential stability of  $e_\rho$  itself can not guarantee that  $\rho_{3,3}(t) > 0 \quad \forall, t \geq t_0$ . Considering only the exponential stability of  $e_\rho$  one gets:

$$-\|e_{\rho,i}(t_0)\| e^{-\kappa_i(t-t_0)} + \rho_{d,i} \leq \rho_{3,i} \leq \|e_{\rho,i}(t_0)\| e^{-\kappa_i(t-t_0)} + \rho_{d,i} \quad (7.38)$$

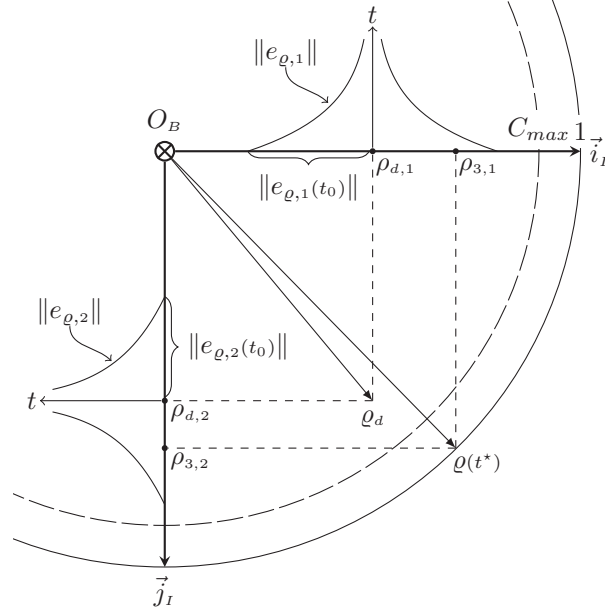


Figure 7.7: This figure illustrates that only the exponential convergence of  $e_\rho$  can not guarantee that  $\|\rho\| < 1$  for every  $t \geq t_0$ . In the depicted case although the inequalities (7.38) hold there might exist a time  $t^*$  for which  $\|\rho(t^*)\| = 1$ .

for  $i = 1, 2$ . The above inequality indicates that there might exist initial conditions  $e_\rho(t_0)$ , a desired vector  $\rho_d$  and a time  $t^*$  such that  $\|\rho(t^*)\| = 1$ . This case is depicted in Figure 7.7. Therefore, the question that arises is what happens when  $\|\rho\| \rightarrow 1$ . Of course the goal is for every  $t \geq t_0$  to hold  $\|\rho\| < 1$ .

From (7.32) the rates of change of the vector  $\rho_3(t)$  in the  $x$  and  $y$  direction of the inertia frame are given by:

$$\dot{\rho} = \dot{\rho}_d - \Lambda_1 e_\rho - \frac{k}{\rho_{3,3}} e_\rho + Z_0(\Theta) e_\omega \quad (7.39)$$

Consider the quadratic function  $R(\|\rho\|) = (1/2) \|\rho\|^2$  of  $\|\rho\|$ . The objective is to prove that each time  $\|\rho\|$  tends to the vicinity of 1, then  $\dot{R}(\|\rho\|) \leq 0$ . The derivative of  $R(\|\rho\|)$  is:

$$\begin{aligned} \dot{R}(\|\rho\|) &= \rho^T \dot{\rho} = \rho^T \dot{\rho}_d - \rho^T \Lambda_1 e_\rho - k \frac{\rho^T e_\rho}{\rho_{3,3}} + \rho^T Z_0(\Theta) e_\omega \\ &\leq \rho^T \dot{\rho}_d - \rho^T \Lambda_1 e_\rho + \|\rho\| \|Z_0(\Theta)\| \|e_\omega\| - k \frac{\rho^T e_\rho}{\rho_{3,3}} \end{aligned}$$

$$\begin{aligned}
&\leq \dot{R}(\|\varrho_d\|) + e_\varrho^T \dot{\varrho}_d - \varrho^T \Lambda_1 e_\varrho + \|e_\omega(t_0)\| e^{-\zeta(t-t_0)} - k \frac{\varrho^T e_\varrho}{\rho_{3,3}} \\
&\leq \dot{R}(\|\varrho_d\|) + (\|\dot{\varrho}_d\| + \lambda \|\varrho\|) \|e_\varrho\| + \|e_\omega(t_0)\| e^{-\zeta(t-t_0)} - k \frac{\varrho^T e_\varrho}{\rho_{3,3}} \\
&\leq \dot{R}(\|\varrho_d\|) + \|e_\varrho(t_0)\| (\|\dot{\varrho}_d\| + \lambda) e^{-\kappa(t-t_0)} + \|e_\omega(t_0)\| e^{-\zeta(t-t_0)} \\
&\quad - k \frac{\varrho \varrho^T - \varrho^T \varrho_d}{\sqrt{1 - \|\varrho\|^2}} \\
&\leq \dot{R}(\|\varrho_d\|) + 2 (\|\dot{\varrho}_d\| + \lambda) e^{-\kappa(t-t_0)} + \|e_\omega(t_0)\| e^{-\zeta(t-t_0)} \\
&\quad - k \frac{\|\varrho\| (\|\varrho\| - \|\varrho_d\|)}{\sqrt{1 - \|\varrho\|^2}} \\
&\leq \|\chi(t, \varrho_d, \dot{\varrho}_d, \|e_\omega(t_0)\|)\| - \frac{\varpi(\|\varrho\|)}{\sqrt{1 - \|\varrho\|^2}} = \bar{R}(\|\chi(\cdot)\|, \|\varrho\|)
\end{aligned}$$

where  $\kappa = \min(\kappa_1, \kappa_2)$ ,  $\lambda = \max(\lambda_{1,1}, \lambda_{1,2})$  and:

$$\begin{aligned}
\chi(\cdot) &= \dot{R}(\|\varrho_d\|) + 2 (\|\dot{\varrho}_d\| + \lambda) e^{-\kappa(t-t_0)} + \|e_\omega(t_0)\| e^{-\zeta(t-t_0)} \\
\varpi(\cdot) &= k \|\varrho\| (\|\varrho\| - C_{max})
\end{aligned}$$

When  $\|\varrho\|$  lies inside the set  $C_{max} = (C_{max} - 1)$  it is obvious that  $\varpi(\|\varrho\|) > 0$ . By solving  $\bar{R}(\|\chi(\cdot)\|, \|\varrho\|) < 0$ , with respect to  $\|\varrho\|$  when  $\|\varrho\| \in C_{max}$ , after some algebraic calculations it is easy to show that there exists a  $C^*(\|\chi(\cdot)\|)$ , with  $C_{max} < C^*(\cdot) < 1$  for every  $\|\chi(\cdot)\| \in \mathbb{R}$ , such that when  $\|\varrho\| > C^*$  then  $\dot{R}(\|\varrho\|) < 0$ . The value of  $C^*$  is given by:

- If  $C_{max} > 0$  then:

$$C^*(\gamma_1) = \frac{C_{max} + \gamma_1 \sqrt{\gamma_1^2 + 1 - C_{max}^2}}{1 + \gamma_1^2}$$

where:

$$\gamma_1(\|\chi(\cdot)\|) = \frac{\|\chi(t, \varrho_d, \dot{\varrho}_d, \|e_\omega(t_0)\|)\|}{k C_{max}}$$

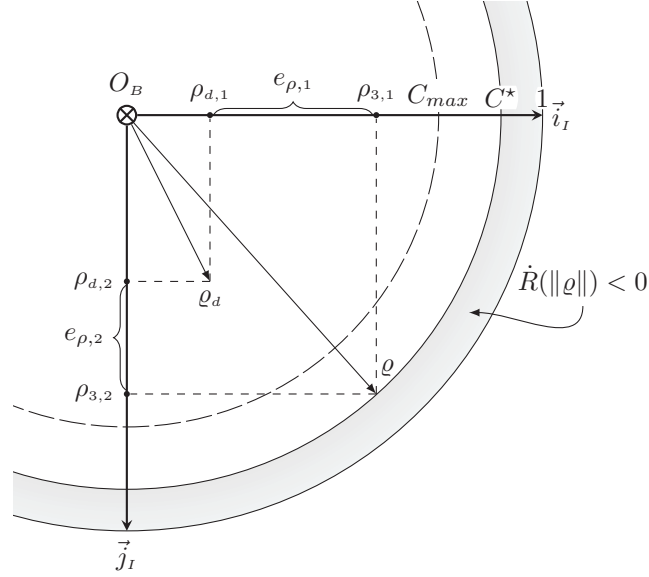


Figure 7.8: This figure illustrates the existence of a value  $C^*$  with  $C_{max} < C^* < 1$  such that when  $\|\varrho\| > C^*$  then  $\dot{R}(\|\varrho\|) < 0$ . The definition of  $R(\|\varrho\|)$  is given in the proof of Theorem 7.2.

- If  $C_{max} = 0$  then  $\|\varrho_d\| = \|\dot{\varrho}_d\| = 0$  for every  $t \geq 0$ , and the value of  $C^*$  is given by:

$$C^*(\gamma_2) = \sqrt{\frac{\gamma_2 \sqrt{\gamma_2^2 + 4} - \gamma_2^2}{2}}$$

where:

$$\gamma_2(\|\chi(\cdot)\|) = \frac{\|\chi(t, 0, 0, \|e_\omega(t_0)\|)\|}{k}$$

Since  $R(\|\varrho\|)$  is a positive definite function of  $\|\varrho\|$  and  $\dot{R}(\|\varrho\|) < 0$  for every  $\|\varrho\| > C^*$  with  $C^* < 1$ , then  $\|\varrho\|$  is decreasing in the interval  $(C^* - 1)$  and never reaches 1, so the helicopter will never overturn. This proves the theorem. A graphic representation clarifying the findings of this proof can be seen in Figure 7.8. □

Due to the fact that  $\rho_{3,3} = C_\theta C_\phi$ , Theorem 7.2 implies that  $|\theta(t)|, |\phi(t)| < \pi/2$  for every  $t \geq t_0$  given that  $|\theta(t_0)|, |\phi(t_0)| < \pi/2$ .

**Lemma 7.1.** *Given that the conditions of Theorem 7.1 are met for the system in (7.36), the dynamics of  $e_{\rho,3}$  will exponentially decay to zero, with the bound:*

$$\|e_{\rho,3}\| \leq \frac{2\sqrt{2}}{c_{min}} \|e_{\varrho}(t_0)\| e^{-\kappa(t-t_0)}$$

where  $\kappa = \min(\kappa_1, \kappa_2)$ .

*Proof.* From Theorem 7.2 it has been proved that  $\rho_{3,3} > 0$  and  $\rho_{d,3} \geq c_{min}$  for every  $t \geq t_0$ . Thus:

$$\rho_{3,3} + \rho_{d,3} \geq c_{min} \Rightarrow \frac{1}{\rho_{3,3} + \rho_{d,3}} \leq \frac{1}{c_{min}}$$

Regarding  $e_{\rho,3}$  one has:

$$\begin{aligned} e_{\rho,3} &= \rho_{3,3} - \rho_{d,3} = \frac{\rho_{3,3}^2 - \rho_{d,3}^2}{\rho_{3,3} + \rho_{d,3}} = \frac{-\rho_{3,1}^2 - \rho_{3,2}^2 + \rho_{d,1}^2 + \rho_{d,2}^2}{\rho_{3,3} + \rho_{d,3}} \\ &= \frac{-(\rho_{3,1} + \rho_{d,1})(\rho_{3,1} - \rho_{d,1}) - (\rho_{3,2} + \rho_{d,2})(\rho_{3,2} - \rho_{d,2})}{\rho_{3,3} + \rho_{d,3}} \\ &= \frac{-e_{\varrho,1}(\rho_{3,1} + \rho_{d,1}) - e_{\varrho,2}(\rho_{3,2} + \rho_{d,2})}{\rho_{3,3} + \rho_{d,3}} \end{aligned}$$

The norm of  $e_{\rho,3}$  will be:

$$\begin{aligned} \|e_{\rho,3}\| &\leq \left\| \frac{\rho_{3,1} + \rho_{d,1}}{\rho_{3,3} + \rho_{d,3}} \right\| \|e_{\varrho,1}\| + \left\| \frac{\rho_{3,2} + \rho_{d,2}}{\rho_{3,3} + \rho_{d,3}} \right\| \|e_{\varrho,2}\| \\ &\leq \frac{2\sqrt{2}}{c_{min}} \|e_{\varrho}\| \leq \frac{2\sqrt{2}}{c_{min}} \|e_{\varrho}(t_0)\| e^{-\kappa(t-t_0)} \end{aligned}$$

□

An immediate consequence of Theorem 7.1 and Lemma 7.1 is the following property, which summarizes the bounds of the norm  $\|e_{\rho}\|$ . Those bounds are useful in the analysis of the translational error dynamics.

**Property 7.3.** *Given that Theorem 7.1 and Lemma 7.1 hold,  $\|e_{\rho}\|$  will have the following bounds:*

7.3.1.  $\|e_{\rho}\| \leq 2$

7.3.2. For the components of the error vector  $e_\rho$ :

$$\|e_{\rho,i}\| \leq \epsilon_i \|e_\rho(t_0)\| e^{-\kappa(t-t_0)}$$

where  $\epsilon_i = 1$  for  $i = 1, 2$  and  $\epsilon_3 = 2\sqrt{2}/c_{min}$ .

7.3.3. The vector  $e_\rho$  is exponentially stable for every  $e_\rho(t_0) \in \mathcal{E} \times \mathcal{P}$  with the exponentially decaying bound:

$$\|e_\rho\| \leq \frac{c_{min} + 2\sqrt{2}}{c_{min}} \|e_\rho(t_0)\| e^{-\kappa(t-t_0)}$$

*Proof.* Due to orthonormality  $\|\rho_3\|, \|\rho_d\| = 1$ . Consequently, Property 7.3.1 is derived by:

$$\begin{aligned} \|e_\rho\| &= \sqrt{(\rho_3 - \rho_d)^T (\rho_3 - \rho_d)} = \sqrt{\rho_3^T \rho_3 + \rho_d^T \rho_d - 2\rho_3^T \rho_d} \\ &= \sqrt{2 - 2\rho_3^T \rho_d} \leq 2 \end{aligned}$$

Property 7.3.2 can be easily derived by Theorem 7.1 and Lemma 7.1. For the exponential bound of Property 7.3.3 the following will hold:

$$\begin{aligned} \|e_\rho\| &\leq \|e_\rho\| + \|e_{\rho,3}\| \\ &\leq \|e_\rho(t_0)\| e^{-\kappa(t-t_0)} + \frac{2\sqrt{2}}{c_{min}} \|e_\rho(t_0)\| e^{-\kappa(t-t_0)} \\ &\leq \frac{c_{min} + 2\sqrt{2}}{c_{min}} \|e_\rho(t_0)\| e^{-\kappa(t-t_0)} \\ &\leq \frac{c_{min} + 2\sqrt{2}}{c_{min}} \|e_\rho(t_0)\| e^{-\kappa(t-t_0)} \end{aligned}$$

□

Lemma 7.1 and Property 7.3.3 provide a very conservative bound on  $\|e_{\rho,3}\|$  and  $\|e_\rho\|$ . However, the useful attribute of those is the exponential decay of  $e_{\rho,3}$  and  $e_\rho$ , which is necessary for the stability analysis of the translational error dynamics.

In this Section, Theorem 7.1 establishes the exponential stability of the attitude error  $[e_\psi \ e_\theta \ e_\omega]^T$ . In addition Theorem 7.2 guarantees that the helicopter will not overturn in its effort to track the reference trajectory, achieving the bounding condition  $|\phi|, |\theta| < \pi/2$  for every  $t \geq t_0$ . Based on those two results, from Property 7.3.3, the exponential decay of the orientation error  $e_\rho$  follows.

## 7.6 Stability of the Translational Error Dynamics

This Section examines the stability of the translational error dynamics. The first step towards the stability analysis is to perform the following linear state transformation:

$$y = \begin{bmatrix} y_1 \\ y_2 \end{bmatrix} = \begin{bmatrix} I_{3 \times 3} & I_{3 \times 3} \\ 0 & I_{3 \times 3} \end{bmatrix} \begin{bmatrix} e_p \\ e_v \end{bmatrix} \quad (7.40)$$

The state transformation above will facilitate the stability analysis of this Section. The resulting form of the translational dynamics is:

$$\dot{y} = f(y) + g(t, y)e_\rho = G(t, y, e_\rho) \quad (7.41)$$

where:

$$f(y) = \begin{bmatrix} y_2 - \Sigma_2(y_2 + \Sigma_1(Wy_1)) \\ -\Sigma_2(y_2 + \Sigma_1(Wy_1)) \end{bmatrix} \quad g(t, y) = - \begin{bmatrix} I_{3 \times 3} \\ I_{3 \times 3} \end{bmatrix} U(t, y) \quad (7.42)$$

The following properties are required to prove global asymptotic stability of the system in (7.41).

**Property 7.4.** *For the nominal system:*

$$\dot{y} = f(y) \quad (7.43)$$

with  $f(y)$  defined in (7.42),  $y = 0$  is an equilibrium point. Given that, for the saturation levels of the vector  $S$  (defined in (7.20)), the following inequalities hold:

1.  $L_{2,i} \leq M_{2,i}$  and  $L_{1,i} \leq M_{1,i}$  for  $i = 1, 2, 3$ .
2.  $M_{1,i} < \frac{1}{3}L_{2,i}$  for  $i = 1, 2, 3$ .

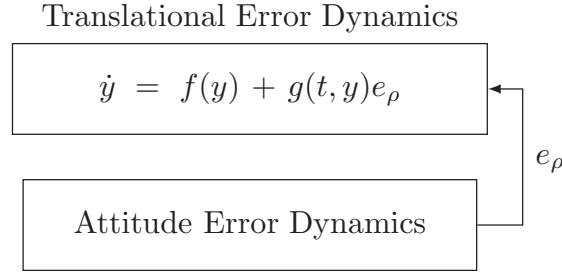


Figure 7.9: Block diagram of the complete helicopter dynamics after the transformation of the translational error states.

Then, based on the findings of [102], the nominal system of (7.43) is GAS.

The resulting helicopter dynamics after the state transformation can be seen in Figure 7.9. The translational dynamics subsystem can be viewed as a perturbed UGAS nominal system where the perturbation term is driven by  $e_\rho$ . The final form of the complete helicopter dynamics is a nonlinear cascaded time-varying system. The stability properties for this class of systems has been investigated in [63]. According to [63], in order for the solutions of the system in (7.41) to be UGAS, the following sufficient conditions should hold simultaneously:

- C.1: The nominal system of (7.43) is UGAS
- C.2: The integral curves of  $e_\rho$  are UGAS
- C.3: The solutions of the system in (7.41) are uniformly globally bounded (UGB).

Conditions C.1 and C.2 are guaranteed by Properties 7.4 and 7.3.3, respectively. The system in (7.41) is not Input to State Stable (ISS). The ISS property would significantly facilitate the proof of condition C.3. Consequently, a different approach is followed, which exploits the Lipschitz properties of  $G(t, y, e_\rho)$  with respect to  $y$  and the bounds of  $e_\rho$  provided by Property 7.3.

**Property 7.5.** *The function  $f(y)$  defined in (7.42), is globally Lipschitz in  $y$ , with Lipschitz constant:*

$$D_f = \sqrt{6}(1 + 2^\Sigma L_2 + 2w_{max}^\Sigma L_1^\Sigma L_2)$$

where  $w_{max} = \max(w_1, w_2, w_3)$  and  ${}^{\Sigma}L_1, {}^{\Sigma}L_2$  positive constants such that:

$$\forall s_1, s_2 \in \mathbb{R}^3 \quad |\Sigma_i(s_1) - \Sigma_i(s_2)| \leq {}^{\Sigma}L_i |s_1 - s_2| \text{ for } i = 1, 2.$$

*Proof.* For the function  $f : \mathbb{R}^6 \rightarrow \mathbb{R}^6$  defined in (7.42), for any  $y, z \in \mathbb{R}^6$  the following inequalities will hold:

$$\begin{aligned} \|f(y) - f(z)\| &= \\ &= \left\| \begin{bmatrix} y_2 - z_2 - \Sigma_2(y_2 + \Sigma_1(Wy_1)) + \Sigma_2(z_2 + \Sigma_1(Wz_1)) \\ -\Sigma_2(y_2 + \Sigma_1(Wy_1)) + \Sigma_2(z_2 + \Sigma_1(Wz_1)) \end{bmatrix} \right\| \\ &\leq |y_2 - z_2 - \Sigma_2(y_2 + \Sigma_1(Wy_1)) + \Sigma_2(z_2 + \Sigma_1(Wz_1))| \\ &\quad + |-\Sigma_2(y_2 + \Sigma_1(Wy_1)) + \Sigma_2(z_2 + \Sigma_1(Wz_1))| \\ &\leq |y_2 - z_2| + 2|-\Sigma_2(y_2 + \Sigma_1(Wy_1)) + \Sigma_2(z_2 + \Sigma_1(Wz_1))| \\ &\leq |y_2 - z_2| + 2{}^{\Sigma}L_2 |y_2 - \Sigma_1(Wy_1) - z_2 + \Sigma_1(Wz_1)| \\ &\leq (1 + 2{}^{\Sigma}L_2) |y_2 - z_2| + 2w_{max} {}^{\Sigma}L_1 {}^{\Sigma}L_2 |y_1 - z_1| \\ &\leq (1 + 2{}^{\Sigma}L_2 + 2w_{max} {}^{\Sigma}L_1 {}^{\Sigma}L_2) (|y_1 - z_1| + |y_2 - z_2|) \\ &\leq (1 + 2{}^{\Sigma}L_2 + 2w_{max} {}^{\Sigma}L_1 {}^{\Sigma}L_2) \sqrt{6} \|y - z\| \end{aligned}$$

Therefore  $f(y)$  is globally Lipschitz in  $y$ . □

The existence of  ${}^{\Sigma}L_1, {}^{\Sigma}L_2$  is guaranteed by property P.5 of Definition 7.1.

**Property 7.6.** For any vector function  $d(t) \in \mathbb{R}^3$  that is uniform continuous with respect to  $t$  and  $\|d(t)\| \leq \delta_0$  for every  $t \geq t_0$  with  $\delta_0$  a positive constant, the function  $g(t, y)d(t) := \Gamma(t, y)$  is globally Lipschitz in  $y$  with Lipschitz constant:

$$D_g(\delta_0) = \delta_0 ({}^{\Sigma}L_2 + w_{max} {}^{\Sigma}L_1 {}^{\Sigma}L_2) \sqrt{12} \frac{U_{max}}{U_{min}}$$

*Proof.* Let  $a(t) = -\ddot{p}_r^I + g e_3$ . For the function  $\Gamma(t, y) = g(t, y)d(t)$  with  $\Gamma : [0, \infty) \times \mathbb{R}^6 \rightarrow \mathbb{R}^6$ , for any  $y, z \in \mathbb{R}^6$  the following inequalities will hold:

$$\begin{aligned}
\|\Gamma(t, y) - \Gamma(t, z)\| &\leq \sqrt{2} \|d(t)U(t, y) - d(t)U(t, z)\| \\
&\leq \delta_0 \sqrt{2} \|U(t, y) - U(t, z)\| \leq \delta_0 \sqrt{2} \left\| \frac{U^2(t, y) - U^2(t, z)}{U(t, y) + U(t, z)} \right\| \\
&\leq \frac{\delta_0 \sqrt{2}}{2U_{min}} \|2a^T(t)(S(y) - S(z)) \\
&\quad + (S(y) + S(z))^T(S(y) - S(z))\| \\
&\leq \frac{\delta_0}{\sqrt{2}U_{min}} \left( 2\|a(t)\| + \|S(y) + S(z)\| \right) \|S(y) - S(z)\| \\
&\leq \delta_0 \sqrt{2} \frac{U_{max}}{U_{min}} |\Sigma_2(y_2 + \Sigma_1(Wy_1)) - \Sigma_2(z_2 + \Sigma_1(Wz_1))| \\
&\leq \delta_0 \sqrt{2} \frac{U_{max}}{U_{min}} (\Sigma L_2 |y_2 - z_2| + w_{max} \Sigma L_1 \Sigma L_2 |y_1 - z_1|) \\
&\leq \delta_0 (\Sigma L_2 + w_{max} \Sigma L_1 \Sigma L_2) \sqrt{12} \frac{U_{max}}{U_{min}} \|y - z\|
\end{aligned}$$

The existence of  $U_{min}, U_{max}$  is guaranteed from Property 7.2 given that Property 7.1 is satisfied and the second derivatives of  $p_r^I(t)$  coordinates are bounded. The above inequality implies that there always exists a Lipschitz constant for every appropriate choice of  $p_r^I(t)$  and for every bounded  $d(t) \in \mathbb{R}^3$ . Therefore  $g(t, y)d(t)$  is globally Lipschitz in  $y$ .  $\square$

The following lemma is an immediate consequence of Properties 7.5 and 7.6.

**Lemma 7.2.** *For any vector  $d(t)$  defined in Property 7.6, the perturbed system:*

$$\dot{y} = f(y) + g(t, y)d(t) := \Pi(t, y) \quad (7.44)$$

*is globally Lipschitz in  $y$  with Lipschitz constant:*

$$D_0(\delta_0) = D_f + D_g(\delta_0)$$

Therefore, the solutions of (7.44) exist, are unique and do not have a finite escape time for any arbitrarily large time interval.

The error vector  $e_\rho$  is continuous and from Property 7.3.1  $\|e_\rho\| \leq 2$  for every  $e_\rho(t_0) \in \mathcal{E}$ . Therefore:

**Lemma 7.3.** *Based on Lemma 7.2, due to the continuity and boundedness of the vector  $e_\rho$ , the system in (7.41) is globally Lipschitz in  $y$ , with Lipschitz constant  $D = D_0(2)$ , therefore the solutions of (7.41) exist, are unique and do not have a finite escape time for any arbitrarily large time interval.*

Lemma 7.3 is of particular interest for the proof of the following theorem, which guarantees the global uniform boundedness of the solutions of the system in (7.41).

**Theorem 7.3.** *Given that Theorems 7.1 and 7.2 hold, the solutions of the system given by (7.41) are UGB for every time  $t \geq t_0$ .*

*Proof.* The nominal system

$$\dot{z} = f(z) \quad (7.45)$$

of (7.43), based on [102] is globally asymptotically stable (GAS). Since it is an autonomous system, it will be uniformly globally bounded (UGB) as well. Therefore for any  $\delta > 0$  (arbitrarily large) there exists  $\beta > 0$  which may depend on  $\delta$  such that:

$$\|z(t_0)\| \leq \delta \Rightarrow \|z(t)\| \leq \beta(\delta) \quad \forall t \geq t_0$$

For the perturbed term of the system in (7.41), for any  $y \in \mathbb{R}^6$  using Property 7.3.1 the following bound will hold:

$$\|g(t, y)e_\rho\| \leq \sqrt{2} \|U(t, y)e_\rho\| \leq 2\sqrt{2}U_{max} = E$$

Applying the Gronwall-Bellman inequality to the integral curves of the nominal (7.45) and perturbed system (7.41), with  $z(t_0) = y(t_0) \leq \delta$  for any finite time interval with  $t \geq t_0$  one obtains:

$$\begin{aligned} \|y(t)\| - \|z(t)\| &\leq \|y(t) - z(t)\| \leq \frac{E}{D} \left[ e^{D(t-t_0)} - 1 \right] \\ \Rightarrow \|y(t)\| &\leq \beta(\delta) + \frac{E}{D} \left[ e^{D(t-t_0)} - 1 \right] = B(\delta, t - t_0) \end{aligned} \quad (7.46)$$

with  $D$  defined in Lemma 7.3. Let  $y_{1,i}, y_{2,i}$  and  $e_{\rho,i}$  with  $i = 1, 2, 3$  denote the  $i^{th}$  component of the vectors  $y_1, y_2$  and  $e_\rho$  correspondingly. The dynamics of the  $i^{th}$  component of the perturbed system (7.41) will be:

$$\begin{aligned} \dot{y}_{1,i} &= y_{2,i} - \sigma_{2,i}(y_{2,i} + \sigma_{1,i}(w_i y_{1,i})) - \gamma_i(t, y, e_{\rho,i}) \\ \dot{y}_{2,i} &= -\sigma_{2,i}(y_{2,i} + \sigma_{1,i}(w_i y_{1,i})) - \gamma_i(t, y, e_{\rho,i}) \end{aligned}$$

where  $\gamma_i(t, y, e_{\rho,i}) = U(t, y)e_{\rho,i}$ . Using Property 7.3.2 one has:

$$\begin{aligned} \|\gamma_i(t, y, e_{\rho,i})\| &= \|U(t, y)e_{\rho,i}\| \\ &\leq U_{max} \|e_{\rho,i}\| \leq U_{max} \epsilon_i \|e_{\rho,i}(t_0)\| e^{-\kappa(t-t_0)} \\ &\leq 2U_{max} \epsilon_i e^{-\kappa(t-t_0)} \end{aligned}$$

To prove uniform boundedness of  $y$  it is sufficient to show uniform boundedness of  $y_{1,i}, y_{2,i}$  for  $i = 1, 2, 3$ . From this point forward of this proof, the subscript  $i$  will be omitted to ease the notation.

From the exponential decaying bound of  $\gamma(\cdot)$  there always exists a finite time  $T^* = t_0 + t^*$  with  $t^* \geq 0$  such that:

$$2U_{max} \epsilon e^{-\kappa t^*} \leq \frac{L_1}{4}$$

Consider the Lyapunov function  $V_2 = \frac{1}{2}y_2^2$ . From the above inequality and using  $t_0 = T^* - t^*$ , the derivative of  $V_2$  along the trajectories of the perturbed system will be:

$$\begin{aligned}\dot{V}_2 &= -y_2\sigma_2(y_2 + \sigma_1(wy_1)) - y_2U(t, y)e_\rho \\ &\leq -y_2\sigma_2(y_2 + \sigma_1(wy_1)) + |y_2|U_{max}\epsilon \|e_\rho(t_0)\| e^{-\kappa(t-t_0)} \\ &\leq -y_2\sigma_2(y_2 + \sigma_1(wy_1)) + |y_2|2U_{max}\epsilon e^{-\kappa t^*} e^{-\kappa(t-T^*)} \\ &\leq -y_2\sigma_2(y_2 + \sigma_1(wy_1)) + |y_2|\frac{L_1}{4}e^{-\kappa(t-T^*)}\end{aligned}$$

For every  $\|y_2\| \geq M_1 + \frac{L_1}{2} = \delta_2$  and for every  $t \geq T^*$  one will get:

$$\begin{aligned}\dot{V}_2 &\leq -y_2\sigma_2(y_2 + \sigma_1(wy_1)) + \frac{L_1}{4}|y_2| \leq -\frac{L_1}{2}|y_2| + \frac{L_1}{4}|y_2| \\ &\leq -\frac{L_1}{4}|y_2|\end{aligned}$$

Then from [43, Theorem 4.18] for every  $|y_2(T^*)| \geq \delta_2$  and for every  $t \geq T^*$  there exists a  $\mathcal{KL}$  function  $\beta_2$  and a finite time  $t_1 \geq 0$  dependent of  $y_2(T^*)$  and  $\delta_2$  such that the integral curve of  $y_2(t)$  satisfies:

$$\begin{aligned}\|y_2(t)\| &\leq \beta_2(\|y_2(T^*)\|, t - T^*) & \forall T^* \leq t \leq T_1 \\ \|y_2(t)\| &\leq \delta_2 & \forall t \geq T_1\end{aligned}$$

where  $T_1 = T^* + t_1$ . Clearly, if  $|y_2(T^*)| \leq \delta_2$  then  $|y_2(t)| \leq \delta_2$  for every  $t \geq T^*$  rendering  $t_1 = 0$  and  $T_1 = T^*$ . Those facts indicate that there always exist a finite time  $T_1 \geq T^*$  after which the integral curve of  $y_2(t)$  will remain bounded in the set  $\Delta_2 = \{y_2 : |y_2| \leq \delta_2\}$  for any initial condition  $y_2(t_0) \in \mathbb{R}$ . Moreover, the asymptotic convergence (or the confinement when  $t_1 = 0$ ) of  $y_2(t)$  to the bounded set  $\Delta_2$  begins at the finite time  $T^*$ . Lemma 7.3 guarantees that the trajectory of  $y_2(t)$  does not have a finite escape time in the interval  $[t_0 T^*]$  and remains bounded.

From (7.46), given that  $\|y_2(t_0)\| \leq \delta$  the trajectory of  $y_2(t)$  for  $t \in [t_0, T^*]$  will be bounded by  $\|y_2(t)\| \leq B(\delta, t^*) = B_2(\delta)$ . Hence, for every  $\delta > 0$  with  $\|y_2(t_0)\| \leq \delta$ :

$$\|y_2(t)\| \leq \max \left( B_2(\delta), \beta_2(B_2(\delta), 0), \delta_2 \right) = R_2(\delta) \quad \forall t \geq t_0$$

Obviously the bound  $R_2(\delta) > 0$  is independent from  $t_0$ . Therefore, the solution  $y_2(t)$  is UGB.

After the time threshold  $T_1$  the argument of the saturation function  $\sigma_2$  will be bounded by:

$$|y_2 + \sigma_1(wy_1)| \leq |y_2| + |\sigma_1(wy_1)| \leq 2M_1 + \frac{L_1}{2} \leq \frac{5}{6}L_2 \quad (7.47)$$

To this extent, when  $t \geq T_1$ , the saturation function  $\sigma_2(\cdot)$  operates in its linear region. Continuing the above procedure, consider the Lyapunov function  $V_1 = \frac{1}{2}y_1^2$ . The derivative of  $V_1$  for every  $t \geq T_1$  will be:

$$\dot{V}_1 = y_1(-\sigma_1(wy_1) - U(t, y)e_{\rho,i}) \leq -y_1\sigma_1(wy_1) + \frac{L_1}{4}|y_1|$$

Consequently, for every  $|y_1| \geq L_1/w = \delta_1$  and  $t \geq T_1$  will yield,  $\dot{V}_1 \leq -\frac{3}{4}L_1|y_1|$ . Once more there exists a  $\mathcal{KL}$  function  $\beta_1$  and a finite time  $t_2$  depended of  $y_1(T_1)$  and  $\delta_1$  such that when  $|y_1(T_1)| \geq \delta_1$ , the integral curve of  $y_1(t)$  satisfies:

$$\begin{aligned} \|y_1(t)\| &\leq \beta_1(\|y_1(T_1)\|, t - T_1) & \forall T_1 \leq t \leq T_2 \\ \|y_1(t)\| &\leq \delta_1 & \forall t \geq T_2 \end{aligned}$$

where  $T_2 = T_1 + t_2$ . If  $|y_1(T_1)| \leq \delta_1$  then  $y_1(t)$  remains bounded in the set  $\Delta_1 = \{y_1 : |y_1| \leq \delta_1\}$  for every  $t \geq T_1$  rendering  $t_2 = 0$ . In either case for any initial condition  $y_1(t_0) \in \mathbb{R}$  there exists a finite time  $T_2 \geq T_1$  after which the trajectory  $y_1(t)$  remains bounded in the set  $\Delta_1$ . The convergence (or the confinement when  $t_2 = 0$ ) of  $y_1(t)$  to  $\Delta_1$  starts when  $t \geq T_1$ . The existence of  $y_1(t)$  in the time interval  $[t_0, T_1]$  is guaranteed by Lemma 7.3.

From (7.46), given that  $\|y_1(t_0)\| \leq \delta$  the trajectory of  $y_1(t)$  for  $t \in [t_0, T_1]$  will be bounded by  $\|y_1(t)\| \leq B(\delta, t^* + t_1) = B_1(\delta, t_1)$ . Hence, for every  $\delta > 0$  and  $t \geq t_0$  with  $\|y_1(t_0)\| \leq \delta$ :

$$\|y_1(t)\| \leq \max\left(B_1(\delta, t_1), \beta_1(B_1(\delta, t_1), 0), \delta_1\right) = R_1(\delta, t_1)$$

The time  $t_1$  is dependent on the value  $y_2(T^*)$  and  $\delta_2$ . Both of them are independent of  $t_0$ . To this extent  $R_1(\delta, t_1)$  does not depend on the initial time  $t_0$  which proves the uniform global boundedness of the trajectory  $y_1(t)$ .

Since  $y_{1,i}(t), y_{2,i}(t)$  are UGB for  $i = 1, 2, 3$  then same holds for the complete states  $y_1(t), y_2(t)$  of the system in (7.41).  $\square$

Theorem 7.3 satisfies the remaining condition C.3 which is required to guarantee that the solutions of (7.41) are UGAS. Based on the work of [63, 94, 103] the stability of the helicopter translational error dynamics is formally stated in the following theorem:

**Theorem 7.4** ([63, 103]). *Given that the nominal system in (7.43) is UGAS (Property 7.4), the orientation error  $e_\rho$  is exponentially convergent and bounded (Property 7.3), and the solutions of (7.41) are UGB (Theorem 7.3), then the solutions of the perturbed system in (7.41) are UGAS.*

Theorems 7.1, 7.2 and 7.4 guarantee that the controller design objectives are met. More specific, for any desired position reference trajectory  $p_r^I$  with bounded higher derivatives satisfying the requirements of Property 7.1 and for every desired yaw heading  $\psi_r$ :

$$\begin{aligned} \lim_{t \rightarrow \infty} \|p^I - p_r^I\| &= 0 & \lim_{t \rightarrow \infty} \|\psi - \psi_r\| &= 0 \\ \text{and } |\theta(t)|, |\phi(t)| &< \pi/2 \quad \forall t \geq t_0 \end{aligned}$$

for any initial condition  $[p^I(t_0) \ v^I(t_0) \ \omega^B(t_0) \ \psi(t_0)]^T \in \mathbb{R}^{10}$  given that the helicopter is not initially overturned ( $|\theta(t_0)|, |\phi(t_0)| < \pi/2$ ).

## 7.7 Numeric Simulation Results

This Section presents the numeric simulation results of the control algorithm. For the helicopter model, the complete representation of the thrust vector is used given in (7.8), which includes the parasitic elements  $X_M, Y_M$  and  $Y_T$ . However, the controller design was based on the simplified force vector representation of (7.9). Furthermore, the total body force and moment vectors of (7.8) and (7.10) are additionally perturbed by the total drag force and moment vectors  $f_d^B$  and  $\tau_d^B$ , respectively. The drag forces and moments are produced by the effect of the relative wind velocity and air pressure, to the surfaces of the helicopter's fuselage, vertical fin and horizontal stabilizer. To represent the complete drag force and moment vectors we have adopted the model given in [66], which is a simplified version of the more elaborate description presented in [29]. Those vectors are:

$$f_d^B = \begin{bmatrix} -d_x^f v_{a,x}^B V_\infty \\ -d_y^f v_{a,y}^B V_\infty - d_y^{vf} |v_{vf}| v_{vf} \\ -d_z^f (v_{a,z}^B + u_i) V_\infty + d_z^{hs} |v_{hs}| v_{hs} \end{bmatrix} \quad \tau_d^B = \begin{bmatrix} z_t d_y^{vf} |v_{vf}| v_{vf} \\ -x_{hs} d_z^{hs} |v_{hs}| v_{hs} \\ -x_t d_y^{vf} |v_{vf}| v_{vf} \end{bmatrix} \quad (7.48)$$

where  $d_x^f, d_y^f, d_z^f, d_y^{vf}, d_z^{hs}$  are constant parameters that depend on the air density as well as the geometry of the fuselage, the vertical fin and horizontal stabilizer. The constant  $u_i$  denotes the main rotor's induced velocity while  $x_{hs}$  is the coordinate of the horizontal stabilizer in the  $\vec{i}_B$  direction of the body frame. The relative wind velocity vector  $v_a^B = [v_{a,x}^B \ v_{a,y}^B \ v_{a,z}^B]^T$  is given by  $v_a^B = v^B - v_w^B$ , where  $v_w^B$  denotes the wind velocity in the body frame coordinates. The rest of the velocity components involved in the drag force and moment model, are:

$$v_{vf} = v_{a,y}^B + x_{tr} \quad v_{hs} = v_{a,z}^B - x_{hs} q \quad (7.49)$$

$$V_\infty = \sqrt{(v_{a,x}^B)^2 + (v_{a,y}^B)^2 + (v_{a,z}^B + u_i)^2} \quad (7.50)$$

In addition to the wind effects, the numeric simulator includes the servo dynamics which are typically represented by a first order filter [30]. Therefore, the servo outputs  $\bar{T}_M, \bar{T}_T$  of the main

and tail rotor are given by:

$$\tau_s \dot{\bar{T}}_M = -\bar{T}_M + T_M \quad \tau_s \dot{\bar{T}}_T = -\bar{T}_T + T_T \quad (7.51)$$

where  $\tau_s$  is the rotors time constant. The applied flapping angles  $\bar{a}$ ,  $\bar{b}$  are produced by the flapping dynamics model established in [30, 70], namely:

$$\tau_f \dot{\bar{a}} = -\tau_f \omega_y - \bar{a} + a \quad \tau_f \dot{\bar{b}} = -\tau_f \omega_x - \bar{b} + b \quad (7.52)$$

where  $\tau_f$  is the main rotor's dynamics time constant. The flapping angles  $a$ ,  $b$  are also saturated to  $\pm 0.25 \text{ rad}$ , complying with realistic limitations of actual rotor configurations. The nominal helicopter model parameters, used by the controller, are obtained by [29] for the MIT's small scale helicopter X-Cell .60 and presented in Table 7.1. The parameters related to the drag forces and moments as well as the servos time constants are given in Table 7.2. The actual helicopter model of the simulator, includes parametric uncertainty that reach a difference of up to 30% with respect to the nominal values used by the controller. All of the above uncertainty injection is necessary for investigating the robust capabilities of the controller under model and parametric uncertainty which occurs in real life applications.

The proposed control scheme can be easily modified in order to include integral components that will attenuate the steady state tracking error, caused by the parametric and model uncertainty. In particular, the nested saturation vector  $S$  and the desired angular velocity component  $r_d$  (defined in (7.20) and (7.27), respectively), can be enhanced with the position and yaw integral error, as follows:

$$S(\eta_p, y_1, y_2) = \Sigma_3 \left( y_2 + \Sigma_2 \left( W_2 y_1 + \Sigma_1 (W_1 (\eta_p + y_1)) \right) \right) \quad (7.53)$$

$$r_d = \frac{C_\theta}{C_\phi} \left[ \dot{\psi}_r - \frac{S_\phi}{C_\theta} q - \lambda_\psi e_\psi - \lambda_\eta \eta_\psi \right] \quad (7.54)$$

Table 7.1: Helicopter parameters.

---


$$\mathcal{I} = \text{diag}(0.18, 0.34, 0.28) \text{ kg} \cdot \text{m}^2, m = 8.2 \text{ kg}, g = 9.81 \text{ m/sec}^2$$

$$x_t = -0.91 \text{ m}, z_t = -0.08 \text{ m}, z_m = -0.235 \text{ m}, x_m = y_m = y_t = 0$$

$$K_\beta = 52 \text{ N} \cdot \text{m/rad}, C^M = 0.004452 \text{ m}/\sqrt{N}, D^M = 0.6304 \text{ N} \cdot \text{m}$$


---

Table 7.2: Drag and servo parameters.

---


$$d_x^f = 0.06, d_y^f = 0.132, d_z^f = 0.09, d_y^{vf} = 0.0072, d_z^{hs} = 0.006 \text{ kg/m},$$

$$x_{hs} = -0.71 \text{ m}, u_i = 4.2 \text{ m/sec}, \tau_s = 0.1 \text{ sec}, \tau_f = 0.1 \text{ sec}$$


---

Table 7.3: Controller gains.

$M_{3,i}$	22	$\Lambda_1$	$\text{diag}(3,1,3,1)$
$L_{3,i}$	21.5	$\Lambda_2$	$\text{diag}(6,6,3)$
$M_{2,i}$	7	$W_1$	$\text{diag}(8,8,8)$
$L_{2,i}$	6.5	$W_2$	$\text{diag}(0.1,0.1,0.1)$
$M_{1,i}$	2	$\lambda_\psi$	2
$L_{1,i}$	1.5	$\lambda_\eta$	2
for $i = 1, 2, 3$		$k$	0.1

where  $\dot{\eta}_p = e_p, \dot{\eta}_\psi = e_\psi, \lambda_\eta > 0$  and  $W_1, W_2$  are diagonal matrices of positive gains. In this case, the requirements of Property 7.4 become,  $L_{i,j} \leq M_{i,j}$  for  $i, j = 1, 2, 3$  while  $M_{j,i} < L_{j+1,i}$  for  $j = 1, 2$  and  $i = 1, 2, 3$ .

The controller performance, in terms of tracking accuracy and dexterity, was tested by the execution of two different maneuvers. For the first maneuver, the helicopter reaches a set point while its velocity exponentially decreases and its heading remains constant. The desired trajectory

for the first maneuver is:

$$p_r^I(t) = \begin{pmatrix} 20 - 20e^{-0.25t} \\ -30 + 30e^{-0.25t} \\ -10 + 10e^{-0.45t} \end{pmatrix} \quad \psi_r(t) = 0$$

The second maneuver is composed of two parts. In the first part the helicopter lifts vertically for 7 seconds. Then it performs an “8 shaped” curved path while it continues to lift. Throughout the whole maneuver the vertical velocity is exponentially decreasing while the heading remains constant. For the second maneuver, the desired position and heading are:

$$p_r^I(t) = (0 \quad 0 \quad -7(1 - e^{-0.3t}))^T \quad \text{for } t \leq 7$$

$$p_r^I(t) = \begin{pmatrix} 20(1 - \cos \frac{2\pi}{23}(t - 7)) \\ 10 \sin(\frac{4\pi}{23}(t - 7)) \\ -7(1 - e^{-0.3t}) \end{pmatrix} \quad \text{for } t > 7$$

$$\psi_r = 0$$

During the execution of both of the maneuvers, the components of the wind speed in the inertia coordinates are (in  $m/sec$ ):

$$v_w^I(t) = 2 \sin(t) \quad v_w^I(t) = 2 \cos(0.75t + \pi/2) \quad v_w^I(t) = 0$$

The controller gains associated with the attitude dynamics are tuned based on the gain requirements of Theorem 7.1. They are sufficiently high in order for the helicopter to rapidly obtain its desired orientation. The saturation gains are tuned based on the gain requirements of Property 7.4. In addition,  $\ddot{p}_{r,z}^I$  and  $M_{3,3}$  comply with Property 7.1. To compensate the effect of the anti-torque  $Q_M$  and the model uncertainty, a steady state value of the flapping angles is required. This steady state value, through the parasitic forces  $X_M, Y_M$  and  $Y_T$  causes an offset in the translational position error. This steady state offset is minimized by increasing the gains of the diagonal matrices

Table 7.4: Controller outline.

$$\begin{aligned}
 v_d^I &= \dot{p}_r^I \\
 \rho_d &= \frac{-\ddot{p}_r^I + ge_3 + S(e_p, e_v)}{\|-\ddot{p}_r^I + ge_3 + S(e_p, e_v)\|} \\
 T_M &= m \|-\ddot{p}_r^I + ge_3 + S(e_p, e_v)\| \\
 \begin{bmatrix} p_d \\ q_d \end{bmatrix} &= Z^{-1}(\Theta) \left( \dot{q}_d - \Lambda_1 e_q - \frac{k}{\rho_{3,3}} e_q \right) \\
 r_d &= \frac{C_\theta}{C_\phi} \left[ \dot{\psi}_r - \frac{S_\phi}{C_\theta} q - \lambda_\psi e_\psi \right] \\
 \tilde{v} &= \mathcal{I} \dot{\omega}_d^B + \hat{\omega}_d^B \mathcal{I} \omega^B - e_\psi \alpha(\phi, \theta)^T - \Lambda_2 e_\omega \\
 v_c &= A^{-1}(T_M) [-B(T_M) + \tilde{v}]
 \end{aligned}$$

$W_1, W_2$ . The controller gains used for the simulation are shown in Table 7.3. The choice of the linear saturation function satisfying the requirements of Definition 7.1 is the following:

$$\sigma(s) = \begin{cases} s & |s| \leq L \\ \text{sgn}(s) \left[ \sin\left(\frac{|s|-L}{2(M-L)}\pi\right) \frac{M-L}{\pi} + \frac{1}{2}(|s|-L) + L \right] & L < |s| \leq 2M - L \\ \text{sgn}(s)M & |s| > 2M - L \end{cases}$$

The position response in the inertia coordinates, versus the desired trajectories with respect to time, are illustrated in Figure 7.10 and Figure 7.11 for the two maneuvers. The helicopter position in inertia coordinates is illustrated in Figure 7.12 and Figure 7.13. The orientation angles, for the two control schemes, are depicted in Figure 7.14 and Figure 7.15. Finally, the rotors thrusts and the flapping angles can be seen in Figure 7.16 and Figure 7.17. The numerical results illustrate the controller's successful tracking performance. Even though, the proposed design is a model based controller, it exhibits significant robustness attributes towards considerable parametric and model uncertainty. Figures 7.14 and 7.15 indicate that the roll and pitch bound which guarantee that the helicopter will not overturn, is met even in the aggressive part of the maneuvers.

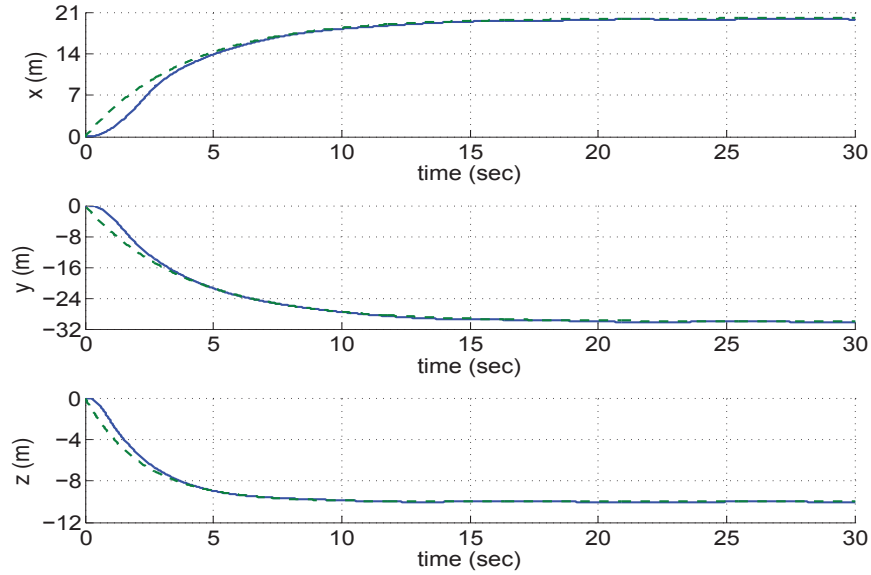


Figure 7.10: *First maneuver*: Reference position trajectory (dashed line) and actual helicopter trajectory (solid line ) expressed in the inertial coordinates with respect to time.

## 7.8 Remarks

This Chapter has presented a backstepping position and heading tracking controller for helicopters. The helicopter model is represented by the rigid body equations of motion enhanced by a simplified model of force and torque generation. The controller assumes full availability of all the helicopter's state variables of the translational and attitude dynamics. The design outline follows a typical backstepping design for feedback systems. The choice of the pseudo controls is taken with caution avoiding unnecessary terms cancellations. This results in a controller that includes a minimal amount of terms required to stabilize the overall system. A summary of the controller inputs and pseudo controls is given in Table 7.4.

The main idea of the design is the use of the direction and magnitude of the thrust vector to stabilize the position error dynamics. The choice of the backstepping pseudo controls results in two interconnected subsystems representing the translational and attitude dynamics errors correspondingly.

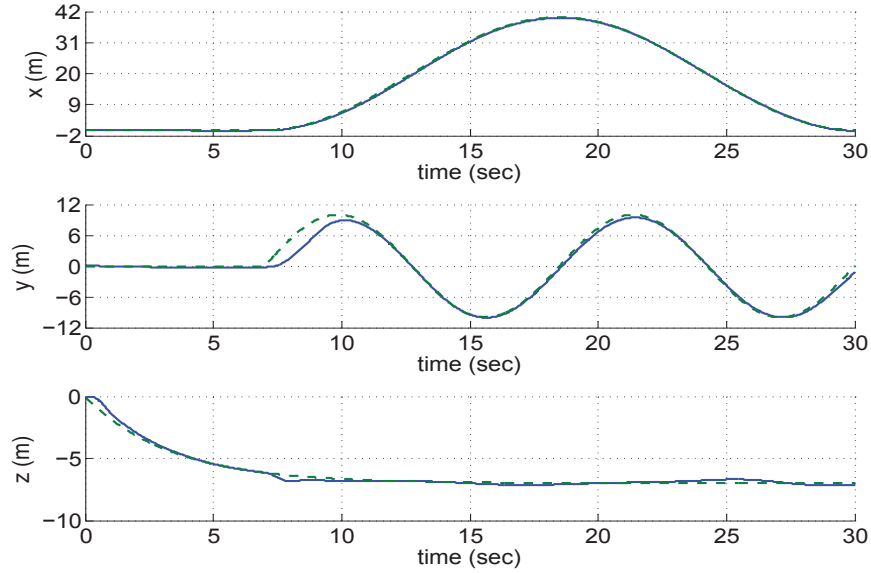


Figure 7.11: *Second maneuver*: Reference position trajectory (dashed line) and actual helicopter trajectory (solid line) expressed in the inertial coordinates with respect to time.

The translational error dynamics are controlled by a nested saturation feedback term and at the same time are perturbed by a bounded function of the directional error. The attitude control design is based on the structural properties of the rotation matrix and it is enhanced with special terms that can guarantee that the helicopter will not overturn in its effort to track the predefined position reference trajectory. The attitude error dynamics will be rendered exponentially stable driving the translational error dynamics globally uniformly asymptotically stable.

The philosophy of this work dictates that for each controller design a standard identification procedure is proposed that will provide the model parameters of the helicopter based on experimental flight data. The applicability of the controller is limited if the designer does not have a practical method to extract the model parameters of the helicopter. The parametric identification of nonlinear continuous dynamic systems can only take place in the time domain. However, time domain parametric identification methods for flight systems are computationally inefficient and less effective compared to frequency domain identification methods [105]. In the time domain approach each iteration of the identification algorithm requires the integration of the nonlinear differential equations of the system for the calculation of the cost function value. This procedure

significantly increases the computational load. In addition, in real life applications the controller algorithm is executed in a microprocessor on board the helicopter. The processing of the algorithms takes place in discrete time and the sampling effect should be taken into account.

Although the proposed controller exhibits significant robustness to parametric uncertainty, still a fair knowledge of the model parameters is necessary. Due to the lack of an efficient identification method the testing of the proposed algorithm is restricted only to numeric simulations based on the MIT's *X-Cell .60* small scale helicopter parameters.

The goal of the next Chapter is to present a backstepping algorithm based on the discrete non-linear helicopter dynamics. The discretization of the helicopter dynamics facilitates the identification procedure since a simple recursive least square algorithm can be used for the determination of the model parameters based on the flight data. Due to the discretization of the helicopter dynamics the new design is not equivalent with the backstepping controller described in this Chapter. The proposed controller of the next Chapter provides a practical solution which can be directly applied to real life applications. The performance of the controller is evaluated using the *X-Plane* simulator.

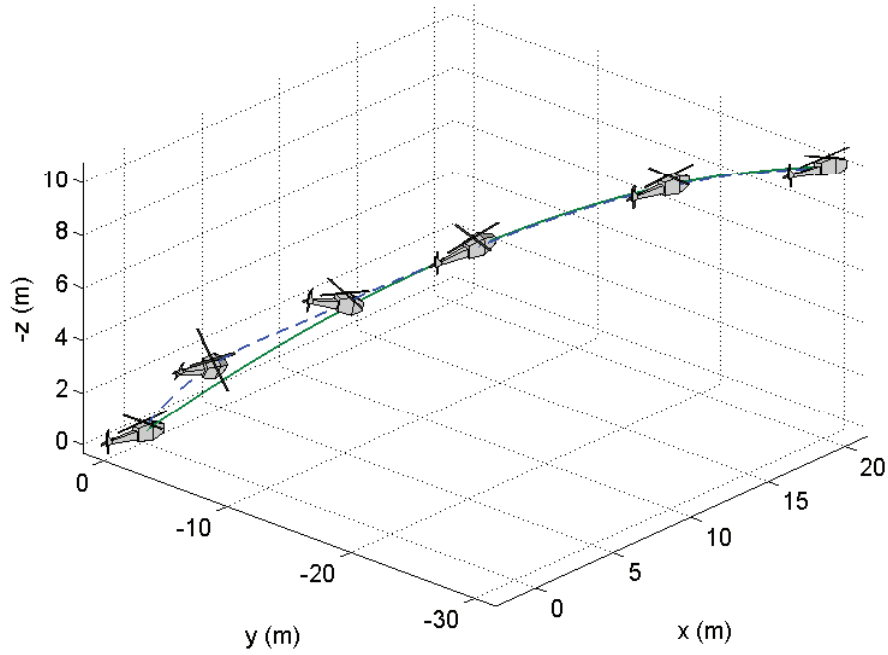


Figure 7.12: *First maneuver*: Reference position trajectory (solid line) and actual helicopter trajectory (dashed line) with respect to the inertial axis.

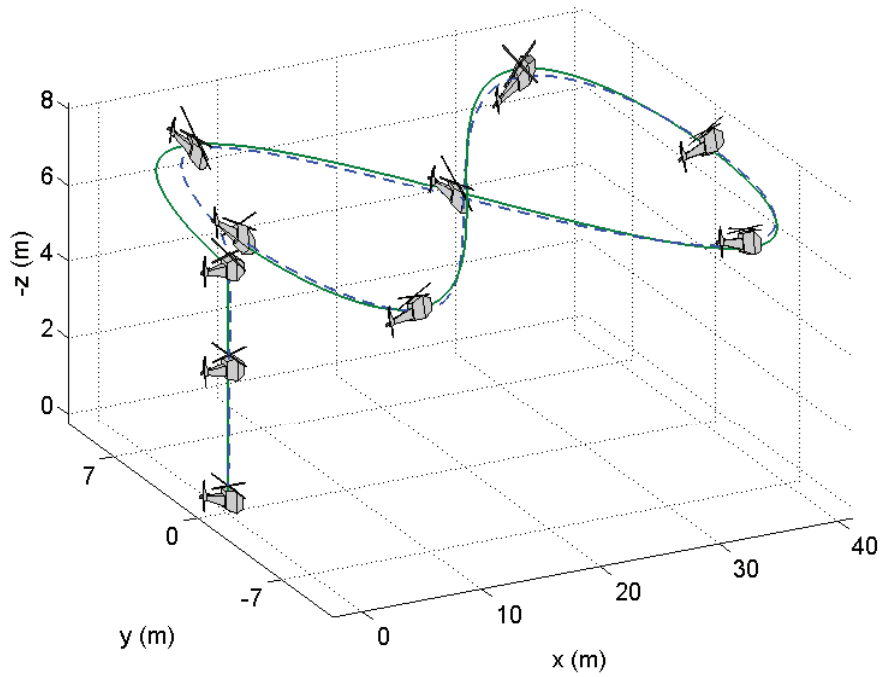


Figure 7.13: *Second maneuver*: Reference position trajectory (solid line) and actual helicopter trajectory (dashed line) with respect to the inertial axis.

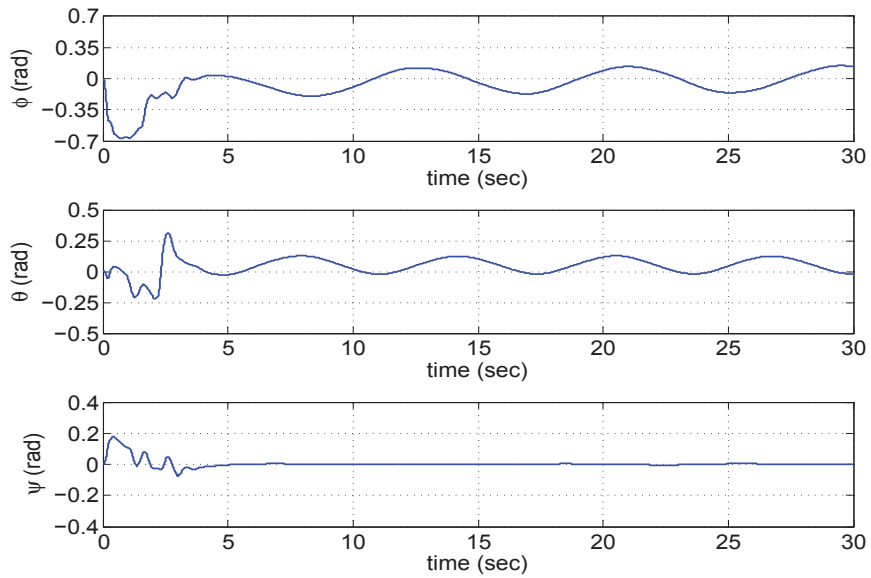


Figure 7.14: *First maneuver*: Euler's orientation angles.

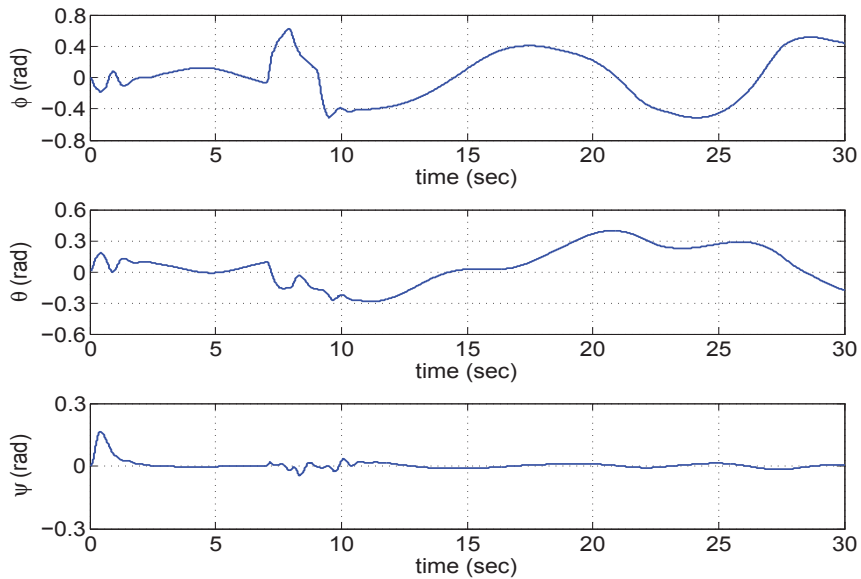


Figure 7.15: *Second maneuver*: Euler's orientation angles.

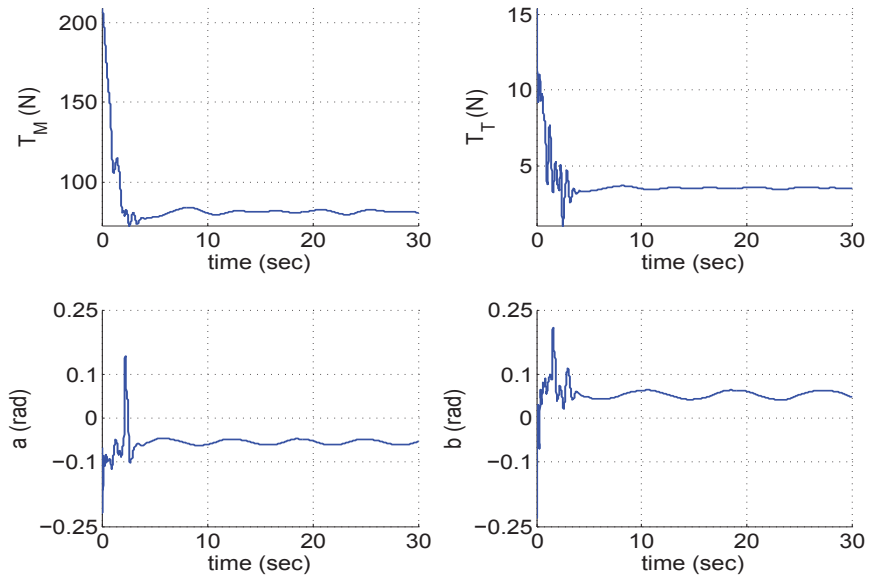


Figure 7.16: *First maneuver*: Main and tail rotor thrust  $T_M, T_T$  and the flapping angles  $a, b$ .

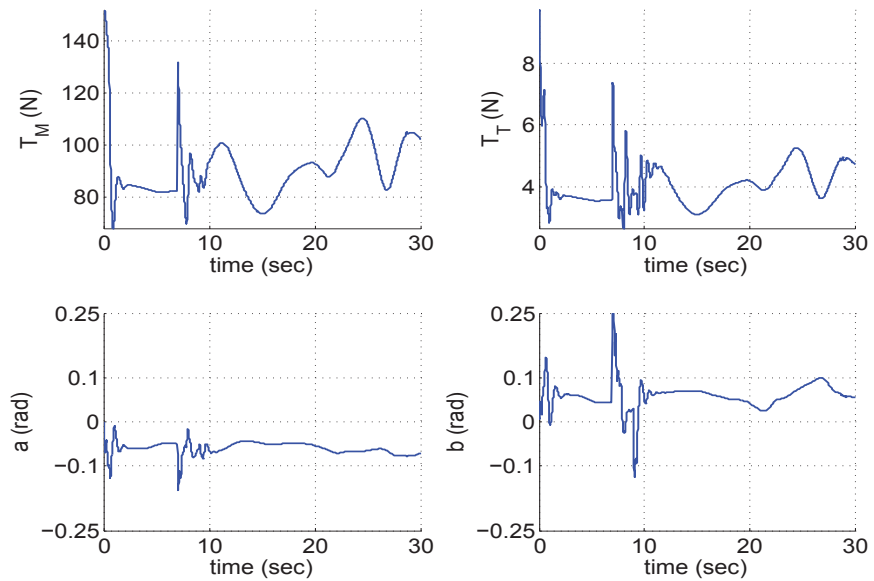


Figure 7.17: *Second maneuver*: Main and tail rotor thrust  $T_M, T_T$  and the flapping angles  $a, b$ .

## Chapter 8: Time Domain Parameter Identification and Applied Discrete Nonlinear Control for Small Scale Unmanned Helicopters

This Chapter deals with the dual problem of parametric identification and nonlinear control of helicopters. The goal of this Chapter is the development of practical identification and control solution for direct application to an autonomous helicopter flight system. Although most controller designs are in continuous time, this chapter considers the discrete time dynamics of the helicopter. The shift of the initial helicopter control problem to the discrete time is twofold: Control algorithms are executed by microprocessors. The discretization effect of the helicopter dynamics should be accounted by the controller. In addition, time domain parametric identification is much simpler and computationally more efficient when the system equations are discretized.

A simple Recursive Least Square (RLS) algorithm is used for the parameter identification in the time domain, the objective being the derivation of system dynamics that are both minimal in complexity and accurate for control design in discrete time. The controller is designed based on a discrete time backstepping technique, for the tracking of predefined position and yaw trajectories. The developed controller provides design freedom in the convergence rate for each state variable of the cascade structure. This is of particular interest since control of the convergence rate in each level of the cascade structure provides better flight results. Both the identification part and control performance are evaluated using *X-Plane*.

### 8.1 Introduction

The concept of backstepping control for continuous time systems in a cascade form has been well studied and analyzed [43] including adaptive modifications [49] to cope with systems includ-

ing parameter uncertainties. In the case of the discrete time systems there has been significant less work to the specific field. The most distinctive work is from [112] dealing with the adaptive backstepping control for discrete time systems.

The first objective of this Chapter is the design of a nonlinear controller for tracking of predefined position and yaw trajectories. A discrete time backstepping controller based on the nonlinear discretized equations of the helicopter is proposed. The controller provides more design freedom compared to the continuous backstepping counterpart algorithm proposed in [11, 21], since the convergence rate of each state variable of the cascade structure can be manipulated. Furthermore, the stability of the resulting dynamics can be simply inspected by the eigenvalues of a linear system without the necessity of Lyapunov's functions. Those eigenvalues are determined by the designer.

The second task of this Chapter is to examine a standard Recursive Least Square (RLS) algorithm for parameter estimation of the nonlinear discrete time dynamics of the helicopter. Both the identification and the control results were successfully tested in *X-Plane* for the *Raptor 90 SE RC* helicopter.

## 8.2 Discrete System Dynamics

The discrete nonlinear model of the helicopter dynamics is derived by direct discretization of the continuous time model presented in the previous Chapter. The TPP dynamics are assumed to be very fast in comparison with the rigid body dynamics and only their steady state effect will be regarded. This is a typical assumption that takes place in the nonlinear controller designs that exists in the literature. The dynamics of the flapping motion are treated as unmodeled uncertainty which is compensated by the robustness of the control algorithm. Therefore, regarding the TPP angles the following hold:

$$a = K_a u_{lon} \quad (8.1)$$

$$b = K_b u_{lat} \quad (8.2)$$

where  $K_a, K_b$  are constant parameters. The magnitude of the main and tail rotor thrust will be considered proportional to the collective control commands, therefore:

$$T_M = K_M u_{col} \quad (8.3)$$

$$T_T = K_T u_{ped} \quad (8.4)$$

where  $T_M, T_T$  are the magnitude of the forces of the main and tail rotor respectively while  $K_M, K_T$  are constant parameters.

Using (8.1)-(8.4) and by ignoring the effect of the anti-torque  $Q_M$  to (7.10) for simplification purposes, a compact form of the external torque applied to the helicopter is:

$$\tau^B = \tilde{A}v_c + \tilde{B}u_{col} \quad (8.5)$$

where

$$v_c = (u_{lat}u_{col} \ u_{lon}u_{col} \ u_{ped})^T \quad (8.6)$$

with  $\tilde{A} \in \mathbb{R}^{3 \times 3}$  and  $\tilde{B} \in \mathbb{R}^{3 \times 1}$  being parameter matrices.

From (7.1), (7.13), (7.3), (7.14), (7.5) by using Euler's implicit method for the approximation of the continuous derivatives, the following equations are obtained:

$$p_{k+1}^I = p_k^I + T_s v_k^I \quad (8.7)$$

$$v_{k+1}^I = v_k^I + \alpha_1 R_k e_3 u_{col,k} + \alpha_2 e_3 \quad (8.8)$$

$$\omega_{k+1}^B = \omega_k^B + \Pi(\omega_k^B) \mathbb{I}(\mathcal{I}, T_s) + A' v_{c,k} + B' u_{col,k} \quad (8.9)$$

$$\Theta_{k+1} = \Theta_k + T_s \Psi(\Theta_k) \omega_k^B \quad (8.10)$$

$$R_{k+1} = R_k + T_s R_k \hat{\omega}_k^B \quad (8.11)$$

where  $e_3 = [0 \ 0 \ 1]^T$  and  $T_s$  denotes the sampling period. In (8.9)  $\Pi(\omega_k^B)$  is a matrix of  $\mathbb{R}^{3 \times p}$  composed only by nonlinear functions of the angular velocities while  $\mathbb{I}(\mathcal{I}, T_s)$  is a vector of  $\mathbb{R}^{p \times 1}$

composed by inertia terms and multiplied by the sampling period  $T_s$ . Both of them satisfy:

$$\Pi(\omega_k^B)\mathbb{I}(\mathcal{I}, T_s) = T_s \mathcal{I}^{-1}[\mathcal{I}\omega_k^B \times \omega_k^B] \quad (8.12)$$

Regarding the rest of the terms in (8.8),(8.9) the following holds:

$$\alpha_1 = -\frac{T_s K_M}{m} \quad (8.13)$$

$$\alpha_2 = T_s g \quad (8.14)$$

$$A' = T_s \mathcal{I}^{-1} \tilde{A} \quad (8.15)$$

$$B' = T_s \mathcal{I}^{-1} \tilde{B} \quad (8.16)$$

An important observation should be given regarding the discrete approximation of (8.11). Integration of translational and rotation dynamics of a rigid body's motion under a potential requires special attention. From [57] Runge-Kutta methods do not preserve the Lie group structure of the configuration space. Most importantly the quantity  $R_{k+1}R_{k+1}^T$  drifts from the identity matrix as the simulation time increases. A more accurate integration of (7.3) could take place by the use of discrete variational integrators [35, 57], which preserve the geometric properties of the Lie group. The disadvantage of this approach is that the proposed structure of the discrete equations -although providing more accurate numerical solutions- is very complicated for control design. To this extent an important condition for (8.7)-(8.11) is that the sampling frequency is small enough that (8.11) can be considered as a perturbation value of the rotation matrix. The experimental results have illustrated that a frequency of  $50Hz$  is adequate enough for (8.11) to provide accurate results even up to a horizon of two time steps given the current value of the configuration matrix and can be used for control design.

### 8.3 Discrete Backstepping Algorithm

Consider a helicopter described by the difference equations (8.7)-(8.11). The objective is to design a nonlinear controller stabilizing the position  $p_k^I$  and the yaw angle  $\psi_k$  to the reference values  $p_{r,k}^I$  and  $\psi_{r,k}$ , respectively.

#### 8.3.1 Angular Velocity Dynamics

Considering (8.9) an obvious control choice for canceling out the nonlinear terms of the angular velocity dynamics is:

$$v_{c,k} = A'^{-1} \left( -\omega_k^B - \Pi(\omega_k^B) \mathbb{I}(\mathcal{I}, T_s) - B' u_{col,k} + \tilde{v}_k \right) \quad (8.17)$$

where  $\tilde{v}_k = [\tilde{v}_{1,k} \ \tilde{v}_{2,k} \ \tilde{v}_{3,k}]^T$ . The angular dynamics become:

$$\omega_{k+1}^B = \tilde{v}_k \quad (8.18)$$

while:

$$\begin{bmatrix} u_{lat,k} \\ u_{lon,k} \\ u_{ped,k} \end{bmatrix} = \begin{bmatrix} u_{col,k} & 0 & 0 \\ 0 & u_{col,k} & 0 \\ 0 & 0 & 1 \end{bmatrix}^{-1} v_{c,k} \quad (8.19)$$

The existence of the inverse of the left matrix on the right hand side of (8.19) is guaranteed by the fact that the collective control  $u_{col,k}$  should be at all times different than zero since in flight operation some thrust is needed to compensate for the weight force.

#### 8.3.2 Translational Dynamics

The equation of translational velocity is given by (8.8). Using the notation of Chapter 7, let  $R_k = [\rho_{1,k} \ \rho_{2,k} \ \rho_{3,k}]$  where  $\rho_{i,k}$  with  $i = 1, 2, 3$  are the column vectors of the rotation matrix. Then

the difference equation of the translational velocity can be written as:

$$v_{k+1}^I = v_k^I + \alpha_1 \rho_{3,k} u_{col,k} + \alpha_2 e_3 \quad (8.20)$$

The column vector  $\rho_{3,k}$  is a unit vector with changing direction depending on the Euler angles. The idea similar to Chapter 7 and [21] is to change the direction of  $\rho_{3,k}$  and at the same time adjust the magnitude of  $u_{col,k}$  to a desired vector which will control the translational velocity dynamics. Therefore the dynamics of  $\rho_{3,k} u_{col,k}$  are the function which should be forwarded in time to develop the backstepping scheme. Let  $u_{col,k+1} = \mu_k$ , and by considering (8.11) and also  $\hat{\omega}_k^B e_3 = -\hat{e}_3 \omega_k^B$  then:

$$\begin{aligned} \rho_{3,k+1} u_{col,k+1} &= R_{k+1} e_3 \mu_k \\ &= R_k e_3 \mu_k - T_s R_k \hat{e}_3 \omega_k^B \mu_k \\ &= R_k (e_3 - T_s \hat{e}_3 \omega_k^B) \mu_k \end{aligned} \quad (8.21)$$

Let  $\mu_{k+1} = \zeta_k$  then by forwarding in time the above equation becomes:

$$\begin{aligned} \rho_{3,k+2} u_{col,k+2} &= R_{k+1} (e_3 - T_s \hat{e}_3 \omega_{k+1}^B) \mu_{k+1} \\ &= R_{k+1} (e_3 - T_s \hat{e}_3 \tilde{v}_k) \zeta_k \\ &= R_{k+1} \begin{bmatrix} T_s \tilde{v}_{2,k} \zeta_k \\ -T_s \tilde{v}_{1,k} \zeta_k \\ \zeta_k \end{bmatrix} = \mathcal{X}_k \end{aligned} \quad (8.22)$$

where  $\mathcal{X}_k$  is a vector as defined below. From (8.22) the following equalities hold:

$$\zeta_k = e_3^T R_{k+1}^T \mathcal{X}_k \quad (8.23)$$

$$\begin{bmatrix} \tilde{v}_{1,k} \\ \tilde{v}_{2,k} \end{bmatrix} = \begin{bmatrix} -T_s \zeta_k & 0 \\ 0 & T_s \zeta_k \end{bmatrix}^{-1} \begin{bmatrix} \rho_{2,k+1}^T \mathcal{X}_k \\ \rho_{1,k+1}^T \mathcal{X}_k \end{bmatrix} \quad (8.24)$$

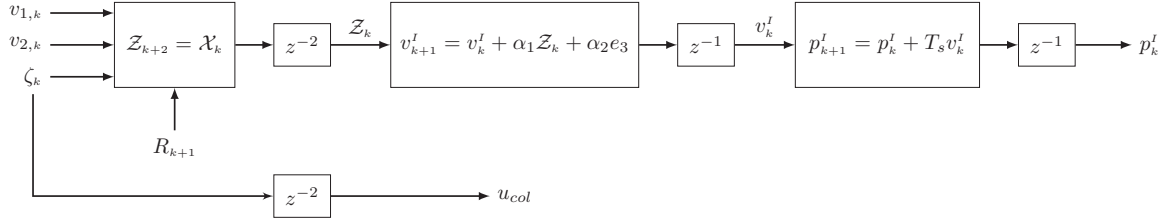


Figure 8.1: Interconnection of the helicopter dynamics using (8.23)-(8.27). The term  $z^{-1}$  denotes a unit time delay.

Since  $\zeta_k = u_{col,k+2}$  the existence of the invertible of the left matrix on the right hand side of (8.24) is guaranteed by the fact that the collective control  $u_{col,k}$  should be different from zero since in flight operation some thrust is needed to compensate for the weight force.

Let  $\mathcal{Z}_{k+i} = \rho_{3,k+i} u_{col,k+i}$  with  $i \in \mathbb{N}$ . The associated equations related with the translational dynamics up to now are:

$$p_{k+1}^I = p_k^I + T_s v_k^I \quad (8.25)$$

$$v_{k+1}^I = v_k^I + \alpha_1 \mathcal{Z}_k + \alpha_2 e_3 \quad (8.26)$$

$$\mathcal{Z}_{k+2} = \mathcal{X}_k \quad (8.27)$$

The error dynamics of the  $p^I$ ,  $v^I$  and  $\mathcal{Z}$  state variables are:

$$e_{p,k+1} = p_{k+1}^I - p_{r,k+1}^I = -p_{r,k+1}^I + p_k^I + T_s v_{d,k}^I + T_s e_{v,k} \quad (8.28)$$

$$e_{v,k+1} = v_{k+1}^I - v_{d,k+1}^I = -v_{d,k+1}^I + v_k^I + \alpha_1 \mathcal{Z}_{d,k} + \alpha_2 e_3 + \alpha_1 e_{z_{d,k}} \quad (8.29)$$

$$e_{z,k+2} = \mathcal{Z}_{k+2} - \mathcal{Z}_{d,k+2} = -\mathcal{Z}_{d,k+2} + \mathcal{X}_k \quad (8.30)$$

Choose the desired values:

$$v_{d,k}^I = \frac{1}{T_s} [p_{r,k+1}^I - p_k^I + K_1 e_{p,k}] \quad (8.31)$$

$$\mathcal{Z}_{d,k} = \frac{1}{\alpha_1} [v_{d,k+1}^I - v_k^I + K_2 e_{v,k} - \alpha_2 e_3] \quad (8.32)$$

$$\mathcal{X}_k = \mathcal{Z}_{d,k+2} + \Lambda_1 e_{z,k+1} + \Lambda_2 e_{z,k} \quad (8.33)$$

where  $K_1, K_2, \Lambda_1, \Lambda_2$  are diagonal gain matrices. After applying the desired values of (8.31)-(8.33) to the translational dynamics described (8.28)-(8.30) one obtains:

$$\begin{bmatrix} e_{p,k+1} \\ e_{v,k+1} \\ e_{z,k+2} \\ e_{z,k+1} \end{bmatrix} = \begin{bmatrix} K_1 & T_s & 0 & 0 \\ 0 & K_2 & 0 & \alpha_1 \\ 0 & 0 & \Lambda_1 & \Lambda_2 \\ 0 & 0 & 1 & 0 \end{bmatrix} \begin{bmatrix} e_{p,k} \\ e_{v,k} \\ e_{z,k+1} \\ e_{z,k} \end{bmatrix} \quad (8.34)$$

The eigenvalues of the above equality are determined by the gains  $K_1, K_2$  and the polynomial  $z^2 - \Lambda_1 z - \Lambda_2$ . Provided that the eigenvalues of the above system lie inside the unit circle the translational dynamics will be globally asymptotically stable. This result is very important since the convergence rate of the error variables can be determined by the designer. By tuning the gains of the diagonal matrices appropriately, smoothness in the flight behavior can be achieved. Real flight implications of this design are significant. Due to the fact that small scale helicopters are very sensitive to control inputs, regulating the convergence rate improves the flight behavior.

### 8.3.3 Yaw Dynamics

The yaw dynamics are obtained by Equation (8.10) and more specifically:

$$\psi_{k+1} = \psi_k + T_s \Psi_3(\Theta_k) \omega_k^B \quad (8.35)$$

where  $\Psi_3(\Theta_k)$  has been defined in (7.24). Let  $e_{\psi,k} = \psi_k - \psi_{r,k}$  be the error in the yaw, then the yaw error dynamics will be:

$$e_{\psi,k+1} = -\psi_{r,k+1} + \psi_k + T_s \Psi_3(\Theta_k) \omega_k^B \quad (8.36)$$

The above equation will be shifted forward in time in order for the control commands to appear.

This leads to:

$$\begin{aligned}
 e_{\psi,k+2} &= -\psi_{r,k+2} + \psi_{k+1} + T_s \Psi_3 (\Theta_{k+1}) \omega_{k+1}^B \\
 &= -\psi_{r,k+2} + \psi_{k+1} + T_s \Psi_3 (\Theta_{k+1}) \tilde{v}_k \\
 &= -\psi_{r,k+2} + \psi_{k+1} + T_s \left( \frac{S_{\phi_{k+1}}}{C_{\theta_{k+1}}} \tilde{v}_{2,k} + \frac{C_{\phi_{k+1}}}{C_{\theta_{k+1}}} \tilde{v}_{3,k} \right)
 \end{aligned} \tag{8.37}$$

An obvious choice for the selection of the value of  $\tilde{v}_{3,k}$  which will cancel out the nonlinear terms and stabilize the yaw error dynamics is:

$$\tilde{v}_{3,k} = \frac{C_{\theta_{k+1}}}{C_{\phi_{k+1}}} \left[ -\frac{S_{\phi_{k+1}}}{C_{\theta_{k+1}}} \tilde{v}_{2,k} + \frac{1}{T_s} (\psi_{r,k+2} - \psi_{k+1} + M e_{\psi,k+1}) \right] \tag{8.38}$$

where  $M$  is a diagonal matrix of gains where the absolute value of each diagonal entry is smaller than unity. Applying the above value for  $\tilde{v}_{3,k}$  the yaw error dynamics become  $e_{\psi,k+2} = M e_{\psi,k+1}$  which implies the asymptotic convergence of  $e_{\psi,k}$  to zero. The control design is summarized by the following algorithm:

- Initialization: At the initial step, when the algorithm is executed for first time set  $u_{col}(0)$  equal to a very small quantity close to zero. This will guarantee the existence of the invertible matrix in (8.19).
- Execution at time step  $k$ : At any given time step  $k$  the full state vector is considered available. To calculate the desired control commands obtained by the backstepping algorithm the following steps should be followed.

– Step 1: Calculate

(i)  $R_{k+1}$  from (8.11).

(ii)  $v_{k+1}^I$  from (8.8).

(iii)  $v_{k+2}^I$  from:

$$v_{k+2}^I = v_{k+1}^I + \alpha_1 R_{k+1} e_3 \mu_k + \alpha_2 e_3$$

- Step 2: Calculate sequentially the following equations:

$$p_{k+1+i}^I = p_{k+i}^I + T_s v_{k+i}^I$$

for  $i = 0, 1, 2$ .

- Step 3: Calculate sequentially the following equations:

$$v_{d,k+i}^I = \frac{1}{T_s} [- (p_{k+i}^I - p_{r,k+1+i}^I) + K_1 (p_{k+i}^I - p_{r,k+i}^I)]$$

for  $i = 0, 1, 2, 3$ .

- Step 4: Calculate sequentially the following equations:

$$\mathcal{Z}_{d,k+i} = \frac{1}{\alpha_1} \{ - (v_{k+i}^I - v_{d,k+1+i}^I) + K_2 (v_{k+i}^I - v_{d,k+i}^I) - \alpha_2 e_3 \}$$

for  $i = 0, 1, 2$ .

- Step 5: Calculate  $\mathcal{X}_k$  from (8.33).
- Step 6: Calculate  $\zeta_k$  from (8.23) and  $\tilde{v}_{1,k}$ ,  $\tilde{v}_{2,k}$  from (8.24).
- Step 9: Calculate
  - $\Theta_k$  from (8.10).
  - $\tilde{v}_{3,k}$  from (8.38).
- Step 10: Calculate  $v_{c,k}$  from (8.17).
- Step 11: Calculate the control commands  $u_{lat,k}$ ,  $u_{lon,k}$  and  $u_{ped,k}$  from (8.19).
- Step 12: Set the following values:

$$u_{col,k} = \mu_k$$

$$\mu_k = \zeta_k$$

## 8.4 Parameter Estimation Using Recursive Least Squares

An important part of the design before the implementation of the flight control algorithm is the parameter estimation of the difference equations (8.8), (8.9). Suggestions for online algorithms [81] are RLS or Gradient Descent methods. In this Chapter a standard RLS algorithm is used. The form of the RLS algorithm can be found in most textbooks related with parameter identification [69]. Let  $y_k$  be the measurement vector where  $y_k \in \mathbb{R}^n$  and  $\theta_k \in \mathbb{R}^N$  is the parameters vector which is going to be estimated. Then, the measurement vector can be modeled as:

$$y_{k+1} = h_k \hat{\theta}_k \quad (8.39)$$

where  $h_k \in \mathbb{R}^{n \times N}$ , while the measurement will be considered clear from noise. The estimates of the parameter vector are provided by the iterative execution of the following algorithm each time a new measurement becomes available:

$$K_{k+1} = P_k h_k^T [h_k P_k h_k^T + I_{n \times n}]^{-1} \quad (8.40)$$

$$P_{k+1} = [I_{N \times N} - K_{k+1} h_k] P_k \quad (8.41)$$

$$\hat{\theta}_{k+1} = \hat{\theta}_k + K_{k+1} [y_{k+1} - h_k \hat{\theta}_k] \quad (8.42)$$

The series of calculations for the above RLS algorithm as indicated by [69] is  $P_k \rightarrow K_{k+1} \rightarrow P_{k+1} \rightarrow \hat{\theta}_{k+1}$ . The initialization of the algorithm is suggested to be  $P_0 = \alpha I_{N \times N}$  where  $\alpha$  is a very large number and for the  $\hat{\theta}_0$  a good initial guess of the parameters or just a zero vector.

For the difference equations (8.8), (8.9) describing the translational and angular velocities of the helicopter the above RLS algorithm can be modified in the following way:

$$y_{k+1} = \begin{bmatrix} v_{k+1}^I - v_k^I \\ \omega_{k+1}^B - \omega_k^B \end{bmatrix} \quad (8.43)$$

$$h_k = \begin{bmatrix} R_k e_3 u_{col,k} & e_3 & 0 & 0 \\ 0 & 0 & \Pi(\omega_k^B) & \Gamma_k \end{bmatrix} \quad (8.44)$$

$$\theta_k^T = [\alpha_1 \ \alpha_2 \ \mathbb{I}^T \ \gamma^T] \quad (8.45)$$

where  $\Gamma_k := \Gamma(u_{lon,k}, u_{lat,k}, u_{ped,k}, u_{col,k})$  is an matrix belonging to  $\mathbb{R}^{3 \times s}$  composed only by the control commands while the vector  $\gamma \in \mathbb{R}^s$  are the parameters associated with the torque vector in such a manner that  $\Gamma_k \gamma = \tau^B$ .

## 8.5 Parametric Model

The identification procedure is an iterative process which requires back and forth testing between modeling and verifying [70, 85]. Based on the system equations described in (8.8) and (8.9) the proposed system dynamics are developed with the dual objective of minimal complexity and satisfactory results. The key feature is to insert the terms that have a dominant effect in the helicopter dynamics and at the same time exclude those that deteriorate or do not effect the identifier. Those key dynamics are obtained from the helicopter dynamic equation for linear and angular velocity by substituting the force and torque generation described in (7.8) and (7.10) respectively. After working back and forth between the system equations and the verification of the experimental results a simplified parametric model was concluded which has physical rational.

The translation velocity dynamics are straightforward and easily identified by equation (8.8). The actual interest and complications is associated with the identification of the angular velocity dynamics. For starters symmetry to the principal axes is assumed. This assumption simplifies significantly the angular velocity dynamics. Therefore  $\Pi(\omega_k^B) = \text{diag}(qr, pr, pq)$  and  $\mathbb{I}(\mathcal{I}, T_s) = (\mathbb{I}_1 \ \mathbb{I}_2 \ \mathbb{I}_3)$ . The second simplification assumes that the position vectors  $\vec{h}_M$  and  $\vec{h}_T$  are aligned with the unitary vectors  $\vec{j}_B$  and  $\vec{k}_B$  respectively. Therefore,  $h_M^B = [0 \ 0 \ z_m]^T$  and  $h_T^B = [x_t \ 0 \ 0]^T$ . Then the parameters associated with the control commands are given by  $\gamma = (\gamma_1 \ \gamma_2 \ \gamma_3)$ . The effect of the command controls to the angular velocity dynamics is given by the matrix  $\Gamma_k = \text{diag}(u_{lat,k}, u_{lon,k}, u_{ped,k})$ . To facilitate the control design the effect of the collective control com-

mand is completely disregarded in the angular velocity dynamics. It is assumed that the collective command takes the trim value  $u_{col} = mg/K_M$ . If  $u_{col}$  takes small values, then the inverse matrix in (8.19) may lead to excessive cyclic and pedal commands. The experimental results indicate that this additional simplification assumption does not have a significant impact neither to the parametric identification nor to the performance of the control algorithm. Then, the parametric model of the angular velocity dynamics is given by:

$$\begin{aligned}
 p_{k+1} &= p_k + \mathbb{I}_1 q_k r_k + \gamma_1 u_{lat,k} \\
 q_{k+1} &= q_k + \mathbb{I}_2 p_k r_k + \gamma_2 u_{lon,k} \\
 r_{k+1} &= r_k + \mathbb{I}_3 q_k p_k + \gamma_3 u_{ped,k}
 \end{aligned} \tag{8.46}$$

## 8.6 Experimental Results

The parameter estimation algorithm and the controller design were tested on the *Raptor 90 SE* model installed in *X-Plane*. The use of *X-Plane* provides a good indication of the applicability of the approach to real flight applications. The lack of any a priori knowledge of the system dynamics, makes it a more realistic validation of the design.

### 8.6.1 Time History Data and Excitation Inputs

An important part of the parameter estimation procedure described in this Chapter, is the collection of the experimental flight test data which are required for the identification of the model. The flight data of the parametric identification procedure are generated by the execution of special excitation inputs to the helicopter. Similarly to the frequency identification case, frequency sweeps were also used for the excitation of the helicopter. The detailed guidelines of the frequency sweeps input signals are given in Section 5.7. For each flight record a computerized frequency sweep is applied to one of the inputs while the rest remain as uncorrelated as possible from the primary

input of interest. During the execution of the frequency sweep it is important the the helicopter does not diverge significantly from the operating point.

Apart from the pedal control  $u_{ped}$  the amplitude of the excitations is adjusted in such a manner that the helicopter will not drift away significantly from the hover trimmed operation. Since the *Raptor* model installed in *X-Plane* does not include a yaw damper or a gyro, the behavior of the helicopter's heading was much more sensitive than the one accounted in actual small scale helicopters. The design of the excitation signal was much more challenging than the rest of the controls since for the long period of the sweep the yaw velocity increases significantly. The excitation signal applied was based on the frequency sweeps and at the beginning of each sinusoidal waiving the amplitude was determined to preserve the yaw velocity between some bounds.

The individual flight records produced by the implementation of the frequency sweeps are concatenated to a single record. The concatenated record is processed by the RLS algorithm for the estimation of the helicopter's model parameters. The sampling rate for the collection of the flight data was set to 50 Hz.

### 8.6.2 Validation

In order to validate the model the actual helicopter is set to hover mode and doublets (symmetrical pulses) are applied by the control commands. After each doublet the helicopter returns to the hovering mode until another excitation occurs. Those excitations take place for all the control inputs.

The comparison between the actual and estimated translational and rotational velocities can be seen in Figure 8.2 and Figure 8.3, respectively. Based on the data it can be seen that the model also provides sufficient estimates for large variations in the linear velocities. The identified parameters are shown in Table 8.1. The verification results illustrate the predictive capability of the identified model for the horizon of one time step. Each estimated point in Figure 8.2 and Figure 8.3 is generated by substituting the actual value of the helicopter's state and input to the right hand side of the difference equations (8.8) and (8.9).

### 8.6.3 Control Design

All of the control commands were saturated in order to lie in the interval  $[-1 \ 1]$  since *X-Plane* does not accept values out of this scope. However, (8.19) requires that  $u_{col} \neq 0$  for every time step. Therefore, for the execution of the control algorithm a simple linear transformation modified the values of the collective command such that  $u_{col} \in (0 \ 1]$ . For the presentation of the controller results the collective signal was again reverted to the interval  $[-1 \ 1]$ . The modeling simplification involving the matrix  $\Gamma$  resulted in the equality  $v_c = (u_{lat} \ u_{lon} \ u_{ped})^T$ . Instead of the pedal control input described by (8.17) and (8.38) a more simple PD controller with bias was applied with sufficient results. The proposed pedal control command used was

$$u_{ped,k} = -0.5e_{\psi,k} - 0.08\omega_{z,k} - 0.18 \quad (8.47)$$

A second modification that took place was the change of the identified values  $\gamma_1, \gamma_2$ . The backstepping algorithm is design based on the assumption of perfect knowledge of the helicopter dynamics. However, although the identification results were adequate there is still some uncertainty associated with the models parameters especially with the angular velocity dynamics described by (8.9). In cases of parameter uncertainty exact dynamics cancellation is not a good practice. Since the inverse of those values is required for the calculation of the corresponding control command, the smaller the value the higher the control command will be. To this extent those values were modified to regulate the cyclic control commands to achieve the desired tracking performance. The parameters were significantly increased with the new values being  $\gamma_1 = 20, \gamma_2 = 10$ .

In general, the time domain parametric identification was proven to be significantly less effective than the frequency domain identification procedure described in Chapter 5. The main difficulty of the RLS algorithm was encountered in the estimation of the parameters associated with the angular velocity dynamics. Although the verification results were satisfactory, the estimated parameters exhibit increased insensitivity of the angular velocity with respect to the control inputs.

Table 8.1: Identified system parameters.

$\alpha_1$	$\alpha_2$	$\mathbb{I}_1$	$\mathbb{I}_2$	$\mathbb{I}_3$	$\gamma_1$	$\gamma_2$	$\gamma_3$
-0.4857	0.0944	0.0256	0.0046	0.0452	0.7854	0.4994	0.1784

Table 8.2: Values of the diagonal gain matrices.

$K_1$	0.92	0.92	0.93
$K_2$	0.93	0.93	0.94
$\Lambda_1$	0	0	0
$\Lambda_2$	0.9	0.9	0.95

The poor performance of the time domain identification can be significantly improved if simple non parametric models of the frequency domain are used as indicators.

The reference maneuver is a trapezoidal velocity profile in the lateral and longitudinal directions identical to the one described in Section 6.7. Throughout the maneuver the reference heading remains constant with the value  $\psi_r = 0$ . The gains of the diagonal matrices used for the backstepping controller can be seen in Table 8.2. The tuning of the controller gains is a very straightforward process. The convergent rate for each error state variable in (8.34) should be faster from the convergent rate of error variables that lie in higher levels of the system. This requirement reflects the natural time scaling between the helicopter dynamics. The translational dynamics are significantly slower than the attitude dynamics. The helicopter velocity responses versus the reference trajectory are illustrated in Figure 8.4. The Euler angles of the helicopter are depicted in Figure 8.5. The position of the helicopter in the inertial coordinates is given in Figure 8.6. Finally the control inputs are shown in Figure 8.7. The performance of the nonlinear controller was excellent. The change in the values of  $\gamma_1, \gamma_2$  parameters resolved the shortcomings of the time domain parameter estimation and resulted to a controller design of high tracking performance.

## 8.7 Remarks

This Chapter has presented a time domain parameter estimation scheme and a nonlinear discrete time control algorithm for helicopters. A simple RLS algorithm is used for the parameter estimation procedure. The excitation signals, used to produce the identification data, were frequency sweeps for each of the control commands. The second task of the Chapter is the design of a nonlinear controller based on the discrete time difference equations of the helicopter. Due to the cascade form of the system a discrete time backstepping method is proposed. The main contribution of this design is the fact that the convergence rate of the cascade system's state variables to their desired values, can be determined by the designer. Tuning those gains appropriately, results in significant improvement of the flight behavior. The above control design considers perfect knowledge of the helicopter dynamics. However as illustrated by the identification results there is a parametric error associated with the angular velocity dynamics. The *X-Plane* simulator is itself a source of uncertainty due to small fluctuation in the sampling rate. The experimental results have illustrated that even in that case the controller is robust enough to deal with both the endogenous and exogenous uncertainty.

The goal of the next Chapter is the development of an improved time domain system identification method. The discrete helicopter dynamics are represented by a Takagi-Sugeno fuzzy model. Instead of using a single nonlinear model for the representation of the helicopter dynamics, the Takagi-Sugeno fuzzy system is an interpolator of multiple nonlinear models which depend on the helicopter's operating condition. The parameters of the Takagi-Sugeno fuzzy system are estimated by the simple RLS algorithm described in this Chapter. The identification results of the fuzzy system indicated significant improvement relative to the parameter estimation approach of this Chapter.

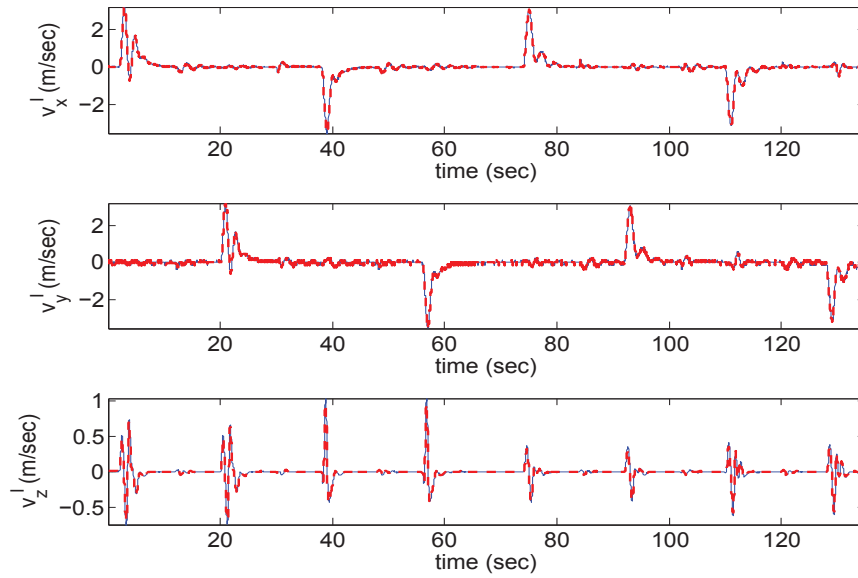


Figure 8.2: Comparison between the actual (solid line) and estimated (dashed line) linear velocities using the verification data.

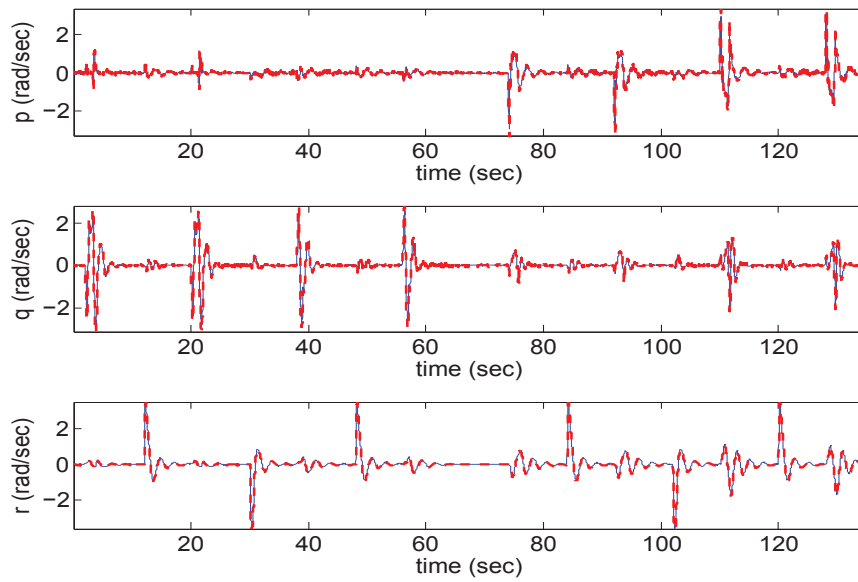


Figure 8.3: Comparison between the actual (solid line) and estimated (dashed line) angular velocities using the verification data.

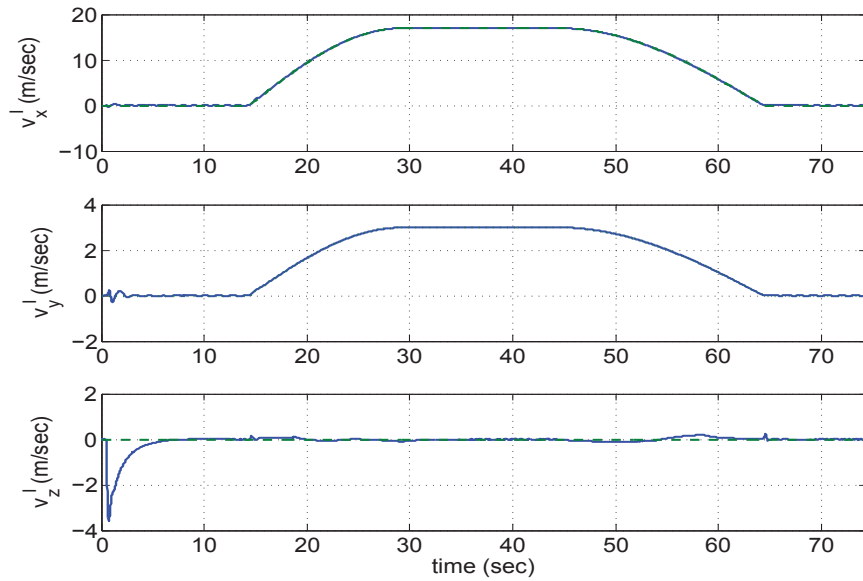


Figure 8.4: Reference trajectory (dashed line) and actual velocity trajectory (solid line) of the helicopter expressed in inertial coordinates with respect to time.

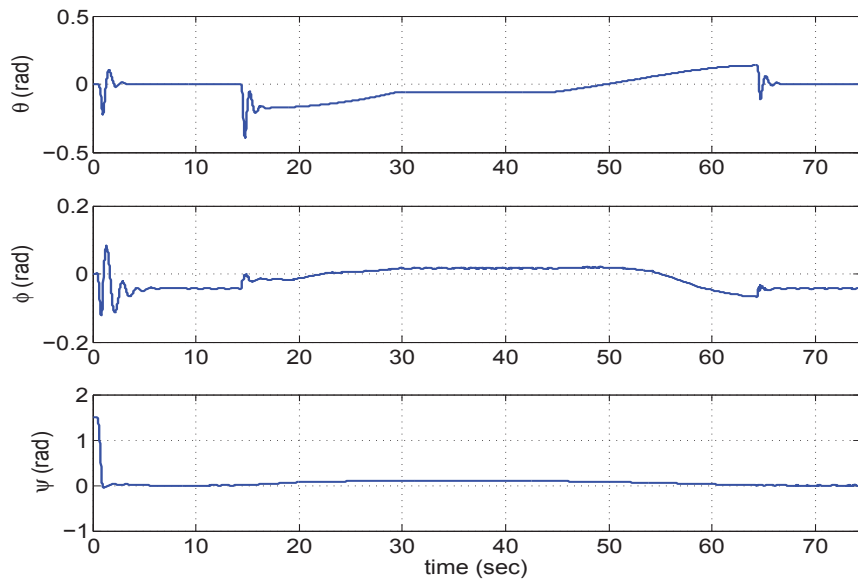


Figure 8.5: Euler's orientation angles.

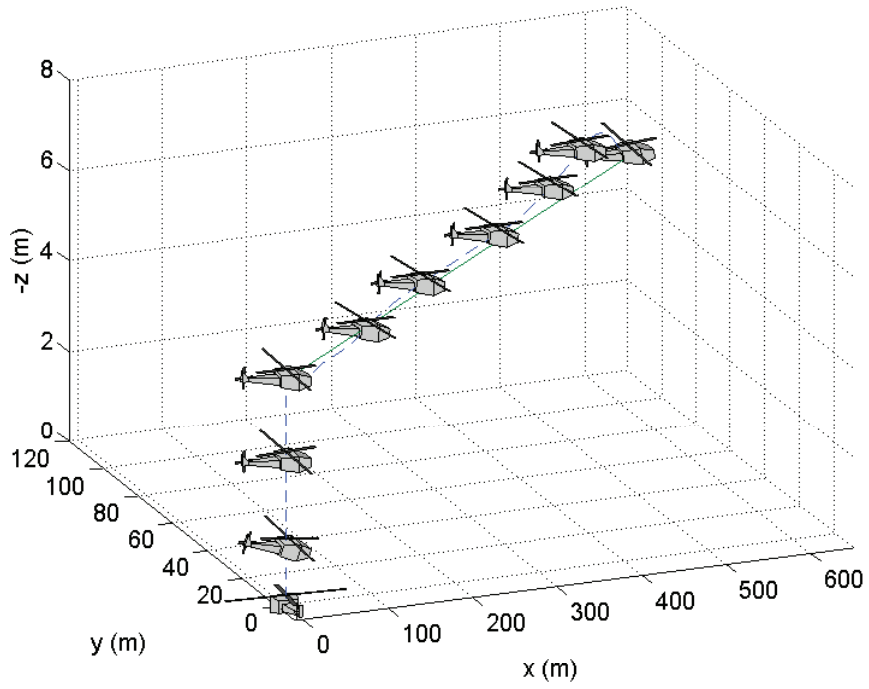


Figure 8.6: Reference position trajectory (solid line) and the actual helicopter position (dashed line) with respect to the inertial axis.

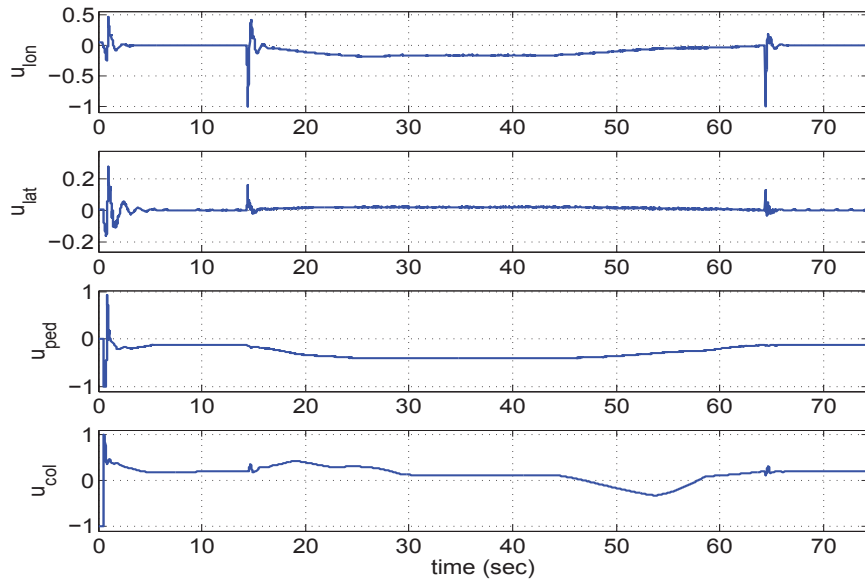


Figure 8.7: Control inputs.

## Chapter 9: Time Domain System Identification for Small Scale Unmanned Helicopters Using Fuzzy Models

The objective of this Chapter is to present a system identification method suitable for helicopter. The proposed model to be identified is a Takagi-Sugeno fuzzy system, representing the translational and rotational velocity dynamics of the helicopter. For the parameter estimation of the Takagi-Sugeno system a classical RLS algorithm is used, which allows the identification to take place on-line since parameter updates are produced whenever a new measurement becomes available. The validity of this approach is tested using *X-Plane*.

### 9.1 Introduction

The objective of this Chapter is to examine a standard technique of fuzzy system identification and its applicability to helicopters. The Chapter illustrates a time domain identification approach that can be implemented on-line in the sense that estimates can be made each time a new state measurement is available. Results illustrate that this method is successful of producing a nonlinear discrete model of relatively low complexity and high accuracy. The resulting model is suitable for the design of model based nonlinear fuzzy controllers.

More specifically, a Takagi-Sugeno fuzzy system is developed based on the discretized dynamics of translational and angular velocity derived in Chapter 8. After the development of the Takagi-Sugeno system, a standard RLS algorithm is used to estimate its parameters. The resulting fuzzy system is an interpolator of nonlinear discrete systems which depends on the helicopter's flight condition.

## 9.2 Takagi-Sugeno Fuzzy Models

This Section illustrates how RLS can be used to identify the parameters of a Takagi-Sugeno fuzzy model [101] used to represent the discrete dynamics of a single state model. This approach will be modified to identify the complete rotorcraft dynamics. The identification of the Takagi-Sugeno system proposed in this paper is based on the method described in [81].

The Takagi-Sugeno fuzzy systems are characterized as “functional fuzzy systems” [81] since their output is a function rather than a membership function center. The fuzzy system is a static nonlinear mapping between the inputs and the outputs and they are composed by  $R$  rules of the form **If-Then**. It will be illustrated how the Takagi-Sugeno system can be used to adjust its parameters in order to provide the best estimate  $\hat{y}(k+1)$  of the state  $y(k)$  given the inputs to the fuzzy system  $(x_1, x_2, \dots, x_n) \in \mathbb{R}^n$ , the state vector  $Y(k) = [y(k), y(k-1), \dots, y(k-m)] \in \mathbb{R}^m$  and the inputs of the plant  $U(k) = [u_1(k), u_2(k), \dots, u_p(k)] \in \mathbb{R}^p$ . Following similar notation of [96] the  $i^{th}$  rule of the rule base can be written as:

**If** ( $F_{x_1}^j$  and  $F_{x_2}^w$  and  $\dots$  and  $F_{x_n}^l$ ) **Then**

$$\hat{y}_i(k+1) = \alpha_{i,1}\Delta_1(Y(k), U(k)) + \dots + \alpha_{i,d}\Delta_d(Y(k), U(k))$$

where  $\hat{y}_i(k+1)$  is the the estimate of  $y(k+1)$  given by the  $i^{th}$  rule. Moreover,  $F_a^b$  is a fuzzy set defined as:

$$F_a^b := \{a, \mu_{F_a^b}(a) : a \in \mathbb{R} \text{ and } \mu_{F_a^b}(a) \in [0 \ 1]\} \quad (9.1)$$

As mentioned in [81, 96] the membership function  $\mu_{F_a^b}(a)$  describes the certainty that the value of  $a$  represented by the linguistic variable  $\tilde{a}$  can be described by the linguistic value  $\tilde{F}_a^b$ . The membership functions considered in this paper are belled shaped Gaussians with or without a saturation portion. Their form can be seen in Table 9.1. The functions  $\Delta_s(Y(k), U(k)) : \mathbb{R}^{m+p} \rightarrow \mathbb{R}$  with  $s = 1, 2, \dots, d$  are used to indicate that the parameter identification can be used for nonlinear dynamic systems which are linear in the parameters. The inference mechanism used to calculate the premise of each rule for this paper will be the dot product. Therefore, the membership function

representing the premise of the above  $i^{th}$  rule will be:

$$\mu_i(x_1, x_2, \dots, x_n) = \mu_{F_{x_1}^j}(x_1)\mu_{F_{x_2}^w}(x_2) \cdots \mu_{F_{x_n}^l}(x_n) \quad (9.2)$$

After-center average defuzzification the estimated output of the identifier will be:

$$\hat{y}(k+1) = \frac{\sum_{i=1}^R \hat{y}_i(k+1)\mu_i}{\sum_{i=1}^R \mu_i} \quad (9.3)$$

where  $\mu_i$  denotes the premise of  $i^{th}$  rule  $\mu_i(x_1, x_2, \dots, x_n)$  for convenience. Let:

$$\xi_i = \frac{\mu_i}{\sum_{i=1}^R \mu_i} \quad (9.4)$$

and:

$$\xi^T(k) = [\Delta_1(k)\xi_1 \cdots \Delta_1(k)\xi_R \cdots \Delta_d(k)\xi_1 \cdots \Delta_d(k)\xi_R] \quad (9.5)$$

$$\theta^T = [\alpha_{1,1} \cdots \alpha_{R,1} \cdots \alpha_{1,d} \cdots \alpha_{R,d}] \quad (9.6)$$

where  $\xi(k)$  and  $\theta$  are vectors of  $\mathbb{R}^{Rd}$ . From the above the estimated state can be written as:

$$\hat{y}(k+1) = \xi^T(k)\theta \quad (9.7)$$

The identification of the parameter vector  $\theta$  takes place with the RLS algorithm described in Section 8.4. The estimates of the parameter vector using RLS are provided by the following algorithm:

$$K(k+1) = P(k)\xi(k)[\xi^T(k)P(k)\xi(k) + 1]^{-1} \quad (9.8)$$

$$P(k+1) = [I_{dR \times dR} - K(k+1)\xi^T(k)]P(k) \quad (9.9)$$

$$\hat{\theta}(k+1) = \hat{\theta}(k) + K(k+1)[y(k+1) - \xi^T(k)\hat{\theta}(k)] \quad (9.10)$$

Table 9.1: Gaussian membership functions.

Left	$\mu^l(x) = \begin{cases} 1 & \text{if } x \leq c^l \\ \exp\left(-\frac{1}{2}\left(\frac{x-c^l}{\sigma^l}\right)^2\right) & \text{otherwise} \end{cases}$
Centers	$\mu(x) = \exp\left(-\frac{1}{2}\left(\frac{x-c}{\sigma}\right)^2\right)$
Right	$\mu^r(x) = \begin{cases} 1 & \text{if } x \geq c^r \\ \exp\left(-\frac{1}{2}\left(\frac{x-c^r}{\sigma^r}\right)^2\right) & \text{otherwise} \end{cases}$

The series of calculations for the above RLS algorithm as indicated by [69] is  $P_k \rightarrow K_{k+1} \rightarrow P_{k+1} \rightarrow \hat{\theta}_{k+1}$ . The initialization of the algorithm is suggested to be  $P(0) = \alpha I_{dR \times dR}$  where  $\alpha$  is a very large number and for the  $\hat{\theta}(0)$  a good initial guess of the parameters or just a zero vector.

At this point it should be mentioned that the inputs to the fuzzy system  $(x_1, x_2, \dots, x_n)$  could be a subset of the state vector. In general the choice of the inputs to the fuzzy system should be descriptive values of the operational condition of the system to be identified.

### 9.3 Proposed Takagi-Sugeno System for Helicopters

As previously stated, the main objective of this paper is to identify a Takagi-Sugeno fuzzy system that best describes the discrete dynamic behavior of the actual helicopter. Based on the system equations presented in (8.8) and (8.9) a Takagi-Sugeno system will be developed with the dual objective of minimal complexity and satisfactory results. The Takagi-Sugeno model is based on the simplification assumptions of Section 8.5.

As indicated by (8.8) the velocity dynamics depend on the orientation of the helicopter and the force vector. The proposed Takagi-Sugeno system representing the translational dynamics will have as input the translational velocity vector  $v^l(k)$ . Let the system be composed by  $R_1$  fuzzy rules then the  $i^{th}$  will be:

**If** ( $F_{v_x}^j$  and  $F_{v_y}^w$  and  $F_{v_z}^\epsilon$ ) **Then**

$$\begin{aligned}\hat{v}_x^I(k+1)_i &= v_x^I(k) + a_1^i [\sin \phi(k) \sin \psi(k) + \cos \phi(k) \sin \theta(k) \cos \psi(k)] u_{col}(k) \\ \hat{v}_y^I(k+1)_i &= v_y^I(k) + a_1^i [\sin \phi(k) \cos \psi(k) - \cos \phi(k) \sin \theta(k) \sin \psi(k)] u_{col}(k) \\ \hat{v}_z^I(k+1)_i &= v_z^I(k) + a_1^i [\cos \phi(k) \cos \theta(k)] u_{col}(k) + a_2^i\end{aligned}\quad (9.11)$$

where  $F_{v_x}^j$ ,  $F_{v_y}^w$  and  $F_{v_z}^\epsilon$  are fuzzy sets representing the linguistic values of the linguistic variables  $\tilde{v}_x^I$ ,  $\tilde{v}_y^I$  and  $\tilde{v}_z^I$ . For the angular velocities, let's assume that the fuzzy system is composed by  $R_2$  rules with the  $i^{th}$  rule being:

**If** ( $F_p^e$  and  $F_q^g$  and  $F_r^c$ ) **Then**

$$\begin{aligned}p(k+1)_i &= p(k) + b_1^i q(k)r(k) + \gamma_1^i u_{lat}(k)u_{col}(k) \\ q(k+1)_i &= q(k) + b_2^i p(k)r(k) + \gamma_2^i u_{lon}(k)u_{col}(k) \\ r(k+1)_i &= r(k) + b_3^i q(k)p(k) + \gamma_3^i u_{ped}(k)\end{aligned}\quad (9.12)$$

where  $F_p^e$ ,  $F_q^g$  and  $F_r^c$  are fuzzy sets representing the linguistic values of the linguistic variables  $\tilde{p}$ ,  $\tilde{q}$  and  $\tilde{r}$  respectively. The parameters of the fuzzy system are unknown. The RLS algorithm can be used so the above equation in order to provide an estimate of the Takagi-Sugeno parameters at each time step that a new measurement is available.

## 9.4 Experimental Results

Similar to Chapter 8, the validation of the model took place for the *Raptor 90 SE* in the *X-Plane* simulator. The sampling rate was set to  $50Hz$ . For the collection of the identification data the same excitation inputs were used with the ones described in Section 8.6.1.

Table 9.2: Gaussian centers and spreads.

Output	Linguistic Variables	Left		Centers		Right	
		$c^l$	$\sigma^l$	$c$	$\sigma$	$c^r$	$\sigma^r$
$\hat{v}^I$	$\tilde{v}_x^I$	-0.5	0.01	0	1	0.5	0.01
	$\tilde{v}_y^I$	-1	0.03	0	3	1	0.03
	$\tilde{v}_z^I$	-1	0.3	0	0.3	1	0.3
$\hat{q}$	$\tilde{q}$	-1.5	0.01	0	6	1.5	0.01
	$\tilde{r}$	-4	0.01	0	8	4	0.01
	$\tilde{p}$	-0.5	1	*	*	0.5	1
$\hat{r}$	$\tilde{q}$	*	*	*	*	*	*
	$\tilde{r}$	-0.5	0.01	0	8	0.5	0.01
	$\tilde{p}$	-1.5	0.03	0	6	1.5	0.03
$\hat{p}$	$\tilde{q}$	-2	0.03	0	6	2	0.03
	$\tilde{r}$	-0.5	0.01	0	8	0.5	0.01
	$\tilde{p}$	*	*	*	*	*	*

Table 9.3: Mean error of the Takagi-Sugeno RLS in comparison with RLS identification over the verification data.

State Estimate	Mean error		Improvement
	Fuzzy RLS	RLS	
$\tilde{v}_x^I$ m/sec	0.0456	0.0457	0.2%
$\tilde{v}_y^I$ m/sec	0.0049	0.0052	5.7%
$\tilde{v}_z^I$ m/sec	0.0253	0.0255	0.7%
$\tilde{q}$ deg/sec	1.0432	1.2050	13.4%
$\tilde{r}$ deg/sec	2.2671	4.0852	43.7%
$\tilde{p}$ deg/sec	1.5554	1.8629	16.5%

#### 9.4.1 Tuning of the Membership Functions Parameters

The centers and the spreads of the Gaussian membership functions of the rotorcraft's Takagi-Sugenano fuzzy system, described by (9.11)-(9.12), are given in Table 9.2. The (\*) symbol indicates that the specific linguistic variable does not participate in the rule base. The choice of these parameters has been based on intuitive criteria rather than an optimizing method over the training set. The main idea is that the linguistic values corresponding to hover operation should have a wide spread in order to dominate over the linguistic variables that correspond to other flight operations. The left and right membership functions are used as supportive means to describe the behavior of the system when the rotorcraft operates outside the bounds of the hover mode. Instead of this intuitive approach there are many optimizing methods to determine the membership function parameters over the training set. A gradient descent tuning method for determining the membership function parameters, is given in [81], however gradient descent should be used to tune the fuzzy model parameters as well. More advance methods for updating the rule base and the parameters of the fuzzy system, by supervised and unsupervised learning, is presented in [1].

#### 9.4.2 Validation

In order to validate the model, the *Raptor 90 SE* is set to hover mode. The applied control commands are periodically perturbing the rotorcraft to a new hover state until a new excitation occurs. Those excitations take place for all the control inputs.

The comparison between the actual and estimated translational and rotational velocities is shown in Figure 9.1 and Figure 9.2 correspondingly. The mean error over the identification data is illustrated in Table 9.3. The same Table presents the mean error of the RLS identification procedure using the straight forward model of (8.8), (8.9) instead of a Takagi-Sugenano fuzzy model. The fuzzy model has a significant improvement in the angular velocity dynamics, which are the biggest identification challenge. The verification results show the success of the approach since the

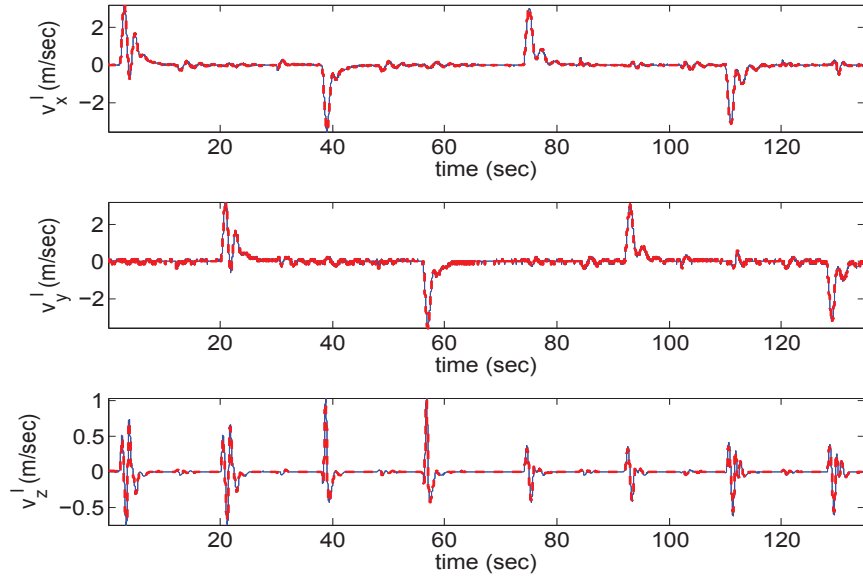


Figure 9.1: Comparison between the actual (solid line) and estimated (dotted line) linear velocities using the verification data.

associated error are small and bounded even in the case of high excitations. Based on the data it can be seen that the model also provides sufficient estimates for large variations in the velocities.

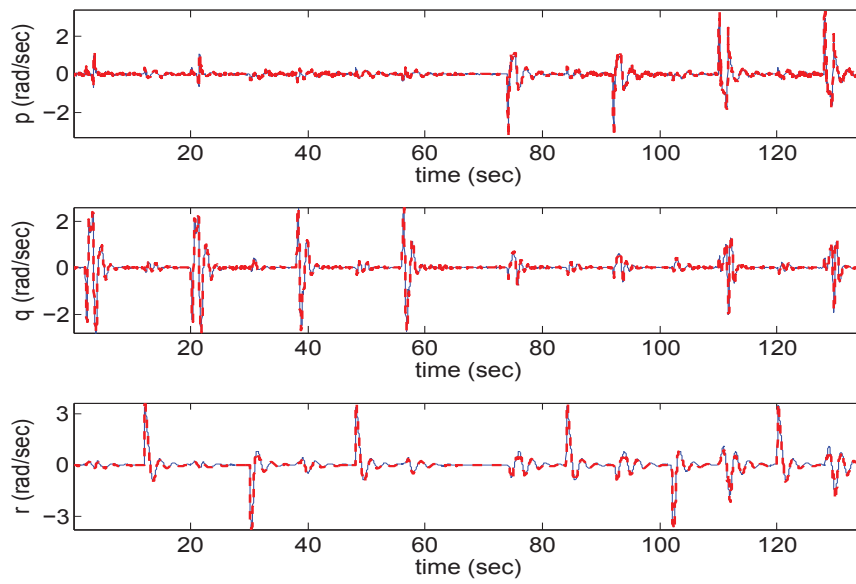


Figure 9.2: Comparison between the actual (solid line) and estimated (dotted line) angular velocities using the verification data.

## Chapter 10: Comparison Studies

This Chapter provides an extensive evaluation and comparison of the controller designs that have been introduced in this research. Evaluation of the flight control systems takes is a function the execution of several flight maneuvers that aim to test the controller designs in terms of stability and tracking accuracy. The test maneuvers are produced by reference position (or velocity) and yaw reference trajectories. The reference trajectories are specially designed in order to examine the performance of the controller designs in multiple operating conditions that cover a wide portion of the flight envelope. Some of the reference trajectories are particularly aggressive investigating the physical limitations of the helicopter. The controllers where tested for the *Raptor 90 SE* RC helicopter which operates in the *X-Plane*flight simulator environment. Details regarding the experimental platform to which the experiments where conducted are given in in Section 5.10.1.

### 10.1 Summary of the Controller Designs

The comparison study involves the evaluation of three controller designs that have been investigated throughout this dissertation. This Section provides a brief summary of these designs. Two of the designs are presented in Chapter 6. The third controller is described in Chapter 8.

The first design is a tracking controller based on the linearized helicopter dynamics. The control law is separated into two static feedback loops. The first is responsible for the regulation of the longitudinal/lateral dynamics and the second is responsible for the regulation of the yaw/heave motion. The controller design is based on the structure of a parametric linear model proposed in [70]. The parametric linear model is given in (6.2) and represents the helicopter dynamics at hover. The controller is additionally enhanced with the integral of the position error. The inclusion of the

integrator dynamics achieves the attenuation of steady state errors due to parametric and modeling uncertainty. The *Raptor 90 SE* linear model identified parameters are given in Table 5.4. The gain values for the two feedback loops of the control law are given in Table 6.1.

The second controller design is based on four independent SISO feedback loops. The control law completely disregards the cross coupling between the helicopter dynamics and assigns a PID controller in each input of the helicopter. The main advantage of this approach is its simplicity since the particular design does not require any knowledge of the helicopter model and the feedback gains can be empirically tuned. The gains for each PID feedback loop are given in Table 6.2.

The third design is a discrete time nonlinear backstepping controller. The flight control system is based on the nonlinear helicopter model composed a full description of the equations of motion. The attitude dynamics and the collective command are used to manipulate the orientation and the magnitude of the thrust vector that is responsible for the generation of the helicopter propulsive forces. The values of the Raptor's nonlinear model parameters are given in Table 8.1. The controller gains are given in Table 8.2.

## 10.2 Experimental Results

The performance of the controllers in terms of tracking accuracy and dexterity is examined by the execution of four different maneuvers. Two of the maneuvers involve velocity tracking while the rest of them require position tracking. Most of the maneuvers require aggressive flight operation which is translated by increased attitude angles and thrust magnitude. The maneuvers are specially designed such that the helicopter transitions to multiple operating flight modes. The execution of the maneuvers forces the helicopter to cover a wide area of the flight envelope and in some cases to reach its physical limits.

### 10.3 First Maneuver: Forward Flight

The first maneuver under investigation requires the cruising of the helicopter by tracking a simple forward flight routine. The reference trajectory is a trapezoidal velocity profile. The heading of the helicopter remains constant throughout the execution of the maneuver with  $\psi_r = 0$ . The forward flight maneuver is composed by five parts. In the first part the helicopter is set to hover by lifting vertically from its starting point from the ground. In the second part of the maneuver, the helicopter accelerates forward. After reaching a certain velocity the helicopter is cruising with constant speed. In the fourth part of the maneuver the helicopter decelerates until its velocity reaches zero. Then, is set to hover again. The reference velocity profile is given by:

$$\begin{aligned}
 v_r^I(t) &= 0 && \text{for } t \leq 18 \\
 v_r^I(t) &= \left( 0 \quad 0 \quad 22 \sin\left(\frac{\pi}{30}(t - 18)\right) \right)^T && \text{for } 18 < t \leq 33 \\
 v_r^I(t) &= 22 && \text{for } 33 < t \leq 48 \\
 v_r^I(t) &= \left( 0 \quad 0 \quad 22 \sin\left(\frac{\pi}{40}(t - 48)\right) \right)^T && \text{for } 48 \leq t \leq 68 \\
 v_r^I(t) &= 0 && \text{for } t > 68
 \end{aligned}$$

The reference velocity and the response of helicopter velocity response produced by the three controllers is depicted in Figure 10.1. The pitch, roll and yaw angles acquired during the execution of the maneuvers for the three designs are depicted in Figure 10.2. The control inputs generated by the flight control systems are shown in Figure 10.3. The position and the orientation of the helicopter during the execution of the maneuvers is shown in Figure 10.4.

During the execution of the maneuver the helicopter reaches a maximum velocity of  $22 \text{ m/sec}$ . Based on extreme flight tests, the maximum possible forward velocity that the Raptor can reach is  $25 \text{ m/sec}$ . This is the pick velocity that the RC model can acquire due to the power limitations of the main rotor. From Figure 10.2 it is apparent that the forward velocity and acceleration of the

helicopter is manipulated by the pitch angle  $\theta$ . All the controller designs successfully tracked the reference velocity trajectory.

#### 10.4 Second Maneuver: Aggressive Forward Flight

The second maneuver is an aggressive version of the previous one. The flight task involves a similar forward flight profile, however, in this case the helicopter is expected to acquire higher acceleration. Thus, the helicopter should reach its maximum velocity in a shorter time interval. Since the longitudinal/lateral acceleration of the helicopter has been proven to be proportional to the pitch/roll angles, a higher tilting of the fuselage is expected during the execution. The interest of this maneuver focus on the acceleration phase. Again, the reference heading remains constant with  $\psi_r = 0$ . The reference velocity trajectory profile is given by:

$$\begin{aligned}
 v_r^I(t) &= 0 && \text{for } t \leq 18 \\
 v_r^I(t) &= \left( 0 \quad 0 \quad 22 \sin\left(\frac{\pi}{14}(t-18)\right) \right)^T && \text{for } 18 < t \leq 25 \\
 v_r^I(t) &= 22 && \text{for } 25 < t \leq 40 \\
 v_r^I(t) &= \left( 0 \quad 0 \quad 22 \sin\left(\frac{\pi}{40}(t-40)\right) \right)^T && \text{for } 40 \leq t \leq 60 \\
 v_r^I(t) &= 0 && \text{for } t > 60
 \end{aligned}$$

The reference velocity trajectory and the velocity response of the three designs is depicted in Figure 10.5. The pitch, roll and yaw angles during the execution of the maneuver are illustrated in Figure 10.6. The generated control inputs for the three designs are shown in Figure 10.7. The position and orientation of the helicopter to the Cartesian space is shown in Figure 10.8.

Figure 10.6 indicates that due to the aggressive acceleration of the helicopter the pitch angle takes a significantly higher value compared to the previous case study. For the nonlinear back-stepping design the pitch angle may reach a value of up to  $60^\circ$ . In addition, during the acceleration phase, the collective command  $u_{col}$  is saturated to its maximum value. The simultaneous

tilting of the fuselage and the increase to the thrust magnitude produce the propulsive force that is necessary for the aggressive portion of the maneuver. From the three designs, the PID and the nonlinear controller exhibit higher pitch angles compared to the linear design. During this phase, since the helicopter is already operating with its maximum available thrust power, the high tilt of the fuselage decreases the vertical component of the thrust vector. The decrease of the thrust's vertical component makes the weight of the helicopter the dominant force in the vertical direction. This fact results to the diving motion of the helicopter which is apparent in Figure 10.8(b) and Figure 10.8(c). Specially in the case of the PID controller, the helicopter almost touches the ground. The diving motion, continuous until the helicopter accumulates sufficient momentum in the longitudinal direction, and the absolute value of the pitch angle is decreased. This effect is purely related with the gain selection of the controllers. In the PID and nonlinear design the gain choice impose significantly faster convergence to the longitudinal/lateral motion compared to the heave dynamics. Therefore the controllers prioritize these dynamics over the vertical motion. The diving motion would be negligible in the ideal case that the controller had unlimited power resources and the magnitude of the thrust force could compensate any decrease to the vertical component of the main rotor thrust caused by the tilting of the fuselage.

### 10.5 Third Maneuver: 8 Shaped

For the third maneuver the helicopter is required to execute an “8 shaped” curved path. The heading of the helicopter remains constant throughout the execution of the maneuver. This maneuver is a position tracking challenge. The maneuver is composed by three parts. In the first phase the helicopter lifts vertically from the starting point and it is set to hover mode. In the second part of the maneuver the helicopter is expected to curve an “8 shaped” path in the longitudinal and lateral direction while its altitude remains constant. At the end of the path the helicopter is set to hover again. The reference position trajectory is given by:

$$p_r^I(t) = \begin{pmatrix} 0 & 0 & -5 \end{pmatrix}^T \quad \text{for } t \leq 15$$

$$p_r^I(t) = \begin{pmatrix} 20 \left[ 1 - \cos\left(\frac{\pi}{20}(t - 15)\right) \right] \\ -14 \sin\left(\frac{\pi}{10}(t - 15)\right) \\ -5 \end{pmatrix} \quad \text{for } 15 < t \leq 55$$

$$p_r^I(t) = \begin{pmatrix} 0 & 0 & -5 \end{pmatrix}^T \quad \text{for } t > 55$$

The reference position trajectory versus the position responses of the three controllers are illustrated in Figure 10.9. The orientation angles of the helicopter during the execution of the maneuvers for the three controllers designs are depicted in Figure 10.10. The control inputs for the three designs are shown in Figure 10.11.

The tracking performance of the controller designs was satisfactory. All of the controllers accurately succeed the tracking task of this more involved coordinate motion. In general, tracking controllers require that the reference trajectories are smooth (the reference functions and their higher derivatives are continuous). A close inspection to the particular continuous trajectory indicates that its first derivative is a piecewise continuous function. The points of discontinuity are located in the end and the start points of the 8 shaped curve execution when the helicopter initiates and finalizes to hover. The discontinuities in the first derivative of the reference trajectory results in instantaneous transient jumps in the control inputs. To avoid these transients it is preferable to use differentiable functions as references. If the generation of such trajectories is not practical or limiting and such transients are hazardous for the operation of the helicopter, it is suggested that the reference trajectories are processed by an appropriate low pass filter that attenuates the the high frequency components of the signal.

## 10.6 Fourth Maneuver: Pirouette

The final maneuver under investigation is the most challenging since it involves the simultaneous and synchronized helicopter motion in all directions of the configuration space. Similarly with the previous trajectories the helicopter is initially set to hover. In the main part of the maneuver,

the helicopter is required to execute a circular motion in the longitudinal and lateral directions. During the execution of the circular motion the helicopter is simultaneously ascending vertically with exponentially decreasing velocity. This results to a spiral motion of the helicopter around a fictional cylinder. At the execution of the fifth spiral a correction maneuver sets the helicopter at the sender of the cylinder. The reference trajectory is given by:

$$\begin{aligned}
 p_r^I(t) &= (0 \quad 0 \quad -3)^T && \text{for } t \leq 15 \\
 p_r^I(t) &= \begin{pmatrix} 5 \left[ 1 - \cos\left(\frac{\pi}{5}(t-15)\right) \right] \\ -5 \sin\left(\frac{\pi}{5}(t-15)\right) \\ -23 + 20e^{-0.06(t-15)} \end{pmatrix} && \text{for } 15 < t \leq 65 \\
 p_r^I(t) &= \begin{pmatrix} 2.5 \left[ 1 - \cos\left(\frac{\pi}{5}(t-65)\right) \right] \\ -2.5 \sin\left(\frac{\pi}{5}(t-65)\right) \\ -23 + 20e^{-3} \end{pmatrix} && \text{for } 65 < t \leq 70 \\
 p_r^I(t) &= (0 \quad 0 \quad -22.0043)^T && \text{for } t > 70
 \end{aligned}$$

The reference trajectory and the helicopter position responses for the three controller designs are illustrated in Figure 10.13. The orientation angles are depicted in Figure 10.14. The control inputs generated by the controllers are depicted in Figure 10.15. Finally, the position and orientation of the helicopter for each controller design during the execution of the maneuver is illustrated in Figure 10.16.

The last maneuver was possibly the most challenging. It is a relative aggressive trajectory since in certain time instances the roll angle of the helicopter reaches a value close to  $60^\circ$ . Obviously, the performance of all the controllers is satisfactory even for this demanding maneuver.

## 10.7 Remarks

The extensive comparison and flight testing presented in this Chapter, provides some very useful observations related with the proposed designs and the helicopter control problem in general. All the controller designs which were under investigation in this comparative study, exhibit robustness and high accuracy tracking capabilities even for reference trajectories that expect composite and aggressive helicopter motion.

The first remark is associated with the linear controller design. Theoretically, the identified linear model of the *Raptor 90 SE* provides a quasi-steady dynamic description which is limited to mild flight operation (hover, cruising with low speed). However, the executed maneuvers required the operation of the helicopter in several operating conditions. In certain cases the reference trajectories imposed the operation of the helicopter in aggressive and high agile maneuvers that required attitude angles of up to  $60^\circ$ . In such operations even the linearity assumptions of the model are violated. A single controller, based only on the identified hover model was adequate.

The success of the linear design is attributed to three key characteristics. The frequency domain identification method produces models of high fidelity and accuracy. The procedure itself, provides significant understanding of the helicopter dynamics. This insight is evaluated and exploited by the controller design. Furthermore, although theoretically, the model is limited only to a neighborhood of a certain operating condition, in reality it covers a relative wide area of the flight envelope. The second characteristic is the decomposition of the controller design to two feedback laws, each of them responsible for a different subsystem of the helicopter dynamics. This idea passes the physical flight intuition to the mathematical development of the controller.

A second remark worth mentioning, is the performance of the PID design. A similar comment about this issue has been already made in Section 6.7. It was expected that the PID performance would be significantly inferior compared to the rest designs. However, the flight results indicate that the PID controller exhibits satisfactory behavior. The success of the PID controller is attributed to the attenuated cross coupling effect amongst the Raptor dynamics. This fact is supported by the off-axis responses of the helicopter illustrated in Figure 5.3. This Figure illustrates

that the magnitude of the  $q/u_{lat}$  and  $p/u_{lon}$  responses lie in the zone of  $-20$  to  $-40$  dB. This is an indicator of negligible cross coupling between the helicopter dynamics.

Finally, the most interesting remark is the following observation: The motion and control responses of all the controller designs are similar given that the tracking objective is achieved. This fact indicates that during the execution of a reference maneuver the helicopter motion and nominal inputs are constrained. The constrained motion depends on the reference trajectory itself. For any method that achieves asymptotic convergence of the helicopter outputs to their reference values, after the occurrence of some initial transients, the helicopter state and control inputs will asymptotically reach a manifold, which is dictated by the functional controllability of the system equations [66]. The simplest approximate description of this manifold is given by the desired state vector  $x_d$  presented in Section 6.2. For example, based on (6.30) the desired pitch and roll angles are given by:

$$\theta_d = \frac{1}{-g} [\dot{u}_r - X_u u_r] \quad \phi_d = \frac{1}{g} [\dot{v}_r - Y_v v_r]$$

The above equation indicates that the pitch and roll angles at a steady-state condition are proportional to the reference lateral/longitudinal acceleration and velocity of the helicopter. Any discontinuities to the reference velocity and acceleration will appear to the attitude angles as well. The ability of the approximated linear model to provide the description of this steady-state manifold is attributed to the differential flatness property [47]. The knowledge of this steady-state vector can be exploited in the development of trajectory generators. For instance, from the above equation, the designer will know what attitude angles are expected during the execution of a predefined reference velocity profile.

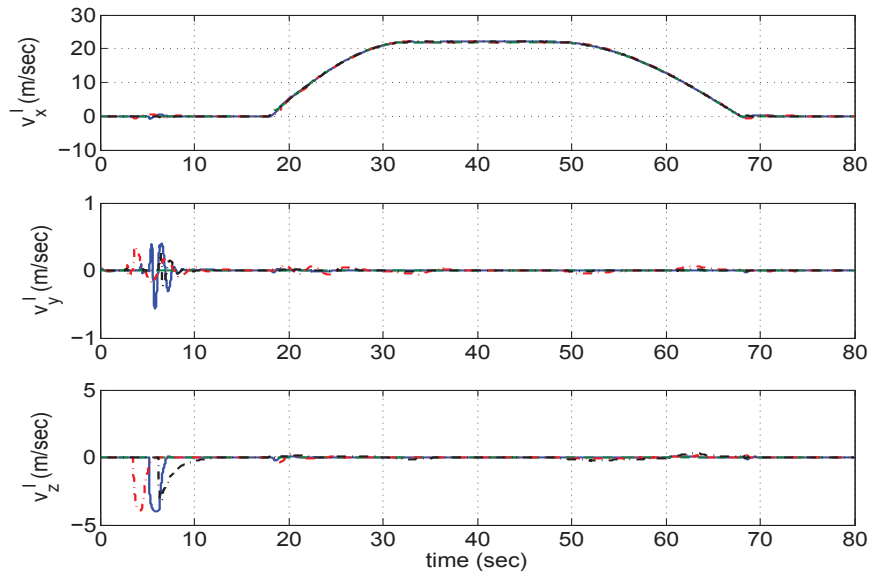


Figure 10.1: *First maneuver (Forward flight)*: Reference velocity trajectory (green dashed line) and actual velocity trajectory of the linear (solid blue line), PID (red dashed dotted line), nonlinear (dashed dotted black line) controller designs, expressed in inertial coordinates with respect to time.

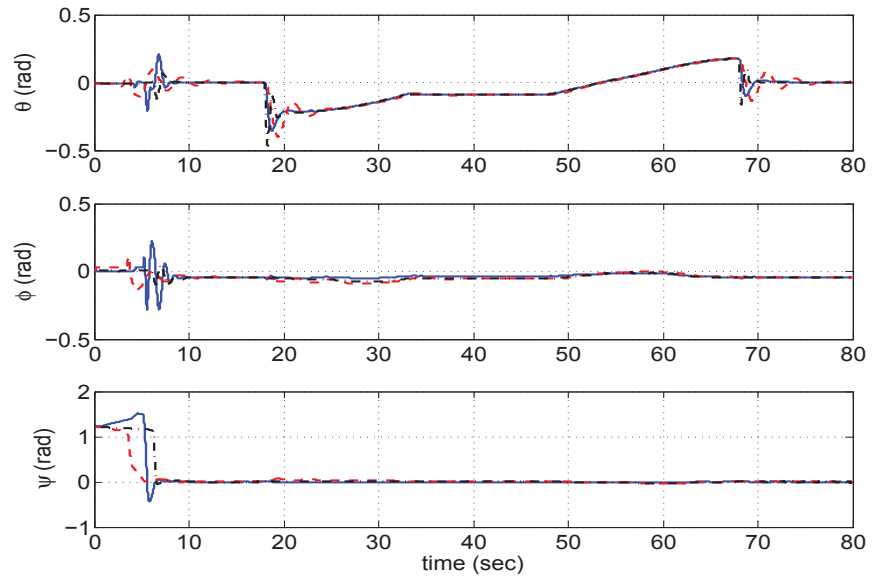


Figure 10.2: *First maneuver (Forward flight)*: Orientation angles of the linear (solid blue line), PID (dashed red line) and nonlinear (dashed dotted black line) controllers designs.

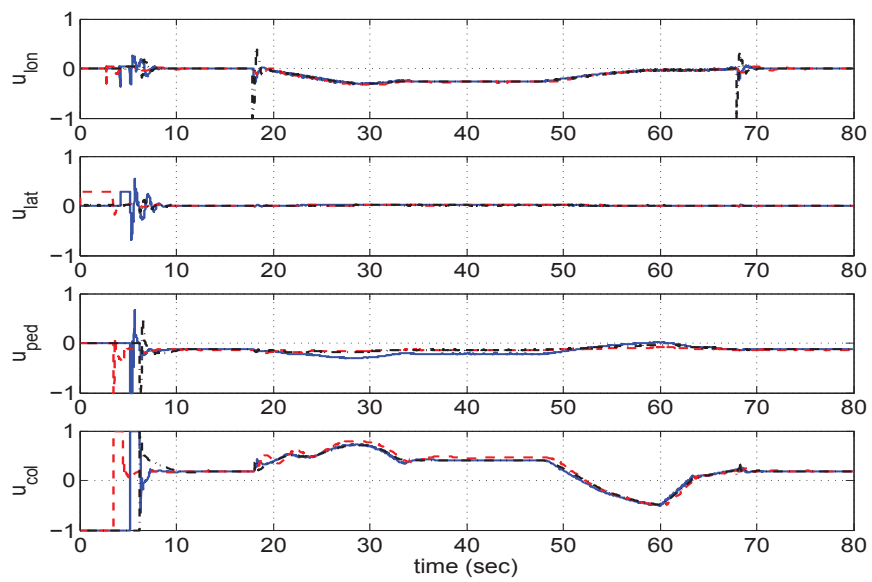
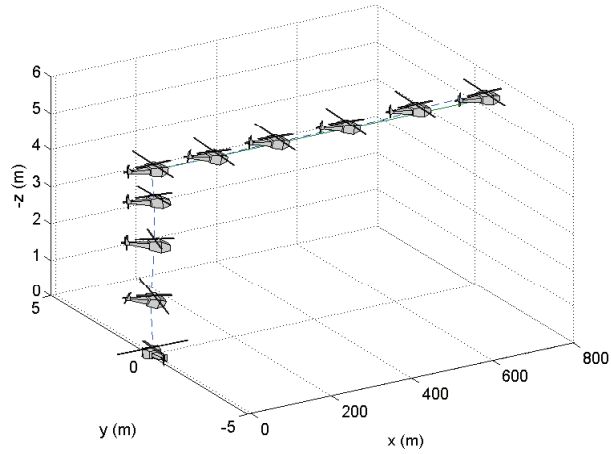
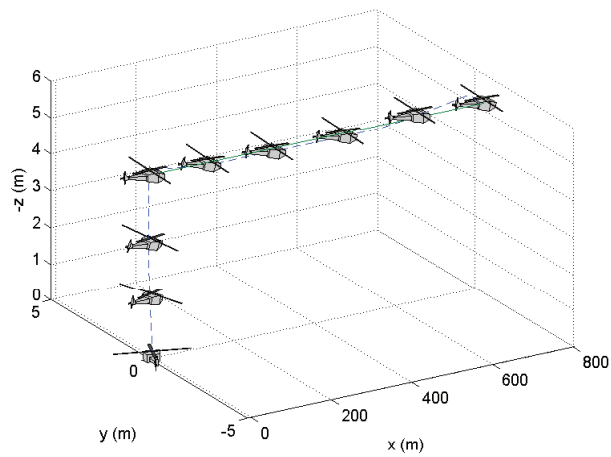


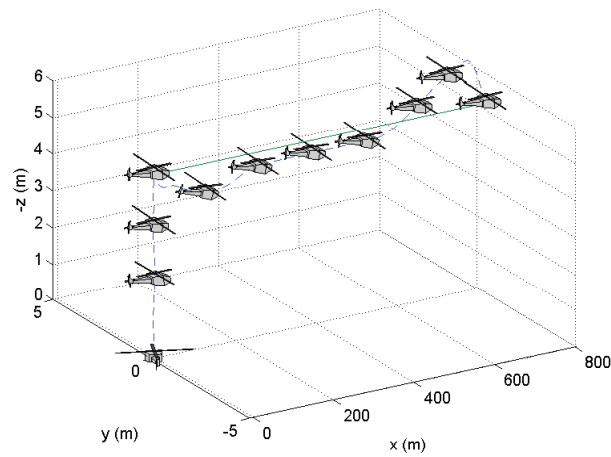
Figure 10.3: *First maneuver (Forward flight)*: Control inputs of the linear (solid blue line), PID (dashed red line) and nonlinear (dashed dotted black line) controller designs.



(a) Linear controller.



(b) PID controller.



(c) Nonlinear controller.

Figure 10.4: *First maneuver (Forward flight)*: Reference position trajectory (solid line) and actual trajectory of the controller designs (dashed line) with respect to the inertial axis.

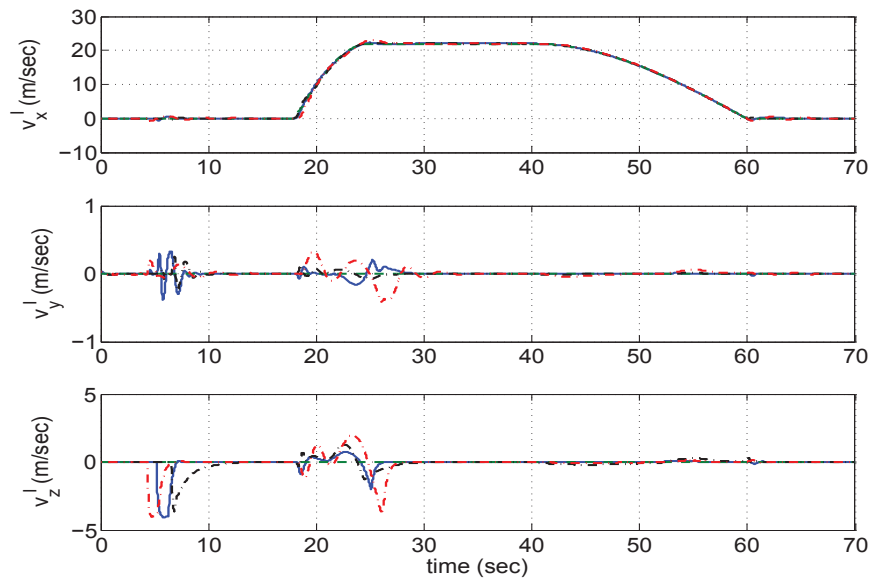


Figure 10.5: *Second maneuver (Aggressive forward flight)*: Reference velocity trajectory (green dashed line) and actual velocity trajectory of the linear (solid blue line), PID (red dashed dotted line), nonlinear (dashed dotted black line) controller designs, expressed in inertial coordinates with respect to time.

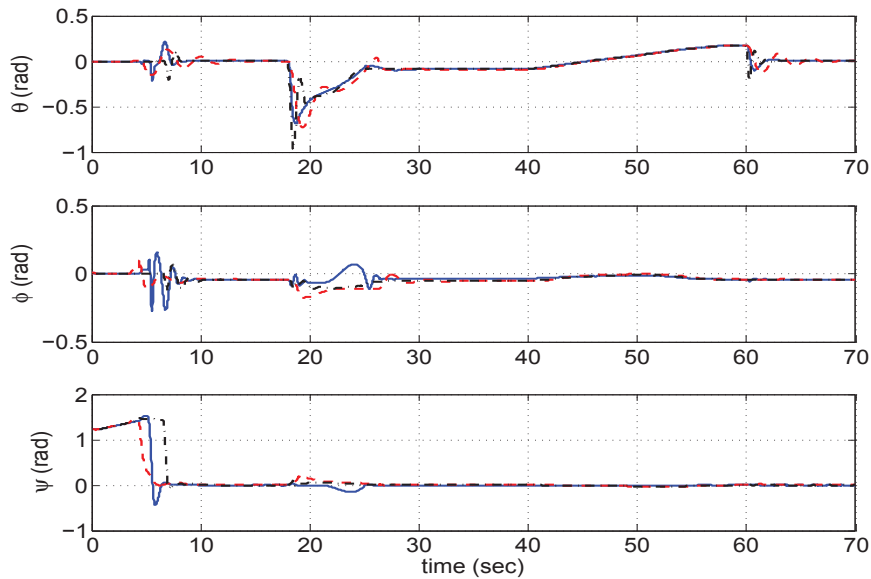


Figure 10.6: *Second maneuver (Aggressive forward flight)*: Orientation angles of the linear (solid blue line), PID (dashed red line) and nonlinear (dashed dotted black line) controllers designs.

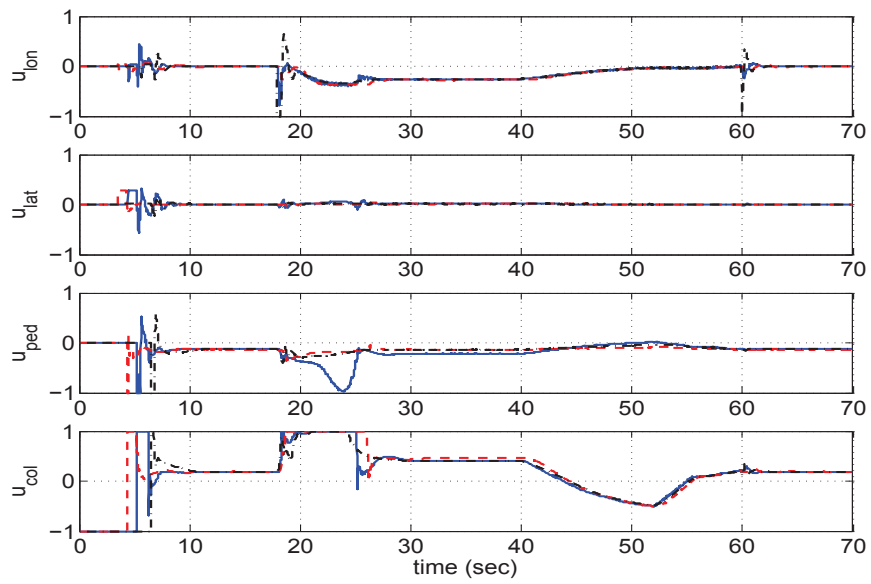
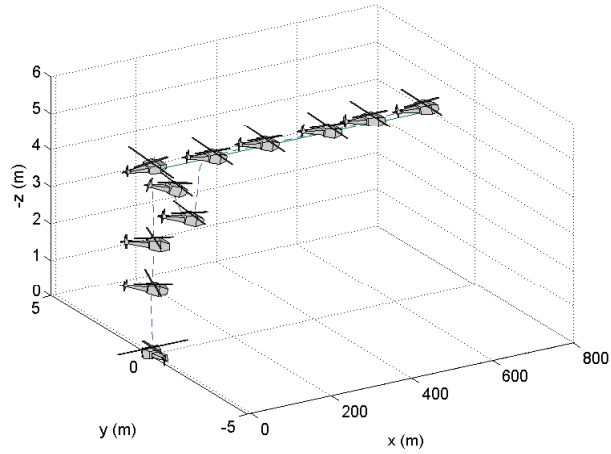
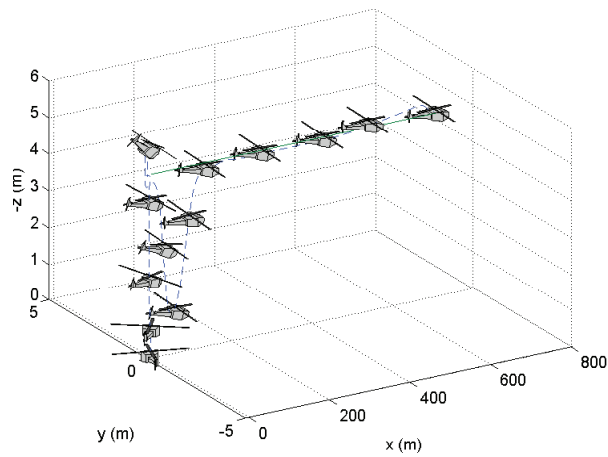


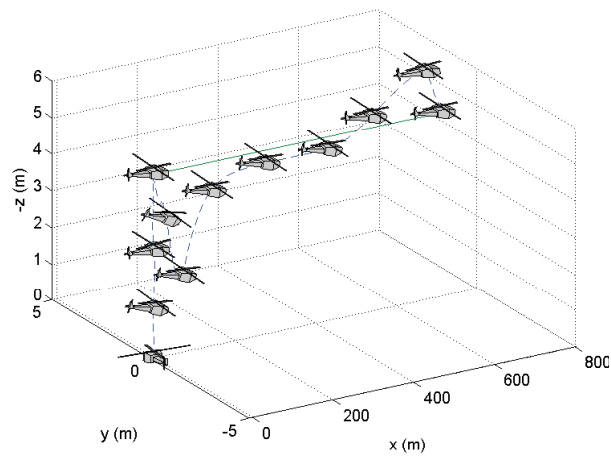
Figure 10.7: *Second maneuver (Aggressive forward flight)*: Control inputs of the linear (solid blue line), PID (dashed red line) and nonlinear (dashed dotted black line) controller designs.



(a) Linear controller.



(b) PID controller.



(c) Nonlinear controller.

Figure 10.8: *Second maneuver (Aggressive forward flight)*: Reference position trajectory (solid line) and actual trajectory of the controller designs (dashed line) with respect to the inertial axis.

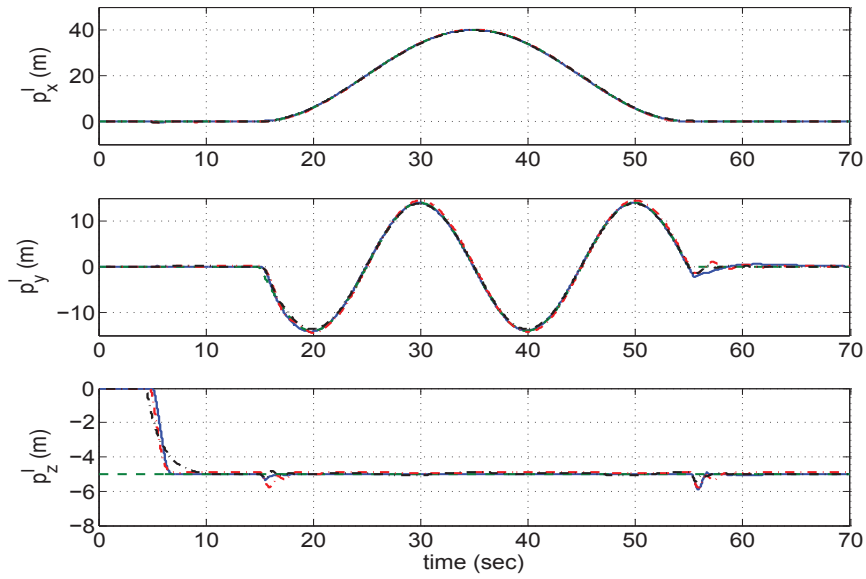


Figure 10.9: *Third maneuver (8 shaped)*: Reference position trajectory (green dashed line) and actual position trajectory of the linear (solid blue line), PID (red dashed dotted line), nonlinear (dashed dotted black line) controller designs, expressed in inertial coordinates with respect to time.

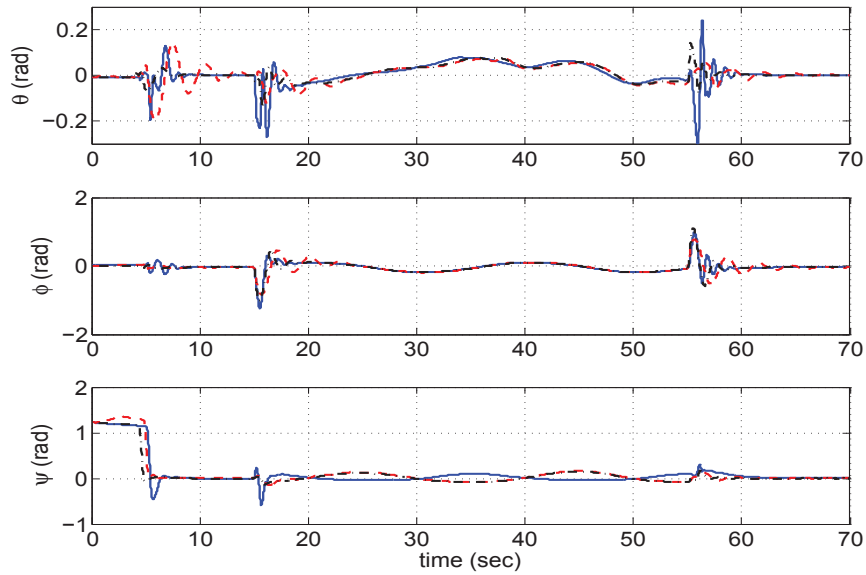


Figure 10.10: *Third maneuver (8 shaped)*: Orientation angles of the linear (solid blue line), PID (dashed red line) and nonlinear (dashed dotted black line) controllers designs.

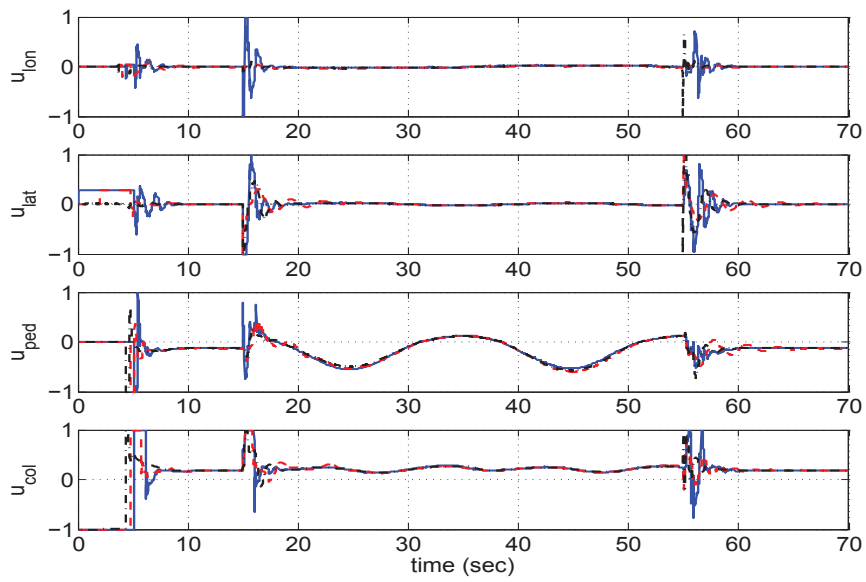
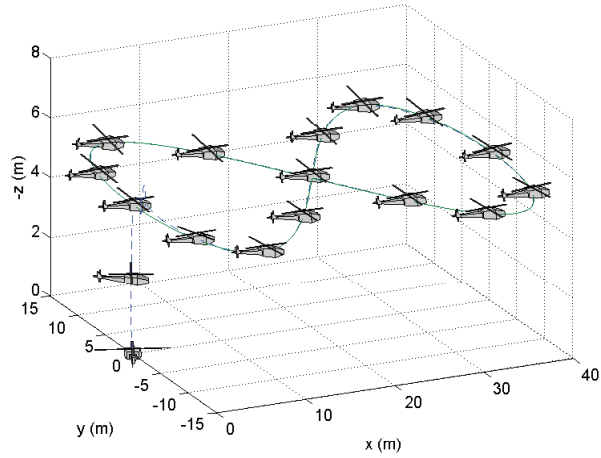
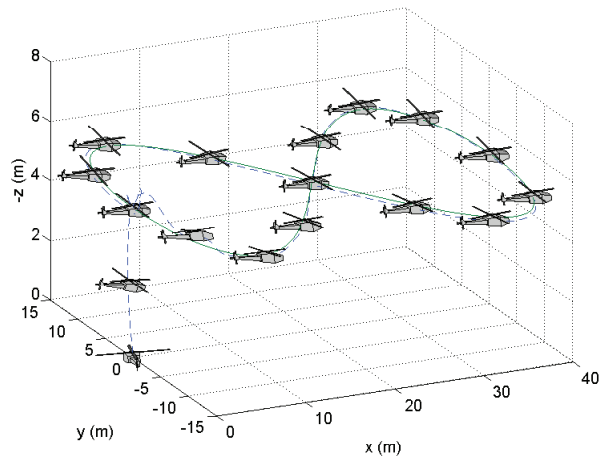


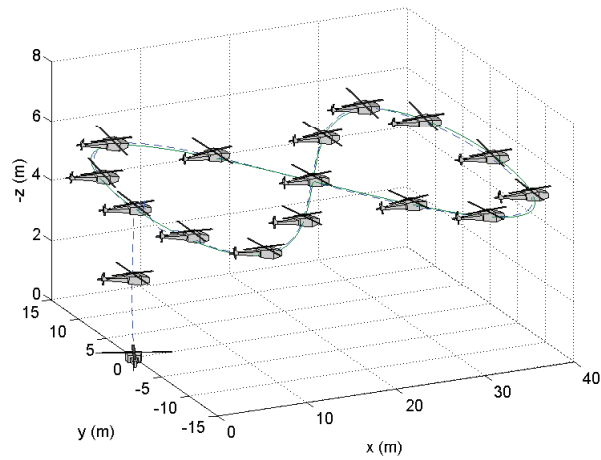
Figure 10.11: *Third maneuver (8 shaped)*: Control inputs of the linear (solid blue line), PID (dashed red line) and nonlinear (dashed dotted black line) controller designs.



(a) Linear controller.



(b) PID controller.



(c) Nonlinear controller.

Figure 10.12: *Third maneuver (8 shaped)*: Reference position trajectory (solid line) and actual trajectory of the controller designs (dashed line) with respect to the inertial axis.

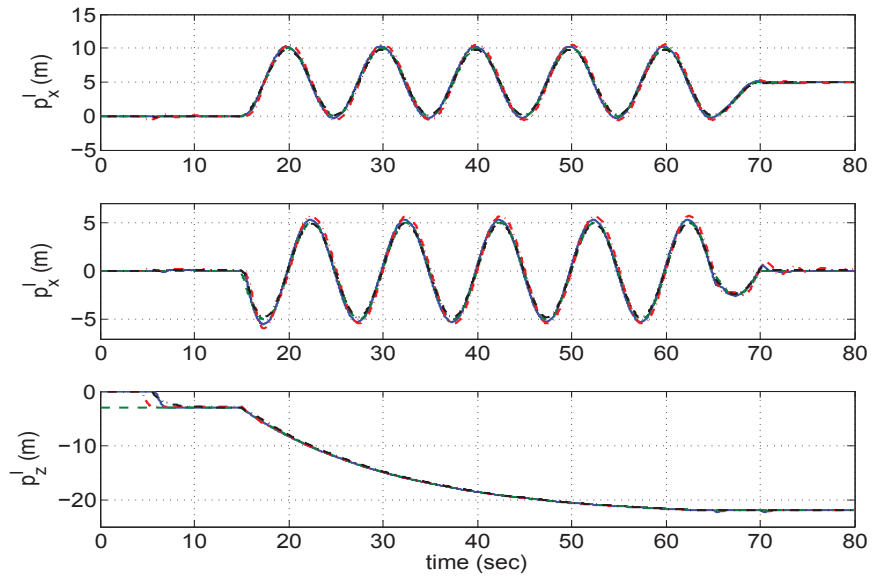


Figure 10.13: *Fourth maneuver (Pirouette)*: Reference position trajectory (green dashed line) and actual position trajectory of the linear (solid blue line), PID (red dashed dotted line), nonlinear (dashed dotted black line) controller designs, expressed in inertial coordinates with respect to time.

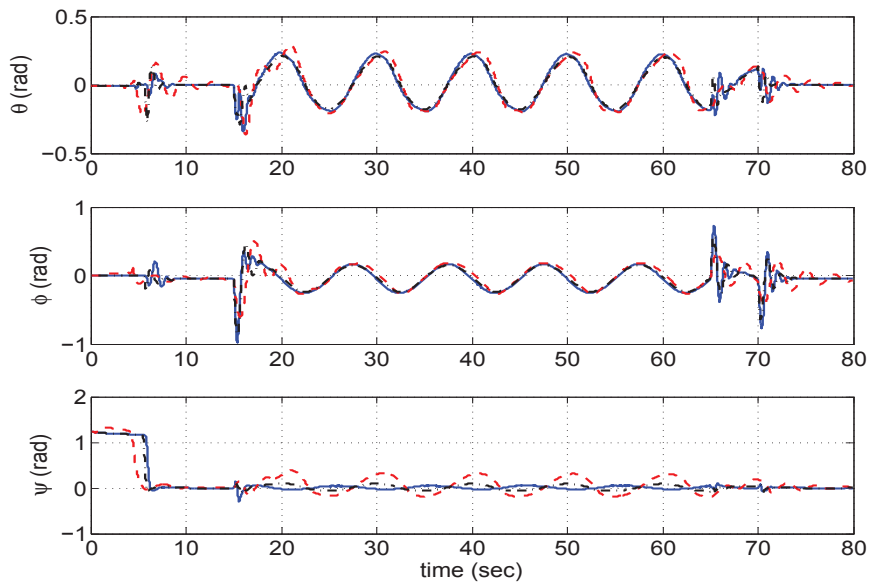


Figure 10.14: *Fourth maneuver (Pirouette)*: Orientation angles of the linear (solid blue line), PID (dashed red line) and nonlinear (dashed dotted black line) controllers designs.

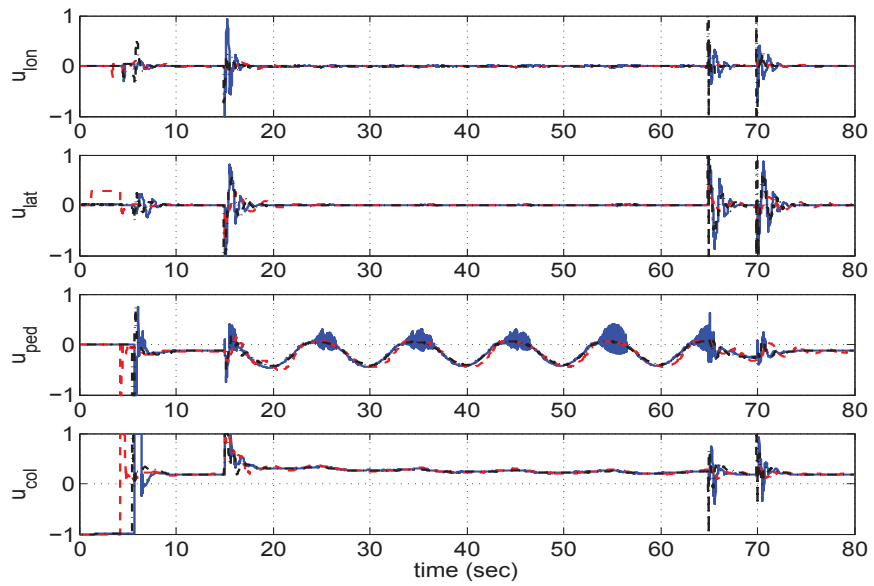
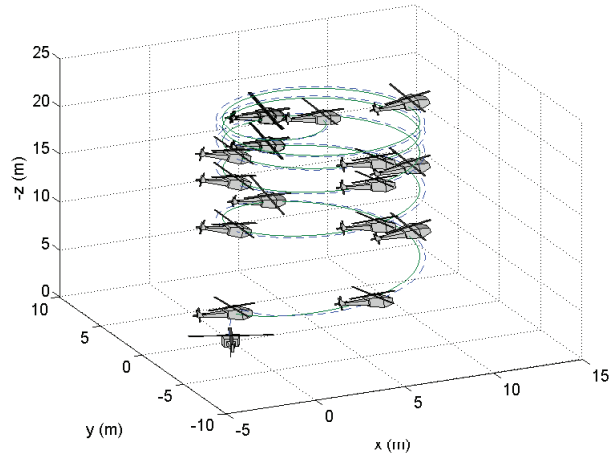
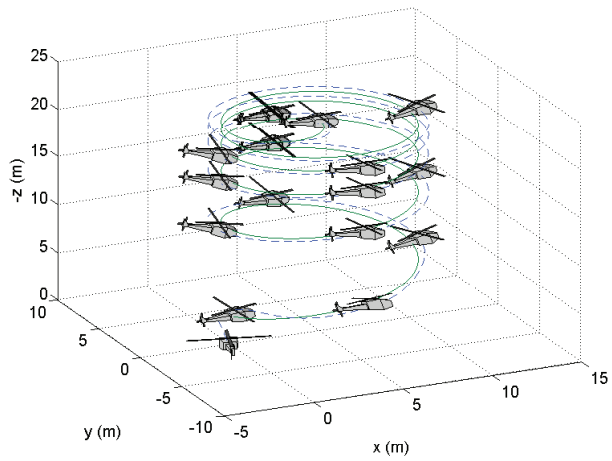


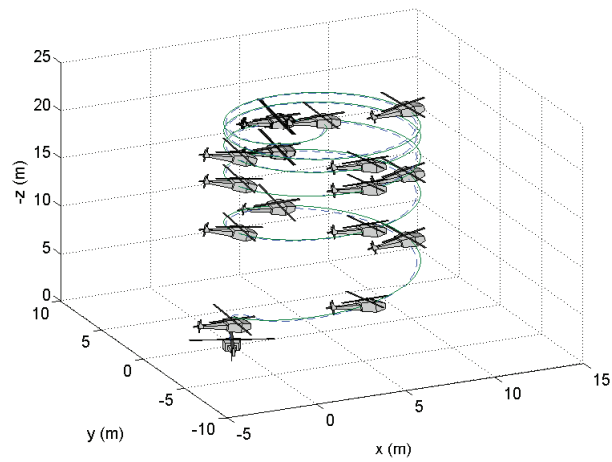
Figure 10.15: *Fourth maneuver (Pirouette)*: Control inputs of the linear (solid blue line), PID (dashed red line) and nonlinear (dashed dotted black line) controller designs.



(a) Linear controller.



(b) PID controller.



(c) Nonlinear controller.

Figure 10.16: *Fourth maneuver (Pirouette)*: Reference position trajectory (solid line) and actual trajectory of the controller designs (dashed line) with respect to the inertial axis.

## Chapter 11: Conclusions and Future Work

Helicopters are highly nonlinear systems with significant dynamic coupling. In general, they are considered to be much more unstable than fixed wing aircraft. The goal of this dissertation has been to examine the design problem of autonomous flight controllers for small scale helicopters.

Modern control techniques are model based, in the sense that the controller architecture depends on the dynamic description of the system to be controlled. This principle applies to helicopter as well, therefore, the flight control problem is tightly connected with the helicopter modeling challenge.

The helicopter dynamics can be represented by both linear and nonlinear models of ordinary differential equations. The model description should accurately predict the helicopter response for any given input. The order and the structure of each model is postulated based on standard laws of physics and aerodynamics accompanied by certain simplification assumptions that reduce as much as possible the complexity of the description. The parametric models should encapsulate the dynamic behavior of a large family of small scale helicopters. Linearized helicopter models have a limited range of validity which is limited to a flight operation in the vicinity of a certain operating point. On the other hand, nonlinear model provide a relative global description of the flight envelope. It is important that the mathematical model is accurate yet manageable enough for the design of a control system.

In this research the linear and nonlinear models structure and order are adopted by widely acknowledged works in the area of the helicopter control and identification. The linear model is adopted by [70] and it consists of a coupled system of the helicopter motion variables and the main rotor flapping dynamics. In the case of the nonlinear representation structure, this work

adopts the model proposed in [47]. This model consists of the helicopter nonlinear dynamic equations of motion enhanced by a simplified model of force and torque generation.

Based on the above parametric model representations, this work introduces several controller designs. The objective of each flight control system is for the helicopter to track a predefined position (or velocity) and yaw reference trajectories. All the proposed controller designs neglect the coupling between the helicopter forces and moments. In particular, we disregard the produced forces from the main rotor flapping motion and the tail rotor in the longitudinal and lateral directions of the body-fixed frame. This is a typical assumption that takes place in most controllers for helicopter that exist in the literature. These parasitic forces have a minimal effect on the translational dynamics compared to the propulsive forces produced by the attitude change of the helicopter. Therefore, this assumption has physical sense. As indicated in [47] the approximate model is feedback linearizable and, therefore, in feedback form. In this work, both linear and nonlinear proposed controllers use concepts from the backstepping recursive design methodology which is suitable for systems of this form.

After establishing a mathematical control framework based on a generic parametric helicopter model, the final step for the implementation of the controller is the extraction of the numeric values of the model parameters. The model parameters should be chosen such that the predicted responses of the model match the actual flight data of the helicopter. The process of extracting the numeric values of the model parameters based on experimental flight data lie in the field of system identification. The system identification procedures are further classified to frequency domain and time domain. The frequency domain identification is much more superior in terms of calculation complexity and accuracy compared to the time domain approaches. However, the main disadvantage of the frequency domain identification is that it is restricted only to linear models.

At this point we need to make clear that the main focus of this work lies in the theoretical development of the flight controllers. Each derived controller is attached with the most suitable system identification approach in order to experimentally validate the applicability of the design. In a real-life application the theoretical control framework is worthless if the helicopter model

parameters are unavailable. The examination of several identification schemes indicate which are the most suitable practices for the extraction of the helicopter parameters.

### 11.1 Summary of Contributions

A summary of the main contributions presented in this work is:

- A multivariable tracking controller based on the linear helicopter dynamics. The proposed design has significant advantages relative to the internal model and integral control approach. The main contribution of this design is its ability to pass the intuitive notion of helicopter manned piloting to the mathematical development of the autonomous controller. This is achieved by separating the helicopter dynamics into two interconnected subsystems representing the longitudinal/lateral and yaw/heave motion, respectively. By disregarding the effect of the forces produced by the flapping motion of the main rotor, the approximated subsystems are in feedback form and, therefore, differentially flat. Due to the differential flatness of the system dynamics, a desired state and input can be determined, composed by the components of the reference output and their higher derivatives. The desired state can be easily and systematically determined by the backstepping approach. When the helicopter state is regulated to this desired state, the tracking error tends asymptotically to zero. Similarly to [47], the desired state vector can be used for the design of meaningful trajectories. The overall control law is a superposition of the desired input and an output feedback component. The output feedback component can be chosen by any design that exists in the literature. The design also allows the scheduling of multiple similar controllers based on linear models of the same structure.
- A tracking control design based on the helicopter nonlinear dynamic model adopted by [47]. This design adopts the backstepping design principle for nonlinear systems in feedback form. The pseudo controls for each level of the feedback system are appropriately chosen to stabilize the overall helicopter dynamics. The pseudo controls combine nested saturation

feedback laws and a novel control strategy for the stabilization of the attitude dynamics. One of the novelties of the proposed controller is its minimalistic design. By using advance stability analysis concepts only the necessary pseudo control terms are included for the stabilization of the system, which are significantly less than existing backstepping designs. Furthermore, apart from stabilizing the attitude dynamics, the control design can guarantee that the helicopter will not overturn for every allowed reference trajectory. The intense theoretical analysis that is used for the derivation of the control design emerges important concepts that should be accounted in the helicopter flight controllers. Such concepts involve the expected range of the pitch and roll angles for aggressive reference maneuvers and the effects of the actuators saturation limits in the helicopter performance.

- A tracking controller based on the discretized nonlinear helicopter dynamics. The control problem is set to the discrete time since time domain system identification is much simpler and computationally efficient. In addition, the control algorithms are executed by micro-processors, therefore, the discretization effect should be accounted by the controller. The main contribution of the developed controller is the design freedom to the convergence rate for each state variable of the cascade structure of the feedback system. This is of particular interest since control of the convergence rate in each level of the cascade structure provides better flight results. The stability of the resulting dynamics can be simply inspected by the eigenvalues of a linear error without the necessity of Lyapunov's functions. The time domain identification takes place with a simple RLS algorithm.
- Finally the the time-domain identification results can be further improved if the discrete nonlinear dynamics are represented by a Takagi-Sugeno fuzzy system. After the development of the Takagi-Sugeno system, a standard RLS algorithm is used to estimate its parameters. The resulting fuzzy system is an interpolator of nonlinear discrete systems which depends on the helicopter flight condition.

## 11.2 Results and Real-Life Implementation

The linear tracking, the discrete backstepping and the PID (introduced in Chapter 6) controller designs were successfully tested in *X-Plane* flight simulator to a Raptor 90 SE RC helicopter. An extensive comparison took place where each flight controller was expected to track several aggressive and dexterous maneuvers. Although the linear helicopter model is theoretically limited only in a neighborhood around hover, a single controller based only on the identified hover model was adequate. The satisfactory performance of the PID design is attributed to the attenuated cross coupling effects amongst the *Raptor 90 SE* dynamics.

For a real-life application it is common engineering intuition to start with the less complex approach. Therefore the first choice should be the PID controller with the four SISO loops. If the cross coupling effect among the system dynamics is significant then the MIMO linear tracking controller should be adopted. Finally, if the linear controller fails to achieve tracking in a wide range of the flight envelope then the nonlinear scheme should be applied.

## 11.3 Future Work

Additional features can be incorporated to the proposed controller designs for their reliable implementation to actual small scale helicopter platforms. Future work involves:

- The helicopter dynamics are characterized by significant parametric and model uncertainty. The proposed controllers are proven to be significantly robust. In all the designs the certainty equivalence principle was adopted. According to that the identified model is considered by the control engineer as the actual helicopter model. A theoretical framework that examines the uncertainty effects to the controller performance would be an important contribution to the flight control design problem.
- Most controller designs neglect the coupling between forces and moments. Therefore, only practical stability of the helicopter can be achieved based on the approximated models.

An interesting research avenue would be to theoretically study the boundedness and error margins introduced by the approximate models.

- In real-life applications the measured sensor signals exhibit significant noise levels which are further deteriorated by the helicopter's engine vibrations. The consequences of noise and the implementation effects of Kalman filtering to the controller design should be further analyzed.

## List of References

- [1] P.P. Angelov and D.P. Filev. An approach to online identification of Takagi-Sugeno fuzzy models. *IEEE Transactions on Systems, Man, and Cybernetics, Part B: Cybernetics*, 34:484–498, 2004.
- [2] N. Antequera, M. Santos, and J.M. De la Cruz. A helicopter control based on eigenstructure assignment. In *IEEE Conference Emerging Technologies and Factory Automation*, 2006.
- [3] J.S. Bay. *Linear State Space Systems*. McGraw-Hill, 1999.
- [4] M. Bejar, A. Isidori, L. Marconi, and R. Naldi. Robust vertical/lateral/longitudinal control of a helicopter with constant yaw-attitude. In *44th IEEE Conference on Decision and Control, and 2005 European Control Conference. CDC-ECC*, 2005.
- [5] J.S. Bendat and A.J. Piersol. *Random Data: Analysis & Measurement Procedures*. Willey InterScience, 1971.
- [6] P. Bendotti and J.C. Morris. Robust hover control for a model helicopter. In *Proceedings of the American Control Conference*, 1995.
- [7] A.R.S. Bramwell, G. Done, and D. Balmford. *Bramwell's Helicopter Dynamics*. Butterworth Heinemann, 2001.
- [8] A. Budiyoona and S.S. Wibowob. Optimal tracking controller design for a small scale helicopter. *Journal of Bionic Engineering*, 4(4):271–280, 2007.
- [9] C.I. Byrnes, F.D. Priscoli, and A. Isidori, editors. *Output regulation of uncertain nonlinear systems*. Birkhauser, 1997.

- [10] G. Cai, B.M. Chen, K. Peng, M. Dong, and T.H. Lee. Modeling and control system design for a UAV helicopter. In *14th Mediterranean Conference on Control and Automation*, 2006.
- [11] P. Castillo, R. Lozano, and A.E. Dzul. *Modelling and Control of Mini-Flying Machines*. Springer-Verlag, 2005.
- [12] P.C. Chandrasekharan. *Robust Control of Linear Dynamical Systems*. Academic Press, 1996.
- [13] R. Chen. Effects of primary rotor parameters on flapping dynamics. Technical Report TP-1431, NASA, 1980.
- [14] A.J. Prasad, J.V.R. Corban, J.E. Calise. Implementation of adaptive nonlinear control for flight test on an unmanned helicopter. In *Proceedings of the 37th IEEE Conference on Decision and Control*, volume 4, pages 3641–3646, December 1998.
- [15] J.E. Corban, A.J. Calise, J.V.R. Prasad, J. Hur, and N. Kim. Flight evaluation of adaptive high-bandwidth control methods for unmanned helicopters. In *AIAA Guidance, Navigation, and Control Conference*, 2003.
- [16] J.J. Craig. *Introduction to Robotics: Mechanics and Control*. Prentice Hall, 2004.
- [17] J.C. Doyle, B.A. Francis, and A. Tannenbaum. *Feedback Control Theory*. Macmillan, 1992.
- [18] M.E. Dreier. *Introduction to Helicopter and Tiltrotor Flight Simulation*. AIAA Education Series, 2007.
- [19] D. Ernst, K. Valavanis, and J. Craighead. Automated process for unmanned aerial systems controller implementation using MATLAB. In *14th Mediterranean Conference on Control and Automation, 2006. MED '06*, 2006.
- [20] B. Etkin. *Dynamics of Flight: Stability and Control*. John Wiley & Sons, 1959.
- [21] I. Fantoni and R. Lozano. *Nonlinear Control for Underactuated Mechanical Systems*. Springer-Verlag New York, Inc, 2001.
- [22] M. Fliess, J. Levine, P. Martin, and P. Rouchon. Flatness and defect of nonlinear systems: Introductory theory and applications. *International Journal of Control*, 61:1327–1361, 1995.

- [23] G.F. Franklin, J.D. Powell, and A. Emami-Naeini. *Feedback Control of Dynamic Systems*. Prentice Hall, 2002.
- [24] E. Frazzoli, M.A. Dahleh, and E. Feron. Trajectory tracking control design for autonomous helicopters using a backstepping algorithm. In *Proceedings of the American Control Conference*, volume 6, pages 4102–4107, 2000.
- [25] D. Fujiwara, J. Shin, K. Hazawa, and K. Nonami.  $\mathcal{H}_\infty$  hovering and guidance control for an autonomous small-scale unmanned helicopter. In *International Conference on Intelligent Robots and Systems*, 2004.
- [26] J. Gadewadikar, F. Lewis, K. Subbarao, and B. Chen.  $\mathcal{H}_\infty$  static output-feedback control for rotorcraft. *Journal of Intelligent and Robotic Systems*, 54:629–646, 2008.
- [27] J. Gadewadikar, F. Lewis, K. Subbarao, and B. Chen. Structured  $\mathcal{H}_\infty$  command and control-loop design for unmanned helicopters. *Journal of Guidance, Control, and Dynamics*, 31:1093–1102, 2008.
- [28] J. Gadewadikar, F.L. Lewis, K. Subbarao, K. Peng, and B.M. Chen.  $\mathcal{H}_\infty$  static output-feedback control for rotorcraft. In *AIAA Guidance, Navigation, and Control Conference and Exhibit*, 2006.
- [29] V. Gavrillets, B. Mettler, and E. Feron. Dynamical model for a miniature aerobatic helicopter. Technical report, Massachusetts Institute of Technology, 2001.
- [30] V. Gavrillets, B. Mettler, and E. Feron. Nonlinear model for a small-size acrobatic helicopter. In *AIAA Guidance, Navigation, and Control Conference and Exhibit*, 2001.
- [31] D.T. Greenwood. *Principles of Dynamics*. Prentice-Hall, 1965.
- [32] N. Guenard, T. Hamel, and V. Moreau. Dynamic modeling and intuitive control strategy for an "X4-flyer". In *International Conference on Control and Automation*, pages 141–146, 2005.
- [33] T. Hamel, R. Mahony, R. Lozano, and J. Ostrowski. Dynamic modeling and configuration stabilization for an X4-flyer. In *15th Triennial World Congress of IFAC*, 2002.

- [34] N. Hovakimyan, N. Kim, A.J. Calise, J.V.R. Prasad, and N. Corban. Adaptive output feedback for high-bandwidth control of an unmanned helicopter. In *AIAA Guidance, Navigation, and Control Conference*, 2001.
- [35] I.I. Hussein, M. Leok, A.K. Sanyal, and A.M. Bloch. A discrete variational integrator for optimal control problems on  $SO(3)$ . In *45th IEEE Conference on Decision and Control*, 2006.
- [36] A. Isidori, L. Marconi, and A. Serrani. *Robust Autonomous Guidance*. Springer-Verlang, 2003.
- [37] A. Isidori, L. Marconi, and A. Serrani. Robust nonlinear motion control of a helicopter. *IEEE Transactions on Automatic Control*, 48:413–426, 2003.
- [38] E.N. Johnson and S.K. Kannan. Adaptive flight control for an autonomous unmanned helicopter. In *AIAA Guidance, Navigation and Control Conference*, 2002.
- [39] E.N. Johnson and S.K. Kannan. Adaptive trajectory control for autonomous helicopters. *Journal of Guidance, Control, and Dynamics*, 28:524–538, 2005.
- [40] W. Johnson. *Helicopter Theory*. Princeton University Press, 1980.
- [41] R.E. Kalman and R.S. Bucy. New results in linear filtering and prediction theory. *Journal of Basic Engineering*, 83:95–108, 1961.
- [42] F. Kendoul, D. Lara, I. Fantoni-Coichot, and R. Lozano. Real-time nonlinear embedded control for an autonomous quadrotor helicopter. *Journal of Guidance, Control and Dynamics*, 30:1049–1061, 2007.
- [43] H.K. Khalil. *Nonlinear Systems*. Prentice Hall, 2002.
- [44] H.J. Kim and D.H. Shim. A flight control system for aerial robots: algorithms and experiments. *Control Engineering Practice*, 11:1389–1400, 2003.
- [45] N. Kim, A. J. Calise, N. Hovakimyan, J. V. R. Prasad, and E. Corban. Adaptive output feedback for high-bandwidth flight control. *Journal of Guidance, Control and Dynamics*, 25:993–1002, 2002.

- [46] V. Klein and E.A. Moreli. *Aircraft System Identification Theory and Practice*. AIAA Education Series, 2006.
- [47] T.J. Koo and S. Sastry. Output tracking control design of a helicopter model based on approximate linearization. In *Proceedings of the 37th IEEE Conference on Decision and Control*, volume 4, pages 3635–3640, 1998.
- [48] T.J. Koo and S. Sastry. Differential flatness based full authority helicopter control design. In *Proceedings of the 38th IEEE Conference on Decision and Control*, 1999.
- [49] M. Krstic, I. Kanellakopoulos, and P.V. Kokotovic. *Nonlinear and Adaptive Control Design*. Wiley-Interscience, 1995.
- [50] R. Kureemun, D. J. Walker, B. Manimala, and M Voskuijl. Helicopter flight control law design using  $\mathcal{H}_\infty$  techniques. In *IEEE Conference On Decicion and Control*, 2005.
- [51] M. La Civita. *Integrated modeling and robust control for full envelope flight of robotic helicopters*. PhD thesis, Carnegie Mellon University, 2002.
- [52] M. La Civita, W.C. Messner, and T. Kanade. Modeling of small-scale helicopters with integrated first-principles and system identification techniques. In *Proceedings of the 58th Forum of the American Helicopter Society*, volume 2, pages 2505–2516, 2002.
- [53] M. La Civita, G. Papageorgiou, W. Messner, and T. Kanade. Design and flight testing of a high-bandwidth  $\mathcal{H}_\infty$  loop shaping controller for a robotic helicopter. In *AIAA Guidance, Navigation, and Control Conference and Exhibit*, 2002.
- [54] M. La Civita, G. Papageorgiou, W.C. Messner, and T. Kanade. Integrated modeling and robust control for full-envelope flight of robotic helicopters. In *Proceedings of IEEE International Conference on Robotics and Automation*, pages 552– 557, 2003.
- [55] M. La Civita, G. Papageorgiou, W.C. Messner, and T. Kanade. Design and flight testing of an  $\mathcal{H}_\infty$  controller for a robotic helicopter. *Journal of Guidance, Control, and Dynamics*, pages 485–494, 2006.
- [56] E.H. Lee, H. Shim, L. Park, and K. Lee. Design of hovering attitude controller for a model helicopter. In *Proceedings of Society of Instrument and Control Engineers*, pages 1385–1390, 1993.

- [57] T. Lee, N.H. McClamroch, and M. Leok. Optimal control of a rigid body using geometrically exact computations on SE(3). In *45th IEEE Conference on Decision and Control*, 2006.
- [58] J.G. Leishman. *Principles of Helicopter Aerodynamics*. Cambridge University Press, 2000.
- [59] W. Levine and M. Athans. On the determination of the optimal constant output feedback gains for linear multivariable systems. *Transactions on Automatic Control*, 15:44–48, 1970.
- [60] F.L. Lewis and V.L. Syrmos. *Optimal Control*. Wiley-InterScience, 1995.
- [61] L. Ljung. *System Identification*. Prentice-Hall, 1987.
- [62] L. Ljung. *System Identification: Theory for the User*. Prentice Hall, 1999.
- [63] A. Loria and E. Panteley. *Advanced Topics in Control Systems Theory: Lecture Notes from FAP 2004*, chapter 2, pages 23–64. Springer-Verlag, 2005.
- [64] R. Mahony and T. Hamel. Robust trajectory tracking for a scale model autonomous helicopter. *International Journal of Robust and Nonlinear Control*, 14(12):1035 – 1059, 2004.
- [65] R. Mahony, T. Hamel, and A. Dzul. Hover control via Lyapunov control for an autonomous model helicopter. In *Proceedings of the 38th IEEE Conference on Decision and Control*, volume 4, pages 3490–3495, 1999.
- [66] L. Marconi and R. Naldi. Robust full degree-of-freedom tracking control of a helicopter. *Automatica*, 43:1909–1920, 2007.
- [67] L. Marconi and R. Naldi. Aggressive control of helicopters in presence of parametric and dynamical uncertainties. *Mechatronics*, 1:381–389, 2008.
- [68] D. McFarlane and K. Glover. A loop-shaping design procedure using  $\mathcal{H}_\infty$  synthesis. *IEEE Transactions on Automatic Control*, 37:759–769, 1992.
- [69] J. M. Mendel. *Lessons in estimation theory for signal processing, communications, and control*. Prentice Hall PTR, 1995.

- [70] B. Mettler. *Identification Modeling and Characteristics of Miniature Rotorcraft*. Kluwer Academic Publishers, 2003.
- [71] B. Mettler, T. Kanade, and M. B. Tischler. System identification modeling of a model-scale helicopter. Technical report, Carnegie Mellon University, 2000.
- [72] B. Mettler, M.B. Tischler, and T. Kanade. System identification of small-size unmanned helicopter dynamics. In *Presented at the American Helicopter Society 55th Forum*, May 1999.
- [73] Mitra. *Digital Signal Processing: A Computer-Based Approach*. McGraw-Hill, 2006.
- [74] A. Moerder, D. Calise. Convergence of a numerical algorithm for calculating optimal output feedback gains. *IEEE Transactions on Automatic Control*, 30(9):900– 903, 1985.
- [75] R.M. Murray, L. Zexiang, and S. Sastry. *A Mathematical Introduction to Robotic Manipulation*. CRC Press, 1994.
- [76] A.V. Oppenheim, R.W. Shafer, and J.R. Buck. *Discrete-Time Signal Processing*. Prentice Hall, 1999.
- [77] A.V Oppenheim, A.S. Willsky, and I.T. Young. *Signals and Systems*. Prentice Hall, 1983.
- [78] H. Ozbay. *Introduction to Feedback Control Theory*. CRC Press, 1999.
- [79] G.D. Padfield. *Helicopter Flight Dynamics: The Theory and Application of Flying Qualities and Simulation Modeling*. AIAA Education Series, 1996.
- [80] G. Papageorgiou and K. Glover.  $\mathcal{H}_\infty$  loop-shaping: Why is it a sensible procedure for designing robust flight controllers. In *AIAA Conference on Guidance, Navigation and Control*, 1999.
- [81] K.M. Passino and S. Yurkovich. *Fuzzy Control*. Prentice Hall, 1998.
- [82] S. Pieper, J.K. and Baillie and K.R. Goheen. Linear-quadratic optimal model-following control of a helicopter in hover. In *American Control Conference*, 1994.

- [83] E. Prempain and I. Postlethwaite. Static  $\mathcal{H}_\infty$  loop shaping control of a fly-by-wire helicopter. *Automatica*, 41:1517–1528, 2005.
- [84] R.W. Prouty. *Helicopter Performance, Stability and Control*. Krieger Publishing Company, 1995.
- [85] I.A. Raptis, K.P. Valavanis, A. Kandel, and W.A. Moreno. System identification for a miniature helicopter at hover using fuzzy models. Submitted in the 47th IEEE Conference on Decision and Control, 2008.
- [86] E. Seckel. *Stability and Control of Airplanes and Helicopters*. Academic Press, 1964.
- [87] J.S. Shamma and M. Athans. Analysis of gain scheduled control for nonlinear plants. *IEEE Transactions on Automatic Control*, 35:898–907, 1990.
- [88] H. Shim, T.J. Koo, F. Hoffmann, and S. Sastry. A comprehensive study of control design for an autonomous helicopter. In *Proceedings of the 37th IEEE Conference on Decision and Control*, volume 4, pages 3653–3658, 1998.
- [89] H.D. Shim, H.J. Kim, and S. Sastry. Control system design for rotorcraft-based unmanned aerial vehicles using time-domain system identification. In *Proceedings of the 2000 IEEE International Conference on Control Applications*, pages 808–813, 2000.
- [90] J. Shin, K. Nonami, D. Fujiwara, and K. Hazawa. Model-based optimal attitude and positioning control of small-scale unmanned helicopter. *Robotica*, 23:51–63, 2005.
- [91] M. Sira-Ramirez, H. and Zribi and S. Ahmad. Dynamical sliding mode control approach for vertical flight regulation in helicopters. In *Control Theory and Applications*, volume 141, 1994.
- [92] S. Skogestad and I. Postlethwaite. *Multivariable Feedback Control*. Wiley, 1996.
- [93] T. Soderstrom and P. Stoica. *System Identification*. Prentice Hall, 1989.
- [94] E.D. Sontag. Remarks on stabilization and input-to-state stability. In *Proceedings of the 28th IEEE Conference on Decision and Control*, volume 2, pages 1376–1378, 1989.

- [95] M.W. Spong, S. Hutchinson, and M. Vidyasagar. *Robot Modeling and Control*. Wiley, 2005.
- [96] J.T. Spooner and K.M. Passino. Stable adaptive control using fuzzy systems and neural networks. *IEEE Transactions on Fuzzy Systems*, 4:339–359, 1996.
- [97] X.D. Sun and T. Clarke. Application of hybrid  $\mu/\mathcal{H}_\infty$  control to modern helicopters. In *International Conference on Control*, 1994.
- [98] H.J. Sussmann and P.V. Kokotovic. The peaking phenomenon and the global stabilization of nonlinear systems. *IEEE Transactions on Automatic Control*, 36:424–440, 1991.
- [99] V.L. Syrmos, C. Abdallah, and P. Dorato. Static output feedback: A survey. In *33rd Conference on Decision and Control*, 1994.
- [100] V.L. Syrmos, C. Abdallah, P. Dorato, and K. Grigoriadis. Static output feedback: A survey. Technical report, University of New Mexico, 1995.
- [101] T. Takagi and M. Sugeno. Fuzzy identification of systems and its applications to modeling and control. *IEEE Transactions on Systems, Man, and Cybernetics*, 15:116–132, 1985.
- [102] A.R. Teel. Global stabilization and restricted tracking for multiple integrators with bounded controls. *Systems & Control Letters*, 18:165–171, 1992.
- [103] A.R. Teel. Using saturation to stabilize a class of single-input partially linear composite systems. In *IFAC NOLCOS'92 Symposium*, pages 379–384, 1992.
- [104] M.B. Tischler and M.G. Cauffman. Frequency-response method for rotorcraft system identification: Flight applications to BO-105 coupled fuselage/rotor dynamics. *Journal of the American Helicopter Society*, 3:3–17, 1992.
- [105] M.B. Tischler and R.K. Remple. *Aircraft and Rotorcraft System Identification*. AIAA Education Series, 2006.
- [106] K.P. Valavanis, editor. *Advances in Unmanned Aerial Vehicles State of the Art and the Road to Autonomy*, volume 33 of *Intelligent Systems, Control and Automation: Science and Engineering*. Springer, 2007.

- [107] M.J. Van Nieuwstadt. *Trajectory Generation for Nonlinear Control Systems*. PhD thesis, California Institute of Technology, 1997.
- [108] D.J. Walker and I. Postlethwaite. Advanced helicopter flight control using two-degree-of-freedom  $\mathcal{H}_\infty$  optimization. *Journal of Guidance, Control and Dynamics*, 19:461–468, 1996.
- [109] M.F. Weilenmann, U. Christen, and H.P. Geering. Robust helicopter position control at hover. In *American Control Conference*, 1999.
- [110] M.F. Weilenmann and P. Hans. A test bench for rotorcraft hover control. In *AIAA Guidance, Navigation and Control Conference*, pages 1371–1382, 1993.
- [111] J.H. Williams. *Fundamentals of Applied Dynamics*. John Wiley & Sons, 1996.
- [112] J. Zhao and I. Kanellakopoulos. Adaptive control of discrete-time strict-feedback nonlinear systems. *Proceedings of the American Control Conference*, 1:828–832, 1997.
- [113] K. Zhou, J.C. Doyle, and K. Glover. *Robust and Optimal Control*. Prentice Hall, 1996.

## Appendices

## Appendix A: Backstepping Control

This Appendix provides a mathematical background of the recursive backstepping control method. The presented material is a summary of more detailed descriptions that can be found in [43, 49]. Lyapunov-based controller design can be systematically tackled by a recursive design procedure called backstepping. Backstepping is suitable for strict-feedback systems which are also known as “lower triangular”. An example of a strict-feedback systems is:

$$\begin{aligned}\dot{\xi}_1 &= f_1(\xi_1) + g_1(\xi_1)\xi_2 \\ \dot{\xi}_2 &= f_2(\xi_1, \xi_2) + g_2(\xi_1, \xi_2)\xi_3 \\ &\vdots \\ \dot{\xi}_{r-1} &= f_{r-1}(\xi_1, \xi_2, \dots, \xi_{r-1}) + g_{r-1}(\xi_1, \xi_2, \dots, \xi_{r-1})\xi_r \\ \dot{\xi}_r &= f_r(\xi_1, \xi_2, \dots, \xi_r) + g_r(\xi_1, \xi_2, \dots, \xi_r)u\end{aligned}\tag{A.1}$$

where  $\xi_1, \dots, \xi_r \in \mathbb{R}$  and  $u \in \mathbb{R}$  is the control input. A typical feedback linearization approach in most cases leads to cancellation of useful nonlinearities. Backstepping design exhibit more flexibility compared to feedback linearization since they do not require that the resulting input-output dynamics to be linear. Cancellation of potentially useful nonlinearities can be avoided resulting to less complex controllers.

The main idea is to use some of the state state variables of (A.1) as “virtual controls” or “pseudo controls”, and depending on the dynamics of each state design intermediate control laws. The backstepping design is a recursive procedure where a Lyapunov function is developed for the entire system. The Lyapunov function can guarantee that the overall dynamics are uniformly globally stable. The recursive procedure can be easily expanded from the nominal case of a system augmented by an integrator. This case study is also referred to as integrator backstepping. Based on the design principles of the integrator backstepping, the control design can be easily expanded

## Appendix A: (continued)

for the case of strict-feedback systems given by (A.1). More particular, consider the system:

$$\dot{\eta} = f(\eta) + g(\eta)\sigma \quad (\text{A.2})$$

$$\dot{\sigma} = u \quad (\text{A.3})$$

where  $[\eta \ \xi]^T \in \mathbb{R}^{n+1}$  is the state vector and  $u \in \mathbb{R}$  is the control input. The objective is the design of a state feedback control law such that  $\eta, \sigma \rightarrow 0$  as  $t \rightarrow \infty$ . It is assumed that both  $f$  and  $g$  are known. This system can be viewed as a cascade connection of two components. The first component is (A.2) with  $\sigma$  as input and the second component is the integrator (A.3). The main design idea is to treat  $\sigma$  as a virtual control input for the stabilization of  $\eta$ . Assume that there exist a smooth state feedback control law  $\sigma = \phi(\eta)$ , with  $\phi(0) = 0$ ; such that the origin of:

$$\dot{\eta} = f(\eta) + g(\eta)\phi(\eta) \quad (\text{A.4})$$

is asymptotically stable. Assume that for the choice of  $\phi(\eta)$  we know a Lyapunov function  $V(\eta)$  such that:

$$\frac{\partial V}{\partial \eta} [f(\eta) + g(\eta)\phi(\eta)] \leq -W(\eta), \quad \forall \eta \in \mathbb{R}^n \quad (\text{A.5})$$

where  $W(\eta)$  is positive definite. By adding and subtracting  $g(\eta)\phi(\eta)$  on the right hand side of (A.2), one has:

$$\dot{\eta} = f(\eta) + g(\eta)[\sigma - \phi(\eta)] \quad (\text{A.6})$$

$$\dot{\sigma} = u \quad (\text{A.7})$$

Denote by  $e_\sigma$  the error between the state  $\sigma$  and the pseudo control  $\phi(\eta)$ , that is:

$$e_\sigma = \sigma - \phi(\eta) \quad (\text{A.8})$$

## Appendix A: (continued)

Writing the initial system in the  $(\eta, e_\sigma)$  coordinates, one has:

$$\dot{\eta} = [f(\eta) + g(\eta)\phi(\eta)] + g(\eta)e_\sigma \quad (\text{A.9})$$

$$\dot{e}_\sigma = u - \dot{\phi}(\eta) \quad (\text{A.10})$$

Since  $f$ ,  $g$  and  $\phi$  are known, one of the advantages of the backstepping design is that it does not require a differentiator. In particular, the derivative  $\dot{\phi}$  can be computed by using the expression:

$$\dot{\phi} = \frac{\partial \phi}{\partial \eta} [f(\eta) + g(\eta)\sigma] \quad (\text{A.11})$$

Setting  $u = v + \dot{\phi}$ , where  $v \in \mathbb{R}$  is a nominal control input, the transformed system takes the form:

$$\dot{\eta} = [f(\eta) + g(\eta)\phi(\eta)] + g(\eta)e_\sigma \quad (\text{A.12})$$

$$\dot{e}_\sigma = v \quad (\text{A.13})$$

which is similar to the initial system, except that now the first component has an asymptotically stable origin when the input is zero. Using this procedure the pseudo control  $\phi(\eta)$  has been “back stepped” through the integrator from  $u = v + \dot{\phi}(\eta)$ . The knowledge of  $V(\eta)$  is exploited in the design of  $v$  for the stabilization of the overall system. Using:

$$V_c(\eta, \sigma) = V(\eta) + \frac{1}{2}e_\sigma^2 \quad (\text{A.14})$$

as a Lyapunov function candidate, we obtain:

$$\begin{aligned} \dot{V}_c &= \frac{\partial V}{\partial \eta} [f(\eta) + g(\eta)\phi(\eta)] + \frac{\partial V}{\partial \eta} g(\eta)e_\sigma + e_\sigma v \\ &\leq -W(\eta) + \frac{\partial V}{\partial \eta} g(\eta)e_\sigma + e_\sigma v \end{aligned} \quad (\text{A.15})$$

## Appendix A: (continued)

The control input  $v$  is chosen as:

$$v = -\frac{\partial V}{\partial \eta}g(\eta) - ke_\sigma, \quad k > 0 \quad (\text{A.16})$$

Substituting the above choice of  $v$  to (A.15), one has:

$$\dot{V}_c \leq -W(\eta) - ke_\sigma^2 \quad (\text{A.17})$$

which shows that the origin  $(\eta = 0, e_\sigma = 0)$  is asymptotically stable. Since  $\phi(0) = 0$ , and  $e_\sigma \rightarrow 0$  as  $t \rightarrow \infty$ ; then the origin  $(\eta = 0, \sigma = 0)$  is asymptotically stable as well. Substituting for  $v$ ,  $e_\sigma$ , and  $\dot{\phi}$ , the final form of the control law is:

$$u = \frac{\partial \phi}{\partial \eta}[f(\eta) + g(\eta)\sigma] - \frac{\partial V}{\partial \eta}g(\eta) - k[\sigma - \phi(\eta)] \quad (\text{A.18})$$

### **About the Author**

Ioannis A. Raptis was born in Athens, Greece in 1979. He received his Dipl-Ing. in Electrical and Computer Engineering from the Aristotle University of Thessaloniki, Greece and his Master of Science in Electrical and Computer Engineering from the Ohio State University in 2003 and 2006, respectively. From 2005 until 2006 he conducted research at the Locomotion and Biomechanics Laboratory of the Ohio State University. In 2006 he joined the Unmanned Systems Laboratory at the University of South Florida. Since 2006 he is pursuing his Ph.D. degree in the department of Electrical Engineering at the University of South Florida. His research interests include nonlinear systems control theory, nonlinear control of electromechanical/robotic systems and rotorcraft/aircraft system identification and control.